



UNIVERSITAT DE
BARCELONA

Synthesis of ethers as oxygenated additives for the gasoline pool

Jordi Hug Badia i Córcoles



Aquesta tesi doctoral està subjecta a la llicència *Reconeixement- SenseObraDerivada 3.0. Espanya de Creative Commons.*

Esta tesis doctoral está sujeta a la licencia *Reconocimiento - SinObraDerivada 3.0. España de Creative Commons.*

This doctoral thesis is licensed under the *Creative Commons Attribution-NoDerivatives 3.0. Spain License.*



UNIVERSITAT DE
BARCELONA

Programa de doctorat d'Enginyeria i Tecnologies Avançades

Synthesis of ethers as oxygenated additives for the gasoline pool

Jordi Hug Badia i Córcoles

Directors:

Dr. Carles Fité Piquer i Dr. Roger Bringué Tomàs

Departament d'Enginyeria Química i Química Analítica, Universitat de Barcelona

Barcelona, setembre de 2016

Contents

Abstract

1. General introduction	1
1.1 Global energy trends	3
1.2 Biofuels	4
1.3 Fuel ethers	5
1.4 Industrial production of fuel ethers	8
1.5 Ion-exchange resins.....	13
1.6 Catalytic activity of acidic ion-exchange resins	16
1.7 Kinetics of fuel ethers syntheses over ion-exchange resins.....	19
1.8 Scope of the thesis	23
1.9 Organization of the thesis.....	24
2. Experimental section	27
2.1 Chemicals.....	29
2.2 Catalysts	30
2.3 Apparatus and analysis	32
2.3.1 Fixed bed reactor system.....	32
2.3.2 Batch reactor system.....	34
2.4 Auxiliary devices	35
3. Chemical equilibrium of the liquid-phase etherification of isobutene with C ₁ to C ₄ linear primary alcohols	37
3.1 Introduction.....	39
3.2 Experimental.....	39
3.2.1 Chemicals and catalysts.....	39
3.2.2 Apparatus and procedure.....	40
3.2.3 Analysis.....	41
3.2.4 Calculations	41
3.3 Results and discussion.....	41
3.3.1 Reaction systems.....	41
3.3.2 Experimental results	44
3.3.2.1 MTBE synthesis	44
3.3.2.2 ETBE synthesis	46
3.3.2.3 PTBE synthesis	47
3.3.2.4 BTBE synthesis	49

3.3.3 Thermodynamic properties.....	50
3.4 Conclusions.....	56
4. Byproducts formation in the ethyl <i>tert</i> -butyl ether (ETBE) synthesis.....	57
4.1 Introduction.....	59
4.2 Experimental.....	60
4.2.1 Chemicals and catalysts.....	60
4.2.2 Apparatus and procedure.....	61
4.2.3 Analysis.....	61
4.2.4 Calculations.....	62
4.3 Results and discussion.....	63
4.3.1 TMP-1 and TMP-2 formation.....	65
4.3.2 DEE formation.....	67
4.3.3 TBA formation.....	68
4.3.4 ESBE formation.....	70
4.3.5 Catalysts comparison.....	72
4.4 Conclusions.....	74
5. Effect of reaction media and ion-exchange resins properties on the liquid-phase etherification of isobutene with C ₁ to C ₄ linear primary alcohols.....	77
5.1 Introduction.....	79
5.2 Experimental.....	79
5.2.1 Chemicals and catalysts.....	79
5.2.2 Apparatus, procedure and analysis.....	80
5.2.3 Calculations.....	80
5.3 Results and discussion.....	81
5.3.1 Reaction system.....	81
5.3.2 Preliminary experiments.....	82
5.3.3 Effect of the linear primary alcohol on the alkyl <i>tert</i> -butyl ether syntheses.....	84
5.3.4 Relations between swollen-state morphology and catalytic activity.....	87
5.4 Conclusions.....	93
6. Catalytic activity and accessibility of acidic ion-exchange resins in liquid-phase etherification reactions.....	95
6.1 Introduction.....	97
6.2 Experimental.....	98

6.3 Results and discussion	98
6.3.1 Reactants molecular size and accessibility	98
6.3.2 Resins swollen-state morphology	100
6.3.3 Relations between swollen-state morphology and catalytic activity	101
6.3.3.1 MTBE experiments	102
6.3.3.2 Generalization of the empirical model	104
6.4 Conclusions	108
7. Simultaneous liquid-phase etherification of isobutene with ethanol and 1-butanol over macroreticular acidic ion-exchange resins	109
7.1 Introduction	111
7.2 Experimental	111
7.2.1 Chemicals and catalysts	111
7.2.2 Apparatus, procedure and analysis	112
7.2.3 Calculations	112
7.3 Results and discussion	113
7.3.1 Catalyst screening	113
7.3.2 Effect of the initial concentration on the simultaneous etherification ...	117
7.3.3 Effect of temperature on the simultaneous etherification	121
7.3.4 Comparison between simultaneous system and individual syntheses ...	124
7.4 Conclusions	126
8. Kinetics of the liquid-phase synthesis of alkyl tertiary butyl ethers over Amberlyst™ 35	127
8.1 Introduction	129
8.2 Experimental	130
8.2.1 Chemicals and catalyst	130
8.2.2 Apparatus, procedure and analysis	131
8.2.2.1 Batch reactor	131
8.2.2.2 Fixed-bed reactor	132
8.3 Results and discussion	132
8.3.1 Experimental results	132
8.3.2 Systematic kinetic modeling	134
8.3.3 Model selection and model averaging	139
8.3.4 Fitting of the kinetic data	141
8.3.4.1 Synthesis of PTBE	141
8.3.4.2 Synthesis of BTBE	146

8.3.4.3 Simultaneous syntheses of ETBE and BTBE	156
8.3.5 Comparison of kinetic equations	161
8.4 Conclusions	164
9. Summary and future lines of research.....	165
9.1 Summary of the main conclusions	167
9.1.1 Conclusions regarding the chemical equilibrium of alkyl <i>tert</i> -butyl ethers syntheses	167
9.1.2 Conclusions regarding the byproducts formation in the ETBE synthesis ..	167
9.1.3 Conclusions regarding the effect of the reaction media on reaction rates and the relations between catalysts properties and resins catalytic behavior	168
9.1.4 Conclusions regarding the isobutene etherification with ethanol and 1-butanol to produce ETBE and BTBE	169
9.1.5 Conclusions regarding the kinetics of the liquid-phase synthesis of alkyl <i>tert</i> -butyl ethers over Amberlyst TM 35	169
9.2 Future lines of research	170
List of publications, work in progress and conference contributions	171
Appendices	175
I. Additional information	177
II. Estimation methods	186
III. Estimated properties	199
List of tables and figures.....	203
Literature.....	211
Resum en català.....	219
Agraïments.....	243

Abstract

Functionalized ion-exchange resins are polymer-based materials that can be used as catalysts, in a wide variety of chemical reactions, to achieve highly selective formation of desired products at cost-effective rates. Among these catalysts, sulfonic ion-exchange resins have become critical in major industrial processes, such as the etherification of isoolefins to obtain branched ethers.

The production of branched ethers, which are oxygenated antiknocking additives for gasoline, became massive after the phase out of lead-based compounds in the 1990s. Among the commercial ethers which are used nowadays, the most important ones, in terms of their global market share, are methyl *tert*-butyl ether (MTBE) and ethyl *tert*-butyl ether (ETBE). These ethers are industrially obtained by means of the catalytic reaction between 2-methylpropene (isobutene) and methanol or ethanol, respectively, over sulfonic macroreticular ion-exchange resins.

On the other hand, the use of reactants obtained from renewable feedstocks to produce fuel components is convenient, since it allows reducing the carbon footprint of transportation fuels in a context in which the global vehicle fleet is growing. In this sense, the trend has been to use biomass-derived ethanol as an alternative to carbon-based alcohols. Nevertheless, this option has generated some concerns regarding its competition with food supplies. Alternatively, the use of other alcohols, such as 1-propanol and 1-butanol, which can also be obtained through fermentative processes, is becoming more attractive, given that they would not compete with food supplies. Etherification of isobutene with these alcohols would produce heavier ethers (i.e., propyl *tert*-butyl ether, PTBE, and butyl *tert*-butyl ether, BTBE, respectively), which have potential benefits as gasoline additives. Nowadays, this is one of the alternatives at hand to achieve an actual improvement of the gasoline formulation in the short- midterm.

Even though the industrial-scale production of MTBE and ETBE is today widely spread, relevant physicochemical aspects regarding ion-exchange resins have not been completely understood. Therefore, studies aimed at providing a deeper insight into the catalytic behavior of these materials are of interest. The present PhD thesis contains several studies related to the catalytic performance of sulfonic macroreticular ion-exchange resins in the liquid-phase syntheses of MTBE, ETBE, PTBE, and BTBE.

Topics included in the present thesis are related to the chemical equilibrium of the mentioned reactions, the byproducts formation, the effect of the medium properties on the etherification reaction rates, the relationships between catalysts properties and catalytic activity, the simultaneous production of ETBE and BTBE, and the kinetics of some of the studied reaction systems.

1. General introduction

1.1 Global energy trends

World population is expected to increase by about 1.5 billion people within the next 20 years, reaching 8.8 billion in 2035, which represents a 17% increase [1]. Over the same period, projections on GDP per person growth indicate a sharper increase, mainly driven by growths in China and India [2]. Per capita energy consumption typically grows consistently with GDP until economies shift from energy-intensive industries, e.g., manufacturing, towards less energy-demanding ones, e.g., service industries, hence global energy demand is expected to increase considerably within the next years [2,3].

Among energy production sources, fossil fuels will continue to dominate largely the global market share, with an expected loss from 86% today to 81% by 2035. The largest gain in the market share concerning non-fossil fuels is expected to come from biofuels (from around 3% to 8%), overtaking nuclear power first and hydro in the early 2030s [2].

Liquid fuels demand will grow mainly due to the transport sector. The global vehicle fleet is expected to increase especially in non-OECD countries (88% of the growth by 2035). Since fuel economy has improved in recent years, transport fuel demand will have a limited growth (Figure 1.1).

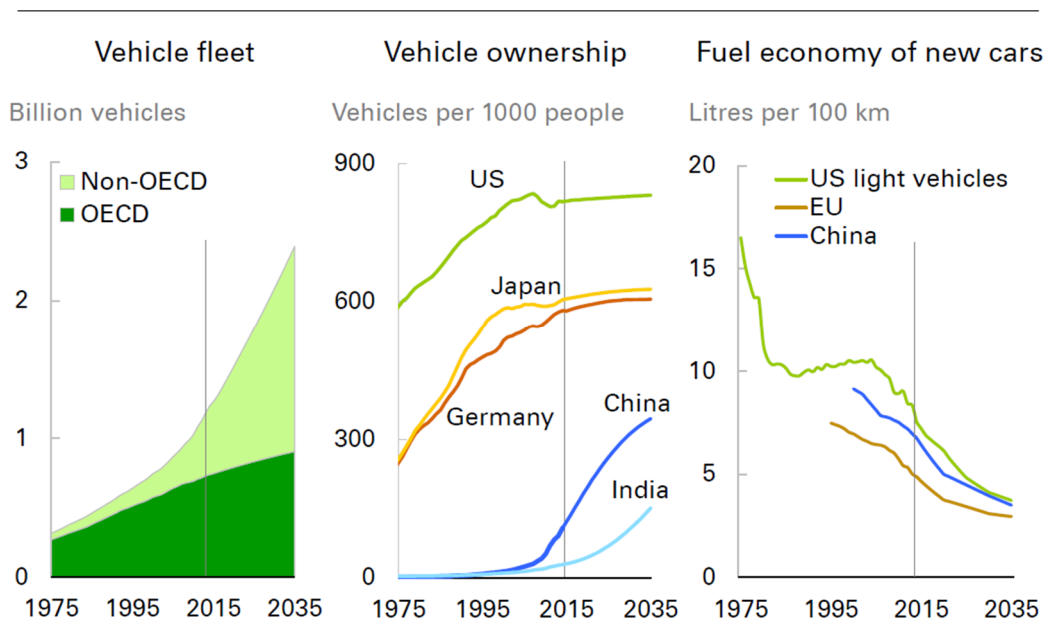


Figure 1.1 Projections on transport [2]

The dominant position in transport fuel demand will still be held by oil, but the share of non-oil alternatives will grow from 5% to 11% in 2035, led by gas and biofuels [4]. In fact, global biofuels production grew by 7.4% in 2014, driven by increases in the US (+5.6%), Brazil (+5.5%), Indonesia (+40.4%), and Argentina (+30.9%), and 0.9% in 2015 [5,6]. The current legislation struggle towards the abatement of CO₂ emissions is likely to continue affecting the transport sector by expanding the introduction of biofuels to newer markets (China, India and Southeast Asia) and encouraging the implementation of advanced biofuels.

1.2 Biofuels

Biofuels production growth has been mainly based on the ethanol production by hydrolysis and fermentation of edible feedstocks, like sugar cane, corn, wheat, or maize. The US and Brazil alone accounted for 83% of the global fuel ethanol production in 2014 [7].

Ethanol can be directly blended with gasoline at any percentage. Blends containing up to 10%vol. of anhydrous ethanol (E10) can be used in most modern internal combustion engines without modifications and they are already available in several countries. E20 to E25 blends are mandatory in Brazil, E85 blends can be found in US and Europe for flexible-fuel vehicles, and E100 blends are used in Brazilian neat ethanol vehicles [8].

Direct addition of ethanol to base gasoline enhances some desirable properties for fuels due to its high octane number¹ and heat of vaporization. Ethanol is also believed to reduce CO₂, particulate, and NO_x emissions. However, ethanol has numerous disadvantages, such as its high hygroscopicity and miscibility with water, and its low energy content and vapor pressure, among others [11]. In addition to this, ethanol production competes with food supplies and promotes invasive plantations [7]. Some properties regarding different ethanol-blended fuels are listed in Table 1.1.

Table 1.1 Properties of fuels blended with different amounts of ethanol

Fuel	Property ^a		
	Reid vapor pressure [kPa]	Research octane number	Heat of combustion [MJ kg ⁻¹]
E0	48.26	85.3	45.12
E5	55.16	89.7	44.15
E10	55.16	92.3	42.87
E15	55.16	94.0	41.61
E20	55.16	99.4	40.51
E85	35 ^b	94-96 ^{c, d}	33.61 ^c
Ethanol	15.8-17.2 ^e	96-113 ^{e, d}	28.55 ^e

^a Unless specified, values from [12]. ^b [13,14]. ^c [15]. ^d (RON+MON)/2. ^e [16].

To overcome some of the issues raised by fuel ethanol production, two main alternatives have been proposed: (i) use of non-edible feedstocks (e.g., cellulosic ethanol from wood, grasses, or the inedible parts of plants) and (ii) use of oxygenates other than ethanol.

¹ The octane number is a numerical representation of the antiknock properties of motor fuel, compared to a standard reference fuel, such as isooctane, which has an octane number of 100. It is also called octane rating [9]. The octane number is determined through two tests, namely Research Octane Number (RON) and Motor Octane Number (MON). RON is determined by running the fuel in a test engine with a variable compression ratio under controlled conditions, and comparing the results with those for mixtures of isooctane and n-heptane. MON is determined by a similar test engine to that used in RON, but with a preheated fuel mixture, higher engine speed (900 rpm instead of 600 rpm for RON), and variable ignition timing to further stress the fuel knock resistance [10].

Cellulosic ethanol does not compete with food supplies but it remains an inconvenient fuel. Among the other oxygenates, a long list of candidates are being considered: on one hand, higher alcohols (which are defined as alcohols with more than two carbon atoms) produced mainly from sugars via fermentation and, on the other hand, nonalcohol oxygenates produced from sugars or lignocellulosic biomass by chemical means. In this sense, a comparison of the blending effects on gasoline properties of ethanol, 1-propanol, 2-propanol, 1-butanol, 2-butanol, 2-methyl-1-propanol, 1-pentanol, 3-methyl-1-butanol, methyl levulinate, ethyl levulinate, butyl levulinate, 2-methyltetrahydrofuran (MTHF), 2-methylfuran (MF), and 2,5-dimethylfuran (DMF) found that these oxygenates reduce the gasoline vapor pressure, with the exceptions of ethanol and 2-propanol. Among other findings, it was also observed that higher alcohols and other oxygenates generally improve vapor lock protection and produce an increase in octane rating, except 1-pentanol and MTHF [17].

The main drawback for nonalcohol oxygenates is that they are at least a decade away from being commercially competitive. Thus, as a mid-term alternative, the interest on higher alcohols has increased lately, especially focused on 1-butanol (which has been given the nickname of biogasoline because of a long list of technical advantages compared to ethanol [18]). Potential shortcomings of 1-butanol are that its toxicity to humans and animals is higher than that of ethanol and gasoline, that there are reasons to believe that it may degrade some automobile materials, and that it is not very safe due to its low flash-point [11,18].

Alternatively, an indirect way to introduce biomass-based alcohols into gasoline is to produce fuel ethers from alcohol addition to olefins. This is a well-established technology since the phase out of lead-based gasoline in the early 1990s.

1.3 Fuel ethers

Fuel ethers are gasoline components with excellent fuel properties: they have high octane number, high energy content, low hygroscopicity, low solubility in water, low vapor pressure, lower oxygen content than alcohols (which, as a result, allows addition of ethers to gasoline in larger amounts and, therefore, harmful gasoline components are diluted), and predictable blending behavior with gasoline (because, unlike alcohols, ethers do not form azeotropes with gasoline) [19].

Etherification reactions involve the addition of an alcohol to the double bond of an olefin. The most relevant examples of fuel ethers are methyl *tert*-butyl ether (MTBE), ethyl *tert*-butyl ether (ETBE), *tert*-amyl methyl ether (TAME), and *tert*-amyl ethyl ether (TAEE). Other quoted candidates would be *tert*-hexyl methyl ether (THME), *tert*-hexyl ethyl ether (THEE), diisopropyl ether (DIPE), and isopropyl *tert*-butyl ether (IPTBE) but, to date, there is no record of their production for blending of gasoline [19,20]. MTBE and ETBE are produced by reaction of isobutene (2-methylpropene) with methanol and ethanol, respectively. Analogously, TAME and TAEE are produced by reaction of the reactive isomers of isoamylene (2-methyl-1-butene and

2-methyl-2-butene) with methanol and ethanol, respectively (Figure 1.2). Properties of some of the most studied fuel ethers are listed in Table 1.2.

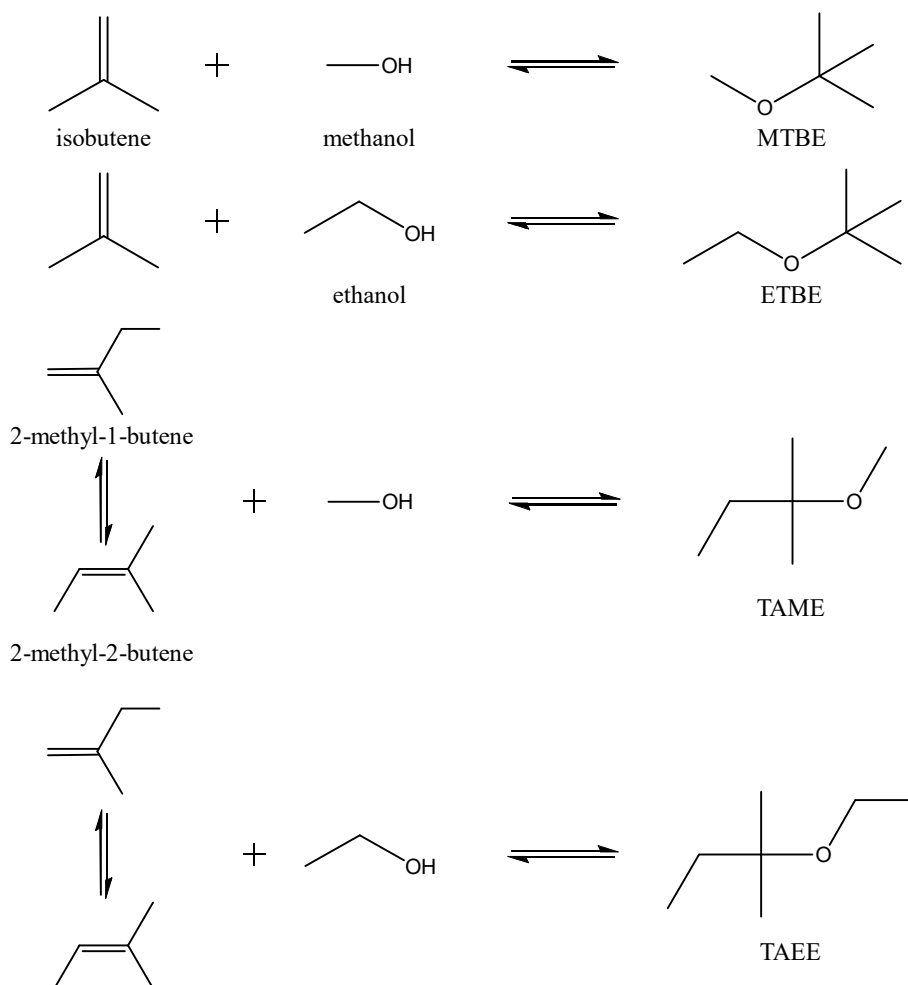


Figure 1.2 Main fuel ethers syntheses reactions

Table 1.2 Properties of some fuel ethers

Fuel ether	Property ^a			
	Reid vapor pressure [kPa]	(RON + MON) / 2	Heat of combustion [MJ kg ⁻¹]	Oxygen content [%wt.]
MTBE	55.12	110	35.2	18.2
ETBE	27.56	112	36.5	15.7
TAME	13.78	105	37.9	15.7
TAEF	12.40 ^b	100	NA	13.8
IPTBE	17.20	105 ^c	NA	13.8
DIPE	34.45	105	37.7	15.7

^a Unless specified, values from [19]. ^b [21]. ^c [22].

Isobutene and isoamylenes are reactive C₄ and C₅ isoolefins, respectively, which are available from fluid catalytic cracking (FCC) and steam cracking (SC) units. Typical C₄ and C₅ cuts from FCC units contain about 25%wt. isobutene and isoamylenes, respectively, whereas SC C₄ cuts usually contain up to 40-50%wt. isobutene [19,23,24].

MTBE was widely used both in US and Europe as octane booster in the reformulated gasoline until, in the early 2000s, it was detected in some US groundwater systems, which led to the replacement of MTBE by isooctane and direct blends of ethanol into gasoline. In Europe, ethanol was mainly introduced through tax incentives generally by replacing MTBE and TAME with ETBE and TAEE. MTBE production sites are distributed over many European countries whereas the ETBE production has been historically located in Germany, France, and Spain. TAME is produced in Italy, France, and Finland. Germany also produces TAEE (Figure 1.3) [20,25].

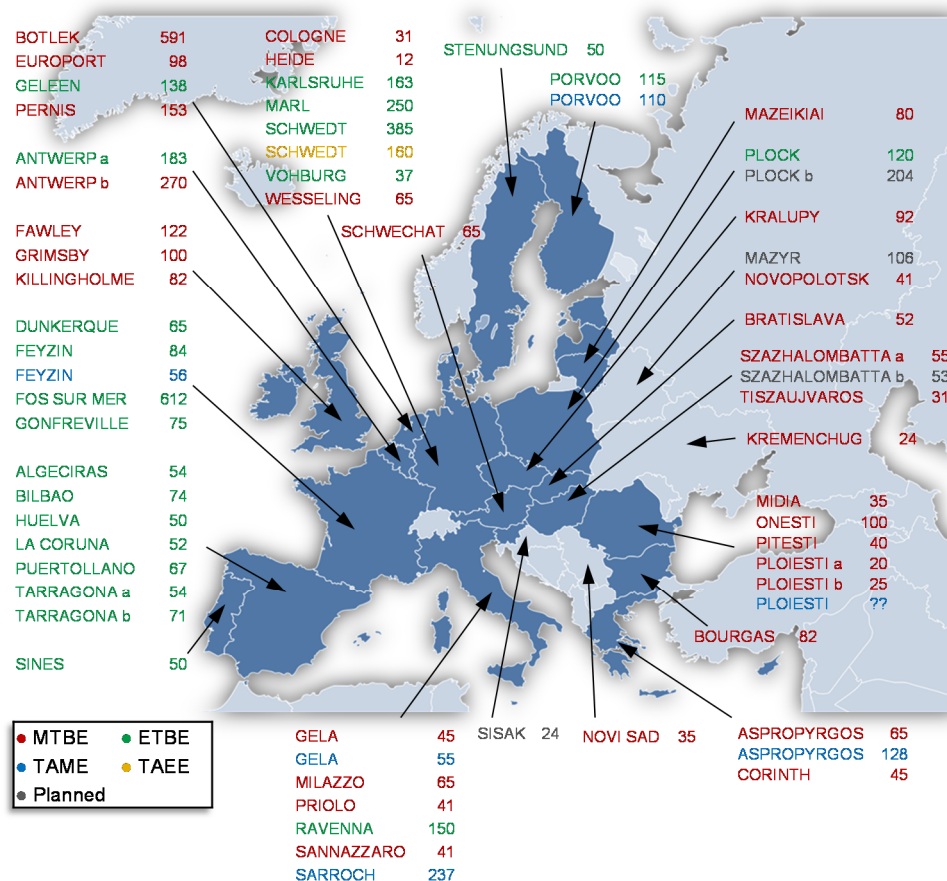


Figure 1.3 European fuel ethers production capacities in 2011 (kt/y) [25]

Among fuel ethers, those produced with alcohols obtained from waste are considered as second generation biofuels and they are hence favored by European legislation. In this sense, methanol can be recovered from raw glycerin, a waste product from biodiesel production, to produce MTBE or TAME [26]. On the other hand, biomass-based ethanol can be produced as indicated in the previous section and, consequently, it raises the same concerns regarding its competition with food supplies but, unlike directly-blended ethanol, ETBE or TAEE are convenient additives for gasoline.

To date, only methanol and ethanol have been used to etherify isoolefins at industrial scale, the main reasons being that oil-based methanol was relatively cheap at the time this process was conceived (1970s), and that the most straightforward choice to substitute methanol was ethanol. Use of alcohols with longer hydrocarbon chains, which would produce heavier ethers, has received very little attention. Potential benefits of blending heavier ethers are that they have higher energy content and boiling point, lower vapor pressure and solubility in water, and they allow a larger dilution effect of harmful gasoline components.

In order to select which heavier alcohols could be chosen to produce the corresponding ethers, different aspects must be considered. Firstly, octane rating of the resulting ethers would be higher if secondary (or branched) alcohols were chosen over primary alcohols, e.g., reaction between isobutene and 2-propanol produces IPTBE which has a higher octane number than propyl *tert*-butyl ether (PTBE), produced by reaction between isobutene and 1-propanol (IPTBE: RON = 109-115, MON = 98-102 [22,27]; PTBE: RON = 109, MON = 92 [22]). Secondly, thermodynamics and kinetics of the candidate syntheses must be evaluated before designing industrial units, e.g., IPTBE reaction is less thermodynamically favored and proceeds at slower rates than PTBE, which results in higher concentration of unreacted reactants and byproducts when synthesizing IPTBE and, therefore, would require more downstream efforts to separate the desired product [22]. Thirdly, within the framework of biofuels, any candidate alcohol should be obtained from biomass-based synthesis routes, e.g., primary alcohols are more abundant as fermentation products than secondary (or branched) alcohols.

As examples, 1-propanol and 1-butanol can be used to etherify isobutene, producing PTBE and butyl *tert*-butyl ether (BTBE), respectively. Use of even larger primary alcohols would produce ethers with much poorer octane rating, which would not be advised (in fact, BTBE octane rating is rather low –MON = 81 [28]–). Both 1-propanol and 1-butanol are industrially produced mainly by means of the oxo process, which consists of a selective hydroformylation and hydrogenation of linear olefins from FCC in the presence of Rh and Co phosphines [29,30]. Alternative routes for producing them from biomass can be the Guerbet catalysis process (condensation of bioethanol and/or biomethanol) or the ABE fermentation (which produces acetone, 1-butanol and ethanol using microorganisms of the genus *Clostridium*) [31,32]. Recent studies within the field of biotechnology can be found targeting 1-propanol and 1-butanol production with engineered microorganisms, which would be able to further enhance biomass-based production routes for these alcohols [33–35].

1.4 Industrial production of fuel ethers

A brief description of the most important commercial processes regarding fuel ethers production is provided in this section, mainly focused on MTBE and ETBE since, to date, these ethers have the largest installed capacity. Production of analogous ethers using heavier alcohols could be achieved by using the same basic schemes without important modifications.

Typically, industrial units consist of two or more reactors in series followed by separation of the ether from unreacted reactants. Hybrid processes are also used to further increase the purity of the obtained ether, e.g., pervaporation-distillation units to separate the azeotropic mixture of ETBE and ethanol or reactive distillation units to shift the chemical equilibrium to complete conversion by means of continuous separation of the product [36]. The most common sources for reactants are FCC or SC C₄ cuts, containing isobutene, and the designated alcohol, i.e., methanol or ethanol, but *tert*-butyl alcohol (TBA) can also be used instead of isobutene, producing the corresponding ether and a molecule of water.

Institut Français du Pétrole (IFP) process for MTBE

MTBE is produced by addition of methanol to isobutene in the presence of an ion-exchange resin at mild temperature, between 40 and 90 °C, and at enough pressure to maintain the liquid phase. The process can be summarized into four basic steps: *a)* the reaction zone, which contains acid catalyst (preferably AmberlystTM 15), is fed with C₄ cut, methanol, and a recycle stream in the liquid phase; *b)* the reaction effluent is distilled under superatmospheric pressure producing a top effluent formed by C₄ hydrocarbons, including unreacted isobutene, and methanol, and a bottom effluent mainly containing MTBE; *c)* the top effluent is divided into two streams, one of which is discharged and the other one is recycled to the reactor feed; *d)* the bottom effluent, which contains a high concentration of MTBE, is recovered as the product (Figure 1.4) [37].

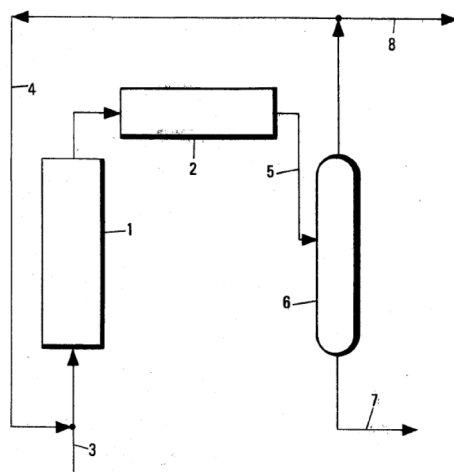


Figure 1.4 IFP process for MTBE. 1: first reactor, 2: second reactor, 3: inlet stream, 4: recycle stream, 5: reactor zone outlet, 6: distillation column, 7: bottom stream from distillation, 8: discharged stream from distillation top effluent [37]

Preferred methanol to isobutene fed molar ratio is between 1.05:1 and 1.4:1. The two reactors should be either fixed or a dispersed bed of catalyst, the first unit operating at a slightly higher temperature than the second one [37].

Several versions of this basic scheme can be found nowadays which can include, for example, a catalytic distillation column as the second reaction section, understoichiometric molar ratio in the reaction zone (to achieve higher ethanol conversions), or alcohol recovery from the product stream and its recycling to the reactor (to achieve higher isobutene conversions) [19,38].

Snamprogetti process for MTBE and TAME

The Snamprogetti process is similar to the IFP one but it includes a second distillation column. In this case, methanol is fed to the first reactor together with the effluent stream of the second distillation column, which contains some isobutene (in the MTBE case). The isobutene conversion in the first reactor is high because there is a high excess of methanol. The outlet stream of the first reactor enters the first distillation column. From the first column, the top effluent contains an olefinic mixture with less than 2% isobutene, and the bottom effluent is a mixture of the produced ether and unreacted methanol. The top effluent is discharged and the bottom effluent, mixed with the olefinic feed, is introduced into the second reactor. In the second reactor, there is an excess of olefin and, as a consequence, the methanol conversion is high. The outlet stream from the second reactor enters the second distillation column in which MTBE (or TAME) is obtained as the bottom effluent and an olefinic stream (poorer in isobutene or isoamylenes) is obtained as the top effluent and recycled back into the first reactor. The recommended liquid hourly space velocity (LHSV) at the first reactor is 5 h^{-1} and, at the second reactor, in the range $20\text{-}50 \text{ h}^{-1}$. Both reactors should operate at $60\text{-}70^\circ\text{C}$. A variation of the described process consists of feeding the olefinic stream to both the first and the second reactor (Figure 1.5) [39].

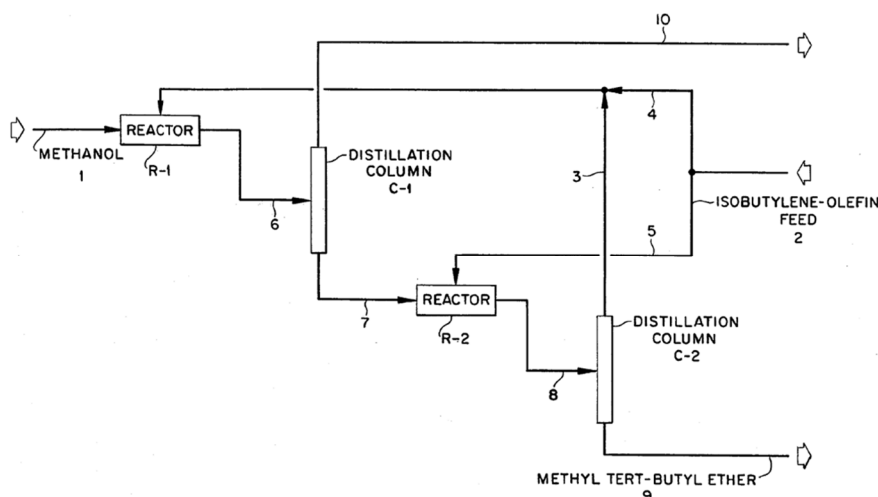


Figure 1.5 Snamprogetti process for MTBE. R-1: first reactor, R-2: second reactor, C-1: first distillation column, C-2: second distillation column, 1: methanol inlet to R-1, 2: olefin inlet stream, 3: C-2 top effluent, 4: olefin inlet to R-1, 5: olefin inlet to R-2, 6: R-1 outlet stream, 7: C-1 bottom effluent, 8: R-2 outlet stream, 9: product outlet stream, 10: discharged C-2 top effluent [39]

Hüls process for ETBE

Small excess of ethanol and C₄ cuts (either from FCC or SC units) are used in the Hüls process to obtain ETBE with acidic ion-exchange resin as catalyst. The reactor zone design depends on the isobutene concentration at the inlet stream. For low isobutene concentration, two adiabatic fixed-bed reactors with an intermediate cooler are used. For high isobutene concentration, a water-cooled multitubular reactor followed by an adiabatic reactor is used or, alternatively, two adiabatic reactors with recycling of the intermediate cooled effluent can also be used.

The reactor outlet is fed to a distillation column, which produces a top effluent, mainly containing butenes and small amounts of ethanol, and an ETBE-ethanol bottom effluent. This bottom stream is usually considered as the final product but, if ethanol needs to be recovered, a second distillation column is used [19].

Philips etherification process

The Philips process, which presents a more complex scheme, also uses ion-exchange resins to etherify isobutene, isoamlyenes, or mixed olefins from FCC or SC units with methanol or ethanol.

Two separate reaction sections are distinguished: in the first one, the reactor outlet stream is fed to a fractionation column to obtain top, bottom, and intermediate effluents, which are fed to the second reaction section, discharged as product (the bottom contains mainly ethers), and recycled, respectively. The outlet stream from the second reactor is fed to a second fractionation column, in which ethers are obtained as the bottom effluent (Figure 1.6) [40].

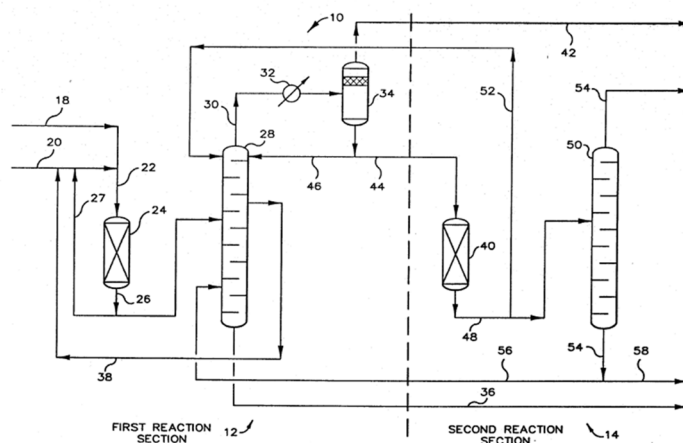


Figure 1.6 Philips etherification process. 10: process system, 12: first reaction section, 14: second reaction section, 18: alcohol feed stream, 20: olefin feed stream, 22: first reactor inlet, 24: first reactor, 26: first reactor outlet, 27: cooling recycle from first reactor, 28: first fractionator, 30: first fractionator top effluent, 32: condenser, 34: accumulator, 36: first fractionator bottom effluent, 38: intermediate stream recycle from first fractionator, 40: second reactor, 42: vapor-phase stream from accumulator, 44: second reactor inlet, 46: recycle from accumulator condensed-phase stream, 48: second reactor outlet, 50: second fractionator, 52: recycle from second reactor outlet, 54: second fractionator effluents, 56: recycle from second fractionator bottom effluent, 58: second fractionator bottom effluent [40]

Texaco process

The Texaco process uses zeolites to obtain MTBE or ETBE from the corresponding alcohol and TBA instead of isobutene. The reaction can be carried out either in a stirred slurry reactor or in a fixed bed reactor at temperatures from 80°C to 200°C, preferably. Preferred alcohol to TBA molar ratio at the reactor inlet stream is from 1:1 to 5:1. Typical product stream can contain up to 50%wt. ether at LHSV around 6 h⁻¹ [41,42].

CDTECH process

In the CDTECH process, the olefinic stream is fed together with the alcohol into a boiling point fixed bed reactor followed by a reactive distillation column where the reaction continues. The produced ether is separated as the bottom effluent. In both the fixed bed reactor and the reactive distillation units, an acidic ion-exchange resin is used as catalyst [38,43].

This process reaches isobutene conversions of 99.99% for the MTBE process and slightly less for the ETBE. Isoamylenes conversion are over 95% for TAME and TAEI [38].

ETHERMAX process

This process also uses reactive distillation technology and similar feeds and catalyst than CDTECH. The most relevant difference with the CDTECH process is that ETHERMAX includes a countercurrent extraction column using water to recover the alcohol from the top effluent of the reactive distillation unit. An alcohol-water distillation column is used to recycle the alcohol to the reactor [38].

NExTAME and NExETHERS processes

NExTAME is an integrated process consisting of reactors and a distillation tower. The reaction reaches chemical equilibrium in the reactors and the resulting product is fed into a distillation column. Unreacted reactants are recycled from the distillation column back into the reactors. No separate alcohol recovery system is required. NExETHERS, which is similar to NExTAME, uses fixed bed reactors and two distillation columns. The excess alcohol is recycled from the second column to remove oxygenates from the olefinic cut [38].

1.5 Ion-exchange resins

Any Brønsted acid can be used as homogeneous or heterogeneous catalyst to produce fuel ethers, such as sulfuric acid, zeolites, heteropolyacids or ion-exchange resins, among others. As seen in the previous section, ion-exchange resins are preferred in industry due to cost-benefit reasons.

Ion-exchange resins are solid organic materials with hydrophilic functional groups bonded to a polymer backbone with hydrophobic character. The polymeric backbone, which is a cross-linked copolymer, consists of an irregular three-dimensional matrix of hydrocarbon chains. Depending on their application, a wide variety of functional groups can be used, ranging from strongly basic systems (with hydroxyl salts of ammonium ions) to strongly acidic ones (based on sulfonic groups), including any combination of them [44].

Two main commercial types of resin can be identified: gel-type resins and macroreticular resins. Gel-type resins present a microporous collapsed structure in dry state and swell in contact with a polar solvent², exhibiting a considerable porosity. Macroreticular resins are composed by agglomerates of gel-type zones, with their respective microporous structure, that form permanent macropores between them, even in the dry state [44–46].

Resins are usually produced by suspension polymerization, which can be broadly summarized as follows: firstly, an organic phase, consisting of a monovinyl-divinyl monomer mixture, a free-radical initiator, and an inert diluent (for macroreticular resins only) is added to a continuous phase (usually an aqueous phase containing additives) under agitation. The organic phase forms small, dispersed droplets in the continuous phase. The reactions of copolymerization and crosslinking take place in the droplets and, as a result, spherical-shaped beads are formed. The inert diluent used for macroreticular resins acts as a porogen and it is soluble in the monomer mixture and insoluble in the continuous phase. In case it is added, the inert diluent is extracted from the beads with a solvent, generating permanent pores. Functionalization of the resins is usually achieved by chemical modification of an already formed copolymer [44,45,47–49].

The ion-exchange resins typically used for fuel ethers production are beads of acidic macroreticular copolymers of polystyrene (PS) chains cross-linked by divinylbenzene (DVB) and functionalized with sulfonic groups. Functionalization is carried out by direct sulfonation of the preformed beads with concentrated sulfuric acid. Both the functionalization and crosslinking degrees play a pivotal role for the resulting properties of the resins. A schematic representation of sulfonated PS-DVB resins structure is shown in Figure 1.7.

² The reaction medium for fuel ethers production is strongly polar, given the presence of alcohols and water (for the case of the TBA synthesis route).

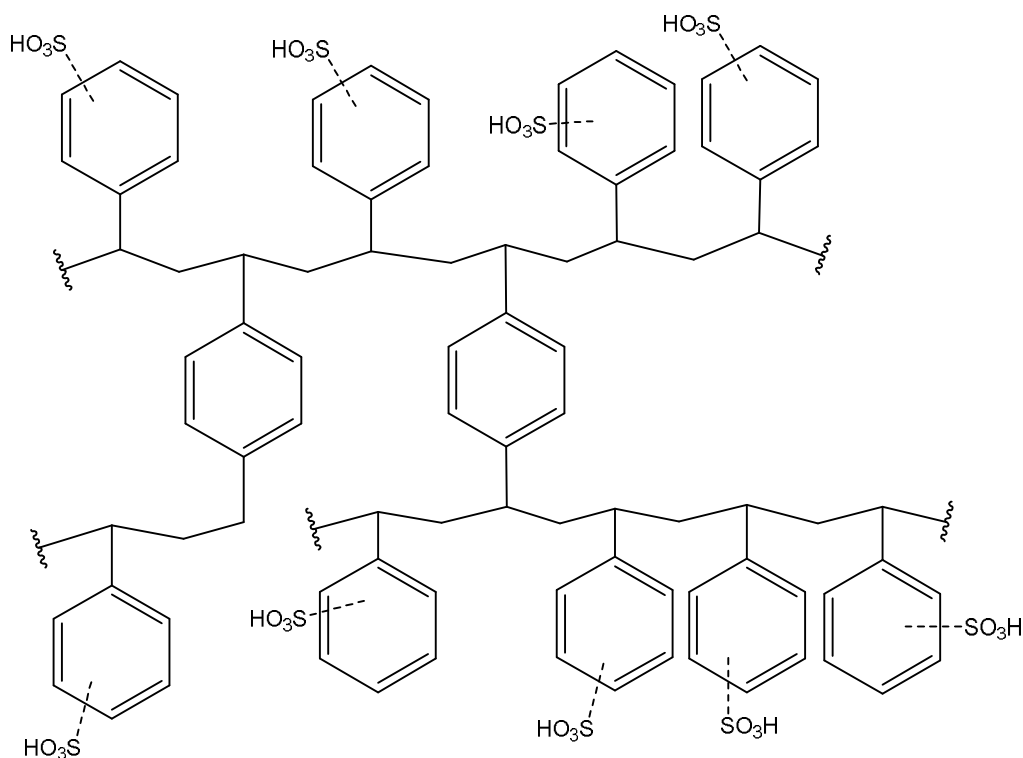


Figure 1.7 Schematic representation of sulfonated PS-DVB ion-exchange resins

With regard to the crosslinking degree, macroreticular resins can be divided into three main groups, depending on the amount of crosslinking agent (expressed as %wt. of DVB in the monomer mixture): low (<9%), medium (9-14%) and high (>14%) crosslinking degree; gel-type resins rarely present more than 12% DVB [50]. The lower the crosslinking degree of a resin, the higher are its elasticity and swelling capacity in contact with a polar medium.

As for the functionalization degree, resins are often classified also into three main groups: partially sulfonated resins, with less than one sulfonic group per styrene ring; conventionally sulfonated (or fully monosulfonated) resins, with about one sulfonic group per styrene ring; and oversulfonated (or hypersulfonated) resins, with more than one sulfonic group per styrene ring. The degree of sulfonation can be controlled by the temperature and time of exposure of the polymers to concentrated sulfuric acid, as well as by using specific solvents to swell the polymer during the sulfonation process, e.g., dichloroethane, methylene chloride or trichloroethylene. In fact, the swelling capacity of a resin affects the ease of permeation of sulfuric acid into it and hence the resulting acid capacity (i.e., the presence of dense domains in highly cross-linked polymers make them difficult to functionalize). At the same time, the introduction of sulfonic groups increases the swelling capacity of a resin when in contact with aqueous environment because the initial lipophilic character of the polymer is changed to a more hydrophilic one [45,51–54].

Information about ion-exchange resins features can be gathered through a wide variety of characterization techniques. Some of them, along with the corresponding determined property, are listed in Table 1.3.

Table 1.3 Popular characterization techniques for ion-exchange resins

Characterization technique	Property	Typical units
Titration against standard base	Acid capacity	meqH ⁺ /g _{cat} or meqH ⁺ /cm ³ _{cat}
Microcalorimetry of ammonia	Acid capacity	meqH ⁺ /g _{cat} or meqH ⁺ /cm ³ _{cat}
	Enthalpy of adsorption	kJ/mol
Karl-Fischer titration	Water content	%wt.
Laser diffraction	Particle size distribution in a given medium	μm
Bulk density determination	Apparent density	g/cm ³
Helium pycnometry	Skeletal density	g/cm ³ _{cat}
Nitrogen reversible adsorption	Surface area	m ² /g _{cat}
	Pore volume	cm ³ /g _{cat}
	Pore diameter	nm
Inverse Steric Exclusion Chromatography (ISEC)	Surface area	m ² /g _{cat}
	Pore volume	cm ³ /g _{cat}
	Pore diameter	nm
	Swollen polymer volume	cm ³ /g _{cat}
Mercury porosimetry	Density, pore volume, pore size distribution and surface area	
Elemental analysis	Composition	%mol. or %wt.
Thermogravimetric analysis (TGA)		
Differential thermal analysis (DTA)		
Infrared spectroscopy		

Among the techniques and properties listed in Table 1.3, it is worth mentioning that there is some lack of characterization techniques able to obtain operando information about resins properties. As example, none of them is able to characterize the resins morphology, i.e., porosity, in the actual reaction medium, which is considered to be crucial for resins catalytic behavior because of the transport restrictions that chemical compounds might experience when permeating through it. Instead, one must consider two opposite situations: either (i) dry state characterization by Mercury-based porosimetry or Nitrogen reversible adsorption³, in which gel-type resins and gel-type zones within macroreticular resins are almost collapsed, or (ii) water-swollen state characterization by ISEC technique, in which the swelling degree is high. However, the information retrieved from either one technique or the other is often useful to establish relationships between morphology and catalytic activity of ion-exchange resins, even though the actual working-state morphology is different from those extreme situations, e.g., [55,56]. On the other hand, infrared techniques, including Diffuse Reflectance Infrared Fourier Transform Spectroscopy (DRIFTS), are able to characterize adsorbed species on a catalyst and to show the evolution of the resin during the reaction [54,57].

³ BET (Brunauer, Emmett and Teller) surface area and BJH (Barret, Joyner and Halenda) mesopore analysis are the most popular methods to obtain morphological properties through Nitrogen reversible adsorption.

In fact, a multi-technique approach is mandatory to characterize these systems in order to establish fundamental understanding of the catalytic behavior of ion-exchange resins under actual working conditions.

1.6 Catalytic activity of acidic ion-exchange resins

Catalysis by ion-exchange resins involves simultaneous processes of diffusion, adsorption, chemical reaction, and desorption. As a consequence, concentration of reactants inside the catalyst, where the reaction occurs, may be different from that in the bulk solution.

Additionally, the polymeric matrix can be structurally influenced by the course of a reaction. Polar solvents, like water or alcohols, swell the matrix (either totally or partially) and could produce acid leaching of the active species from the catalyst to the bulk solution, changing the catalytically-inert character of the solution to an active one [50]. For instance, when resins are swollen in aqueous environment, the hydronium cation becomes the active agent and may present a certain degree of mobility around sulfonic groups. On the contrary, for non-polar environments, the acidic groups are undissociated and reaction takes place through adsorption of reactants on the cluster of active sites [45]. These two opposite situations are schematically represented in Figure 1.8.

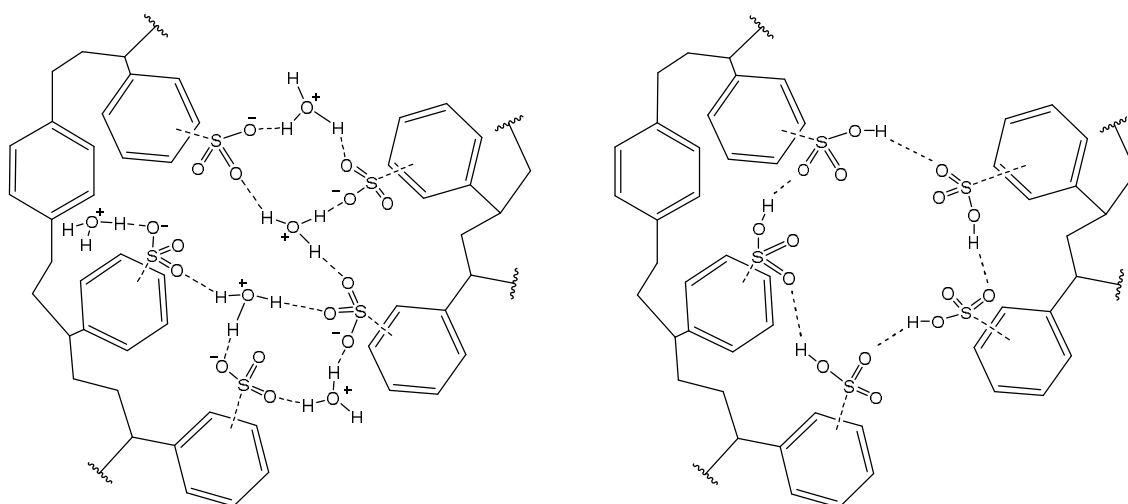


Figure 1.8 Hydrated (left) and undissociated (right) sulfonic groups attached to the polymeric matrix of an ion-exchange resin

From this fact, specific and general acid catalysis can be distinguished. The former, proceeds similarly to homogeneous catalysis by soluble acids and becomes evident at high concentration of polar compounds. The latter, which is an actual heterogeneous catalytic step, takes place at low concentration of polar compounds and it is faster than specific catalysis [58,59].

On the other hand, as commented earlier, resins structural properties have a determinant impact on their catalytic behavior. For instance, the matrix of gel-type resins is homogeneous, with no discontinuities, which results in almost no catalytic activity unless reactants are capable of swelling the matrix themselves –or if a convenient

solvent is added–, because the only active sites to be reached would be those located on the beads surface, which represent an insignificant proportion of the active sites within a resin. In contrast, reactants can permeate easier through macroreticular resins because of the existence of interstices between the agglomerates of gel-type zones [50].

Manufacturers can tailor resins pore size distribution and swelling capacity to enhance selectivity towards desired products via sieve action, favoring or limiting the transport of certain molecules through the catalyst, hence affecting their ability to reach active sites and react. The matrix expansion degree can be regulated by selecting the amount of crosslinking agent and the pore size distribution can be controlled by changing specific variables of the polymer synthesis method, e.g., the temperature profile during polymerization, when the pore structure is being established [46].

As for adsorption processes involved in this type of catalysis, an aspect that needs to be considered is that of competitive adsorption of reactants on resins. Preferential adsorption of specific reactants allows higher concentration of them inside the catalyst and, consequently, selectivity towards the corresponding products is enhanced. For instance, methanol adsorption on AmberlystTM 15 was found to be larger than that of 1-butanol (distribution coefficients between internal and external concentration were 1.14 for methanol and 0.67 for 1-butanol [59]), which led to a higher production of MTBE over BTBE when the two alcohols and isobutene were in contact with the catalyst [59,60].

Another major difference between homogeneous catalysis and catalysis by ion-exchange resins is that the dependence of reaction rates on the concentration of sulfonic groups is non-linear due to the heterogeneity of active sites. This is explained by considering local differences in protons concentration inside the gel-phase of the catalyst and differences between active sites, regarding their activity level [59,61,62]. The non-uniform distribution of active sites allows reaching high local concentrations of protons inside the catalysts that can be explained by Hammett-type acidity functions [50].

Differences in the activity level displayed by internal and external active sites have been quoted in literature, e.g., [63,64]. According to those studies, active sites located at the surface of the gel-type phase are less active than those located at inner regions. As a tentative explanation to this fact, it can be assumed that inner sites would be more prone to be arranged in such local spatial distributions that coordination of reactants to multiple active sites could be accomplished. Thus, participation of several groups would be preferentially achieved by inner active sites and hence they could stabilize better the reaction intermediate.

To date, one of the most successful approaches to provide information about resins working-state morphology and molecular accessibility is based on the ISEC technique assessment. This technique allows determining the meso- and macroporosity formed by resins in swollen-state and distinguishes between volume fractions within the gel-type phase (often referred to as microporosity) in terms of resins polymer density [65,66].

The ISEC technique employs the swollen material to be characterized, i.e., the ion-exchanger, as the steady-state phase in a liquid chromatography column, and measures elution volumes of solutes with a characteristic molecular size. Then, under the considered assumptions: (i) a simple geometric model can describe the macropore system, and (ii) the micropore system can be treated as a discrete set of fractions of different chain density, the mathematical treatment of the data provided by the ISEC analysis provides information on pore volume distributions [45,65,66].

Differences between the activity level displayed both by different resins and by different active sites within a resin are explained by differences in the structure of the polymer skeleton, including the location of sulfonic groups in the catalyst matrix [67,68]. The microporous structure of ion-exchange resins is modeled as a set of discrete volume fractions with different characteristic polymer chain densities (namely, 0.1, 0.2, 0.4, 0.8, and 1.5 nm/nm^3). A number of works can be found in literature targeting the influence of the features characterized through ISEC on the catalytic behavior of resins in different reactions, e.g., [51,53,55,69,70]. The swollen-state morphology of macroreticular ion-exchange resins is schematically depicted in Figure 1.9.

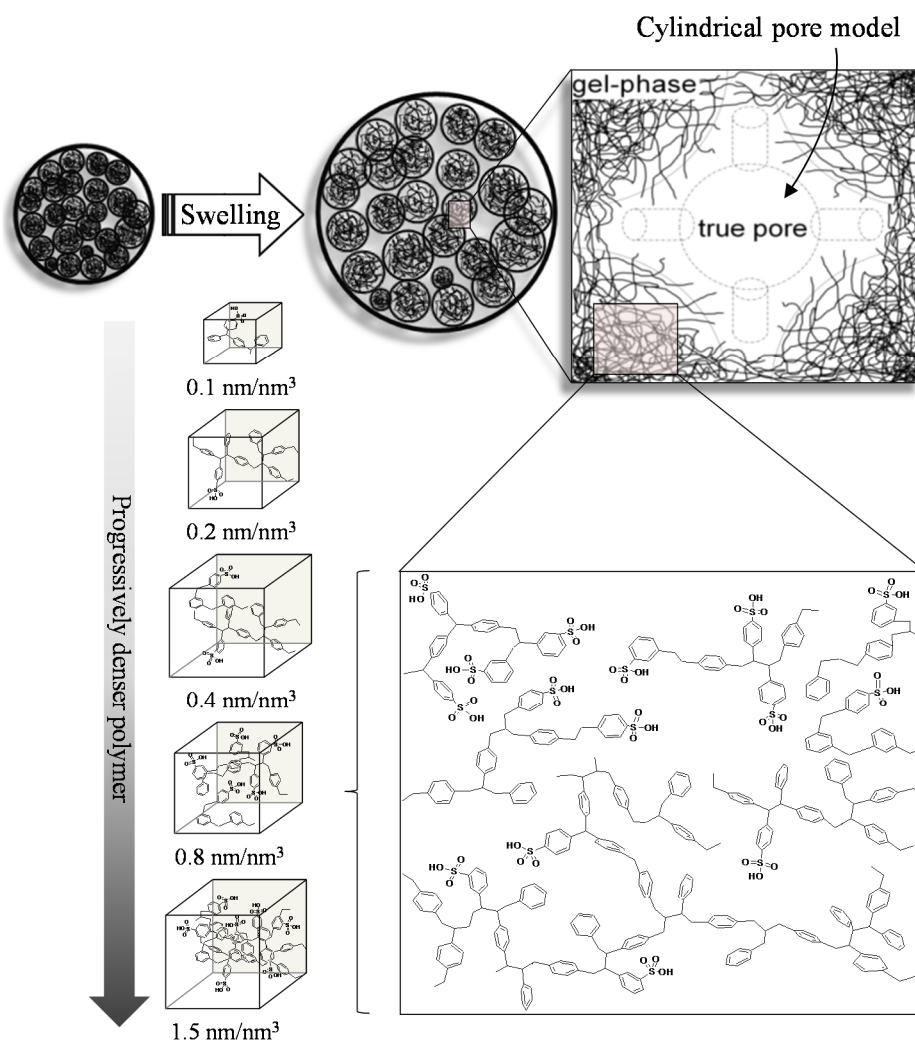


Figure 1.9 Schematic representation of the swollen-state morphology of macroreticular ion-exchange resins (Adapted from [45,71].)

1.7 Kinetics of fuel ethers syntheses over ion-exchange resins

Reaction kinetics in this field are described as a series of elementary steps undergone by reactants and products over the catalysts, namely [72] (Figure 1.10):

1. Diffusion of reactants from the fluid-phase, or bulk, to the surface of the catalyst particle through a boundary layer surrounding it.
2. Intraparticle diffusion of reactants into the catalyst pores from the external layer to the active sites of the catalyst.
3. Adsorption of reactants on the active sites.
4. Surface reaction of adsorbed reactants to produce adsorbed products. This step includes the formation of adsorbed intermediate species.
5. Desorption of reaction products from the active sites.
6. Intraparticle diffusion of products through the pores from the active sites to the external layer the catalyst.
7. Diffusion of products to the fluid-phase from the external surface of the catalyst particle across the boundary layer surrounding it.

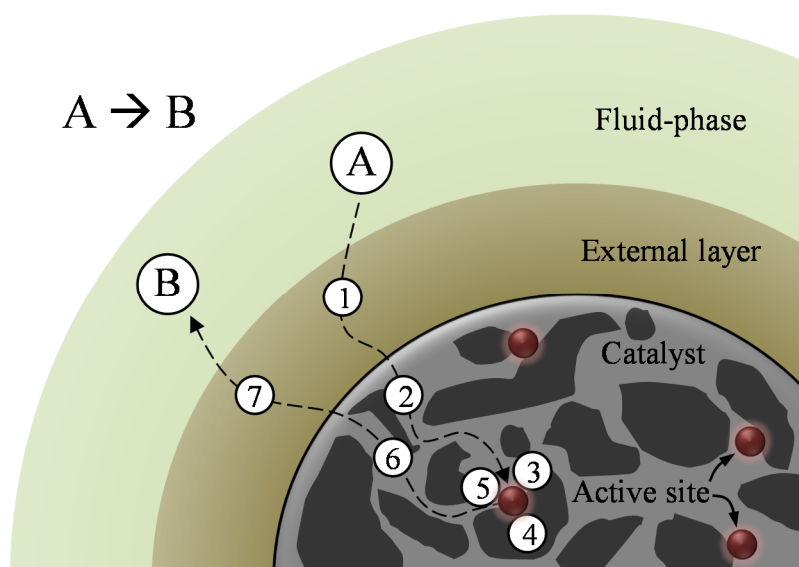


Figure 1.10 Schematic representation of the elementary steps occurring during a catalytic reaction

To obtain a kinetic model for a catalytic reaction, it needs to be considered that steps 1, 3, 4, 5 and 7 take place in series and steps 2 and 6 take place in series-parallel. Steps 3, 4 and 5 are of chemical nature whereas steps 1, 2, 6 and 7 are physical steps of mass transfer. Accordingly, three different regimes of kinetic control can exist: external mass transport control (involving steps 1 and 7), internal mass transport control (steps 2 and 6) and intrinsic reaction kinetics control (steps 3, 4 and 5).

When one of the mentioned steps takes place in a significantly lower rate than the rest, that step is considered to determine the overall rate of the reaction. The physical control regimes can be by-passed by selecting appropriate flow conditions in the reactor (external mass transport) or conveniently small catalyst particles (internal mass

transport). Experimental data must be gathered to determine the conditions at which such phenomena take place at sufficiently fast rates so that the resistance they represent can be regarded as non-significant for each studied reaction. If physical resistances can be neglected, the reactants concentration profile from the bulk solution to the active sites is considered to be flat. Under these conditions, the chemical steps are the rate-determining ones and intrinsic reaction rate kinetic expressions can be computed.

Kinetic expressions are based on three hypotheses: (i) the solid surface contains a fixed number of active sites, (ii) all active sites are identical, and (iii) the active sites reactivity depends exclusively on temperature, not on the amount or nature of any other material that might be present on the solid surface during the reaction. As it might seem obvious from the previous section, assumptions (ii) and (iii) are inaccurate for ion-exchange resins. Still, kinetic expressions obtained under such considerations are successful in explaining the experimental variation of rates based on rational mechanisms through which catalytic reactions can be understood [73,74].

The general approach to obtain kinetic expressions for catalytic reactions is based on the Langmuir-Hinshelwood-Hougen-Watson (LHHW) or Eley-Rideal (ER) mechanisms. In the LHHW formalism, all reactants are considered to be adsorbed on, at least, one catalytic site. In the ER formalism, which is actually a special case of LHHW, not all reactants need to be adsorbed on the active sites and the reaction may proceed by reaction between one adsorbed molecule and a molecule from the fluid-phase [73,74].

In the following lines, a reaction of the type of the ones studied throughout this PhD thesis ($A + B \rightleftharpoons P$) is explained considering an LHHW mechanism.

In order for the reaction to begin, reactants, A and B, must be adsorbed on vacant catalytic sites, σ . Once reactants are adsorbed, the surface reaction between adjacent adsorbed molecules can proceed and a molecule of adsorbed product, P, is produced. Finally, desorption of the product takes place. Equilibrium and rates for each of these elementary steps can be expressed as follows (considering single-site adsorption):

$$\begin{aligned} \text{Adsorption of A:} \quad & A + \sigma \rightleftharpoons A\sigma \\ & K_A = \frac{k_{a,A}}{k_{d,A}} = \left[\frac{\hat{c}_A}{c_A \hat{c}_v} \right]_{Eq} \end{aligned} \quad (1.1)$$

$$r'_{a,A} = k_{a,A} c_A \hat{c}_v - k_{d,A} \hat{c}_A = k_{a,A} \left(c_A \hat{c}_v - \hat{c}_A / K_A \right) \quad (1.2)$$

$$\begin{aligned} \text{Adsorption of B:} \quad & B + \sigma \rightleftharpoons B\sigma \\ & K_B = \frac{k_{a,B}}{k_{d,B}} = \left[\frac{\hat{c}_B}{c_B \hat{c}_v} \right]_{Eq} \end{aligned} \quad (1.3)$$

$$r'_{a,B} = k_{a,B} c_B \hat{c}_v - k_{d,B} \hat{c}_B = k_{a,B} \left(c_B \hat{c}_v - \hat{c}_B / K_B \right) \quad (1.4)$$

Surface reaction: $A\sigma + B\sigma \rightleftharpoons P\sigma + \sigma$

$$\widehat{K} = \frac{\widehat{k}}{\widehat{k}'} = \left[\frac{\widehat{c}_P \widehat{c}_v}{\widehat{c}_A \widehat{c}_B} \right]_{Eq} \quad (1.5)$$

$$r'_s = \widehat{k} \widehat{c}_A \widehat{c}_B - \widehat{k}' \widehat{c}_P \widehat{c}_v = \widehat{k} \left(\widehat{c}_A \widehat{c}_B - \widehat{c}_P \widehat{c}_v / \widehat{K} \right) \quad (1.6)$$

Desorption of P: $P\sigma \rightleftharpoons P + \sigma$

$$K_P = \frac{k_{a,P}}{k_{d,P}} = \left[\frac{\widehat{c}_P}{c_P \widehat{c}_v} \right]_{Eq} \quad (1.7)$$

$$r'_{d,P} = k_{d,P} \widehat{c}_P - k_{a,P} c_P \widehat{c}_v = k_{d,P} \left(\widehat{c}_P / K_P - c_P \widehat{c}_v \right) \quad (1.8)$$

In Equations 1.1 to 1.8, K_j is the adsorption equilibrium constant of the compound j , \widehat{K} is the equilibrium constant of the surface reaction, $r'_{a,j}$ and $r'_{d,j}$ are rates of adsorption and desorption, respectively, r'_s is the surface reaction rate, $k_{a,j}$ and $k_{d,j}$ are rate constants of adsorption and desorption, \widehat{k} and \widehat{k}' are the direct and the indirect surface reaction rate constants, c_j and \widehat{c}_j are the concentrations of the different compounds either in the bulk solution or adsorbed in the catalytic site, and \widehat{c}_v is the concentration of vacant active sites.

Additionally, the thermodynamic equilibrium constant, K , of the overall reaction is:

$$K = \left[\frac{c_P}{c_A c_B} \right]_{Eq} = \frac{\widehat{c}_A}{c_A \widehat{c}_v} \frac{\widehat{c}_B}{c_B \widehat{c}_v} \frac{\widehat{c}_P \widehat{c}_v}{\widehat{c}_A \widehat{c}_B} \frac{c_P \widehat{c}_v}{\widehat{c}_P} = \frac{K_A K_B \widehat{K}}{K_P} \quad (1.9)$$

and the total active sites concentration, \widehat{c}_0 , is:

$$\widehat{c}_0 = \widehat{c}_A + \widehat{c}_B + \widehat{c}_P + \widehat{c}_v \quad (1.10)$$

Given that the steps of adsorption, surface reaction and desorption take place in series (steps 3, 4 and 5 in Figure 1.10), their corresponding rates are equal to each other and to the overall reaction rate, as follows:

$$r' = k_{a,A} \left(c_A \widehat{c}_v - \widehat{c}_A / K_A \right) = k_{a,B} \left(c_B \widehat{c}_v - \widehat{c}_B / K_B \right) = \widehat{k} \left(\widehat{c}_A \widehat{c}_B - \widehat{c}_P \widehat{c}_v / \widehat{K} \right) = k_{d,P} \left(\widehat{c}_P / K_P - c_P \widehat{c}_v \right) \quad (1.11)$$

Since concentrations \widehat{c}_A , \widehat{c}_B , \widehat{c}_P and \widehat{c}_v , are not easy to determine, the above equations need to be combined in order to express the overall reaction rate in terms of concentrations at the fluid-phase, namely c_A , c_B and c_P . The complexity of these expressions, even when considering first-order reactions, makes it advisable trying to simplify them by assuming that one of the involved steps is rate-determining.

If adsorption of reactant A is considered to control the rate of the overall process, reaction rate can be expressed as:

$$-r'_A = -r'_B = r_P = r'_{a,A} = k_{a,A} \left(c_A \widehat{c}_v - \widehat{c}_A / K_A \right) \quad (1.12)$$

In this situation, adsorption of B, desorption of P and surface reaction, can be considered to be in a pseudo-equilibrium situation, from which:

$$\left(c_B \hat{c}_v - \hat{c}_B / K_B\right) \rightarrow 0 \Rightarrow \hat{c}_B \approx K_B c_B \hat{c}_v \quad (1.13)$$

$$\left(\hat{c}_P / K_P - c_P \hat{c}_v\right) \rightarrow 0 \Rightarrow \hat{c}_P \approx K_P c_P \hat{c}_v \quad (1.14)$$

$$\left(\hat{c}_A \hat{c}_B - \hat{c}_P \hat{c}_v / \hat{K}\right) \rightarrow 0 \Rightarrow \hat{c}_A \approx \frac{\hat{c}_P \hat{c}_v}{\hat{K} \hat{c}_B} = \frac{K_A c_P \hat{c}_v}{K c_B} \quad (1.15)$$

Combining and rearranging Equations 1.10, 1.12-15, the resulting kinetic expression is:

$$r' = \frac{k_{a,A} \hat{c}_0 \left(c_A - c_P / K c_B\right)}{1 + \frac{K_I c_P}{K c_B} + K_B c_B + K_P c_P} \quad (1.16)$$

Similarly, if adsorption of B is rate-determining, the final kinetic expression is:

$$r' = \frac{k_{a,B} \hat{c}_0 \left(c_B - c_P / K c_A\right)}{1 + K_A c_A + \frac{K_B c_P}{K c_A} + K_P c_P} \quad (1.17)$$

When the surface reaction is the rate-determining step, adsorption and desorption can be considered to be in pseudo-equilibrium and they can be expressed as:

$$\left(c_A \hat{c}_v - \hat{c}_A / K_A\right) \rightarrow 0 \Rightarrow \hat{c}_A \approx K_A c_A \hat{c}_v \quad (1.18)$$

$$\left(c_B \hat{c}_v - \hat{c}_B / K_B\right) \rightarrow 0 \Rightarrow \hat{c}_B \approx K_B c_B \hat{c}_v \quad (1.19)$$

$$\left(\hat{c}_P / K_P - c_P \hat{c}_v\right) \rightarrow 0 \Rightarrow \hat{c}_P \approx K_P c_P \hat{c}_v \quad (1.20)$$

From Equations 1.10 and 1.18-19, the concentration of vacant active sites is:

$$\hat{c}_v = \frac{\hat{c}_0}{1 + K_A c_A + K_B c_B + K_P c_P} \quad (1.21)$$

And the resulting kinetic expression is:

$$r' = \frac{\hat{k} K_A K_B \hat{c}_0^2 \left(c_A c_B - c_P / K\right)}{\left(1 + K_A c_A + K_B c_B + K_P c_P\right)^2} \quad (1.22)$$

Finally, when desorption of the product is considered to be the rate-determining step, adsorption of reactants A and B are expressed as in Equation 1.18 and 1.19, respectively, and surface reaction should be expressed as:

$$(\hat{c}_A \hat{c}_B - \hat{c}_P \hat{c}_v / \hat{K}) \rightarrow 0 \Rightarrow \hat{c}_P \approx \hat{c}_A \hat{c}_B \hat{K} / \hat{c}_v = K_A K_B \hat{K} c_A c_B \hat{c}_v^2 / \hat{c}_v = K K_P c_A c_B \hat{c}_v \quad (1.23)$$

And the corresponding kinetic equation can be written as:

$$r' = \frac{k_{a,p} K \hat{c}_0 (c_A c_B - c_P / K)}{1 + K_A c_A + K_B c_B + K K_P c_P c_A c_B} \quad (1.24)$$

As it can be observed, Equations 1.16, 1.17, 1.22 and 1.24 present the same general structure, namely:

$$\text{reaction rate} = \frac{[\text{kinetic term}][\text{driving force}]}{[\text{adsorption term}]^n} \quad (1.25)$$

Naturally, expressions stemming from ER formalisms or in which adsorption of reactants could happen in more than one active site at the same time, would require the development of the corresponding equations through a similar approach. In kinetic modeling, it is usual to proceed by proposing several mechanisms and, then, fitting the resulting expressions to the experimental data. Finally, thermodynamically consistent expressions able to explain kinetic data free from mass transport limitations are selected as the most appropriate ones to provide information on the reaction mechanism [74].

1.8 Scope of the thesis

For years, ion-exchange resins have been used as catalysts in major industrial processes, such as in the production of alkyl *tert*-butyl ethers. However, a complete understanding of crucial physicochemical aspects regarding the catalytic behavior of these materials has not yet been achieved. Thus, the main goal of this work is to study the performance of sulfonic, macroreticular ion-exchange resins through their catalytic activity in the synthesis reactions of methyl *tert*-butyl ether (MTBE), ethyl *tert*-butyl ether (ETBE), propyl *tert*-butyl ether (PTBE), and butyl *tert*-butyl ether (BTBE), which are excellent antiknocking additives for gasoline. To accomplish this, the following objectives have been raised:

1. To study the thermodynamic equilibrium of the mentioned syntheses
2. To analyze the products distribution for this type of syntheses and to determine the conditions of formation of byproducts over acidic macroreticular resins
3. To extend the understanding of ion-exchange resins catalytic behavior through relations between their properties and their catalytic activity
4. To study the viability of a proposed process by which ethers can be obtained simultaneously
5. To perform kinetic analyses of the proposed syntheses over promising catalysts

1.9 Organization of the thesis

In Chapter 2, a brief description of the chemicals, catalysts and experimental devices used through the present PhD thesis is provided. Specific descriptions regarding experimental setups and procedures are provided in each section.

Chapter 3 addresses an investigation on the chemical equilibrium of the liquid-phase syntheses of methyl *tert*-butyl ether (MTBE), ethyl *tert*-butyl ether (ETBE), propyl *tert*-butyl ether (PTBE), and butyl *tert*-butyl ether (BTBE) by reaction of isobutene with methanol, ethanol, 1-propanol, and 1-butanol, respectively, using various ion-exchange resins as catalysts in different devices. Thermodynamic properties for these reactions and involved species were estimated, namely molar standard enthalpy and entropy changes of reaction and molar enthalpy change of formation. Comparison of the estimated reaction thermodynamic values among this series of analogous reactions, and with results quoted in the literature, when available, was made.

The study of the products distribution and conditions that favor side reactions taking place along with etherification reactions was focused on the ETBE synthesis, as shown in Chapter 4. To carry out this study, a synthetic C₄ mixture, which emulates FCC C₄ cuts, was used as isobutene source. The presence of byproducts was studied in terms of production and selectivity. The effect of temperature and the influence of the initial ethanol to isobutene molar ratio were also analyzed.

The studies provided in Chapter 5 and Chapter 6 intend to further understand the catalytic behavior of macroreticular acidic ion-exchange resins by analyzing their catalytic activity in the liquid-phase syntheses of MTBE, ETBE, PTBE, and BTBE and to relate it with the resins most relevant properties. To do so, the first approach analysis was focused on assessing the effect of the reaction medium properties variation due to the alcohol size on the reaction rates. An attempt to distinguish which catalysts features have an actual relation with the resins catalytic performance was provided. As a second approach, the resins catalytic activity was correlated to their working-state features when swollen in polar reaction media, such as in etherification processes. In order to cover a wide range of resins properties, sixteen resins were used, which present a wide range of the properties of interest (i.e., acid capacity, sulfonation type, crosslinking degree, and swollen-phase volume fractions distribution).

The simultaneous syntheses of ETBE and BTBE over different acidic macroreticular ion-exchange resins are studied in Chapter 7. Comparison between individual and simultaneous processes was provided, along with a catalytic screening study that allows determining the most suitable catalyst for the simultaneous etherification process. The effect of temperature and of reactants composition on the ethers formation, in terms of conversion, selectivity and reaction rate, was also discussed.

Finally, in Chapter 8, a kinetic study of three reaction systems is provided. These are the individual syntheses of PTBE and BTBE and the simultaneous syntheses of ETBE and BTBE over AmberlystTM 35. Mechanistic kinetic models based on the Langmuir-

Hinshelwood-Hougen-Watson and the Eley-Rideal formalisms, in terms of components activities, was proposed for each studied reaction.

Chapter 9 summarizes the main conclusions reached in this thesis and proposes some future lines of research.

A list of the author's contributions to the scientific community is provided next.

Some additional information regarding experimental data for the previous chapters, as well as information regarding the methods needed to estimate some physical properties, can be found in the Appendix.

Lists of tables, figures and literature references appearing throughout this PhD thesis are provided after the Appendix.

Finally, a brief summary of this work in Catalan is included at the end of the thesis.

2. Experimental section

2.1 Chemicals

As reactants, methanol (max. water content 0.005%wt.), ethanol (max. water content 0.02%wt.), 1-propanol (max. water content 0.005%wt.), 1-butanol (max. water content 0.005%wt.), and either pure 2-methylpropene (isobutene) or a synthetic C₄ mixture as the isobutene source were used. The C₄ mixture composition emulates C₄ fractions from FCC units: 25%wt. of isobutene, 40%wt. of isobutane, and 35% *trans*-2-butene.

As reaction products or byproducts, some chemical standards were used for analytical procedures: 2-methyl-2-propanol (TBA), diethyl ether (DEE), 2-methoxy-2-methylpropane (MTBE), 2-ethoxy-2-methylpropane (ETBE), 2-ethoxybutane (ESBE), 2,4,4-trimethyl-1-pentene (TMP-1) and 2,4,4-trimethyl-2-pentene (TMP-2). 2-methyl-2-propoxypropane (PTBE) and 1-*tert*-butoxybutane (BTBE) were synthesized and purified in our laboratory through liquid-liquid extraction followed by rectification using a Vigreux column.

As auxiliary gases, nitrogen, helium, synthetic air, and hydrogen were also used. Nitrogen was used to pressurize all components of the reaction medium and to impel the liquid mixture through the experimental setups, by difference of pressures. Helium, synthetic air and hydrogen were used for chromatographic analyses.

The source and purity of all used compounds is listed in Table 2.1.

Table 2.1 Source, purity, and analysis of used materials

Compound	Source	Mass fraction purity [%]	Analysis method
methanol	Panreac	≥ 99.8	gas chromatography
ethanol	Panreac	≥ 99.8	gas chromatography
1-propanol	Sigma-Aldrich	≥ 99.7	gas chromatography
1-butanol	Sigma-Aldrich	≥ 99.8	gas chromatography
2-methylpropene	Air Liquide	≥ 99.9	gas chromatography
C ₄ mixture	Abelló-Linde	≥ 99.9	gas chromatography
2-methyl-2-propanol	Panreac	≥ 99.7	gas chromatography
diethyl ether	Panreac	≥ 99.5	gas chromatography
2,4,4-trimethyl-1-pentene	Sigma-Aldrich	≥ 98.0	gas chromatography
2,4,4-trimethyl-2-pentene	Sigma-Aldrich	≥ 98.0	gas chromatography
2-ethoxybutane	TCI Europe	≥ 99.7	gas chromatography
2-methoxy-2-methylpropane	Panreac	≥ 99.9	gas chromatography
2-ethoxy-2-methylpropane	TCI Europe	≥ 95.0	gas chromatography
2-methyl-2-propoxypropane	synthesis ^a	≥ 99.0	gas chromatography
1- <i>tert</i> -butoxybutane	synthesis ^a	≥ 98.0	gas chromatography
nitrogen	Air Liquide	≥ 99.9995	–
helium	Abelló-Linde	≥ 99.998	–
hydrogen	Air Liquide	>99.99	–
synthetic air	Air Liquide	>99.999	–

^a Synthesized and purified in our lab.

2.2 Catalysts

All catalysts used in this PhD thesis were macroreticular, acidic, sulfonated ion-exchange resins of styrene-divinylbenzene (PS-DVB). Most of them were commercial catalysts, namely: Amberlyst™ 15 (A-15, Rohm & Haas SAS, Chauny, France), A-16, A-35, A-36, A-39, A-40, A-46, A-48, A-70, Purolite® CT175 (CT-175, Purolite Ltd., Pontyclun, UK), CT-252, CT-275, and Lewatit® K 2620 (K2620, LANXESS AG, Cologne, Germany). Lab-made partially-sulfonated resins from a previous study [53] were also used, namely: 306, 406, 606 and 806. Main catalysts properties are listed in Table 2.2.

Table 2.2 Physical and chemical properties of catalysts

Catalyst	%DVB ^a	Acid Capacity ^b [meqH ⁺ g _{cat} ⁻¹]	Sulfonation type ^c	$-\Delta H_a^{NH_3}$ ^d [kJ mol ⁻¹]	$d_{p,m}$ ^f [μm]	T_{max} ^h [K]
A-15	High	4.81	C	110 ± 3 ^e	740	393
A-16	Medium	4.80	C	108 ± 3 ^e	600-800 ^g	403
A-35	High	5.32	O	113 ± 3	623	423
A-36	Medium	5.40	O	117 ± 2 ^e	630	423
A-39	Low	4.81	C	111 ± 3 ^e	–	403
A-40	High	5.01	O	111 ± 3 ^e	580-800 ^g	413
A-46	High	0.87	P	108 ± 3 ^e	–	393
A-48	High	5.62	O	113 ± 3 ^e	–	413
A-70	Low	2.65	C	117 ± 2 ^e	570	463
CT-175	High	4.98	C	114 ± 1 ^e	940	403
CT-252	Medium	5.40	O	115 ± 3 ^e	780	403
CT-275	High	5.20	O	113 ± 3	746	403
K2620	High	5.07	O	109 ± 3	620	413
306	High	0.81	P	–	–	–
406	High	0.99	P	–	–	–
606	High	1.89	P	–	–	–
806	High	3.10	P	–	–	–

^a Crosslinking degree considered classification: Low (<9%); Medium (9-14%); High (>14%).

^b Titration against standard base. ^c Conventionally sulfonated (C), oversulfonated (O), and partially sulfonated (P). ^d Ammonia adsorption enthalpy by microcalorimetry. ^e [75]. ^f Mean particle diameter from laser diffraction in air. ^g Mean particle diameter from manufacturer data. ^h Maximum operation temperature as recommended by the manufacturer.

The selected ion-exchange resins include polymers of low (A-39 and A-70), medium (A-16, A-36 and CT-252) and high crosslinking degree (A-15, A-35, A-40, A-46, A-48, CT-175, CT-275, K2620, 306, 406, 606 and 806). As for the sulfonation type, resins include conventionally sulfonated resins, with one sulfonic group per styrene ring, (A-15, A-16, A-39 and CT-175) oversulfonated resins, with more than one sulfonic group per styrene ring (A-35, A-36, A-40, A-48, CT-252, CT-275 and K2620), and partially-sulfonated resins, with less than one sulfonic group per styrene ring (A-46, 306, 406, 606 and 806). Among partially sulfonated resins, local differences in sulfur concentration within the beads have been reported in resins A-46, 306, and 406 [53], and therefore they are considered to be sulfonated mainly on the surface of their microspheres. In the case of A-70, in its manufacture some hydrogen atoms of the polymer chain are substituted by

chlorine atoms to increase the thermal stability of the resin, which improve the resin thermal stability and acid strength, leading to non-significant desulfonation by thermal stress of this resin compared to other PS-DVB resins [76].

Morphological characteristics of the selected resins both in dry and in water-swollen state are shown in Table 2.3.

Table 2.3 Morphological properties of resins both in dry and in water-swollen state

Catalyst	ρ^a [g cm ⁻³]	Dry state: adsorption-desorption of N ₂ at 77 K ^b				Swollen in water: ISEC method			
		S_{BET}^c [m ² g ⁻¹]	S_g [m ² g ⁻¹]	V_g^d [cm ³ g ⁻¹]	$d_{\text{m,pore}}^e$ [nm]	Macro-mesopores			Gel phase
						S_{area} [m ² g ⁻¹]	V_{pore}^e [cm ³ g ⁻¹]	d_{pore}^e [nm]	V_{sp} [cm ³ g ⁻¹]
A-15	1.416	42.0	41.3	0.328	31.8	192	0.616	12.8	0.765
A-16	1.401	1.69	1.75	0.013	29.7	46.2	0.188	16.3	1.129
A-35	1.542	29.0	35.6	0.210	23.7	199	0.720	14.5	0.613
A-36	1.567	21.0	21.2	0.143	27.0	68.0	0.259	15.2	1.025
A-39	1.417	0.09	0.065	0.0003	17.6	56.1	0.155	11.1	1.624
A-40	1.431	0.22	0.32	0.0006	7.5	11.0	0.125	45.5	0.442
A-46	1.137	57.4	54.8	0.263	19.2	186	0.470	10.1	0.523
A-48	1.538	33.8	32.1	0.249	31.0	186	0.568	12.2	0.620
A-70	1.514	0.018 ^f				66.1	0.220	13.3	1.257
CT-175	1.498	28.0	26.6	0.30	45.1	90.7	0.615	27.1	0.908
CT-252	1.493	22.4	19.9	0.221	44.4	132	0.491	14.9	0.981
CT-275	1.506	20.3	30.2	0.377	50.1	209	0.772	14.7	0.806
K2620	1.428	28.7	30.6	0.188	27.3	163.8	0.498	12.2	0.942
306	1.112	38.1	40.6	0.267	26.4	156	0.408	10.5	1.247
406	1.129	35.8	39.6	0.272	27.5	136	0.643	18.9	0.934
606	1.177	30.4	33.5	0.233	27.8	122	0.652	21.3	0.951
806	1.263	26.5	29.0	0.198	28.0	62.2	0.455	29.3	1.250

^a Skeletal density. Measured by Helium displacement (Accupic 1330). ^b Samples dried at vacuum (0.001 MPa, 383 K). ^c BET method (Brunauer-Emmett-Teller). ^d Volume of N₂ adsorbed at relative pressure (P/P₀) = 0.99. ^e $d_{\text{m,pore}} = 4V_g/S_g$ or $d_{\text{pore}} = 4V_{\text{pore}}/S_{\text{area}}$, respectively. ^f Without pretreatment (rinsing) with solvents.

ISEC water-swollen morphology of gel-type phase is shown in Figure 2.1, in which the expanded polymer volume of domains with different characteristic chain density is depicted.

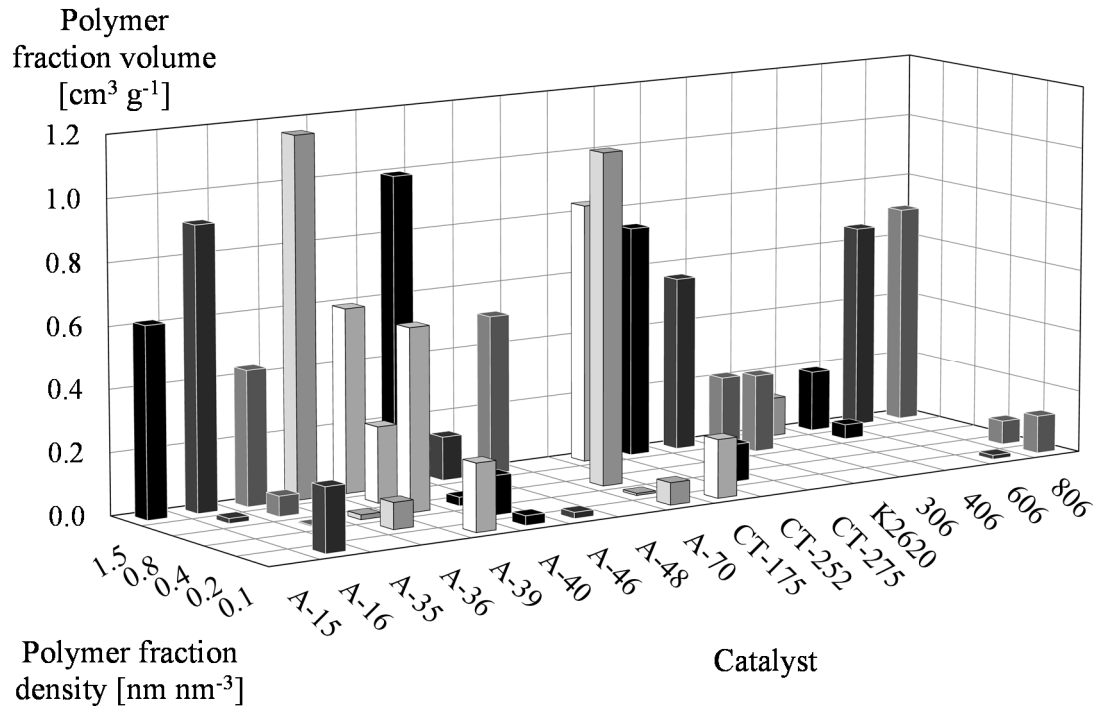


Figure 2.1 ISEC morphological pattern of the gel-type phase

2.3 Apparatus and analysis

Experiments were carried out in two separate devices: a fixed bed reactor system and a batch reactor system. A general description of these experimental setups is provided next.

2.3.1 Fixed bed reactor system

The fixed bed reactor setup (Figure 2.2) consisted in a fixed bed tubular microreactor (length: 150 mm, i.d.: 7 mm) submerged in a thermostatic bath to maintain the reactor at the desired temperature, controlled within ± 0.01 K with a dimethylpolysiloxane thermostatic oil (Therm 180, LAUDA DR. R. WOBSE & CO. KG, Lauda-Königshofen, Germany).

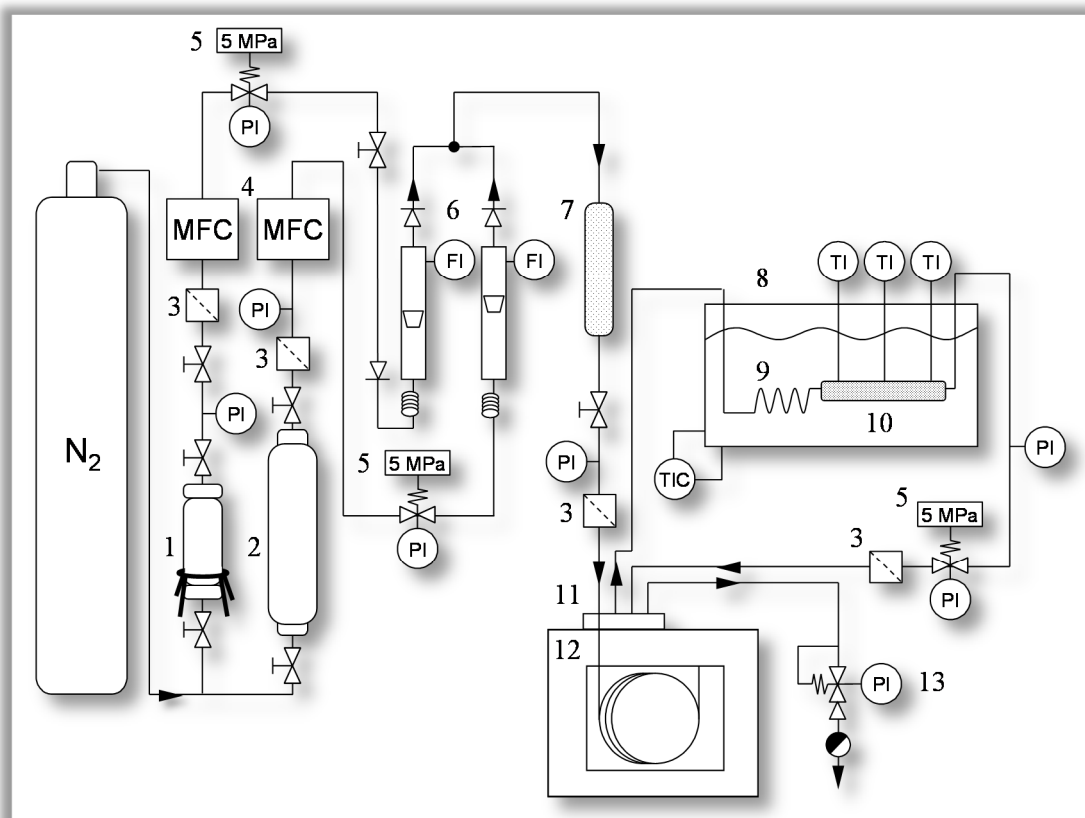


Figure 2.2 Schematic diagram of the fixed bed reactor setup: 1. olefinic cylinder, 2. alcohol reservoir, 3. filter 2 μ m, 4. mass flow controller, 5. safety valve, 6. one-way valve, 7. mixer, 8. thermostatic bath, 9. heating coil, 10. reactor, 11. sampling valves, 12. gas chromatograph, 13. back-pressure regulator

This setup was operated either in differential or in integral regime. In the present reaction systems, differential regime, in which reaction rate can be considered as constant along the reactor, is generally achieved when conversion values do not exceed 10% [19]. Therefore, mass of catalyst in these experiments was chosen to obtain such isobutene maximum conversion values at the desired temperature. When operated under integral regime, no limitations regarding the mass of catalyst were followed, so conversion could reach higher values. Additionally, some integral regime experiments were carried out using up to three reactors build in series.

Samples were taken inline from the reactor inlet and outlet streams through two sampling valves that injected 0.2 μ L of pressurized liquid into an Agilent gas chromatograph 7890A with a flame ionization detector (GC-FID). The GC was equipped with a capillary column (HP-PONA 19091S-001, J&W Scientific, Santa Clara, US; 100% dimethylpolysiloxane, 50 m \times 0.20 mm \times 0.50 μ m). Hydrogen and synthetic air were used for the FID detector. Helium was used as carrier gas. GC oven temperature and carrier gas flow were set to identify and quantify all reactants and products or byproducts, when formed, depending on each considered reaction.

2.3.2 Batch reactor system

The batch reactor setup (Figure 2.3) consisted of a 200 cm³ stainless-steel jacketed batch reactor equipped with a six-blade magnetic stirrer (Autoclave Engineers, Pennsylvania, US). The reactor temperature was controlled within ± 0.1 K by a 1,2-propanediol-water thermostatic mixture.

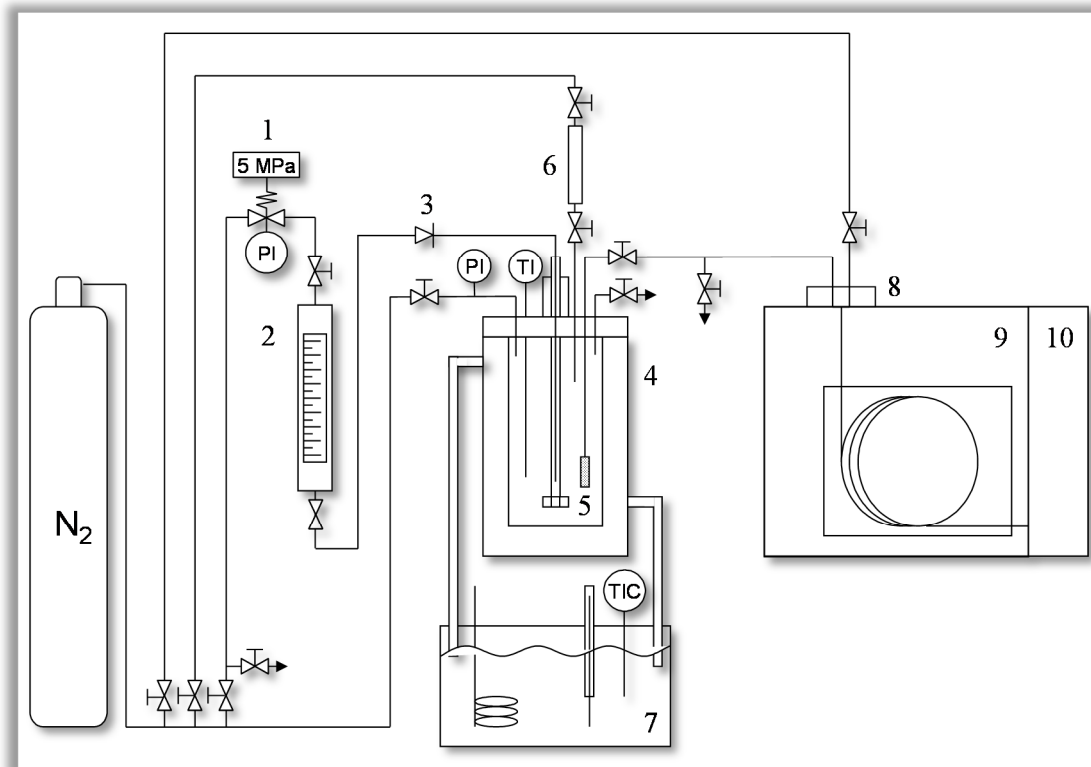


Figure 2.3 Schematic diagram of the batch reactor setup: 1. safety valve, 2. pressure burette, 3. one-way valve, 4. reactor, 5. filter 2 μ m, 6. catalyst injector, 7. thermostatic bath, 8. sampling valve, 9. gas chromatograph, 10. mass selective detector.

A sampling valve (Valco A2CI4WE.2, VICI AG International, Schenkon, Switzerland) is connected to the reactor vessel that can inject 0.2 μ L of pressurized liquid into an Agilent gas chromatograph 6890 attached to a mass selective detector HP5973N (GC-MS). The GC is equipped with a capillary column (HP-PONA 19091S-001, J&W Scientific, Santa Clara, US; 100% dimethylpolysiloxane, 50 m \times 0.20 mm \times 0.50 μ m). The electron source of the mass detector is set to 503 K and the quadrupole is set to 423 K. Helium is used as carrier gas. GC oven temperature and carrier gas flow are set to identify and quantify all reactants and products or byproducts, when formed, depending on each considered reaction.

2.4 Auxiliary devices

Particle size of resins was measured in air by means of a LS 13320 Laser Diffraction Particle Size Analyzer using previously dried catalyst samples at 383 K under vacuum.

Catalyst BET surface area (S_{BET}), pore volume (V_{pore}) and pore diameter (d_{pore}) in dry state were obtained by Nitrogen adsorption-desorption at 77 K (Accusorb ASAP 2020, Micrometrics). Krypton was used for surface areas $< 1 \text{ m}^2\text{g}^{-1}$. S_{BET} was obtained by BET method. V_{pore} was obtained by the volume of gas adsorbed at relative pressure $(P/P_0) = 0.99$. The catalyst samples were previously dried at 383 K under vacuum overnight.

Measurements of both particles size and catalysts porosity were carried out by the Scientific and Technological Centers (CCiT) of the University of Barcelona.

A Karl-Fischer volumetric titrator (Orion AF8), by Thermo Electron Corporation, was used to determine the water content in either solid catalyst or liquid mixture samples.

Prüfsieb test-sieving by Fritsch GmbH (DIN 4188, metal wire) were used to obtain separate fractions of catalyst particles in terms of their sizes. Width apertures ranged from 0.08 to 1.25 mm.

An atmospheric oven and a vacuum oven, both by Memmert, were used for the catalyst samples drying protocol.

Different precision balances were used, namely a HR-120 ($\pm 0.0001 \text{ g}$) by A&D Weighing, a SBA 41 ($\pm 0.001 \text{ g}$) by Scaltec Instruments GmbH, a SI-4002 ($\pm 0.01 \text{ g}$) by Denver Instruments, and a SSH 94 ($\pm 0.5 \text{ g}$) by Scaltec Instruments GmbH.

A Vigreux distillation column (length: 0.4 m) was used to purify propyl *tert*-butyl ether and butyl *tert*-butyl ether.

3. Equilibrium of the liquid-phase etherification of isobutene with C₁ to C₄ linear primary alcohols

THE PRESENT CHAPTER IS AN ADAPTED VERSION OF THE WORK

J.H. Badia, C. Fité, R. Bringué, E. Ramírez, F. Cunill. Thermodynamic analysis of the experimental equilibria for the liquid-phase etherification of isobutene with C₁ to C₄ linear primary alcohols. *Journal of Chemical & Engineering Data*, 61, 2016, 1054-1064.

3.1 Introduction

Experimental studies on thermodynamic properties concerning promising processes are mandatory to determine their viability. In this sense, all major industrially-operated production processes have to be preceded by thorough studies on their equilibrium conditions. Recent examples of this fact, from several disciplines, would be the synthesis of graphene [77,78], pharmaceutical drugs design [79,80] or novel biofuels production [81–83].

Regarding biofuels, new legislation in European countries is pushing ahead with next generation fuels to reinforce the struggle started by the EU with directives 2009/28/EC and 2009/30/EC, which promote the usage of renewable sources and establish fuel reformulation main guidelines. Among fuel additives that help reaching the required standards, oxygenate ethers arise as a feasible alternative. Oxygenate additives like methyl *tert*-butyl ether and ethyl *tert*-butyl ether, obtained by isobutene etherification with methanol and ethanol, respectively, have been already studied since they have been produced worldwide for decades. However, the production of heavier ethers from alkene etherification with larger primary alcohols, such as 1-propanol or 1-butanol, has been scarcely studied.

Prior to scale-up studies on the feasibility of industrializing these processes, thermodynamic properties analyses based on experimental data must be carried out. Actually, thermodynamic information of reacting systems where alkenes and several linear alcohols are involved is scarce. The present chapter, based on a sound experimental work, contributes to fill part of this lack of information.

3.2 Experimental

3.2.1 Chemicals and catalysts

Reactants were methanol, ethanol, 1-propanol, 1-butanol, and either pure 2-methylpropene (isobutene) or the synthetic C₄ mixture as the isobutene source. As main reaction products, 2-methoxy-2-methylpropane (MTBE), 2-ethoxy-2-methylpropane (ETBE), 2-methyl-2-propoxypropane (PTBE), and 1-*tert*-butoxybutane (BTBE), were obtained. As byproducts, 2-methyl-2-propanol (TBA), diethyl ether (DEE), 2,4,4-trimethyl-1-pentene (TMP-1), 2,4,4-trimethyl-2-pentene (TMP-2), and 2-ethoxybutane (ESBE), were detected.

Amberlyst™ 35 (A-35) was used as catalyst in the majority of the experimental work. Other similar ion-exchange resins were tested for comparative purposes: Amberlyst™ 15 (A-15), Purolite® CT275 (CT-275) and Lewatit® K 2620 (K2620).

3.2.2 Apparatus and procedure

Experiments were carried out at constant temperature in the range 313-383 K and 1.5-2.0 MPa to keep all components in the liquid phase. Two different reactors were used to carry out the experiments. The first experimental setup consisted of a series of catalytic fixed bed tubular microreactors (length: 150 mm, i.d.: 7 mm). The second setup consisted of a 200 cm³ stainless-steel jacketed batch reactor. Initial (batch reactor) or fed (tubular reactor) alcohol/isobutene molar ratio ($R_{A/O}^{\circ}$) ranged from 0.6 to 2.4.

As catalysts were supplied in wet state, they were pretreated to reduce their water content. Catalysts were firstly dried at room temperature for 48 h to remove most of the free water from the resin beads and, afterwards, located in an atmospheric oven at 383 K. Catalysts used in the fixed bed reactor system were then kept in the oven for at least 14 h until the experiment was carried out. Catalysts used in the batch reactor system were kept in the atmospheric oven for 2.5 h and, afterwards, placed in a vacuum oven, at 373 K and 0.001 MPa, for 12 h. Final water content in the resin beads after vacuum-drying was 3-5%wt. (analyzed by Karl-Fischer titration in our laboratory).

The number of reactor units build in series and the feed flow-rate in the fixed bed reactor system were chosen for each experiment to achieve a desired liquid hourly space velocity (LHSV) in the range 1.8-20 h⁻¹. Firstly, a weighed amount of oven-dried catalyst was introduced into the designated number of reactors, which were afterwards submerged in a thermostatic bath. Then, only the alcohol was fed to the reactors in order to preheat the catalytic bed and to reduce, as much as possible, the remaining water in the catalyst by alcohol percolation. By means of this procedure, the water content in the resin beads can be reduced to less than 1%wt., when an alcohol volume of more than 10 times the catalytic bed volume is passed through the bed [84]. Afterwards, while the alcohol flow was kept constant, the pressurized C₄ mixture was added to the feed for the reaction to proceed. Then, pressure was fixed at 1.5 MPa in order to ensure all reactants were in the liquid state. From that moment onward, the composition variation at the outlet stream was monitored by repeated chromatographic analyses. When no significant variation of composition was observed between consecutive analyses, the experiment was ended, since it was considered that the system had reached the steady-state.

Regarding the experiments carried out in the batch reactor system, procedure was as follows: the catalyst load, ranging 0.1-10%wt. of the reactant mixture, was introduced into a catalyst injector and pressurized to 2.0 MPa with nitrogen. The corresponding alcohol was introduced into the reactor vessel before the heating, and the stirring (500-750 rpm) were switched on. The isobutene, or the C₄ mixture, was first kept in a pressure burette, and then introduced into the reactor by difference of pressures. Once the reactive mixture reached the desired temperature, controlled within ± 0.1 K by a 1,2-propanediol-water thermostatic mixture, the catalyst was injected. This instant was considered as the starting point for the reaction. Experiments lasted 5-8 h, until the reaction medium composition showed no significant variation in time.

3.2.3 Analysis

In the fixed-bed reactor setup, samples were taken inline from the reactor inlet and outlet streams through two sampling valves that injected 0.2 μL of pressurized liquid into an Agilent gas chromatograph 7890A. In the batch reactor setup, samples were also taken inline from the reaction medium through a sampling valve that injected 0.2 μL of pressurized liquid into an Agilent gas chromatograph 6890 attached to a mass selective detector HP5973N used to identify and quantify the reaction system components. Both GC were equipped with a capillary column (100% dimethylpolysiloxane, 50 m × 0.20 mm × 0.50 μm). GC oven temperature ranged 308-343 K, carrier gas flow (Helium) varied from 0.6 to 1.5 mL/min and the analyses length was 20-45 min depending on the considered reaction.

3.2.4 Calculations

For a chemical reaction at a given time, mass-action ratio, Γ_x , corresponds to the ratio of products molar fractions to reactants molar fractions, each raised to the power of the stoichiometric coefficient, ν . In non-ideal systems, activity coefficients have to be taken into account, as follows:

$$\Gamma_a = \prod_{j=1}^S a_j^{\nu_j} = \prod_{j=1}^S \gamma_j^{\nu_j} \cdot \prod_{j=1}^S x_j^{\nu_j} = \Gamma_\gamma \cdot \Gamma_x \quad (3.1)$$

where S are the species involved in the considered reaction, and Γ_a and Γ_γ are the mass-action ratios expressed in terms of activities, a , and activity coefficients, γ , respectively. In the present systems, activity coefficients were estimated by means of the modified UNIFAC-Dortmund method [85].

In a batch stirred tank reactor, chemical equilibrium is reached when the reaction medium composition becomes constant with time. In a fixed-bed reactor, the outlet stream is considered to be at chemical equilibrium if its composition at the steady state does not change at decreasing flow rate with the same inlet composition and reaction temperature. When the reaction mixture is at chemical equilibrium, mass-action ratio equals to the equilibrium constant, namely $K_x = \Gamma_x$, $K_\gamma = \Gamma_\gamma$, and $K = \Gamma_a$, the latest being the thermodynamic equilibrium constant.

3.3 Results and discussion

3.3.1 Reaction system

The study was focused on the series of analogous syntheses of alkyl *tert*-butyl ether from isobutene and C₁ to C₄ linear primary alcohols. In each part of the experimental work, methanol (MeOH), ethanol (EtOH), 1-propanol (1-PrOH) or 1-butanol (1-BuOH) were used to obtain, respectively, methyl *tert*-butyl ether (MTBE), ethyl *tert*-butyl ether (ETBE), propyl *tert*-butyl ether (PTBE) or butyl *tert*-butyl ether (BTBE) (reactions R1, R2, R3, and R4, respectively, in Figure 3.1).

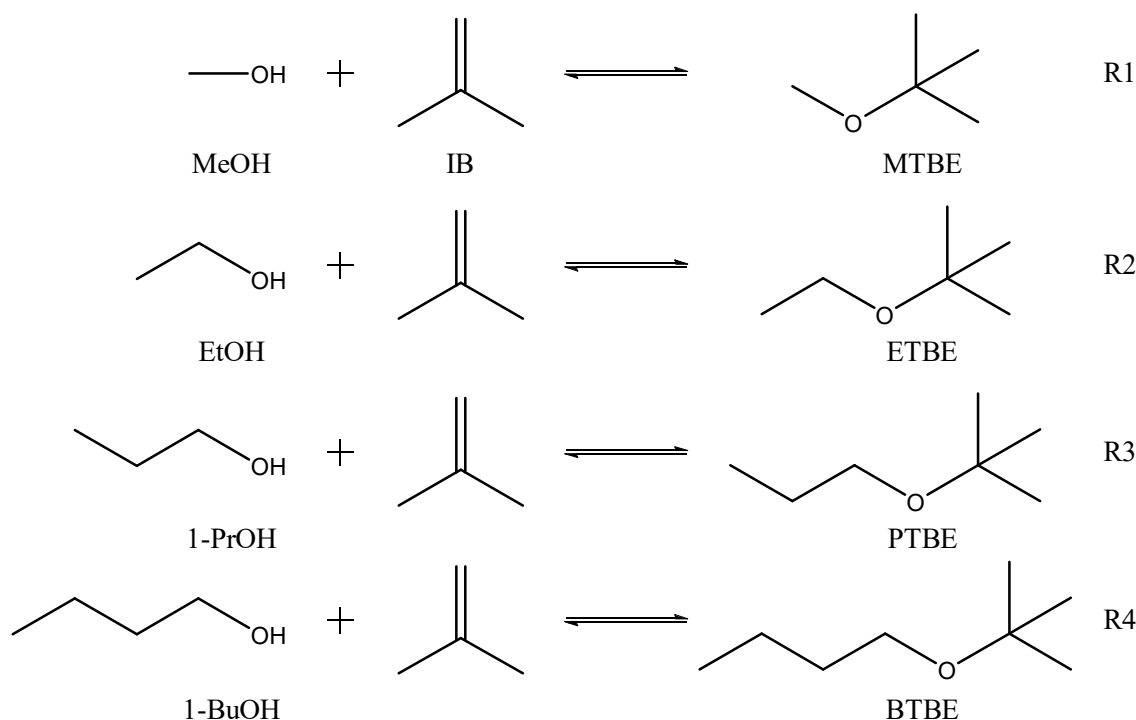


Figure 3.1 Main reactions involved

Possible side-reactions comprise dimerization of isobutene to give TMP-1 and TMP-2, isobutene hydration to give TBA, alcohol dehydration to give water and the corresponding symmetric ether and, as 2-butene is present in the synthetic C₄ mixture, the etherification reaction of 2-butene with alcohol to give the corresponding alkyl *sec*-butyl ether [86,87] (see Chapter 4). Byproducts formation ranged 0-5.5%wt. in the fixed-bed reactor experiments, and 0-15.7%wt. in the batch reactor experiments. When formed, these byproducts were quantified and, therefore, included in the calculations. Given the extension of some side-reactions in the batch experiments and their irreversible nature, e.g., isobutene dimerization, in some runs a pseudo equilibrium situation was reached rather than a true thermodynamic equilibrium situation. The activities relations corresponding to each equilibrium reaction obtained in such experiments were assumed to be equivalent to the equilibrium constant when they were constant in time, within the experimental error.

Regarding the thermodynamic properties, enthalpy, $\Delta_r H^\circ$, entropy, $\Delta_r S^\circ$, and standard free energy, $\Delta_r G^\circ$, changes of each reaction at the temperature T, can be estimated from formation properties of involved compounds by means of the following expressions:

$$\Delta_r H^\circ(T) = \sum_{j=1}^S \nu_j \Delta_f H_j^\circ \quad (3.2)$$

$$\Delta_r S^\circ(T) = \sum_{j=1}^S \nu_j S_j^\circ \quad (3.3)$$

$$\Delta_r G^\circ(T) = \Delta_r H^\circ - T \Delta_r S^\circ \quad (3.4)$$

Among thermochemical data concerning these reaction systems it has been observed: (i) a significant discrepancy in published values for some compounds, or (ii) inexistence of data in the available databases, e.g., BTBE. Therefore, literature values were compared to select the most reliable sources. For non-available values, two different group-contribution methods (Joback method [88] and Modified Benson method [89–91]) were used to obtain estimated values. The modified Benson method estimates were found to present lower discrepancies with available published data and, consequently, these estimates were used for the missing values rather than those obtained by the Joback method. When available, published experimental values were preferred instead of estimates. Used values are listed in Table 3.1.

Table 3.1 Thermochemical data of involved chemical species (standard state, liquid at 1 atm and 298.15 K)

Compound	$\Delta_r H^\circ$ ^a [kJ mol ⁻¹]	S° ^a [J (mol K) ⁻¹]
isobutene	-37.50	215.4 ^b
methanol	-239.2	126.8
ethanol	-277.6	160.7
1-propanol	-302.6	193.6
1-butanol	-327.3	225.8
MTBE	-313.6	265.3
ETBE	-349.9	297.9 ^c
PTBE	-372.2 ^b	333.5 ^b
BTBE	-403.3 ^c	362.7 ^d

^a Unless specified, values have been taken from *CRC Handbook of Chemistry and Physics* [92].

^b Linnekoski et al. [22]. ^c Sharonov et al. [93].

^d Estimated by Modified Benson Method [89–91].

Table 3.2 lists theoretically estimated values of $\Delta_r H^\circ$, $\Delta_r G^\circ$ and $\Delta_r S^\circ$ for each alkyl *tert*-butyl ether syntheses in the liquid phase at 298.15 K, calculated by means of Equations 3.2 to 3.4, and the corresponding thermodynamic equilibrium constants, K , at that temperature according to the following relation:

$$\ln K = \frac{-\Delta_r G^\circ}{RT} = \frac{-\Delta_r H^\circ}{RT} + \frac{\Delta_r S^\circ}{R} \quad (3.5)$$

Table 3.2 Theoretically determined standard enthalpy, free energy and entropy changes, as well as the corresponding thermodynamic equilibrium constants, of alkyl *tert*-butyl ether syntheses in the liquid phase at 298.15 K

Reaction	$-\Delta_r H^\circ$ [kJ mol ⁻¹]	$-\Delta_r G^\circ$ [kJ mol ⁻¹]	$-\Delta_r S^\circ$ [J (mol K) ⁻¹]	K
MTBE	-36.90	-14.0	-76.9	280
ETBE	-34.80	-11.5	-78.2	103
PTBE	-32.10	-9.6	-75.5	48
BTBE	-38.50	-15.1	-78.6	438

To check that the equilibrium constant, K , for each reaction was only a function of temperature, that is, to discard possible pressure effects, the Poynting correction factor, \mathcal{P} , was calculated by means of the following expression [88]:

$$\mathcal{P} = \exp\left(\frac{P-1}{RT} \sum_{j=1}^S v_j V_j\right) \quad (3.6)$$

where V_j is the molar volume of the compound j and P is the pressure expressed in atm. Since values of \mathcal{P} were close to unity for the whole experimental conditions range, the assumption of null pressure effect on equilibrium constants has been accepted.

3.3.2 Experimental results

Thermodynamic equilibrium data have been experimentally obtained for the presented series of analogous reactions. The comparison between experimental equilibrium constants, available literature values, and theoretical constants from formation data is provided in this section for each synthesis.

3.3.2.1 MTBE synthesis

Thermodynamic properties of the MTBE synthesis (reaction R1 in Figure 3.1) have been widely studied throughout the years [23,94–99]. Thus, only few experimental runs were carried out, mainly to compare results to those quoted in literature and to validate the procedure through which equilibrium data were obtained. MTBE experimental data was obtained in the fixed bed reactor system. Experimental conditions regarding these runs are provided in Appendix I (Table A1).

Values of the mass-action ratio of chemical compounds activities, Γ_a , were calculated from the fixed-bed reactor outlet stream composition at steady state operating at two temperatures, using different catalysts, and at LHSV values in the range of 2 to 20 h⁻¹. Results depicted in Figure 3.2 show that, irrespectively of the used catalyst, at LHSV of about 2 h⁻¹ the calculated Γ_a values can be considered equal to the thermodynamic equilibrium constant values, K_{MTBE} , quoted in literature [23,94–99], within the margin of experimental error, for both temperatures. For higher LHSV, Γ_a decreases at increasing LHSV, and reactor outlet stream would not be at equilibrium. In particular, under the same LHSV and temperature conditions, the calculated value of Γ_a is larger when the used catalyst has a higher acid capacity, as a result of its higher catalytic activity.

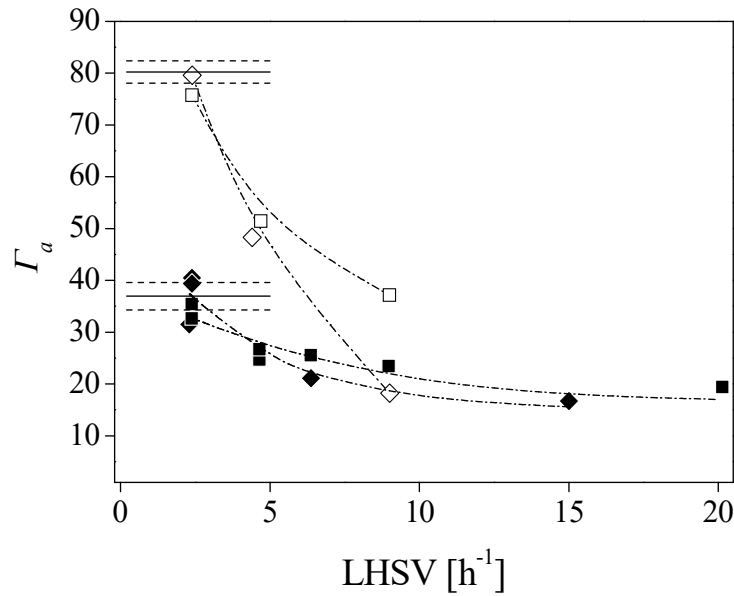


Figure 3.2 Experimental mass-action ratio, Γ_a , variation with LHSV for the MTBE experiments. Mean literature values [23,94–99] of the MTBE thermodynamic equilibrium constant, K_{MTBE} , at each temperature are represented with solid lines, and their respective standard uncertainty margin is represented with dashed lines. Open symbols (T = 323 K): A-15 (\diamond), A-35 (\square). Solid symbols (T = 343 K): A-15 (\blacklozenge), A-35 (\blacksquare)

Figure 3.3 provides a comparison between experimental K_{MTBE} at 323 and 343 K, those quoted in literature, and theoretically determined equilibrium constants at different temperatures. The agreement between results proves that the followed procedure to obtain equilibrium constants is reliable.

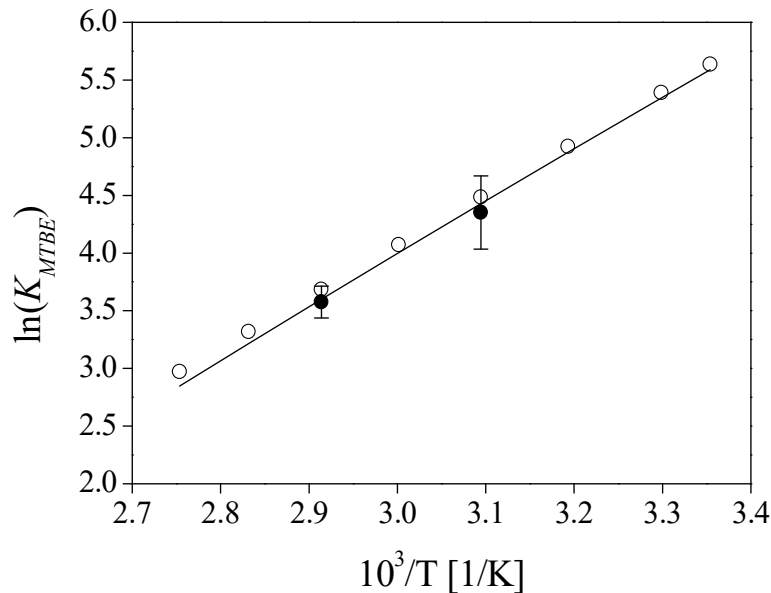


Figure 3.3 Comparison between values for MTBE equilibrium constant. Error bars correspond to uncertainty for 95% level of confidence. Present work (\bullet), theoretically determined values (\circ), and linear fit of literature values [23,94–99] (—)

3.3.2.2 ETBE synthesis

Even though thermodynamics of the ETBE synthesis (reaction R2 in Figure 3.1) have been also extensively dealt with in literature, for instance [100–105], the lack of agreement between sources has often led to a discrepancy between theoretically and experimentally obtained equilibrium constants [105]. In order to confirm the reliability of the experimental equilibrium obtained in this work, ETBE experiments were carried out in two different reactor systems, in a wider temperature range (313–383 K) and using different catalysts. Experimental conditions and results for each individual experiment are provided in Appendix I (Tables A2 and A3).

As example, results of some experimental runs in each setup are provided in Figure 3.4. Figure 3.4 (a), where a batch experiment performed at 323 K, $R_{A/O}^{\circ} = 0.64$, and 10%wt. of A-35 as catalyst load is shown, depicts the evolution in time of each compound molar fraction, x . Given that the catalyst load was high, isobutene and ethanol quickly reacted to give ETBE, which reached a molar fraction that hardly evolved in time, within the margin of experimental error. Concentration of C₄ compounds other than isobutene barely changed during the experiment, because isobutane is an inert compound under the reaction conditions, and 2-butene needs higher temperatures and ethanol initial concentrations to react in a significant extension. Regarding side-reactions, TMP-1 and TMP-2 were the more largely formed byproducts.

Figure 3.4 (b) shows the variation with LHSV of the reactor outlet stream composition, in terms of x_i , for fixed-bed experiments at 333 K, $R_{A/O}^{\circ} = 1.10$, and using A-35 as catalyst. As seen in the figure, no significant variations were detected for different LHSV, what means that ETBE kinetics was fast enough to reach chemical equilibrium at the reactor outlet in all the experimental conditions range.

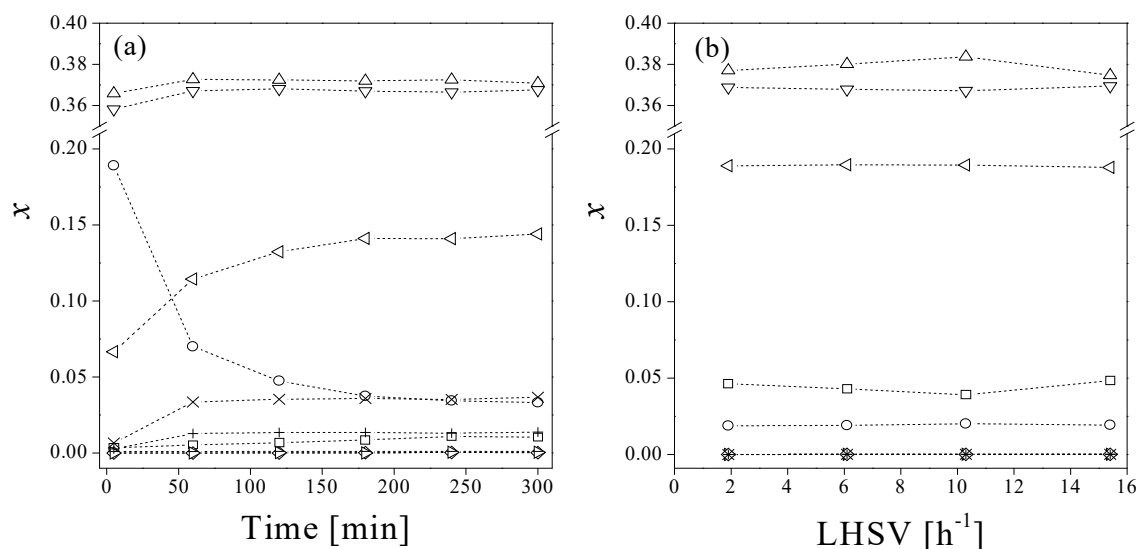


Figure 3.4 Molar fraction evolution in time for the ETBE synthesis in a batch experiment at $T = 323$ K, $R_{A/O}^{\circ} = 0.64$, stirring speed = 500 rpm, A-35, catalyst load = 10% wt. of the reactant mixture (a), and outlet stream steady-state molar fraction variation with LHSV for the ETBE synthesis in fixed-bed experiments at $T = 333$ K, $R_{A/O}^{\circ} = 1.10$, using A-35 as catalyst (b). IB (○), EtOH (□), isobutane (Δ), 2-butene (▽), ETBE (◁), ESBE (▷), DEE (◇), TBA (–), TMP-1 (×) and TMP-2 (+)

Regarding the equilibrium constant values for the ETBE synthesis, the comparison between experimental results, those quoted in the literature and theoretical estimated values is provided in Figure 4. As seen, experimental equilibrium constants, K_{ETBE} , are in a relatively good agreement with both literature and theoretical values. It is noticeable that linear fits applied to experimental results and to K_{ETBE} values derived from the expressions suggested by Jensen and Datta [102] almost coincide in slopes and only a slight discrepancy in intercepts is observed. This fact, adds reliability to the experimental results presented in the present work.

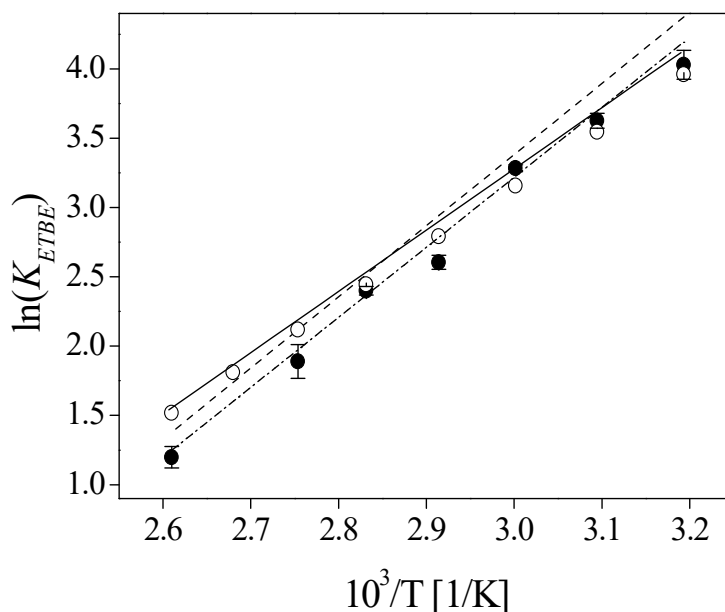


Figure 3.5 Comparison between values for ETBE equilibrium constants. Error bars correspond to uncertainty for 95% level of confidence. Present work (●), theoretically determined (○), linear fit of literature values [100–105] (—), linear fit applied to Jensen and Datta [102] expressions values (- - -), and linear fit applied to present work values (· - · - ·)

3.3.2.3 PTBE synthesis

Studies of thermodynamic properties on the PTBE synthesis (reaction R3 in Figure 3.1) are scarce in literature; only few works that studied this reaction were found [22,59,106,107]. Experiments have been carried out in the batch stirred tank reactor from different initial alcohol/isobutene molar ratio, $R_{A/O}^0$, and at different temperatures, using A-35 as the catalyst. Figure 3.6 shows the evolution in time of the PTBE molar fraction until chemical equilibrium was reached in the different experimental runs. Experimental conditions and results for each individual experiment are provided in Appendix I (Table A4).

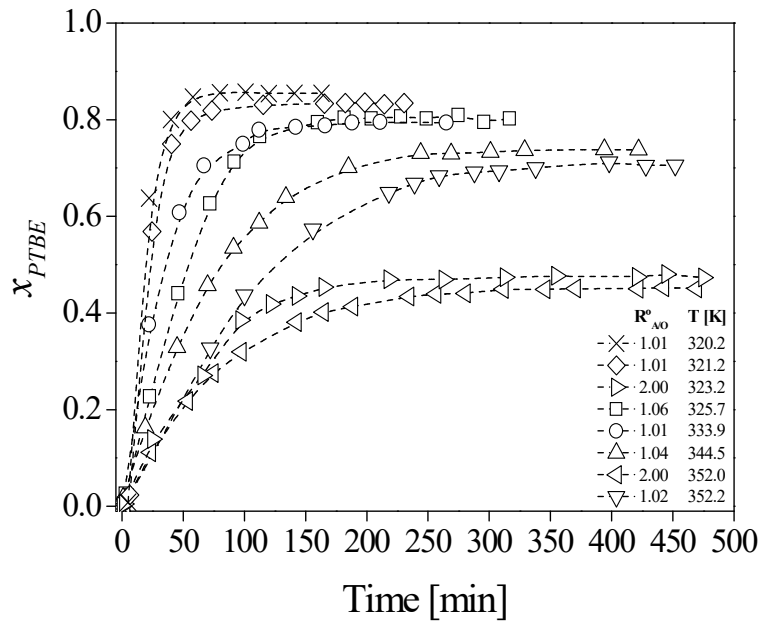


Figure 3.6 Evolution in time of PTBE molar fraction in batch experiments at different R^o_{AO} and temperatures. A-35, catalyst load = 0.1-11%wt., 750 rpm

Figure 3.7 provides a comparison between experimental, published [22], and theoretically estimated values of K_{PTBE} . Although some discrepancies are revealed in that figure, the slope of the linear fit of the theoretically determined equilibrium constants and that of the present work are almost coincident. Regarding values quoted in literature, the trend they describe differs from that described by both experimental K_{PTBE} of the present work and theoretical values.

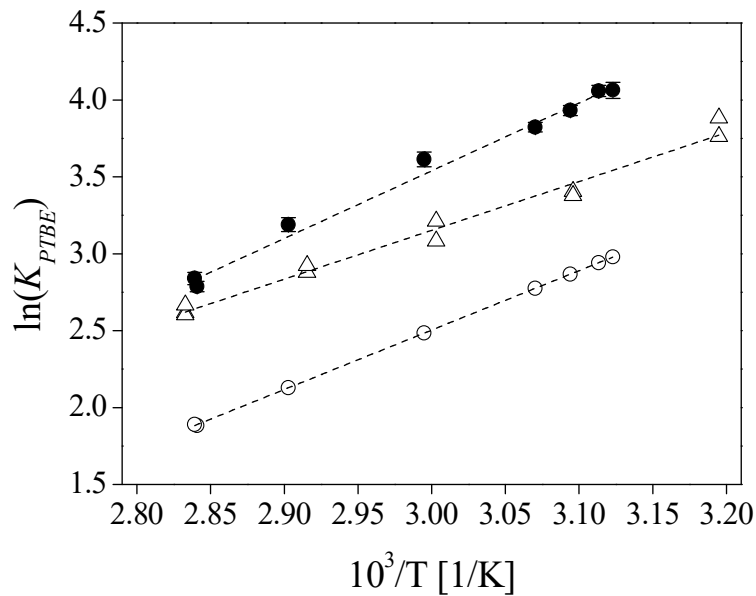


Figure 3.7 Comparison between values for PTBE equilibrium constant. Error bars correspond to uncertainty for 95% level of confidence. Present work (●), literature values [22] (△), and theoretically estimated values (○)

3.3.2.4 BTBE synthesis

Studies concerning BTBE equilibrium are hard to find in literature [93,108]. To study its thermodynamics, we followed the same procedure and varied temperature and initial concentrations to reach equilibrium compositions, using A-35 as the catalyst in the batch reactor. Figure 3.8 shows the evolution in time of the BTBE molar fraction for the different experimental runs until chemical equilibrium was reached, for different $R^{\circ}_{A/O}$ and temperature. Experimental conditions and results for each individual experiment are provided in Appendix I (Table A5).

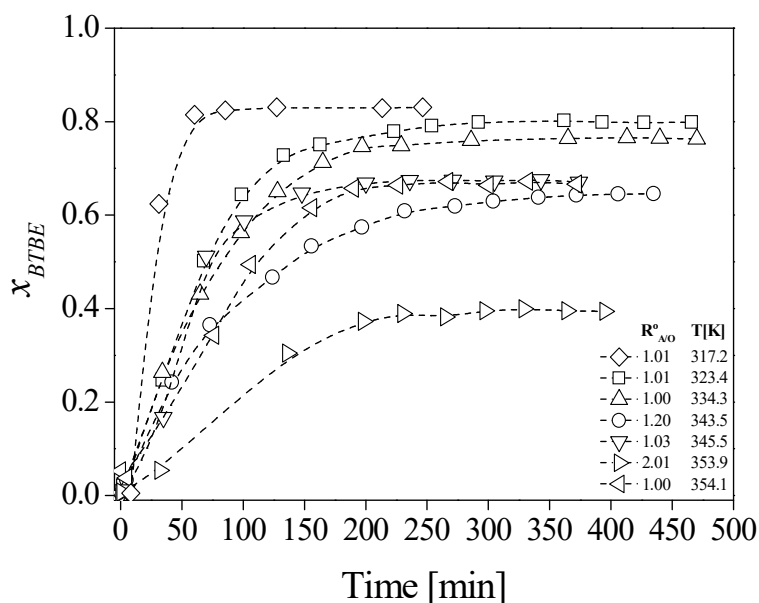


Figure 3.8 Evolution in time of BTBE molar fraction in batch experiments at different $R^{\circ}_{A/O}$ and temperatures. A-35, catalyst load = 0.1-7% wt., 750 rpm

In Figure 3.9, experimental K_{BTBE} values are compared to those reported in literature and to theoretically determined ones. As it can be seen, experimental data from literature [108] and from the present work are coincident, whereas a significant discrepancy can be observed regarding theoretical equilibrium constants. From dashed lines in Figure 3.9, it becomes clear that discrepancies between theoretically estimated and experimental values regard intercepts rather than slopes of linear fits.

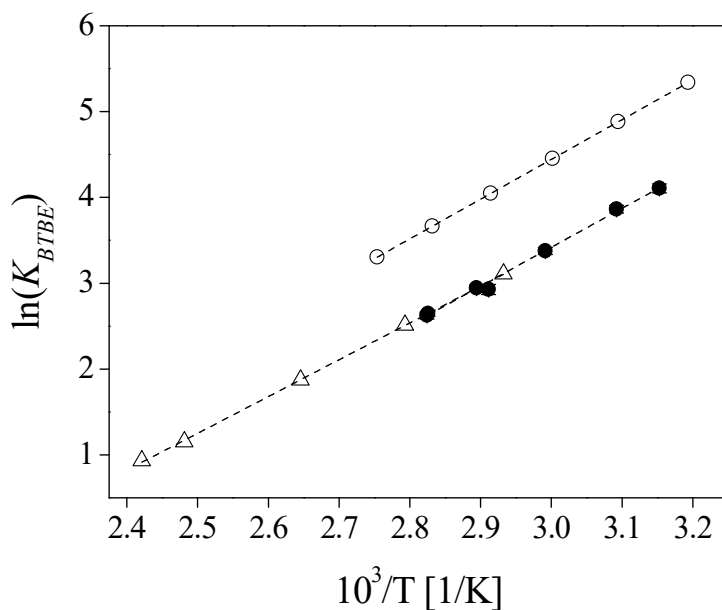


Figure 3.9 Comparison between values for BTBE equilibrium constant. Error bars correspond to uncertainty for 95% level of confidence. Present work (●), literature values [108] (Δ), and theoretically estimated values (○)

3.3.3 Thermodynamic properties

Figure 3.10 depicts $\ln K_i$ versus $1/T$ for the four studied equilibrium reactions, by assuming that the enthalpy change of etherification reactions can be considered constant within the assayed temperature range. As seen in the figure, experimental results fit well to a straight line and therefore reaction enthalpy could be considered independent on temperature ($\Delta_r H^\circ \neq f(T)$).

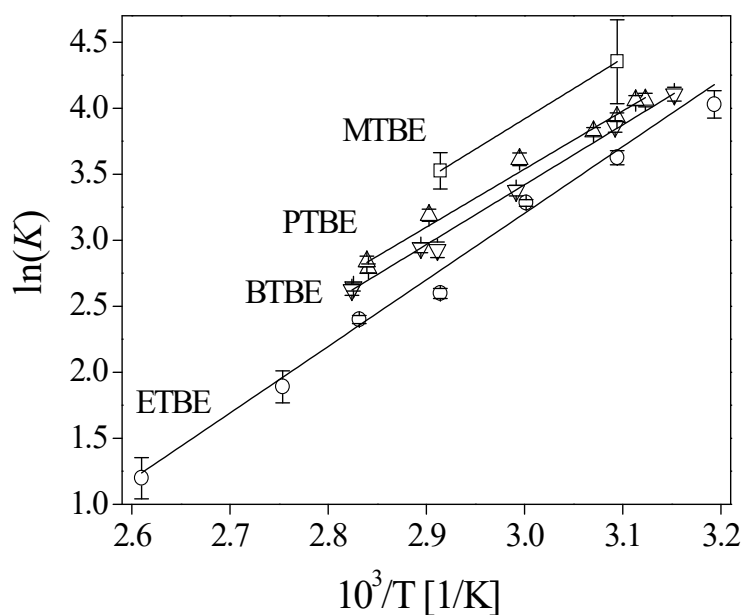


Figure 3.10 Van't Hoff plot when considering reaction enthalpy change constant within the temperature range ($\Delta_r H^\circ \neq f(T)$). Error bars correspond to uncertainty for 95% level of confidence. Solid lines refer to the values predicted using Eqs. 3.7–3.10

The standard molar enthalpy change of reaction, $\Delta_r H^\circ$, can be obtained from the slope and the standard molar entropy change of reaction, $\Delta_r S^\circ$, from the intercept. The resulting fitting equations obtained by least squares regression with the corresponding standard errors are:

$$\ln K_{MTBE} = \frac{(4,540 \pm 1,190)}{T} - (9.7 \pm 3.5) \quad (3.7)$$

$$\ln K_{ETBE} = \frac{(4,860 \pm 210)}{T} - (11.46 \pm 0.60) \quad (3.8)$$

$$\ln K_{PTBE} = \frac{(4,360 \pm 430)}{T} - (9.52 \pm 1.29) \quad (3.9)$$

$$\ln K_{BTBE} = \frac{(4,570 \pm 340)}{T} - (10.30 \pm 0.99) \quad (3.10)$$

Equation 3.7 is shown for comparative purposes, since it presents a considerable uncertainty in its parameters because MTBE experiments were performed at only two temperatures. Thus, the above expression is not recommended to determine thermodynamic properties of the MTBE synthesis. The following expression from literature [96] should be used instead:

$$\ln K_{MTBE} = \frac{(4,703 \pm 96)}{T} - (10.3 \pm 0.1) \quad (3.11)$$

On the other hand, if $\Delta_r H^\circ$ is considered to be temperature dependent, it can be expressed by the Kirchoff equation:

$$\frac{d\Delta_r H^\circ}{dT} = \sum_{j=1}^S \nu_j C_{P_j}^\circ \quad (3.12)$$

where $C_{P_j}^\circ$ are the liquid phase molar heat capacities of the compound j in the considered reaction, which can be calculated by the equation and coefficients shown in Table 3.3.

Table 3.3 Molar heat capacity coefficients of the equation $C_p^\circ [J mol^{-1} K^{-1}] = a + bT + cT^2 + dT^3$, where T is expressed in K

Compound	a _i	b _i	c _i × 10 ³	d _i × 10 ⁵
isobutene ^a	596.89	-4.6357	14.40	-1.372
methanol ^a	1,391.6	-12.364	37.81	-3.719
ethanol ^a	1,422.5	-12.839	40.31	-4.016
1-propanol ^b	277.77	-2.0498	7.476	-0.7170
1-butanol ^b	320.73	-2.2142	7.986	-0.7585
MTBE ^a	53.176	0.7173	-1.533	0.2241
ETBE ^a	83.158	0.5894	-0.864	0.1383
PTBE ^c	-539.7	4.279	-5.96	0
BTBE ^c	-507.8	4.235	-5.93	0

^a Izquierdo et al. [23]. ^b Estimated by Missenard method [88].

^c Determined by differential scanning calorimetry (DSC).

Table 3.3 shows heat capacity coefficients taken from literature, estimated and experimentally determined. Literature values from different sources are reliable beyond doubt. As example, ETBE-related values from different works [23,102,105] lead to the same final results. With respect to unavailable coefficients, estimation of 1-propanol and 1-butanol molar heat capacities by different estimation methods, i.e., Missenard and Růžička-Domalski methods [88,89], lead to values that are similar to those quoted in literature [109] and therefore they can be considered as reliable. Missenard estimates were chosen because overall discrepancies with available databases regarding the four studied alcohols were found to be lower. As for the two missing ethers, i.e., PTBE and BTBE, their molar heat capacity variation with temperature was experimentally determined by differential scanning calorimetry (DSC) analysis in the temperature range of 298 to 368 K. These experimental determinations were carried out at the Scientific and Technological Centers (CCiT) of the University of Barcelona. Coefficients regarding these ethers are thus derived from fitting the equation in Table 3.6 to experimental results. Figure 3.11 shows the molar heat capacity values that were not found in the available literature as a function of temperature.

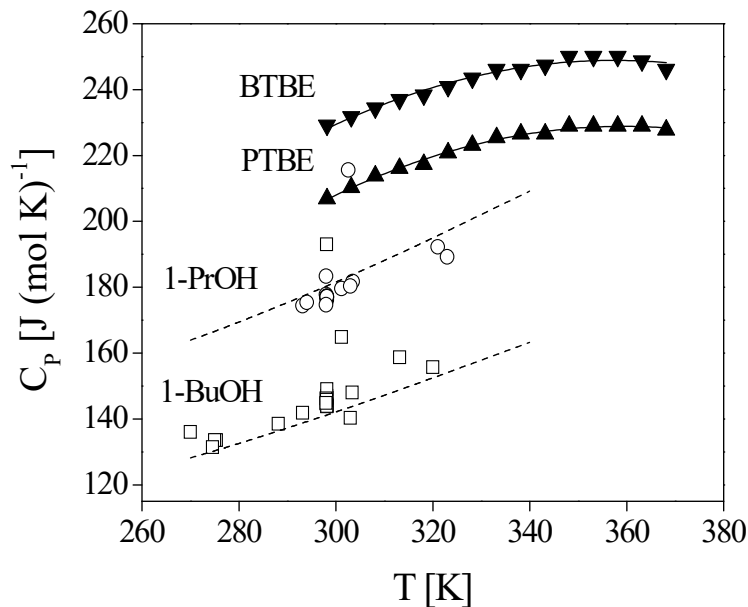


Figure 3.11 Variation of the molar heat capacity with temperature. Solid lines correspond to the equation and parameters in Table 3.6. Dashed lines correspond to estimation of molar heat capacity by Missenard method. Solid symbols refer to experimental determination by DSC: PTBE (▲), BTBE (▼). Open symbols refer to literature values [109]: 1-propanol (○), 1-butanol (□)

The integrated form of the Kirchoff equation, combined with the equation in Table 3.3, gives the following expression:

$$\Delta_r H^o = I_K + aT + \frac{b}{2}T^2 + \frac{c}{3}T^3 + \frac{d}{4}T^4 \quad (3.13)$$

where:

$$a = \sum_{j=1}^S v_j a_j; b = \sum_{j=1}^S v_j b_j; c = \sum_{j=1}^S v_j c_j; d = \sum_{j=1}^S v_j d_j \quad (3.14)$$

The dependence of the equilibrium constant on temperature is described by the Van't Hoff equation:

$$\frac{d \ln K}{dT} = \frac{-\Delta_r H^\circ}{RT^2} \quad (3.15)$$

Equation 3.15, combined with Equation 3.13 and integrated, leads to:

$$\ln K = I_H - \frac{I_K}{RT} + \frac{a}{R} \ln T + \frac{b}{2R} T + \frac{c}{6R} T^2 + \frac{d}{12R} T^3 \quad (3.16)$$

where I_K and I_H are the integration constants. The fit of Equation 3.16 to the experimental values of the equilibrium constants at different temperatures allows obtaining I_K value from the slope and I_H value from the intercept. Figure 3.12 provides the Van't Hoff plot where reaction enthalpy change is considered as a function of temperature ($\Delta_r H^\circ = f(T)$).

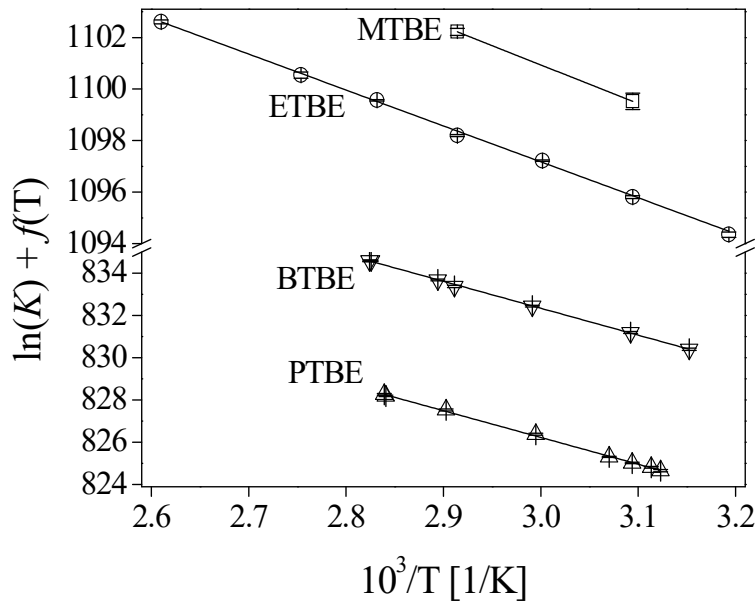


Figure 3.12 Van't Hoff plot considering reaction enthalpy as function of temperature ($\Delta_r H^\circ = f(T)$). 95% confidence intervals are represented with error bars. Solid lines refer to the values predicted by Equation 3.15 with parameters in Table 3.4 for each reaction

Finally, the standard molar entropy and free energy changes of reaction, $\Delta_r S^\circ$ and $\Delta_r G^\circ$, can be evaluated by means of the following expressions:

$$\Delta S^\circ = RI_H + a + a \ln T + bT + \frac{c}{2} T^2 + \frac{d}{3} T^3 \quad (3.17)$$

$$\Delta G^\circ = I_K - RI_H T - aT \ln T - \frac{b}{2} T^2 - \frac{c}{6} T^3 - \frac{d}{12} T^4 \quad (3.18)$$

Parameters of Eqs. 3.13, 3.16-18 are shown in Table 3.4. Summary of thermochemical properties determined for the studied reactions is provided in Table 3.5.

Table 3.4 Temperature dependence parameters of K , $\Delta_r H^\circ$, $\Delta_r S^\circ$, and $\Delta_r G^\circ$, for the considered reactions when $\Delta_r H^\circ = f(T)$. Uncertainties refer to a 95% confidence interval

Reaction	a [J mol ⁻¹ K ⁻¹]	b [J mol ⁻¹ K ⁻²]	c × 10 ³ [J mol ⁻¹ K ⁻³]	d × 10 ⁵ [J mol ⁻¹ K ⁻⁴]	I _K [J mol ⁻¹ K ⁻¹]	I _H [-]
MTBE	-1,935.314	17.717	-53.743	5.3131	122.5 ± 9.9	1,145.2 ± 3.5
ETBE	-1,936.232	18.0641	-55.574	5.5263	117.66 ± 1.68	1,139.62 ± 0.58
PTBE	-1,414.36	10.9645	-27.836	2.089	105.5 ± 3.4	864.31 ± 1.21
BTBE	-1,425.42	11.0849	-28.316	2.1305	105.3 ± 3.0	870.35 ± 1.08

Table 3.5 Standard molar enthalpy (kJ mol⁻¹), entropy (J (mol K)⁻¹) and free energy (kJ mol⁻¹) changes of alkyl *tert*-butyl ether syntheses in the liquid phase at 298.15 K. Uncertainties refer to a 95% confidence interval

Reaction	Property	$\Delta_r H^\circ \neq f(T)$	$\Delta_r H^\circ = f(T)$	Theoret.	Literature			
MTBE	$\Delta_r H^\circ$	-38 ± 10	-37 ± 10	-36.9	-37.7 ^a	-39.1 ± 0.8 ^b	-38.0 ± 0.8 ^b	-36.1 ^c
	$\Delta_r S^\circ$	-80 ± 30	-80 ± 30	-76.9		-85.3 ± 0.5 ^b	-81.7 ± 0.5 ^b	-75.4 ^c
	$\Delta_r G^\circ$	-13 ± 13	-14 ± 13	-14.0	-14.0 ^a	-13.7 ± 0.8 ^b	-13.6 ± 0.8 ^b	-13.7 ^c
ETBE	$\Delta_r H^\circ$	-40.4 ± 1.7	-38.5 ± 1.7	-34.8	-44.3 ± 2 ^d	-41.1 ^e	-35.45 ± 1.94 ^f	-36.3 ± 7.2 ^g
	$\Delta_r S^\circ$	-95 ± 5	-89 ± 5	-78.2		-94.9 ^e	-82.37 ± 5.99 ^f	-81.3 ± 21.4 ^g
	$\Delta_r G^\circ$	-12 ± 2	-12 ± 2	-11.5		-12.8 ^e		-12.1 ± 4.5 ^g
PTBE	$\Delta_r H^\circ$	-36 ± 4	-34 ± 3	-32.1	-26.4 ^h			
	$\Delta_r S^\circ$	-79 ± 11	-71 ± 10	-75.5	-53.0 ^h			
	$\Delta_r G^\circ$	-13 ± 5	-12 ± 4	-9.6				
BTBE	$\Delta_r H^\circ$	-38 ± 3	-35 ± 3	-38.5	-34.8 ± 2.7 ⁱ			
	$\Delta_r S^\circ$	-86 ± 8	-76 ± 9	-78.6	-75.8 ± 7.7 ⁱ			
	$\Delta_r G^\circ$	-12 ± 4	-12 ± 4	-15.1				

^a Rehfinger and Hoffmann [95]. ^b Izquierdo et al. [96]. ^c Wyczesany [98]. ^d Françoisse and Thyron [100].
^e Jensen and Datta [102]. ^f Sharonov et al. [103]. ^g Soto et al. [105]. ^h Linnekoski et al. [22]. ⁱ Sharonov et al. [108]

The estimated values of the thermodynamic properties of the studied reactions are globally in good agreement with the data in the available literature (Table 3.5). In this work, values for MTBE synthesis have been obtained from experimental runs at only two temperatures, with a large relative uncertainty, and, therefore, they are provided for comparative purposes. Consequently, the use of literature values for MTBE is recommended, especially those by Izquierdo et al. [96]. Concerning ETBE synthesis, the estimated values are coincident, within the experimental error, with those reported by Jensen and Datta [102], obtained from both theoretical relations and experimental results, and with those by Soto et al. [105], determined experimentally in a slightly different reaction system, the simultaneous production of ETBE and *tert*-amyl ethyl ether. Values by Françoisse and Thyron [100] are a bit larger, and values by Sharonov et al. [103] agree with theoretical values. There are very few studies in the available literature devoted to thermodynamic equilibrium of PTBE and BTBE synthesis. In the PTBE synthesis, the estimated values are close to the theoretical ones, and differences with Linnekoski et al. [22] are regarded as inconclusive. With respect to BTBE

synthesis, the present results agree with the values reported by Sharonov et al. [108], and they are close to the theoretical ones.

A rather good agreement is observed between experimental and theoretically estimated thermodynamic state functions. Nevertheless, slight differences between theoretical and experimental thermodynamic properties lead to obvious discrepancies regarding theoretical and experimentally obtained equilibrium constants, as it has been already commented, given the exponential dependence defined by the Van't Hoff equation. These discrepancies are particularly evident in the intercepts of the Van't Hoff plots rather than in their slopes. Consequently, discrepancies between theoretical and experimental entropy changes of reaction are larger than between enthalpy changes. As example, the theoretical entropy change of the ETBE synthesis seems to be overestimated, as it can be seen by comparing that value to those reported either in this work or in literature. In this sense, a remark should be made about the thermochemical data used to determine theoretical values: experimentally-based databases should be extended because, even though estimation methods can provide relatively accurate values, small deviations lead to considerable discrepancies with experimental thermodynamic data.

At this point, thermochemical data of formation of the four ethers produced in these reactions have been readjusted accordingly with present experimental data, by considering the reaction enthalpy as a function of temperature ($\Delta_r H^\circ = f(T)$). As seen in Table 3.6, relative differences of readjusted values, compared to those presented in Table 3.2, are quite low and, therefore, they can be considered as acceptable. The general agreement between proposed values and either reported or estimated ones reinforces the reliability of the present study.

Table 3.6 Readjusted thermochemical data of the ethers produced if $\Delta_r H^\circ = f(T)$ (standard state, liquid at 1 atm and 298.15 K)

Compound	$\Delta_r H^\circ$ (difference with literature value ^a) [kJ mol ⁻¹]	S ^o (difference with literature/estimated value ^a) [J (mol K) ⁻¹]
MTBE	-313.5 (0.0%)	264.5 (-0.3%)
ETBE	-353.6 (1.1%)	286.7 (-3.9%)
PTBE	-373.6 (0.4%)	338.5 (1.5%)
BTBE	-399.8 (-0.9%)	365.0 (0.6%)

^a Relative difference of readjusted formation data compared to values in Table 3.2.

Finally, concerning the two alternatives early used on whether to consider the reaction enthalpy change as a function of temperature or not ($\Delta_r H^\circ = f(T)$ or $\Delta_r H^\circ \neq f(T)$), Table 3.7 shows the variation of the enthalpy change of reaction, $\Delta_r H^\circ$, in the temperature range 323-353 K. As seen in the table, maximum relative differences between values are 2.7%, 3.6%, 7.1%, and 7.6%, for the syntheses of MTBE, ETBE, PTBE, and BTBE, respectively. Thus, enthalpies of reaction are more sensitive to temperature variations as the size of the produced ether increases, especially for PTBE and BTBE.

Table 3.7 Estimated values of the liquid phase standard molar enthalpy change of reaction, $\Delta_r H^\circ$, for the studied reactions, when it is considered as temperature dependent

T [K]	$\Delta_r H^\circ$ [kJ mol ⁻¹]			
	MTBE	ETBE	PTBE	BTBE
323	-37.5	-39.3	-35.2	-36.9
333	-37.8	-39.7	-36.0	-37.8
343	-38.1	-40.2	-36.8	-38.7
353	-38.5	-40.7	-37.7	-39.7

The variation with temperature of enthalpy changes of reaction regarding the four studied syntheses are quite close to those previously reported in literature. For instance, observed enthalpy variations in the syntheses of MTBE and ETBE were 3.4% and 3.6%, respectively, over the same temperature range, according to values previously reported [96,105]. On the other hand, also from literature values [22,108], the variation with temperature of PTBE and BTBE enthalpy changes of reaction were 10% and 9%, respectively, over the same temperature range. Therefore, regarding both PTBE and BTBE syntheses, it would be advisable to consider the enthalpy change of reaction as temperature dependent.

3.4 Conclusions

Extensive experimental data are provided to estimate enthalpy, entropy and free energy changes of liquid-phase etherification of isobutene with C₁ to C₄ linear primary alcohols. Experimental equilibrium results for the involved reactions have been proven to be independent of the catalyst and reactor type. All four chemical reactions have been found to be reversible and exothermic. Consequently, the amount of produced ethers at equilibrium decreases at increasing temperature.

If the enthalpy change of reaction is considered as independent on temperature, estimated values of the liquid-phase standard enthalpy changes of the synthesis reactions of MTBE, ETBE, PTBE and BTBE are -38 ± 10 , -40.4 ± 1.7 , -36 ± 4 , and -38 ± 3 kJ mol⁻¹, respectively. If the enthalpy change is considered as a function of temperature, their estimated values at 298.15 K are -37 ± 10 , -38.5 ± 1.7 , -34 ± 3 and -35 ± 3 kJ mol⁻¹, respectively. Reaction enthalpies of PTBE and BTBE synthesis are more sensitive to temperature than those of MTBE and ETBE synthesis.

Liquid-phase standard state thermochemical data concerning the four produced ethers have been estimated as the following enthalpies of formation: -313.5, -353.6, -373.6 and -399.8 kJ mol⁻¹, and the following entropies: 264.5, 286.7, 338.5 and 365.0 J (mol K)⁻¹ for MTBE, ETBE, PTBE and BTBE, respectively.

4. Byproducts formation in the synthesis of ethyl *tert*-butyl ether (ETBE) over acidic macroreticular ion-exchange resins

THE PRESENT CHAPTER IS AN ADAPTED VERSION OF THE WORK

J.H. Badia, C. Fité, R. Bringué, E. Ramírez, F. Cunill. Byproducts formation in the ethyl *tert*-butyl ether (ETBE) synthesis reaction on macroreticular acid ion-exchange resins. *Applied Catalysis A: General*, 468, 2013, 384-394.

4.1 Introduction

The use of fuel ethers and, more specifically, of ethyl *tert*-butyl ether (ETBE), became widely spread in the European Union (EU) since oxygenated ethers were selected as preferred octane enhancers due to consecutive directives regulating gasoline composition. Industrially, ETBE is obtained under mild conditions by means of the heterogeneous catalytic etherification reaction of isobutene with ethanol, in which acidic macroreticular ion-exchange resins of polystyrene–divinylbenzene matrix are used as catalysts [50,110,111].

Reaction byproducts formation in the industrial process is related to the feed alcohol to olefin ratio, to the sources for the two reactants and to the hot-spots that could take place within the catalytic bed, where temperatures above 373 K can be reached. With regard to the reactants sources, isobutene comes mainly from the effluent of two petrochemical units (FCC and SC), along with other four-carbon compounds, resulting in what is known as the C₄ cut. A typical FCC C₄ cut composition includes isobutene, isobutane, butane, linear butenes and others. With respect to ethanol, since the current trend is to produce it from renewable sources, as from biomass by hydrolysis and sugar fermentation, an important amount of water within the alcoholic stream can be present [112].

Main side reactions involve (Figure 4.1): dimerization of isobutene to form 2,4,4-trimethyl-1-pentene (TMP-1) and 2,4,4-trimethyl-2-pentene (TMP-2), and thereof double bond isomerization (reactions 2-4 in the figure), ethanol dehydration to form diethyl ether (DEE) and water (reaction 5 in the figure), isobutene hydration to form of *tert*-butyl alcohol (TBA) (reaction 6 in the figure), and formation of ethyl *sec*-butyl ether (ESBE) by reaction between ethanol and linear butenes of C₄ olefinic cuts (reaction 7 in the figure). Analogous side reactions are expected in the industrial production of other alkyl *tert*-butyl ethers other than ETBE, obtained by isobutene etherification with the corresponding alcohol.

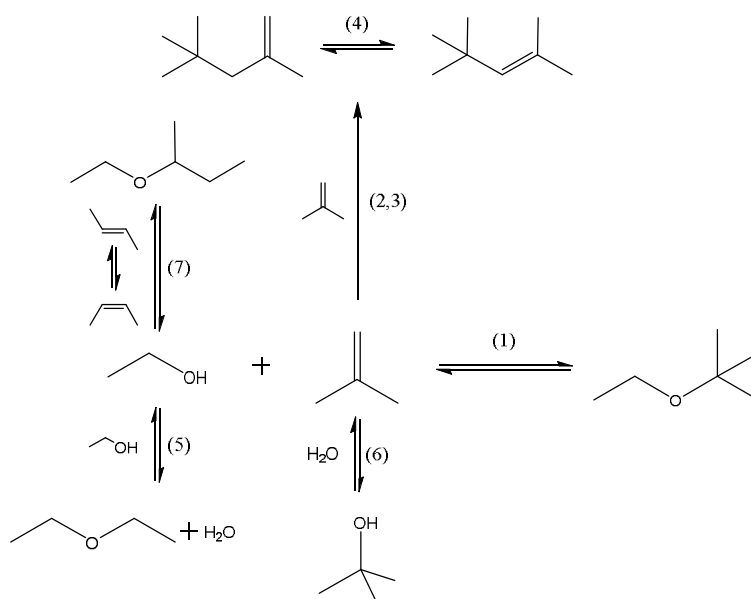


Figure 4.1 Reaction network in the ETBE synthesis using C₄ as isobutene source

In general, byproducts are inconvenient because some of them attenuate the desired properties towards the resulting gasoline mixture (Table 4.1). The presence of TMP-1 and TMP-2 along with the ETBE stream product does not pose any problems for blending, since both compounds have a high octane number. However, they can originate polymers on the catalyst that could act as poison by accumulating in the pores and lowering the accessibility to acid centers [87]. DEE formation enhances higher blending vapor pressure that might increase undesired evaporative emissions, as its vapor pressure is higher than for the rest of possible products [113,114]. Regarding TBA, although its octane number is high, TBA presence in the gasoline blending increases its water solubility, its blending Reid Vapor Pressure (RVP) [115–118], and its oxygen content [119]. Finally, as ESBE has a more linear structure than ETBE, it is assumed that its octane number is lower than that of ETBE. Thus, the effect of the ESBE presence would be to reduce the octane number of the gasoline mixture [120]. Besides, byproducts could cause some problems in the separation units, and in the later use of the unreacted C₄ stream.

Table 4.1 Relevant properties of involved compounds [23,121,122]

Category	Compound	Blending RVP [bar]	(RON + MON) / 2	Boiling Point [K]	Oxygen content [%wt.]	Solubility in water [g / 100 g _{water}]
Main product	ETBE	0.34	110	345	15.7	1.2
	TBA	0.70	101	356	21.6	infinite
Byproduct	TMP-1 and TMP-2	0.11 ^a	~100	374.5	0	0
	DEE	0.60 ^a	low	308	21.6	Partially soluble in cold water
	ESBE	0.10 ^a	low	355	15.7	~ 1
Reactant	EtOH	1.25	113	351	34.7	infinite
	IB	2.6 ^a	low	266.2	0	3.88 · 10 ⁻⁴

^a Since blending Reid Vapor Pressure (RVP) was not available, vapor pressure at 293 K is given instead.

As literature on byproducts formation in alkyl *tert*-butyl ethers syntheses is very scarce, the aim of this chapter is to determine the conditions of formation of the byproducts which are formed simultaneously with these syntheses on acidic macroreticular resins. ETBE synthesis was chosen for its predominance in the EU as oxygenate additive. The studied byproducts are, therefore, DEE, TMP-1, TMP-2, ESBE, and TBA.

4.2 Experimental

4.2.1 Chemicals and catalysts

Reactants were ethanol and the synthetic C₄ mixture as the isobutene source. TBA, DEE, ETBE, ESBE, TMP-1, and TMP-2 were used for analysis purposes.

As catalysts, Amberlyst™ 35 (A-35) was used in the majority of the experimental work and Purolite® CT275 (CT-275) was used for comparative purposes. Pretreatment of the catalyst consisted in removing, as much as possible, their water content. Final water

content in the resin beads was 3-5%wt. (analyzed by Karl-Fischer titration in the laboratory). Additionally, dried catalyst beads were crushed and sieved in order to obtain particle diameters, d_p , ranging 0.25-0.40 mm, what ensures no internal mass transfer influence on the overall reaction rate, as it was determined in previous works [19].

4.2.2 Apparatus and procedure

The experimental setup consisted of a 200 cm³ stainless-steel jacketed batch reactor. The reaction temperature range was 323-383 K, controlled within ± 0.1 K. The system pressure was kept at 2.0 MPa to ensure the liquid phase over the reaction system.

A set of 28 experiments was performed at four different temperatures (323, 343, 363 and 383 K) with three different initial alcohol/olefin molar ratio (nominal ratios considered, $R_{A/O}^0$, were 0.5, 1.0, and 2.0) in order to explore the effect of different conditions on the side reactions that take place during the ETBE synthesis reaction that could be representative of that in industrial conditions. A list of the experimental conditions and results can be found in the Appendix I (Table A6). For reproducibility evaluation purposes, experiments at 383 and 343 K and at $R_{A/O}^0$ equal to 0.5 and 2.0, as well as at intermediate conditions, were repeated at least three times. Experiments at the lowest temperature (323 K) were not repeated as they revealed scarce byproducts formation. The relative standard uncertainty for reactants conversion ranged 0.3-4.4% and the mean relative uncertainty of the mass balances was less than 3%, which is considered an acceptable level of experimental error.

Depending on the assayed $R_{A/O}^0$, the designated amount of ethanol and 10.08 ± 0.02 g of dried catalyst were introduced in the reactor before the heating and the stirring were switched on. Catalyst amounts correspond to a 10%wt. of the whole reacting mixture. Previous experience revealed that no effect of the catalyst load below 11.3%wt. should be expected [123]. Stirring speed was set at 500 rpm to ensure no external mass transfer influence on the overall reaction rate given that, in previous works carried out in the same experimental apparatus, at 363 K and in the range 400-600 rpm, no influence of that physical step for the ETBE synthesis reaction was observed [124]. Additionally, the same conclusion was achieved by other studies at 500-800 rpm stirrer speed [125,126]. Temperature ranged from 323 to 383 K, because it was considered to be representative of the reported temperature profiles in industrial-scale reactors, including possible hot spots. The amount of C₄ mixture, determined by $R_{A/O}^0$, was introduced into the reactor from a pressure burette, impelled by nitrogen, once the desired temperature inside the reactor vessel was reached. This instant was considered as the starting point for the reaction.

4.2.3 Analysis

Samples were taken inline from the reactor medium through a sampling valve that injected 0.2 μ L of pressurized liquid into an Agilent gas chromatograph 6890 attached to a mass selective detector HP5973N (GC-MS). The GC was equipped with a capillary column (100% dimethylpolysiloxane, 50 m \times 0.20 mm \times 0.50 μ m). The oven

temperature was set at 308 K during 45 min. Helium was used as the carrier gas with a flow of 1.5 mL/min.

Up to 11 different chemical species, namely, ethanol, isobutene, ETBE, isobutane, *trans*- and *cis*-2-butene, TBA, DEE, ESBE, TMP-1 and TMP-2, were chromatographically identified in significant amounts depending on the experimental conditions. Besides, other minor byproducts, formed by either the hydration or the oligomerization of 2-butenes, were also detected in the experiments carried out in favorable conditions (excess of olefins and at the highest temperature, 383 K). In particular, 2-butanol, from the hydration of 2-butene, was detected in less than 1.0% of GC area and dimers of 2-butene and/or codimers of 2-butene and isobutene were detected in less than 1.5% of GC area. These minor byproducts were never detected at other working conditions, and they were therefore not taken into further consideration in the calculations. Figure 4.2 is provided as an example chromatogram of an experiment carried out with A-35 as the catalyst, at 383 K, $R_{A/O} = 2.0$, after 300 minutes of reaction.

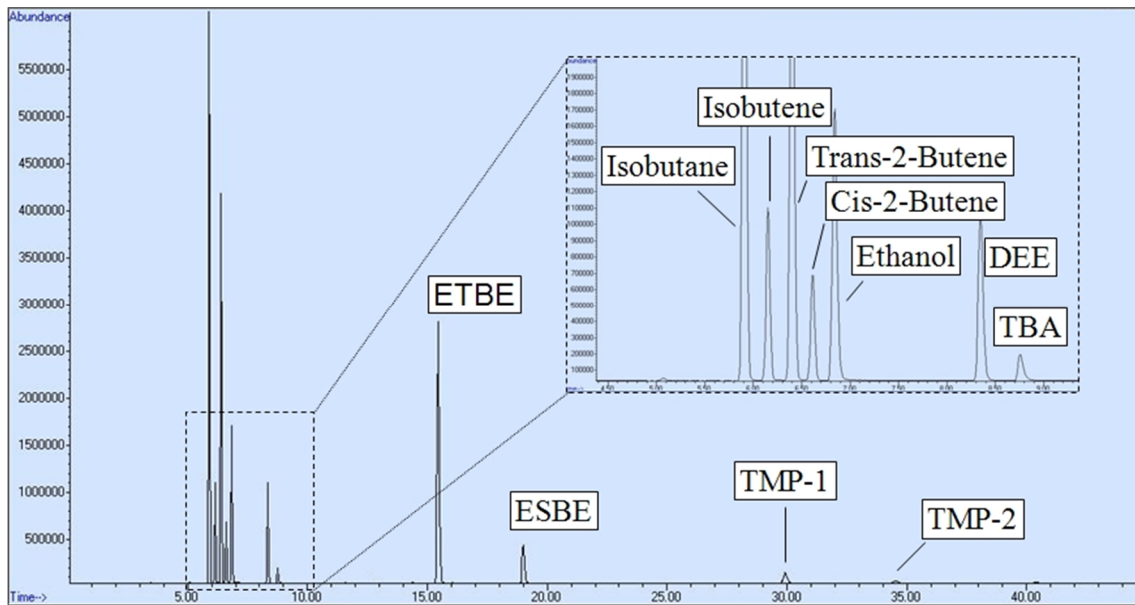


Figure 4.2 Example chromatogram after 300 min of experiment. $T = 383$ K, $R_{A/O} = 2.0$, A-35, catalyst load = 10%wt., $d_p = 0.25$ -0.40 mm, 500 rpm

4.2.4 Calculations

Results were expressed in terms of conversion (X_j) of the main reactants, ethanol and isobutene, and of selectivity (S_j^k), to products and byproducts from them, as follows:

$$X_j = \frac{\text{mole of } j \text{ reacted}}{\text{mole of } j \text{ fed}} \quad (4.1)$$

$$S_j^k = \frac{\text{mole of } j \text{ reacted to produce } k}{\text{mole of } j \text{ reacted}} \quad (4.2)$$

where k is the considered product or byproduct, and j is the reactant (isobutene or ethanol).

4.3 Results and discussion

Figure 4.3 plots molar fraction, x_j , evolution of the chemical species involved in a model experiment, carried out with A-35, at 383 K and $R_{A/O}^0 = 0.5$. Under such conditions, side reactions were strongly favored.

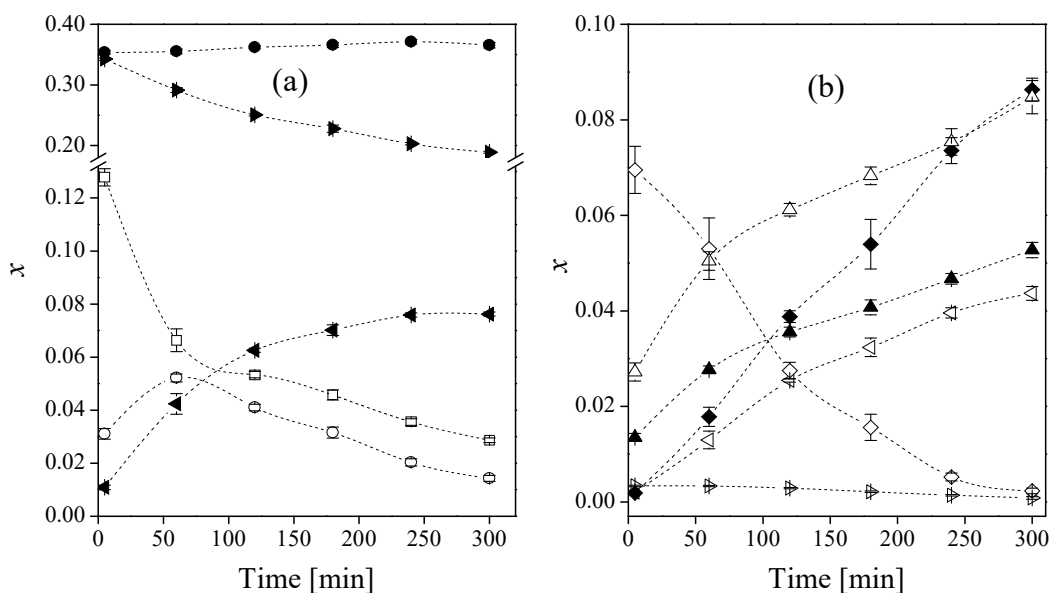


Figure 4.3 Molar fraction evolution of major (a) and minor (b) chemical species. $T = 383$ K, $R_{A/O}^0 = 0.5$, A-35, catalyst load = 10%wt., $d_p = 0.25$ - 0.40 mm, 500 rpm. Error bars refer to the standard uncertainty for replicated experiments. x_{IB} (\square), x_{EtOH} (\circ), $x_{isobutane}$ (\bullet), $x_{trans-2-butene}$ (\blacktriangleright), $x_{cis-2-butene}$ (\blacktriangleleft), x_{ETBE} (\diamond), x_{TBA} (\triangleright), x_{DEE} (\triangleleft), x_{ESBE} (\blacklozenge), x_{TMP-1} (\triangle), x_{TMP-2} (\blacktriangle)

In Figure 4.3a, molar fraction of the main reactants, ethanol and isobutene, as well as other C_4 mixture components (isobutane and linear butenes) are represented. As it can be observed in Figure 4.3b, where ETBE and byproducts molar fraction evolution is represented, byproducts appeared as soon as the reaction began. TMP-1 and TMP-2 were formed quickly and, after 1 hour, their molar fraction increased in an almost linear trend until the end of the experiment. TBA formation was very low; it achieved a very smooth maximum concentration level within the first 60 minutes and then decreased to almost null values. It can be concluded that, initially, isobutene reacted swiftly with the available water in the reaction medium to approach equilibrium (see reaction 6 in Figure 4.1) and, then, the equilibrium position shifted, resulting in the observed decrease in TBA concentration, because of a higher consumption of isobutene in other simultaneous reactions (especially those of isobutene dimerization, reactions 2 and 3 in Figure 4.1). Regarding DEE and ESBE formation, they seem to describe a linear pattern what suggests a continuous evolution towards equilibrium, both reactions being far from that point when the experiment was over. The ETBE concentration drop, reaching null values at the end of the experiment, can be explained by the multiple demands of ethanol and isobutene in the different side reactions in which they were also involved, that led to the ETBE decomposition (reaction 1 in Figure 4.1). Note that ETBE concentration maximum level was reached within the first steps of the experiment, what

means that this reaction proceeded quickly, due to the high temperature and the catalyst loaded (10%wt. of the reacting mixture).

Figure 4.4 plots selectivity vs. conversion of the two main reactants in this experiment. Note that, in Figure 4.4 (both a and b) one can clearly distinguish the points corresponding to the first sample analyzed ($X_{IB} \approx 55\%$ and $X_{EtOH} \approx 71\%$) from the rest. This experimental fact can be explained if the side reactions taking place simultaneously are considered. It seems obvious, by observation of ETBE molar fraction evolution in Figure 4.3b, that probably even before the first sample was analyzed ETBE synthesis reaction had progressed greatly. Then, ETBE decomposition to give isobutene and ethanol took place during the experiment. This is a quite acceptable hypothesis once considered the high temperature and amount of catalyst in the reacting media. In the subsequent analyses during the experiment, reactants conversion increase is due to its progressively higher consumption in side reactions.

It is worth mentioning that, as this model experiment revealed, after enough time of reaction, ETBE concentration could reach null values. As it was the aim of this paper to discuss on side reactions taking place simultaneously with ETBE production, reference time up to 300 minutes was set as the end of the experiments.

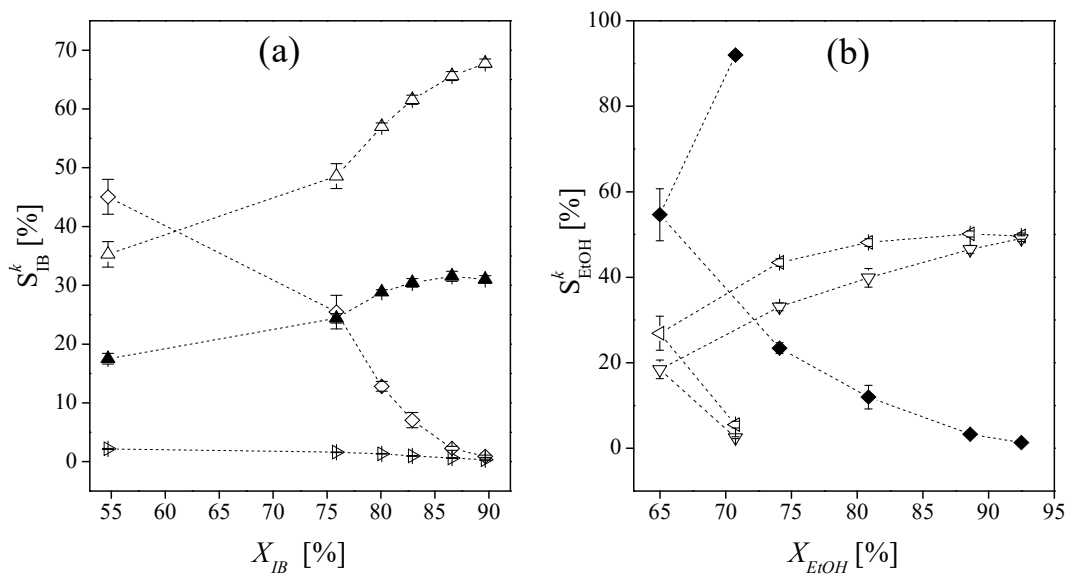


Figure 4.4 Selectivity of isobutene (a) and ethanol (b) towards products vs. total conversion. $T = 383$ K, $R^o_{A/O} = 0.5$, A-35, catalyst load = 10%wt, $d_p = 0.25$ - 0.40 mm, 500 rpm. Error bars refer to the standard uncertainty for replicated experiments. S_{IB}^{ETBE} (\diamond), S_{IB}^{TBA} (\triangleright), S_{IB}^{TMP-1} (Δ),

$$S_{IB}^{TMP-2}$$
 (\blacktriangle), S_{EtOH}^{ETBE} (\blacklozenge), S_{EtOH}^{DEE} (\triangleleft), S_{EtOH}^{ESBE} (∇)

4.3.1 TMP-1 and TMP-2 formation

Isobutene dimerization (reactions 2 and 3 in Figure 4.1) gives TMP-1 and TMP-2. Further oligomerization could originate trimers and tetramers. Additionally, when linear butenes are present, as it is the case of feedstocks from FCC or SC units, linear butenes could react with isobutene to form codimers giving a primary carbocation which, eventually, could be rearranged, forming other trimethylpentenes. Codimerization reactions, though, are known to be slower than isobutene dimerization, according to previous studies on the dimerization/etherification of FCC and SC C₄ hydrocarbons in the presence of methanol [127]. In the present study, codimers, trimers and heavier oligomers were not taken into consideration in the calculations as they were obtained only at the highest temperature and in less than 1.5% of GC area.

It has to be noted that dimers formation was the most relevant side reaction in the production of ETBE. This is in good agreement with the reported data in literature for similar systems, for instance in MTBE, TAME, TAEE, and IPTBE productions [86,87,128].

Isobutene selectivity towards TMP-1 and TMP-2 was enhanced by high temperatures and low R^o_{A/O}. This is coherent because high temperatures and isobutene concentration have been reported to be enhancers for the isobutene dimerization reaction [129,130]. As example, Figure 4.5 plots the selectivity to TMP-1 against temperature at the end of the experiments (t = 300 min). In that figure, a noticeable difference in isobutene selectivity to TMP-1 is observed between experiments carried out at the lowest R^o_{A/O} of 0.5 and that at 2.0. In the former, values of selectivity towards TMP-1 range from less than 30% at low temperatures (323 and 343 K) to more than 60% at 383 K. In the latter, though, almost null values of selectivity are observed except for the experiment carried out at the highest temperature. Experimental series with an R^o_{A/O} of 1.0 constitutes an intermediate situation between the others. Analogous trends were observed for the selectivity of isobutene to TMP-2, reaching values of over 30% at 383 K and R^o_{A/O} = 0.5.

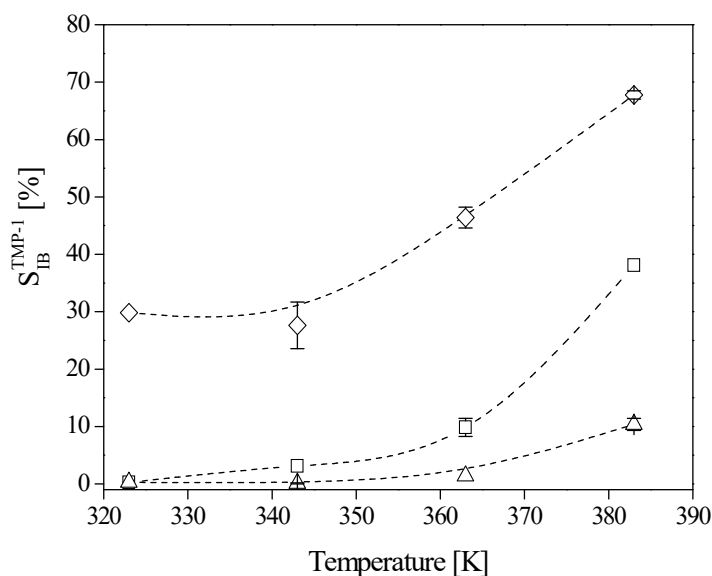


Figure 4.5 Variation with temperature of the isobutene selectivity towards TMP-1 after 300 min of reaction. A-35, catalyst load = 10%wt., $d_p = 0.25\text{-}0.40$ mm, 500 rpm. Error bars refer to the standard uncertainty for replicated experiments. R^o_{A/O} = 0.5 (◇), R^o_{A/O} = 1.0 (□), R^o_{A/O} = 2.0 (Δ)

The enhancement of dimers formation at low molar ratios suggests that isobutene, in a relatively high concentration, is readily adsorbed on non-dissociated sulfonic groups of the catalyst and dimerization reaction follows. This is actually a heterogeneous catalytic step, which is faster than an ionic one (specific acid catalysis), with dissociated protons due to the presence of ethanol in the surroundings of the sulfonic groups (general acid catalysis) [58–60,62,131].

With respect to the isomerization reaction between TMP-1 and TMP-2 (reaction 4 in Figure 4.1), the TMP-1 to TMP-2 molar ratio was monitored throughout each experiment. In the initial stage of the reaction, this ratio quickly achieved values that ranged from 1.5 to 2.6 and remained stable onwards. Similar ratios were also reported in analogous systems involving multiple simultaneous reactions [87]. According to literature, TMP-1 is thermodynamically more favored than TMP-2, resulting in a molar ratio of about 4:1 at equilibrium in the same temperature range (323–383 K) as well as at lower temperatures [132,133] what suggests that, in the present work, isomerization had not yet reach the chemical equilibrium at the end of the experiments (300 min).

It is worth mentioning that isomerization of diisobutenes constitute an exception to the general rule in alkene isomers stability. The general rule states that the more stable alkene is the one in which the double bond is located in intermediate positions of the carbon chain, in order to produce the highest possible substitution of the double bond. However, in isobutene dimers, the more substituted isomer, the trisubstituted TMP-2, is less stable than the disubstituted TMP-1. This fact has been already explained in literature by the internal repulsion between branches in the TMP-2 molecule that arises from the *tert*-butyl group located in the *cis* position to the methyl group [132].

With regard to dimerization reaction rate at high temperatures, TMP-1 was formed swifter than TMP-2 (Figure 4.6). The shape of both dimers production against time suggests irreversible reactions. Reaction rate of the isobutene dimerization increased as $R_{A/O}^0$ decreased, achieving its maximum values at 383 K and at $R_{A/O}^0 = 0.5$.

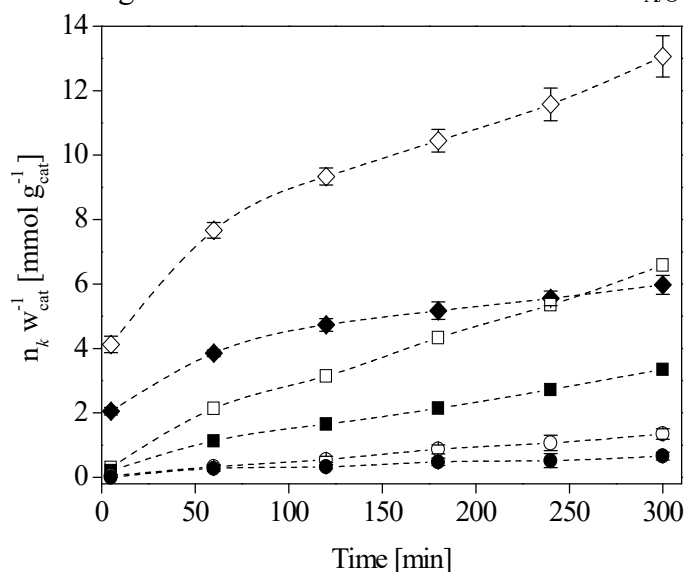


Figure 4.6 TMP-1 and TMP-2 formation vs. time at different $R_{A/O}^0$. n_k is referred to number of moles. $T = 383$ K, A-35, catalyst load = 10%wt., $d_p = 0.25$ - 0.40 mm, 500 rpm. Error bars refer to the standard uncertainty for replicated experiments. Open symbols: TMP-1 ($R_{A/O}^0 = 0.5$ (\diamond), $R_{A/O}^0 = 1.0$ (\square), $R_{A/O}^0 = 2.0$ (\circ)). Solid symbols: TMP-2 ($R_{A/O}^0 = 0.5$ (\blacklozenge), $R_{A/O}^0 = 1.0$ (\blacksquare), $R_{A/O}^0 = 2.0$ (\bullet))

4.3.2 DEE formation

Regarding ethanol dehydration (reaction 5 in Figure 4.1), Figure 4.7 reveals that high temperatures greatly enhanced the selectivity of ethanol towards diethyl ether, reaching levels of almost 50%. At low temperatures (323 and 343 K), no difference in selectivity towards DEE was observed at different $R^{\circ}_{A/O}$. At high temperatures (363 and 383 K), low alcohol concentration ($R^{\circ}_{A/O} = 0.5$) led to higher selectivity to DEE whereas no difference in selectivity was observed between experiments carried out under stoichiometric conditions ($R^{\circ}_{A/O} = 1.0$) or when an excess of ethanol was fed to the reactor ($R^{\circ}_{A/O} = 2.0$). This fact might seem counterintuitive, because an excess of ethanol could be expected to constitute an enhancer of the DEE formation. But as Figure 4.8 illustrates, when an excess of alcohol was fed, ethanol conversion was lower than operating at other $R^{\circ}_{A/O}$.

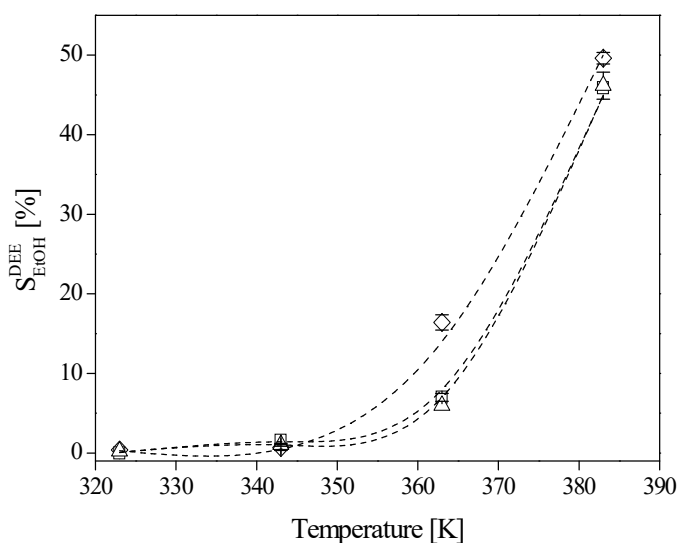


Figure 4.7 Variation with temperature of the ethanol selectivity towards DEE at $t_{\text{exp}} = 300$ min. A-35, catalyst load = 10%wt., $d_p = 0.25\text{-}0.40$ mm, 500 rpm. Error bars refer to the standard uncertainty for replicated experiments. $R^{\circ}_{A/O} = 0.5$ (\diamond), $R^{\circ}_{A/O} = 1.0$ (\square), $R^{\circ}_{A/O} = 2.0$ (Δ)

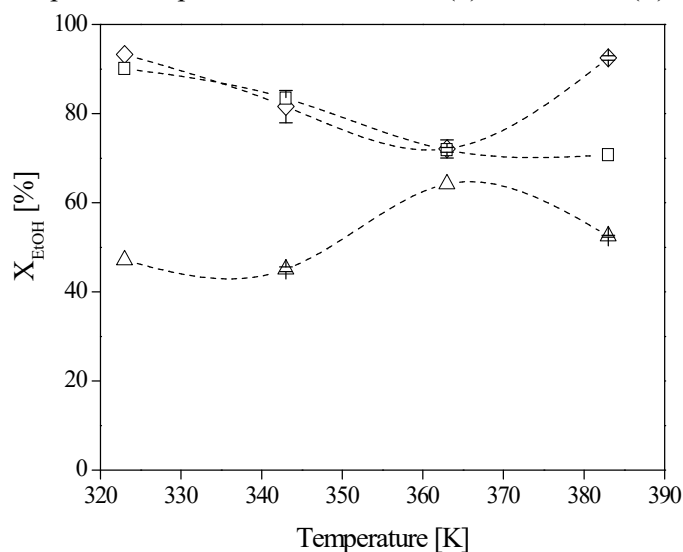


Figure 4.8 Ethanol conversion at $t_{\text{exp}} = 300$ min against temperature at different $R^{\circ}_{A/O}$. A-35, catalyst load = 10%wt., $d_p = 0.25\text{-}0.40$ mm, 500 rpm. Error bars refer to the standard uncertainty for replicated experiments. $R^{\circ}_{A/O} = 0.5$ (\diamond), $R^{\circ}_{A/O} = 1.0$ (\square), $R^{\circ}_{A/O} = 2.0$ (Δ)

In terms of DEE production at the end of every experiment, temperature plays a much more important role than $R_{A/O}^o$ as a DEE promoter. To illustrate it, consider the experiments at 363 K and lower temperatures depicted in Figure 4.9, none of which showed significant differences in terms of DEE production with respect to $R_{A/O}^o$. Nevertheless, at 383 K, an increase in DEE formation is observed as increasing $R_{A/O}^o$. The increase of the reaction medium polarity due to the excess of ethanol affects the catalytic behavior of the catalyst in several ways [134,135] and can account for the increase in the DEE production. Polar molecules, as ethanol, can break the hydrogen network that binds the sulfonic groups and, as a consequence, more inner active centers become accessible to the reactants. When ethanol dehydration takes place, the water released as the reaction proceeds would even enhance this effect. On the contrary, a polar medium solvates the acidic protons of those active centers which present a lower acid strength than the protons bound to the sulfonic groups, thus reducing the reaction rate on each catalytic center [136]. Taking into account these opposed factors, the enhancing effect might be more important than the inhibiting one in the ethanol dehydration reaction at 383 K.

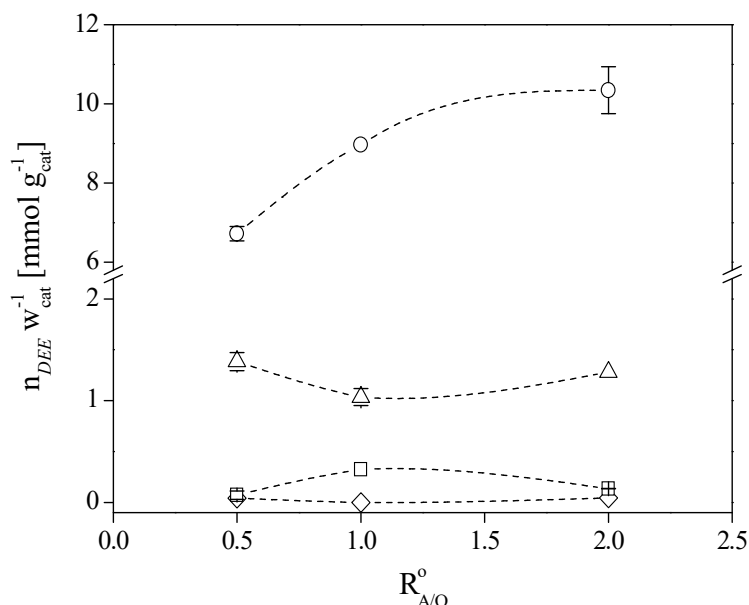


Figure 4.9 DEE formation against $R_{A/O}^o$ at different temperatures at $t_{exp} = 300$ min. A-35, catalyst load = 10%wt., $d_p = 0.25$ - 0.40 mm, 500 rpm. Error bars refer to the standard uncertainty for replicated experiments. T = 323 K (\diamond), T = 343 K (\square), T = 363 K (Δ), T = 383 K (\circ)

4.3.3 TBA formation

Reaction between water and isobutene led to TBA formation (reaction 6 in Figure 4.1). For the present work, water could stem from different sources: the amount of water contained within the ethanol (200 ppm), the remaining moisture hold in the catalyst (3-5%wt.), and the chemically-produced molecules of water proceeding from the dehydration of ethanol.

Figure 4.10 reveals that, at $R_{A/O}^o$ other than 0.5, isobutene selectivity towards TBA at the end of the experiments increased with temperature. At low temperatures (363 K and

lower), no significant differences in the selectivity to TBA can be distinguished between experiments at $R_{A/O}^{\circ} = 1.0$ and 2.0 , whereas for the experiments at $R_{A/O}^{\circ} = 0.5$ the selectivity was slightly lower. At the highest temperature (383 K), the higher the molar ratio, the higher the selectivity towards TBA was. These facts suggest that more polar media enhanced selectivity to TBA.

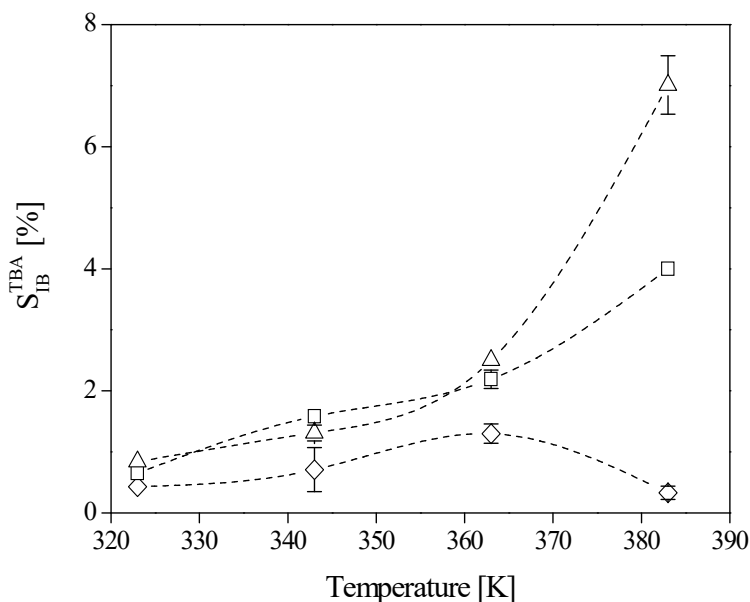


Figure 4.10 Variation with temperature of the isobutene selectivity towards TBA at $t_{\text{exp}} = 300$ min. A-35, catalyst load = 10%wt., $d_p = 0.25\text{-}0.40$ mm, 500 rpm. Error bars refer to the standard uncertainty for replicated experiments. $R_{A/O}^{\circ} = 0.5$ (◇), $R_{A/O}^{\circ} = 1.0$ (□), $R_{A/O}^{\circ} = 2.0$ (△)

Figure 4.11 plots the evolution of the TBA production at $R_{A/O}^{\circ} = 2.0$, that is when the highest amounts of TBA were detected, and at different temperatures. While at lowest temperatures, namely 323 K and 343 K, the TBA content decreased after a maximum value, at the highest temperatures (363 K and 383 K) no maximum value was yet achieved by the time the experiment ended. The former behavior can be explained by assuming that, as TBA is known to reach the equilibrium swiftly [137], water present in the medium reacted readily reacts with isobutene at the initial steps of the experiment and, afterwards, the reverse reaction proceeded since isobutene was consumed by other competitive side reactions, mainly dimerization. The latter behavior can be related to the major extent of the dehydration reaction of ethanol at high temperatures, what produced water that subsequently reacted with isobutene to form more TBA.

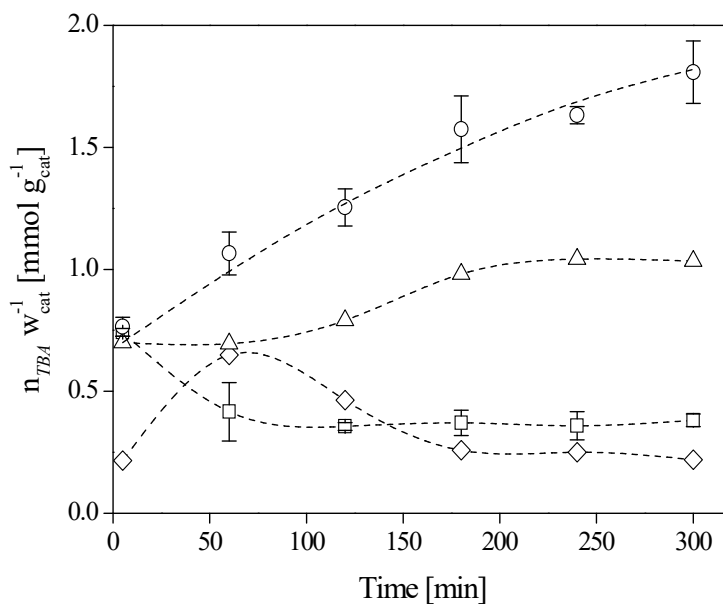


Figure 4.11 Evolution of TBA formation at different temperatures. $R_{A/O}^0 = 2.0$, A-35, catalyst load = 10%wt., $d_p = 0.25\text{-}0.40$ mm, 500 rpm. Error bars refer to the standard uncertainty for replicated experiments. $T = 323$ K (◇), $T = 343$ K (□), $T = 363$ K (△), $T = 383$ K (○)

As reported in literature, water shows a strong inhibitory effect on the ETBE production, even at low contents [137]. This inhibitory effect would disappear progressively as water was consumed to yield TBA, which was produced quickly. However, the simultaneous dehydration of ethanol, enhanced by high temperatures, could lead to higher water production that would account for a sustained consumption of isobutene. This implies that, depending on the experimental conditions, some water can be redelivered to the reaction media, what arises as a potentially modifier factor of the catalytic conditions throughout an experiment. The high polarity of water leads to a combined effect of potentially reducing the activity of sulfonic groups and, simultaneously, swelling the resin, what allows reactants to access to active centers that were initially unreachable [138].

4.3.4 ESBE formation

Etherification of linear butenes with ethanol occurs when linear butenes are present in the C_4 cut used as isobutene source, leading to ESBE formation (reaction 7 in Figure 4.1). In the present work, *trans*-2-butene was included in the synthetic C_4 mixture in order to emulate the presence of these linear butenes in typical sources of isobutene, such as FCC or SC C_4 cuts. It is worth noting that isomerization of *trans*-2-butene present in the initial mixture to *cis*-2-butene was detected. Amounts of *cis*-2-butene reached levels up to 7% of GC area that were taken into account in the calculations. According to literature, *trans*-2-butene is thermodynamically more stable than *cis*-2-butene [139,140].

As shown in Figure 4.12, selectivity to ESBE was strongly favored by high temperatures and low $R_{A/O}$. At low temperatures ($T = 343$ K and lower) no significant amounts of ESBE were detected, but at 363 K and higher, values of selectivity to ESBE

achieved in experiments at $R_{A/O}^{\circ} = 0.5$ were far higher than those achieved under stoichiometric or in excess of alcohol conditions ($R_{A/O}^{\circ} = 1.0$ or 2.0 , respectively).

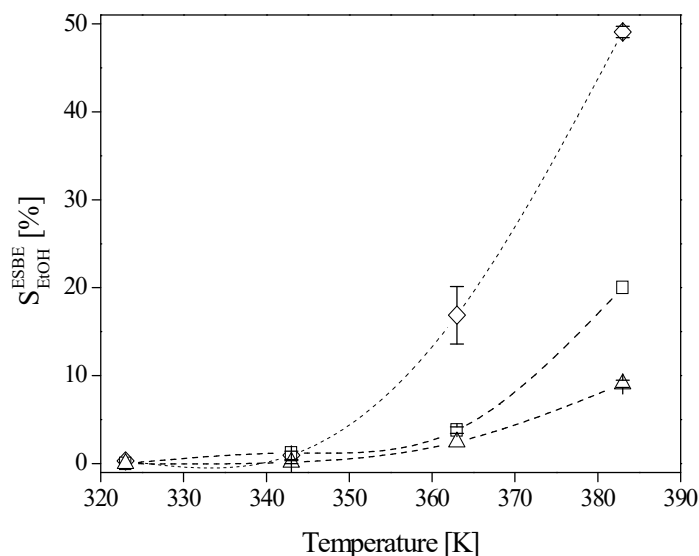


Figure 4.12 Variation with temperature of the ethanol selectivity towards ESBE at $t = 300$ min. A-35, catalyst load = 10%wt., $d_p = 0.25$ - 0.40 mm, 500 rpm. Error bars refer to the standard uncertainty for replicated experiments. $R_{A/O}^{\circ} = 0.5$ (\diamond), $R_{A/O}^{\circ} = 1.0$ (\square), $R_{A/O}^{\circ} = 2.0$ (Δ)

Figure 4.13 reveals that ESBE production evolved linearly with time under the most favorable condition ($R_{A/O}^{\circ} = 0.5$), what suggests that the reaction was far from the equilibrium within the assayed temperature range.

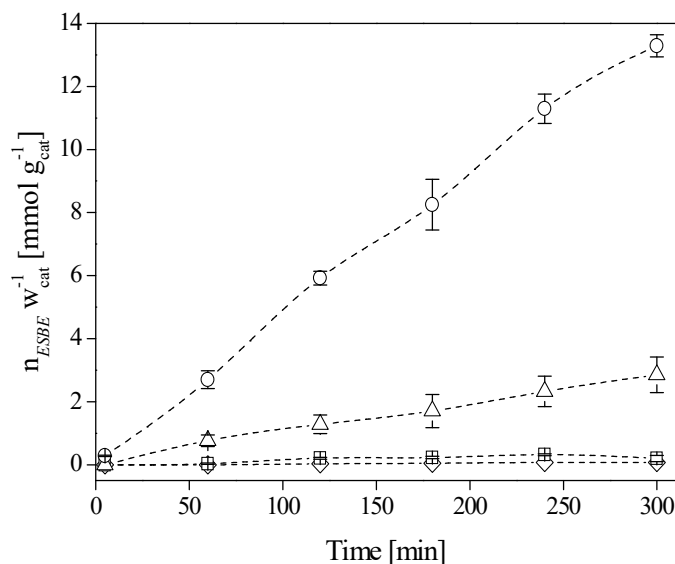


Figure 4.13 ESBE formation vs. time at different temperatures. $R_{A/O}^{\circ} = 0.5$, A-35, catalyst load = 10%wt., $d_p = 0.25$ - 0.40 mm, 500 rpm. Error bars refer to the standard uncertainty for replicated experiments. $T = 323$ K (\diamond), $T = 343$ K (\square), $T = 363$ K (Δ), $T = 383$ K (\circ)

Similar to the one described for the dimers formation at low $R_{A/O}^{\circ}$, a heterogeneous catalytic step can be assumed again. Linear butenes would be able to take the proton directly from the sulfonic groups, because they would be less dissociated due to the lack of ethanol [58–60,62,131]. This assumption was already adopted in a similar study on the side reactions taking place along with the MTBE synthesis [86].

4.3.5 Catalysts comparison

In order to compare possible differences in terms of global behavior of the reaction system due to the catalyst, three representative experiments carried out with A-35 were repeated with CT-275. These experiments were performed at rather high temperatures (363 and 383 K), in order to favor side reactions, and in excess of olefins and under stoichiometric conditions ($R_{A/O}^0 = 0.5$ and 1.0, respectively), in order not to mask a possible influence of $R_{A/O}^0$ by choosing only one initial feed composition. In general, significant differences between both catalysts were observed in terms of ETBE production, total byproducts formation and product distribution, depending on the assayed conditions.

Figure 4.14 plots the evolution of the total byproducts formation in those experiments. Under stoichiometric conditions ($R_{A/O}^0 = 1.0$), no significant differences between catalysts were detected. At 363 K and $R_{A/O}^0 = 0.5$, A-35 led to more byproducts formation than CT-275. At the same $R_{A/O}^0$ and 383 K, byproducts formation increased for both catalysts, as expected, but with a larger production for CT-275. A similar fact has been reported in the oligomerization reaction of 1-hexene for the same resins [141].

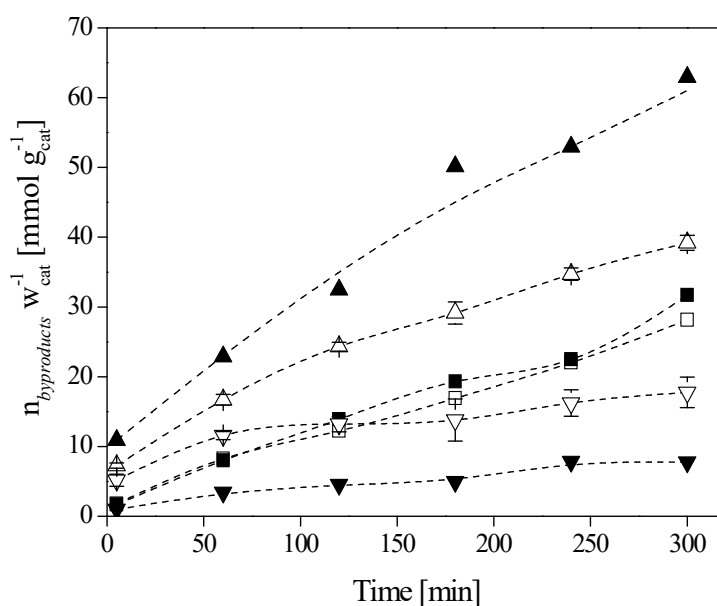


Figure 4.14 Total byproducts formation vs. time with two different catalysts. Catalyst load = 10%wt., $d_p = 0.25\text{-}0.40$ mm, 500 rpm. Error bars refer to the standard uncertainty for replicated experiments. Open symbols: A-35 ($R_{A/O}^0 = 0.5$, $T = 363$ K (▽); $R_{A/O}^0 = 0.5$, $T = 383$ K (△); $R_{A/O}^0 = 1.0$, $T = 383$ K (□)). Solid symbols: CT-275 ($R_{A/O}^0 = 0.5$, $T = 363$ K (▼); $R_{A/O}^0 = 0.5$, $T = 383$ K (▲); $R_{A/O}^0 = 1.0$, $T = 383$ K (■))

According to literature [127], A-35 is expected to be more active than CT-275 due to its higher acid capacity, regardless the difference might be scarce. Accordingly, the higher the activity of a catalyst, the higher the total formation of products and/or byproducts should be expected. Nonetheless, in this particular case, this premise was not accomplished in the experiments at the highest temperature.

After analyzing each byproduct individually, it was determined that the shift of the most active catalyst in the byproducts formation from A-35 to CT-275 as temperature was raised from 363 to 383 K was mainly due to an increase in the isobutene dimers production as well as, though in minor extension, in the ESBE production. This shift could be explained by morphological differences between catalysts. A-35 would experience internal diffusion problems due to its smaller pore diameter that would become apparent at higher temperature, which is when dimerization is more favored. A sufficiently high amount of dimers could eventually block, at least partially, the pores of A-35 and, therefore, hinder the species diffusion for larger molecules as TMP-1, TMP-2, and ESBE. Such phenomenon would not occur, or it could occur in a much lower extension, with CT-275 because it presents a larger pore size (Table 2.3).

With respect to products distribution (Figure 4.15), strong differences were detected between the two resins at 363 K and $R^{\circ}_{A/O} = 0.5$, where A-35 clearly favored isobutene dimerization compared to CT-275. This difference was reduced by increasing the temperature to 383 K, at the same $R^{\circ}_{A/O} = 0.5$, where both catalysts presented similar isobutene selectivity towards each byproduct. Consequently, a higher temperature reduces the effects of the structural catalyst properties on selectivity. Finally, at 383 K and $R^{\circ}_{A/O} = 1.0$, isobutene selectivity towards dimers was more enhanced by A-35 than by CT-275. Selectivity towards TBA was higher for CT-275 than for A-35, what can be explained by the lesser consumption of isobutene due to the competitive irreversible reaction of dimerization. Evolution of ethanol selectivity towards products showed similar trends to those described here.

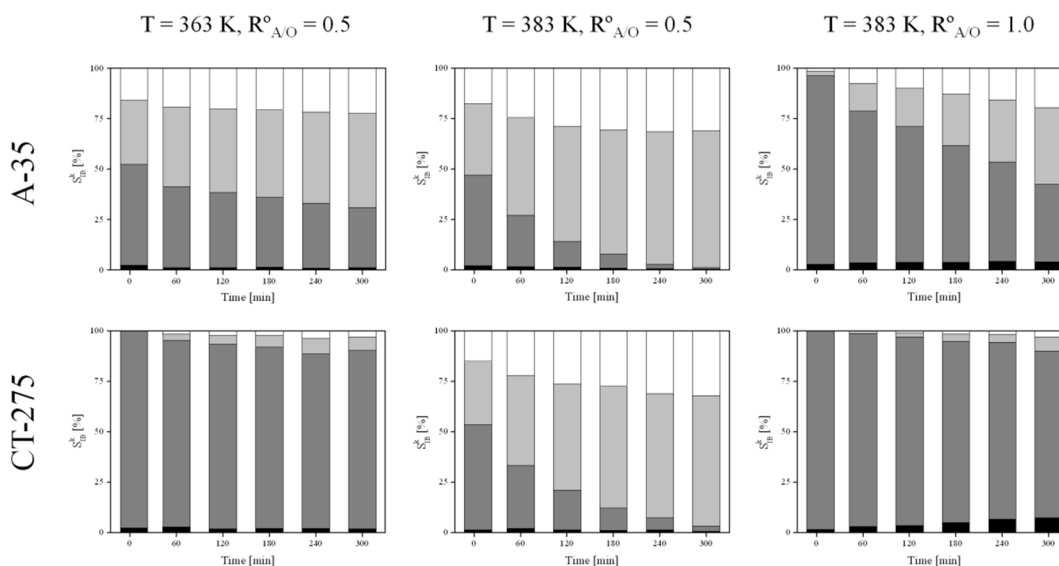


Figure 4.15 Evolution of products distribution in terms of isobutene selectivity to TBA (■), ETBE (■), TMP-1 (■), and TMP-2 (□) with A-35 and CT-275. Catalyst load = 10%wt., $d_p = 0.25\text{-}0.40$ mm, 500 rpm

In order to give an explanation to the results plotted in Figure 4.15, it has to be considered that at high temperatures, namely 363 and 383 K, the fastest reversible reactions, ETBE and TBA, could reach positions close to chemical equilibrium

conditions rapidly, irrespectively of the used catalyst. Then, as slower side reactions proceeded, the reversible reactions could move to the left side, leaving free isobutene that could dimerize. Therefore, Figure 4.15 shows an increasing selectivity towards TMP-1 and TMP-2 through the experiments.

From the catalysts properties standpoint, it is necessary to bear in mind that the most active catalyst for the main reaction is also the most active one for side reactions. So, in general, A-35 was progressively more selective than CT-275 towards larger molecules, as TMP-1 and TMP-2. Additional explanation for such phenomenon could be the slightly higher specific surface area of A-35 that could lead to a more suitable spatial distribution of acid centers to form isobutene dimers. To support this hypothesis, literature data showed that, operating under the same temperature range (343-383 K), in the isobutene dimerization reaction in the presence of *tert*-butyl alcohol, the more selective ion-exchange catalyst assayed for the isobutene dimerization was the one with the highest specific surface area [121]. However, more than two catalysts should be tested in order to establish a proper correlation between the chemical reaction and the catalyst properties.

With regard to the experiments at 383 K and $R^{\circ}_{A/O} = 0.5$, also in Figure 4.15, the almost identical products distribution evolution experienced by the two catalysts evidences that given such favoring conditions –in terms of dimerization reaction–, morphological differences between the catalysts were not significant enough so as to lead to different behavior. Perhaps, in excess of olefin, the resins structures could be partially collapsed and the advantages of A-35 towards dimerization were not shown because the accessibility to its acid centers decreased more than for CT-275.

Considering the three experiments, it has to be pointed out that CT-275 led to higher productions of ETBE than A-35, within the experimental conditions assayed. At 383 K, though, CT-275 also produced more byproducts than A-35.

4.4 Conclusions

Dimerization of isobutene, giving TMP-1 and TMP-2, was the most relevant side reaction. Low molar ratios and high temperatures enhance this reaction. High temperatures enhanced DEE formation. Excess of ethanol produced scarcely more DEE than low molar ratios and that was related to slow kinetics of the ethanol dehydration reaction. At the conditions assayed, TBA was produced in very low quantities. Although at low temperatures, selectivity towards TBA at the end of the experiment was almost zero, at high temperatures, the higher the molar ratio, the higher the selectivity towards TBA. Possible explanation implies a combined effect of the dehydration of ethanol, what produces water, and the readiness with which isobutene reacts with this water. There was a strong effect of the loaded water over this side reaction. ESBE formation was detected only at high temperatures but the selectivity towards it achieved values up to 50%. Low feed molar ratios also enhanced this side reaction.

Finally, it can be stated that high temperatures strongly enhance the formation of all the byproducts studied –kinetics of the side reactions are strongly affected by temperature– whereas initial molar ratios have a strong influence on the nature of side reactions that are favored.

Concerning the catalysts comparison, CT-275 led to higher productions of ETBE than A-35, within the experimental conditions assayed. However, at 383 K, CT-275 also produced more byproducts than A-35.

Minimum ETBE production was detected in experiments at high temperatures and low molar ratios. Selectivity of the two reactants towards ETBE was slightly higher at $R_{A/O}^{\circ} = 2.0$ than at $R_{A/O}^{\circ} = 1.0$. However, at $R_{A/O}^{\circ} = 2.0$, part of the ethanol did not react. Then, in order to minimize side reactions along with the ETBE reaction synthesis, it is advisable to control the cooling system –so hot-spots should be minimized–, to work with molar ratios slightly higher than the stoichiometric one and to keep the feedstock as free from water as possible.

5. Effect of reaction media and ion-exchange resins properties on the liquid-phase etherification of isobutene with C₁ to C₄ linear primary alcohols

THE PRESENT CHAPTER IS AN ADAPTED VERSION OF THE WORK

J.H. Badia, C. Fité, R. Bringué, E. Ramírez, M. Iborra. Relevant properties for catalytic activity of sulfonic ion-exchange resins in etherification of isobutene with linear primary alcohols. *Journal of Industrial and Chemical Engineering*, 42, 2016, 36-45.

5.1 Introduction

The isobutene etherification reaction with linear primary alcohols larger than ethanol might entail a change of the reaction medium properties, in comparison to MTBE and ETBE productions, that can affect the catalytic performance of the ion-exchange resins used as catalysts.

A number of works that studied the etherification of olefins with alcohols of a different number of carbon atoms can be found in literature, where ion-exchange resins were used as catalysts [22,59,104,142–144]. Many of these studies focused on the reactivity of one olefin with one alcohol, while others compared the behavior of various alcohols to draw conclusions on the reaction mechanism and the effect of reactant properties on the etherification. None of these works focused on the catalytic performance of used ion-exchange resins.

In the present chapter, sixteen ion-exchange resins are assayed to compare their performance in the etherification reaction of isobutene with methanol, ethanol, 1-propanol, and 1-butanol. In this way, relations can be established between catalytic activities, resins features and reaction medium properties. Given the large number of properties and characteristics of these catalysts often found in literature, a systematic approach is developed to determine which ones have an actual relation with the resin catalytic performance in this type of reactions.

5.2 Experimental

5.2.1 Chemicals and catalysts

Reactants were methanol, ethanol, 1-propanol, 1-butanol, and a synthetic C₄ mixture as the isobutene source. Additionally, the following chemical standards were used for analytical procedures: 2-methoxy-2-methylpropane (MTBE), 2-ethoxy-2-methylpropane (ETBE), 2-methyl-2-propoxypropane (PTBE), 1-*tert*-butoxybutane (BTBE), 2-methyl-2-propanol (TBA), diethyl ether (DEE), 2,4,4-trimethyl-1-pentene (TMP-1), and 2,4,4-trimethyl-2-pentene (TMP-2).

A total of sixteen ion-exchange resins were used as catalysts. They were all sulfonated macroreticular polymers with a styrene-divinylbenzene backbone. Twelve resins are commercially available, supplied by Rohm & Hass (Amberlyst™ type) and by Purolite® (namely: A-15, A-16, A-35, A-36, A-39, A-40, A-46, A-48, A-70, CT-175, CT-252, and CT-275), and four had been produced in the lab (named as 306, 406, 606, and 806 [53]). Their most relevant characteristics have been listed in Tables 2.2 and 2.3. Pretreatment of catalysts consisted in reducing their water content and crushing and sieving to obtain designated particle size ranges.

The used resins present a wide range of the properties of interest: acid capacity (from 0.8 to 5.6 meqH⁺ / g_{cat}); crosslinking degree (low, medium, and high); and sulfonation type (oversulfonated, conventionally sulfonated, partially sulfonated, and surface sulfonated).

This variety of properties was chosen to cover a wide range of morphological and chemical features to allow identifying which are relevant to the catalytic activity.

5.2.2 Apparatus, procedure and analysis

The experimental setup consisted of a catalytic fixed bed tubular microreactor submerged in a thermostatic bath to maintain the reactor at the desired temperature. In order to get an isothermal reactor bed, catalyst was diluted with silicon carbide of the same particle size range. Silicon carbide had been proven to be inert in terms of reaction. If catalyst dilution were too large, preferential paths or by-passing effects could arise. In a previous work [19], it was found that inert/catalyst mass ratios up to 300 did not affect the kinetic results for the present system. Therefore, dilution was kept under that value for all the experiments to avoid back-mixing and channeling.

Experiments were carried out at 333 K. Reactor feed was free of product, what means null isobutene conversion level at the reactor inlet. Alcohol to olefin molar ratio ($R_{A/O}^0$) at the reactor inlet was set to 1.0.

Firstly, only alcohol was fed and the reactor was submerged in the thermostatic bath, similarly to industrial scale reactor startups. The aim of this procedure is to heat up the catalyst bed and to reduce, as much as possible, the remaining water in the catalyst by alcohol percolation (the final water content in the resin can be considered lower than 1%wt. [84]). Afterwards, the C₄ mixture was added to the reactor feed while maintaining a constant alcohol flow. This moment was considered the beginning of the experiment. Around 3-4 h were needed for each kinetic run to reach the steady state. This fact was verified by repeated chromatographic analysis at the reactor outlet.

Along every experimental run, samples of the reaction medium were taken inline from the reactor inlet and outlet streams through two sampling valves that injected 0.2 μ L of pressurized liquid into an Agilent gas chromatograph 7890A equipped with a capillary column (100% dimethylpolysiloxane, 50 m \times 0.20 mm \times 0.50 μ m). Helium was used as the carrier gas with a flow of 0.75 mL / min. Oven temperature ranged from 308 to 343 K depending on the considered reaction. This analytical system allowed identifying and quantifying the reactants, the inert components of the C₄ mixture, the formed ether and the reaction byproducts, when formed.

5.2.3 Calculations

Experimental results were quantified in terms of reaction rate with respect to isobutene, by means of the following expression, which applies to a plug-flow fixed bed catalytic reactor at differential regime:

$$\text{Reaction rate: } -r_{IB} = \frac{F_{IB}^0 (X_{IB,outlet} - X_{IB,inlet})}{W_{cat}} \quad (5.1)$$

where F_{IB}^0 is the isobutene reference molar flow at null conversion, $X_{IB,outlet}$ is the isobutene conversion at the reactor outlet, $X_{IB,inlet}$, the inlet isobutene conversion, was zero, and W_{cat} is the catalyst mass in dry basis.

$$\text{Relative conversion: } X_{IB} = 1 - \frac{F_{IB,outlet}}{F_{IB,inlet}} \quad (5.2)$$

In order to provide an empirical relationship between catalysts features and reaction rates, a response surface methodology analysis was carried out by means of the stepwise procedure, considering a second-order polynomial expression with interaction terms as follows:

$$y = \beta_0 + \sum_{i=1}^k \beta_i x_i + \sum_{i=1}^k \beta_{ii} x_i^2 + \sum_{i < j=1}^k \sum_{j=1}^k \beta_{ij} x_i x_j \quad (5.3)$$

where y is the response variable, x the independent variables, and β the equation coefficients.

5.3 Results and discussion

5.3.1 Reaction system

The studied reactions were the alkyl *tert*-butyl ether syntheses from isobutene and linear primary alcohols with one to four carbon atoms. Alkyl *tert*-butyl ethers are formed by addition of the corresponding alcohol to isobutene (IB). Methanol (MeOH), ethanol (EtOH), 1-propanol (1-PrOH), or 1-butanol (1-BuOH) were used to obtain, respectively, methyl *tert*-butyl ether (MTBE), ethyl *tert*-butyl ether (ETBE), propyl *tert*-butyl ether (PTBE), or butyl *tert*-butyl ether (BTBE) (Figure 5.1).

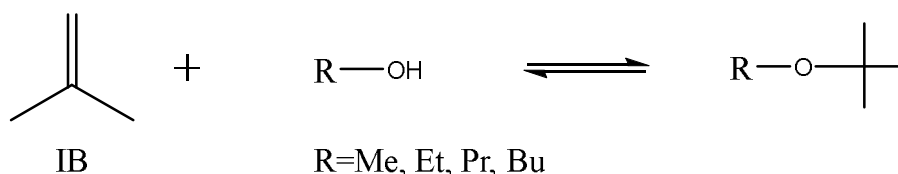


Figure 5.1 Main reactions involved

This type of reactions can be explained by a mechanism consisting in a series of elementary steps. Firstly, reactants adsorb on the resin active sites, then the surface reaction between the adsorbed alcohol and isobutene follows, producing a molecule of adsorbed ether which, finally, desorbs [131]. All reactions should proceed through a similar mechanism, since the only difference is the number of carbon atoms in the alcohol chain.

Possible side-reactions comprise isobutene dimerization to form 2,4,4-trimethyl-1-pentene and 2,4,4-trimethyl-2-pentene, isobutene hydration to form *tert*-butyl alcohol, alcohol dehydration to form the corresponding symmetric ether and water, and etherification of 2-butene from the synthetic C₄ mixture with alcohol to form the corresponding alkyl *sec*-butyl ether. Byproduct formation was avoided (less than 0.3% GC) by setting a relatively low temperature (333 K) and the stoichiometric initial molar ratio alcohol/olefin ($R_{A/O}^0 = 1.0$). These conditions were known to be the less favorable

ones for side-reactions to occur according to literature data on the present reaction systems and similar ones [86,87] (see Chapter 4). In particular, byproducts formation can be dismissed in the present work, because the relative difference of the molar carbon balance applied to every experimental point by considering only the etherification reaction was always below 2%.

5.3.2 Preliminary experiments

To evaluate reaction rates as a basis of the composition change between reactor inlet and outlet using Equation 5.1, the reactor needs to operate under differential regime (i.e., reaction rates can be considered constant along the reactor). For both MTBE and ETBE systems, literature data showed that the reactor behaves differentially when isobutene conversion levels are up to 10% [136,138]. This value has been confirmed experimentally also for PTBE and BTBE systems, as seen in Figure 5.2. Therefore, the mass of catalyst in the experiments was chosen to obtain values of isobutene conversion up to around 10% at 333 K.

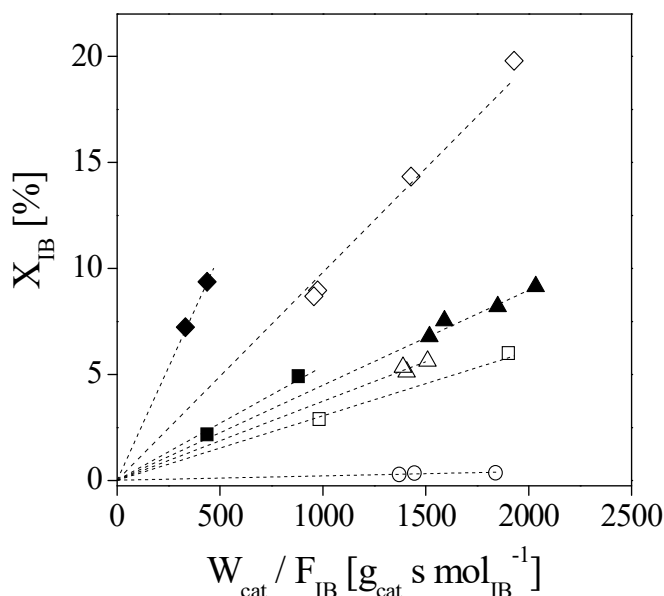


Figure 5.2 Isobutene conversion with different catalysts vs. W_{cat}/F_{IB} at 333 K and $R_{A/O}^0 = 1.0$ for the studied reaction systems. MTBE: A-35 (△) and A-46 (○); ETBE: A-35 (▲); PTBE: CT-275 (◇) and A-39 (□); BTBE: CT-275(◆) and A-39 (■)

With respect to the external mass transfer influence, experiments were carried out at different flow rate values, characterized by the weight hourly space velocity (WHSV), in the four considered reaction systems for a choice of catalysts. Selected resins cover the whole range of catalysts properties. As Figure 5.3 (a and b) shows, the external mass transport influence can be neglected at least for WHSV higher than 500 h⁻¹ at 333 K, which corresponds to a linear velocity higher than 0.17 cm/s calculated for empty tube.

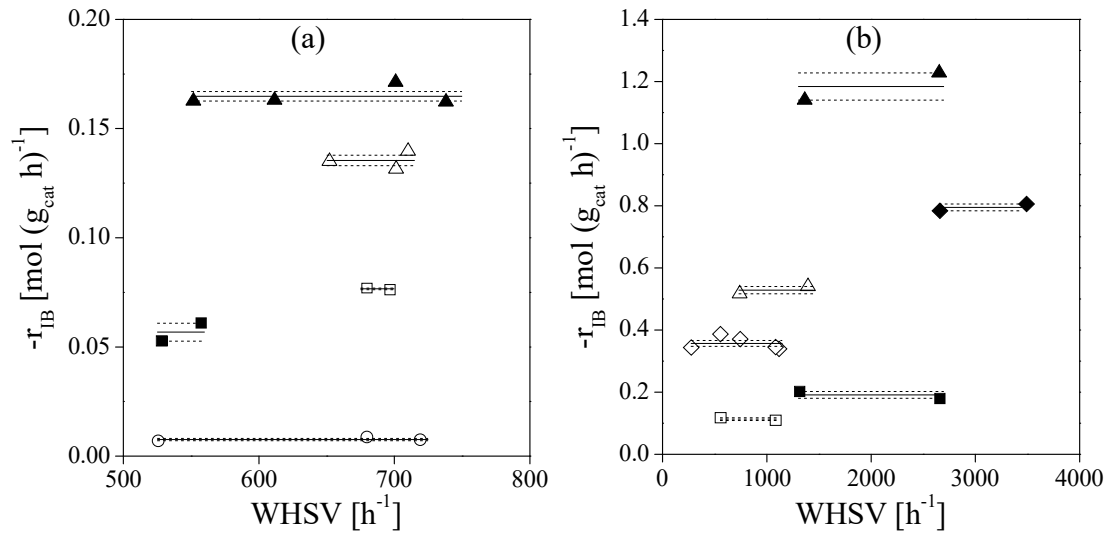


Figure 5.3 Influence of external mass transport on the rate at 333 K and $R^o_{A/O} = 1.0$. (a) MTBE: A-35 (Δ), A-39 (□), A-46 (○); ETBE: A-35 (▲), A-39 (■). (b) PTBE: A-35 (Δ), CT275 (◇), A-39 (□); BTBE: A-35 (▲), CT-275 (◆), A-39 (■). —: mean value; - - -: standard uncertainty margin

Regarding the possible influence of internal mass transfer effects on reaction rates, due to diffusion of species within the resin backbone, these effects would become more apparent with bigger molecular size of involved species, and larger particles for a catalyst with relatively small pore volume, resulting in measured reaction rates lower than without diffusional effects. To cover the wide range of pore volume, experiments for both PTBE and BTBE synthesis reactions were carried out with CT-275 and A-39, which present the largest and the smallest pore volumes, respectively, among the assayed catalysts. As seen in Figure 5.4, internal mass transfer effects can be considered as negligible, within the experimental error, at 333 K and $R^o_{A/O} = 1.0$ for all assayed bead sizes. Since the involved molecules in the MTBE and ETBE reaction systems are smaller, internal mass transfer effects are expected to be non-significant under the same experimental conditions.

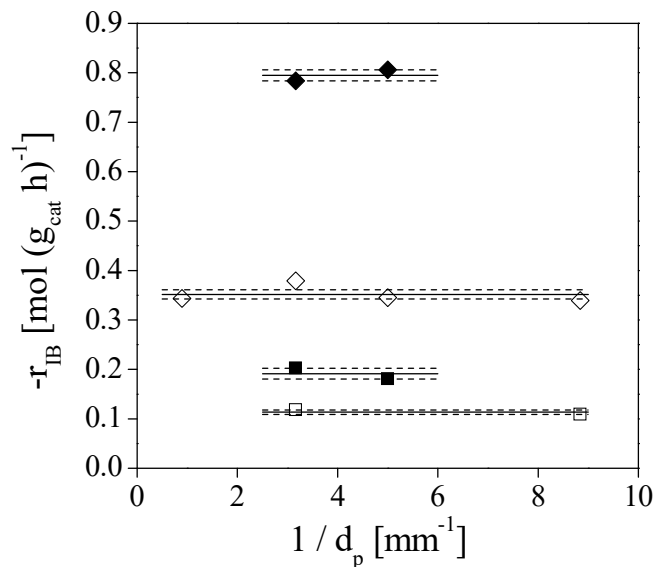


Figure 5.4 Influence of internal mass transport on the rate at 333 K and $R^o_{A/O} = 1.0$
 PTBE: CT-275 (◇) and A-39 (□); BTBE: CT-275 (◆) and A-39 (■)
 (—: mean value; - - -: standard uncertainty margin)

5.3.3 Effect of the linear primary alcohol on the alkyl *tert*-butyl ether syntheses

Table 5.1 lists reaction rates of each assayed ion-exchange resin in the four considered reactions. As seen, reaction rates with respect to the alcohol type followed the order 1-butanol > 1-propanol > ethanol > methanol, already described in literature [59], in the experiments with more active catalysts. These catalysts were A-15, A-35, A-36, A-40, A-48, CT-175, CT-252, and CT-275. In the experiments with less active catalysts, methanol was more reactive than ethanol. These catalysts were A-16, A-39, A-46, A-70, 306, 406, 606, and 806. Regarding the reproducibility of the experimental results presented in Table 5.1, although not all the experiments were replicated, the uncertainties associated to experimentally determined rates range 0.5 to 7%, which is an acceptable level of experimental error. It can be assumed that the uncertainty of the experiments that were not replicated would be of the same order.

Table 5.1 Reaction rates for alkyl *tert*-butyl ethers. Standard uncertainty for replicated experiments is presented. T = 333 K, R^o_{A/O} = 1.0, d_p = 0.25-0.40 mm, WHSV > 500 h⁻¹

Catalyst	$-r_{IB}$ [mol (g _{cat} h) ⁻¹]			
	MTBE	ETBE	PTBE	BTBE
A-15	0.098 ± 0.002	0.117	0.275	
A-16	0.0951 ± 0.0017	0.0812	0.211	0.457
A-35	0.135 ± 0.002	0.1624 ± 0.0002	0.529 ± 0.012	1.228
A-36	0.136	0.140		
A-39	0.0766 ± 0.0005	0.057 ± 0.004	0.113 ± 0.004	0.191 ± 0.011
A-40	0.109	0.126		
A-46	0.0076 ± 0.0005	0.0061	0.0082	0.0186
A-48	0.135	0.152		
A-70	0.0393	0.0240	0.0414	0.0596
CT-175	0.101	0.126		
CT-252	0.114	0.118		
CT-275	0.125	0.133	0.379 ± 0.008	0.795 ± 0.011
306	0.0058	0.0052	0.0064	0.0119
406	0.0084	0.0058	0.0089	0.0160
606	0.01982 ± 0.00013	0.0158	0.0328	0.0583
806	0.0432	0.0380	0.0980	0.2041

In a first approach, the observed reactivity variation can be explained in terms of the used alcohol and the subsequent reaction medium properties variation. Table 5.2 summarizes alcohols most relevant properties.

Table 5.2 Alcohols properties

Alcohol	Number of carbon atoms	Molar weight [g mol ⁻¹]	Molar volume ^a [cm ³ mol ⁻¹]	Molecular length ^b [nm]	Dipole moment ^c [D]	pK _a ^d	Hildebrand solubility parameter, δ [MPa ^{1/2}] ^e
MeOH	1	32.04	42.10	0.30	1.700	15.09	27.9
EtOH	2	46.07	60.20	0.41	1.691	15.93	25.2
1-PrOH	3	60.10	77.64	0.55	1.679	16.10	23.4
1-BuOH	4	74.12	94.28	0.66	1.661	16.10	21.8

^a Hankinson-Brobst-Thomson (HBT) method at 1.5 MPa and 333 K [88,89]. ^b Calculated from the distances and angles of bonds between atoms using ChemBioOffice 2013 software, as it allows drawing molecules in their conformation of minimum energy. ^c [145]. ^d [146]. ^e Estimated at 1.5 MPa and 333 K according to [88,89,145].

From values in Table 5.2, it can be observed that some alcohol properties are correlated with the alcohol length. In this sense, alcohols molar weight, volume, and length increase proportionally with their number of carbon atoms. In contrast, dipole moment and Hildebrand solubility parameter diminish in different manner as the number of carbon atoms increases, while pK_a hardly changes. Isobutene reaction rate for the tested catalysts in the four reaction systems is plotted as a function of some alcohol properties in Figure 5.5.

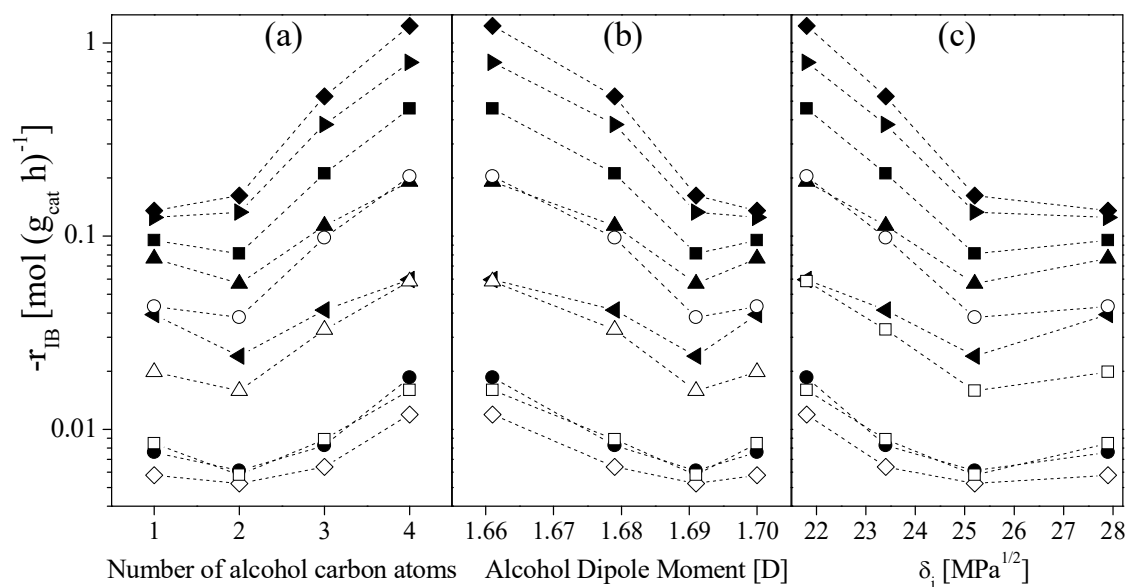


Figure 5.5 Isobutene reaction rate values for different catalysts versus number of alcohol carbon atoms (a), dipole moment (b), and Hildebrand solubility parameter (c). $T = 333 \text{ K}$, $R_{A/O}^{\circ} = 1.0$, $d_p = 0.25\text{-}0.40 \text{ mm}$, $\text{WHSV} > 500 \text{ h}^{-1}$. A-16 (■), A-35(◆), A-39 (▲), A-46 (●), A-70 (◄), CT-275 (►), 306 (◇), 406 (□), 606 (Δ), 806 (○)

Globally, from Figure 5.5a, isobutene reacts faster with larger alcohols: BTBE formation is the fastest reaction, PTBE is about the half, and ETBE and MTBE formation, both similar, are about the third. Reaction rate decreases with alcohol polarity (Figure 5.5b), what could be explained by the ease of more polar compounds to swell the resin backbone and to solvate the acidic protons of the sulfonic groups by breaking the hydrogen bond network. Then, although more catalytic centers become accessible to reactants by the swelling effect, the proton donor-acceptor strength of these centers is reduced by the protons solvation, with a result of lower reaction rates [50,130,136,142,147,148].

On the other hand, as seen in Figure 5.5c, rates generally increase for alcohols presenting lower values of the Hildebrand solubility parameter, δ . This parameter accounts for the interaction between the liquid mixture and the resin: compounds with similar values of δ are likely to present a higher affinity. Thus, alcohols presenting a higher affinity for a resin can permeate easier into it and reach a larger number of active sites, what would contribute to enhance reaction rates. The Hildebrand solubility parameter of each used resin, δ_p , can be estimated at 298 K by a group contribution

method [149], their values ranging 22.4-25.6 MPa^{1/2} (Table 5.3), by means of the following expression:

$$\delta_p = \sqrt{\frac{\sum_i x_i E_{coh,i}}{\sum_i x_i V_i}} \quad (5.4)$$

In Equation 5.4, x_i , $E_{coh,i}$ and V_i correspond, respectively, to the molar fraction, the cohesion energy and the molar volume contribution of the structural group i , present in the resin. At the operating temperature of 333 K, δ_p values are expected to either remain constant or to slightly decrease in comparison to those in Table 5.3 [150]. The value of δ presented by ethanol is globally closer to the δ_p values presented by most resins, with some exceptions: resins A-46, 306, and 406 present δ_p values closer to those of 1-butanol and A-70, 606, and 806 present δ_p values closer to 1-propanol. This fact would be related to the ease of permeation of these alcohols into the catalyst backbone in the mentioned cases.

Table 5.3 Estimated values of each resin Hildebrand solubility parameter at 298 K

Catalyst	δ_p [MPa ^{1/2}] ^a
A-15	24.9
A-16	24.7
A-35	25.4
A-36	25.2
A-39	24.6
A-40	25.1
A-46	22.4
A-48	25.6
A-70	23.2
CT-175	25.0
CT-252	25.2
CT-275	25.2
306	22.4
406	22.5
606	22.9
806	23.6

^a Estimated at 298 K [149]

In the actual reaction medium, though, alcohols only represent a relatively small proportion of the reactive liquid mixture in contact with the resin. Then, if Hildebrand solubility parameters of the mixture, δ_M , are used instead of δ for each alcohol, their differences respect δ_p values are much higher: mean δ_M values were 13.287 ± 0.001 , 13.271 ± 0.007 , 13.75 ± 0.02 , and 13.53 ± 0.04 MPa^{1/2} for MTBE, ETBE, PTBE, and BTBE systems, respectively. As seen in Figure 5.6, $(\delta_p - \delta_M)$ difference values in the syntheses involving 1-propanol and 1-butanol are, globally, slightly smaller than when involving methanol and ethanol. This fact would be related to the observed reactivity gradation.

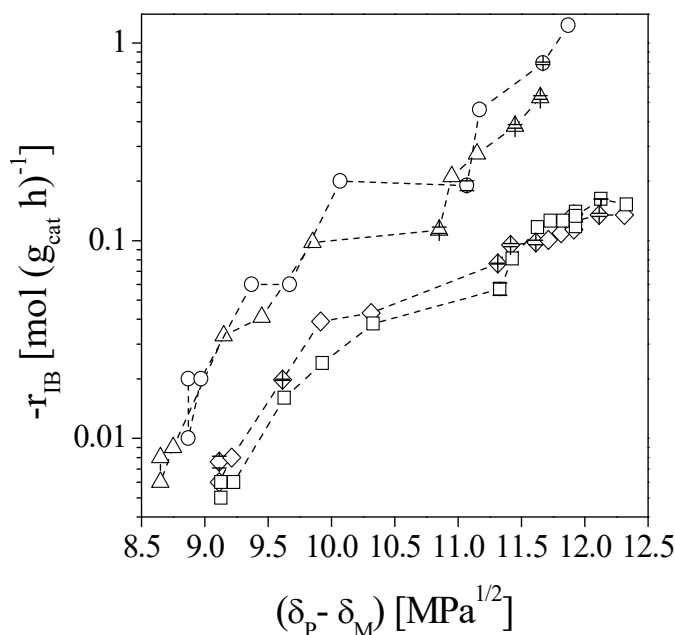


Figure 5.6 Isobutene reaction rate values for each synthesis reaction versus differences between the Hildebrand solubility parameter of the polymer, δ_p , and that of the medium, δ_M . T = 333 K, $R^{\circ}_{A/O} = 1.0$, $d_p = 0.25\text{-}0.40$ mm, $\text{WHSV} > 500$ h⁻¹. MTBE (◇), ETBE (□), PTBE (Δ), BTBE (○)

Figure 5.6 shows a similar trend of the isobutene consumption rate with respect to $(\delta_p - \delta_M)$ difference for every reaction system. This fact supports that the affinity between the resin and the reaction medium would affect similarly the catalytic activity for different reaction systems.

5.3.4 Relation between resins properties and catalytic activity

As seen in both Figures 5.5 and 5.6, the relative reactivity of a given resin compared to the others hardly changes irrespectively of the alcohol, what would indicate a relation between the resin morphological properties and its activity.

Acid capacity is often found in literature for some acid-catalyzed reactions as a key factor of the catalytic activity of a resin, e.g., [59]. In this sense, Figure 5.7, which plots reaction rate against resins acid capacity, shows that reaction rate globally increases as acid capacity increases, but that this trend becomes less clear for highly acidic resins (>4.8 meqH⁺ g_{cat}⁻¹). It has been stated that high sulfonic groups concentration can also have a counter effect regarding accessibility of reactants towards active sites because of steric hindrances [147], what could lower their overall efficiency per active center. As a conclusion, it seems that the acid capacity is not the only determining factor to explain catalysts activity differences. Therefore, to consider the effect of other properties seems necessary to quantify the effect of the catalysts features that have an actual influence on resins catalytic activity.

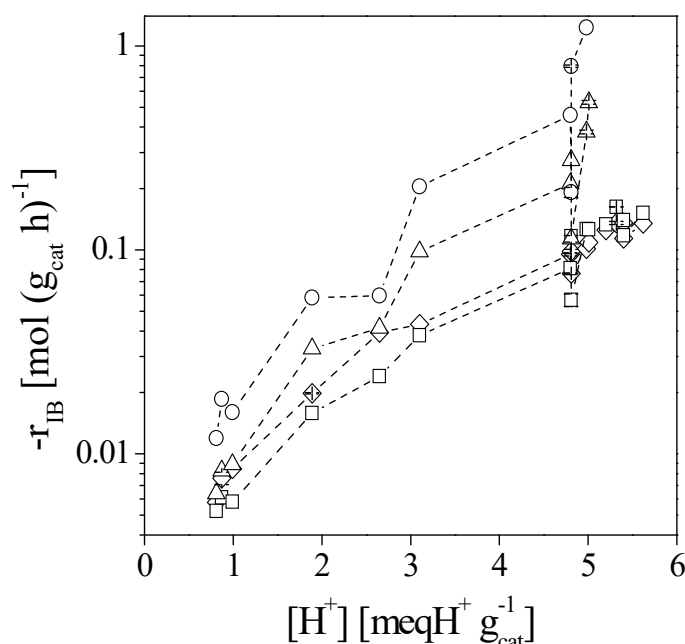


Figure 5.7 Reaction rate as a function of catalysts acid capacity. T = 333 K, R^o_{A/O} = 1.0, d_p = 0.25-0.40 mm, WHSV > 500 h⁻¹. MTBE (◇), ETBE (□), PTBE (△), BTBE (○)

To elucidate significant effects of catalyst characteristics, the main properties (Table 2.2) and the morphological properties in both dry and water-swollen state (Table 2.3) have been taken into account to develop an empirical model that correlates reaction rates and relevant catalyst properties. Dry-state characteristics include the BET (Brunauer-Emmett-Teller) surface area, the BJH (Barret-Joyner-Halenda) desorption cumulative surface area and volume of pores, and the mean pore size. The considered water-swollen state characteristics were the surface area, volume and size of meso-macropores, as well as the specific volume of swollen polymer, which corresponds to the micropore-size cavities in the resins gel-phase, as determined by ISEC technique [45,65,66].

A response surface methodology analysis has been used to find the most significant factors that explain reaction rate variability in terms of resins properties for each reaction system. The searched model consists of an expression with the lowest number of terms in which all parameters and the regression itself are statistically significant within a 95% confidence level. Independent variables were coded each to fit the range -1 to +1. The best empirical model for each reaction was searched among second order polynomials with interaction terms by means of the stepwise procedure. As polynomials are empirical models, square roots of etherification rates, rather than actual rates, were used as response variable, because they provided a better fit, and residuals followed more closely a normal distribution. Table 5.4 lists the parameter values, with their standard uncertainty and *p*-value, the regression F statistic, and the adjusted R² for the resulting best empirical model for each reaction system using coded regressors.

Table 5.4 Data analysis for coded regressors

Reaction		Term				F _{reg}	R ² _{adjusted}
		β ₀	β ₁ ([H ⁺])	β ₂ (V _{sp})	β ₁₂ ^a ([H ⁺]·V _{sp})		
MTBE	Coefficient	0.219	0.141	-0.016	–	577.9	0.987
	p-value	<0.0001	<0.0001	0.0195	–		
	St. uncertainty	0.003	0.004	0.006	–		
ETBE	Coefficient	0.212	0.147	-0.038	-0.029	261.7	0.981
	p-value	<0.0001	<0.0001	0.0013	0.0343		
	St. uncertainty	0.005	0.006	0.009	0.012		
PTBE	Coefficient	0.328	0.259	-0.104	-0.101	169.7	0.981
	p-value	<0.0001	<0.0001	0.0008	0.0046		
	St. uncertainty	0.009	0.014	0.018	0.025		
BTBE	Coefficient	0.477	0.390	-0.200	-0.173	129.3	0.977
	p-value	<0.0001	<0.0001	0.0007	0.0059		
	St. uncertainty	0.017	0.024	0.032	0.041		

^a The ([H⁺]·V_{sp}) term was statistically non-significant for the MTBE system

According to the analysis results, reaction rates depend on the same two resin properties, irrespectively of the considered reaction system: the acid capacity, [H⁺], and the specific volume of swollen polymer, V_{sp}. Results suggest a linear effect of [H⁺] and V_{sp} on $\sqrt{-r_B}$ in every reaction system, and also an interaction effect of [H⁺]·V_{sp}, except for MTBE. Any other resin property effect was found to be statistically non-significant. Table 5.4 shows that each fitted parameter presents the same sign for the different reaction systems, and therefore the corresponding property affects reaction rate in the same sense. For instance, since β₁ is positive, [H⁺] enhances reaction rate, and negative values of β₂ and β₁₂ indicate that both V_{sp} and the interaction term [H⁺]·V_{sp} have a detrimental effect on reaction rates. Moreover, the relative importance of regressors in each reaction system has been assessed to determine the relative effect of each term [151]. Results, plotted in Figure 5.8, show that [H⁺] is by far the factor with the highest relative impact, and it gradually loses weight as the alcohol size increases. In contrast, V_{sp} and the interaction term [H⁺]·V_{sp} have a very low effect on reaction rate in the MTBE system, but their relative importance increases substantially with larger alcohols. This fact can be attributed to the relation of V_{sp} with the empty space between polymer chains of the resin, a factor that becomes more important for larger molecules.

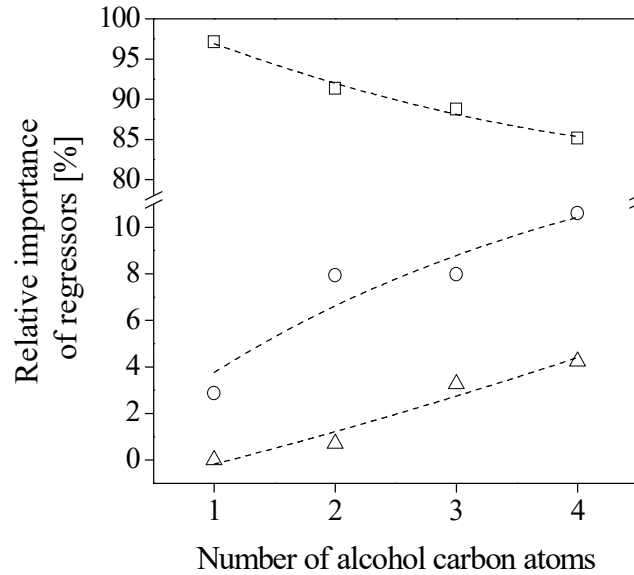


Figure 5.8 Relative importance of regressors versus number of alcohol carbon atoms.

[H⁺] (□), V_{sp} (○) and [H⁺]·V_{sp} (Δ)

The derived expressions, in terms of uncoded regressors, are:

$$\text{MTBE: } \sqrt{-r_{IB}} = +0.0592 + 0.0585 [H^+] - 0.0272 V_{sp} \quad (5.5)$$

$$\text{ETBE: } \sqrt{-r_{IB}} = +0.0124 + 0.0825 [H^+] - 0.0023 V_{sp} - 0.0206 [H^+] V_{sp} \quad (5.6)$$

$$\text{PTBE: } \sqrt{-r_{IB}} = -0.0681 + 0.1796 [H^+] + 0.0520 V_{sp} - 0.0709 [H^+] V_{sp} \quad (5.7)$$

$$\text{BTBE: } \sqrt{-r_{IB}} = -0.0981 + 0.2877 [H^+] + 0.0531 V_{sp} - 0.1217 [H^+] V_{sp} \quad (5.8)$$

where $-r_{IB}$ is expressed in $\text{mol}(\text{g}_{\text{cat}} \text{h})^{-1}$, $[H^+]$ in $\text{meqH}^+ \text{g}_{\text{cat}}^{-1}$, and V_{sp} in $\text{cm}^3 \text{g}_{\text{cat}}^{-1}$. Figure 5.9 compares experimental and predicted reaction rates using Equations 5.5 to 5.8, which shows a satisfactory fit over the whole range of reaction rate values.

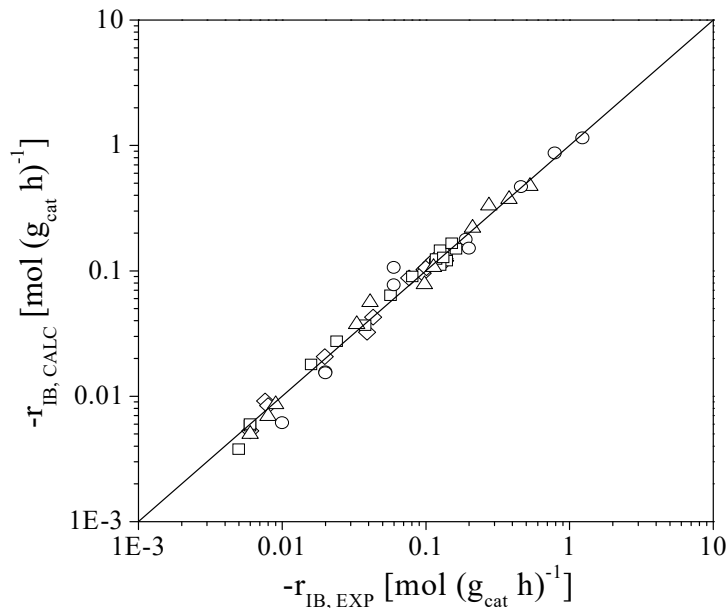


Figure 5.9 Reaction rate fit for the considered reactions. T = 333 K, R^o_{A/O} = 1.0, d_p = 0.25-0.40 mm, WHSV > 500 h⁻¹. MTBE (◇), ETBE (□), PTBE (Δ) and BTBE (○)

As Figure 5.10 illustrates, the shape of the response surface is similar for all considered reactions. Isobutene consumption rates increase with increasing $[H^+]$ and, as larger alcohols are used, a progressively increasing effect of low V_{sp} on rates is observed. On the other hand, the four response surfaces show very low reaction rate values and they are almost not sensitive to V_{sp} for resins with very low acid capacity (surface sulfonated resins 306, 406, and A-46).

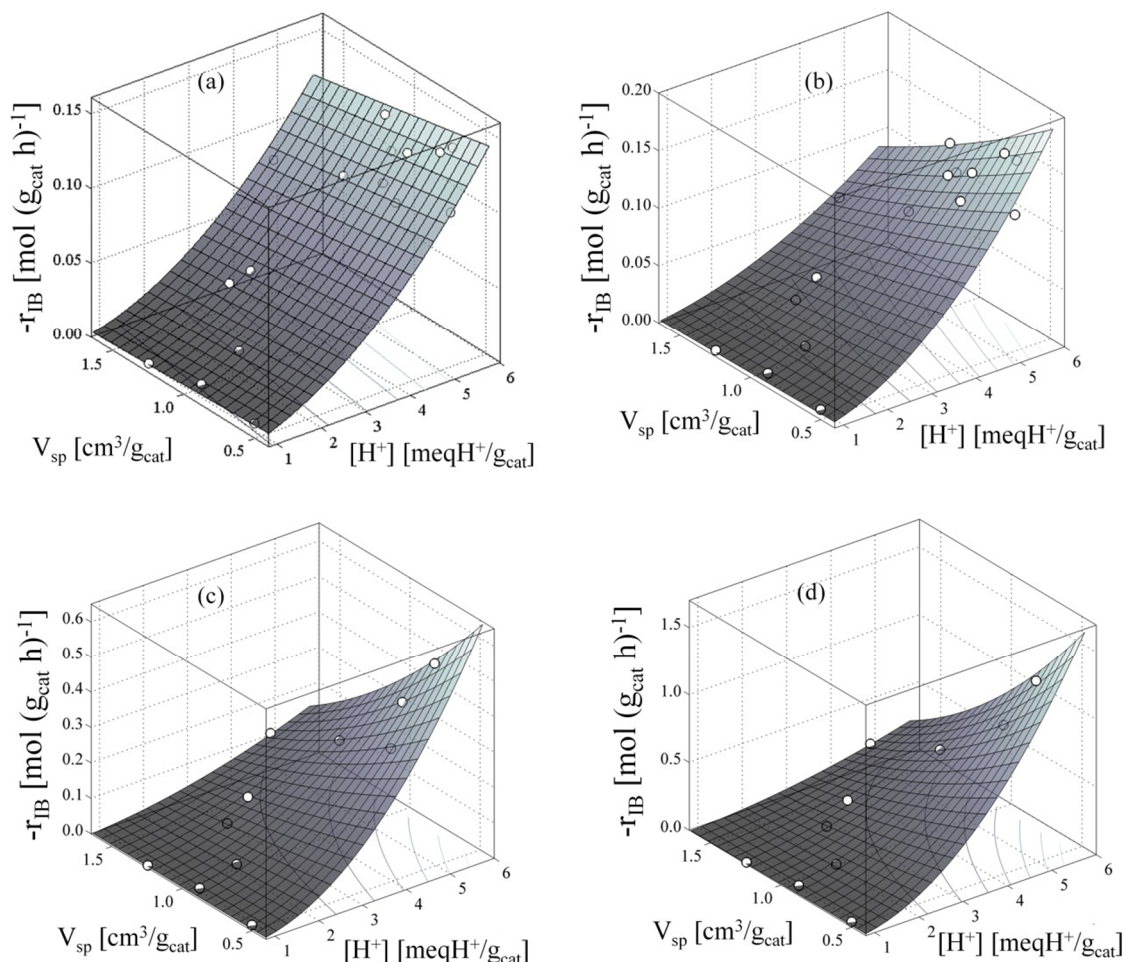


Figure 5.10 Response surfaces for the syntheses of MTBE (a), ETBE (b), PTBE (c), and BTBE (d)

These models allow us to provide an explanation regarding the relation between the resins morphological properties and their activity. As expected, a high acid capacity, $[H^+]$, favors etherification rates. As for the V_{sp} , a low value implies a more rigid structure, less swollen, when the resin is in the reaction medium. Such rigidity entailed faster rates and this effect is more accused for larger alcohols. From a catalyst manufacturer standpoint, this fact implies that maintaining a high active site local concentration in the gel phase and preventing an excessive swelling of the polymer backbone contributes to reach higher reaction rates. On the other hand, in regard to the reaction medium properties variation, present results point out that the reaction of isobutene with larger alcohols is more affected by the spatial conformation, and that the acid capacity of the catalysts plays a less important role.

It can be considered that the molecular size of all reactants is low enough so as not to expect steric hindrances when permeating through the resin network (see Chapter 6). Consequently, a larger network flexibility not only would not enhance etherification rates, by easing reactants transport through it, but it could reduce local concentration of active sites per unit volume, due to the increase of the distance between them. Therefore, a high active sites local concentration would lead to higher rates because reactants could coordinate to multiple active sites at the same time to form products readily.

Given that acid capacity and specific swollen polymer volume are able to explain most of the observed variability of rates, the relative magnitude $[H^+]/V_{sp}$, which can be defined as the active sites concentration in the gel phase [56], seems a reasonable combination of properties to assess the catalytic behavior of different resins (Figure 5.11).

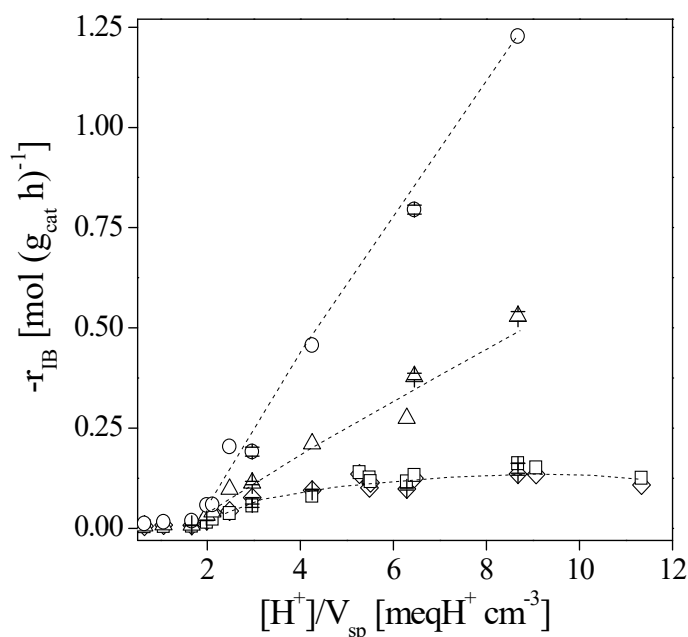


Figure 5.11 Reaction rate vs. $[H^+]/V_{sp}$. T = 333 K, $R_{A/O}^0 = 1.0$, $d_p = 0.25\text{-}0.40$ mm, WHSV > 500 h⁻¹. MTBE (◇), ETBE (□), PTBE (△) and BTBE (○)

Two well defined regions can be observed in Figure 5.11. At low $[H^+]/V_{sp}$ (< 2 meqH⁺ cm⁻³, characteristic of the partially sulfonated resins 306, 406, A-46, and 606) all reactions present very low and similar reaction rate values, probably due to a low amount of adsorbed species on the resins and to a large distance between adjacent active sites. At high $[H^+]/V_{sp}$ (> 2 meqH⁺ cm⁻³), reaction rates increase, attributable to a better coordination of reactant molecules with the active sites, because of the higher concentration of active sites in the gel phase. This reaction rate enhancement is sharper for reactions involving larger alcohols, what supports the idea that the studied reactants do not present steric hindrances, but, on the contrary, reaction of isobutene with larger alcohols is favored by interactions between the resin backbone and the longer hydrocarbon chain of the alcohol. It is worth mentioning that both MTBE and ETBE reaction rates seem to present a maximum value for $[H^+]/V_{sp} = 8.5\text{-}9$ meqH⁺ cm⁻³ and that rates slightly diminish from that value on. To confirm this issue, more experimental data should be gathered for the whole series of the studied reactions.

Finally, cross-matching $[H^+]/V_{sp}$ values with data in Table 5.1, it is observed that the alcohols reactivity followed the order of the alcohols series 1-butanol > 1-propanol > ethanol > methanol for resins with high $[H^+]/V_{sp}$ (5.3–11.3 meqH⁺ cm⁻³), whereas methanol and ethanol swap their position for resins with low $[H^+]/V_{sp}$ (0.6–4.2 meqH⁺ cm⁻³). In this sense, methanol would be able to penetrate deeper than ethanol into the gel phase in resins with low density of active sites (i.e. low $[H^+]/V_{sp}$ values), probably due to its smaller size and, therefore, methanol would access to a large number of active sites than ethanol, with a result of faster reaction rate. On the other hand, methanol would not be able to penetrate any deeper than ethanol into the gel phase in resins with a higher density of active sites (i.e. higher $[H^+]/V_{sp}$ values). In this situation, reactants transport within the gel-phase would be driven only by interactions between the polymer backbone of the resin and the hydrocarbon chain of the alcohol.

5.4 Conclusions

The catalytic performance of ion-exchange resins in the addition of isobutene to a homologous series of four linear primary alcohols to obtain methyl (MTBE), ethyl (ETBE), propyl (PTBE) and butyl *tert*-butyl ether (BTBE) has been studied. Sixteen different ion-exchange resins have been assayed to cover a wide range of properties. Globally, etherification reactions rates, for every resin, present an upward gradation as the alcohol is larger (1-butanol > 1-propanol > ethanol ~ methanol).

The response surface methodology has been applied to the kinetic results for each reaction system to identify the catalyst properties that determine the catalytic activity. In all cases, they were the acid capacity and the specific volume of the swollen polymer gel phase. Acid capacity has been, by far, the most important property, and the specific volume of the swollen polymer gel phase gains weight progressively as the alcohol size increases. An empirical equation for each reaction system has been provided that can explain satisfactorily the experimental reaction rate values, within a 95% confidence level. According to these models, highly-acidic resins with a rigid morphology are the most active catalysts in the present reaction systems.

6. Catalytic activity and accessibility of acidic ion-exchange resins in liquid phase etherification reactions

THE PRESENT CHAPTER IS AN ADAPTED VERSION OF THE WORK

J.H. Badia, C. Fité, R. Bringué, M. Iborra, F. Cunill. Catalytic activity and accessibility of acidic ion-exchange resins in liquid phase etherification reactions. *Topics in Catalysis*, 58 (14), 2015, 919-932.

6.1 Introduction

The role of catalysis in the modern industrial chemistry is crucial. Most industrial catalysts are high-surface-area solids onto which active centers are located. These materials have become today critical to mediate the pathways by which chemical reactions occur, enabling highly selective formation of desired products at rates that are commercially viable [152]. Ion-exchange resins are among the polymer-based catalysts, since active sites are supported on the polymer backbone.

Although nowadays resins are widely used as catalysts in the chemical industry, the understanding of these materials at a molecular scale level has not yet been successfully achieved. For such purpose, an ever-growing set of characterization techniques exists that give light in different ways to the morphological nature of polymeric catalysts. Both classical and modern most relevant physical characterization techniques can be listed as follows: temperature programmed techniques (including thermogravimetry), mass spectrometry, physical adsorption (BET model for determination of specific surfaces), porosimetry (mercury-based measurement of the pore size and size distribution), X-ray technologies, electron microscopy, infrared and Raman spectroscopies, electron spin resonance and magic angle spinning nuclear magnetic resonance [54]. However, none of the listed techniques takes into consideration the micropores generated by the swelling of the polymer skeleton in contact with a liquid. Therefore, one of the most determining aspects in evaluating the interaction of the catalytic behavior of an ion-exchanger with the reacting medium remains unmonitored. As it is known, certain properties of a reaction medium, such as polarity, have been marked to be strongly related to the swelling of the catalysts, allowing a higher accessibility of reactants to the functional groups and, thus, influencing the catalytic activity. Furthermore, the polarity of a reaction medium may vary throughout a reactive process and so would do the catalyst swelling [45,136,153].

Up to date, the only procedure employed to characterize the morphology of ion-exchangers in the swollen state is the Inverse Steric Exclusion Chromatography (ISEC), based on modeling the microporous structure as a set of discrete volume fractions with different characteristic polymer chain densities [65,66]. Even though it is based upon the swelling of ion-exchangers in water (because water was found to be the most suitable solvent in terms of reducing enthalpic interactions between polymer and solute [154]) and a number of industrially-interesting reactions take place in water-free environment, the ISEC technique is appropriate to assess the catalytic behavior in chemical reactions. Use of other solvents different than water is considered difficult, or even not possible [69].

Attempts can be found in the open literature to correlate the rate of a given reaction to structural aspects of ion-exchange resins. In some works, the internal distribution and concentration of sulfonic groups or the reactants accessibility towards them were studied to assess the catalytic activity [52,64,147], or else they discerned between the activity of internal and external sulfonic acid groups [63]. Other works analyzed the swelling properties of sulfonated ion-exchangers [155]. Finally, a number of works found some

correlations between the reaction rate achieved by an ion-exchanger and its functionalization degree [51,59,60,67,68]. For the present work, it was considered appropriate to adapt the approach of Jeřábek et al. [69], who used the ISEC determination of the swollen-state morphology of a series of cationic gel-type ion-exchangers with the same acid capacity to express the observed bisphenol-A synthesis reaction rate as a sum of the contributions of individual fractions of the swollen polymer. Such contributions were expressed by means of the products of the volumes occupied by each fraction, in units of mass of the water-swollen resin, and a specific activity associated with each fraction characteristic polymer chain density (0.1, 0.2, 0.4, 0.8, 1.5 nm nm⁻³).

In connection to the previous chapter, an empirical expression has been developed to determine the contribution of each individual fraction of swollen polymer to the overall rate of the syntheses of methyl, ethyl, propyl and butyl *tert*-butyl ether (MTBE, ETBE, PTBE, and BTBE, respectively), with several ion-exchange catalysts with different physicochemical properties.

6.2 Experimental

The present chapter provides a deeper insight to the results already described in Chapter 5. Therefore, the used materials, the experimental setup and procedure, as well as the experimental reaction rate values are the same as described in the previous chapter.

6.3 Results and discussion

6.3.1 Reactants molecular size and accessibility

The main difference between the considered synthesis reactions is the size of the alcohol with which isobutene reacts. Therefore, reactants molecular size could have implications on the adsorption extent and its penetrability into the polymer network. It could be assumed that the different polymer chain densities of a resin are a measure of the spaces available within the gel-phase. This leads to an assessment of the spatial requirements that a resin will or will not be able to fulfill for a molecule of a particular size to access to its active sites.

The reactants molecular length in their minimum energy conformation, d_m , can be calculated from the distances and angles of bonds between atoms. In order to estimate such magnitudes, ChemBioOffice 2013 software was used, as it allows drawing molecules in the conformation of minimum energy and retrieve length, height and width of molecules. Results show that alcohols are almost linear molecules with a length ranging from 0.30 nm (MeOH) to 0.66 nm (1-BuOH), as indicated in Table 6.1. Isobutene is slightly bigger than ethanol.

Table 6.1 Molecular length, Ogston distribution coefficients, K_O , in different density domains of swollen polymer, molecular weight and random coil diameter, Φ_d , of considered reactants

Polymer chain density [nm nm ⁻³]		0.1	0.2	0.4	0.8	1.5		
Equivalent pore size [nm] ^a		9.3	4.8	2.6	1.5	1.0		
Compound	M [g mol ⁻¹]	Molecular length ^b [nm]	K_O				Φ_d [nm]	
Methanol	32.0	0.30	0.96	0.93	0.86	0.73	0.56	0.19
Ethanol	46.1	0.41	0.95	0.90	0.81	0.66	0.46	0.23
1-propanol	60.1	0.55	0.93	0.87	0.75	0.57	0.34	0.27
1-butanol	74.1	0.66	0.92	0.84	0.70	0.49	0.26	0.31
Isobutene	56.1	0.44	0.95	0.89	0.80	0.64	0.43	0.26

^a From [70]. ^b Estimated by ChemBioOffice 2013 Software (d_m).

To quantify the ease of penetration of a molecule into a porous domain of a certain density, in relation to its quantity in the free solution, the Ogston distribution coefficient, K_O , estimated by [65,70]

$$K_O = \exp\left(-0.25\pi C(d_m + d_c)^2\right) \quad (6.1)$$

provides an indication of which part of a porous system is accessible to spherical molecules with a diameter d_m in a polymer domain of a chain density C . Parameter d_c stands for the diameter of the polymer chain rigid rods ($d_c = 0.4$ nm). According to Equation 6.1, K_O ranges from 1 to 0, what means that either the compound amount is the same inside and outside that gel-phase zone ($K_O = 1$) or else that the compound is completely excluded from that gel-phase zone ($K_O = 0$). Values of K_O in Table 6.1 are consistent with the fact that transport through gradually denser domains is more hindered for larger alcohols than for smaller ones. It is also noticeable that K_O values for a given polymer density decrease progressively as the alcohol size increases. As for the isobutene, K_O values indicate that its mobility through the swollen-state polymer is less hindered than that of 1-PrOH.

Similarly, comparison between the random coil diameter and the equivalent pore size, of the different density domains of a swollen polymer [70], provides information on the spaces between polymer chains that a molecule would require to permeate through it without enthalpic interactions (Table 6.1). The random coil diameter, Φ_d , can be estimated by the equation [46,56]

$$\Phi_d = 0.02457(\overline{M}_w)^{0.5882} \quad (6.2)$$

This is an empirical measure of the space filled by a molecule of molecular weight \overline{M}_w (g/mol). In order to ensure that a molecule can permeate without impediments through a porous system, it is accepted that a value 2.5 times greater than Φ_d is needed. The equivalent pore sizes of the swollen polymer zones depicted in Table 6.1 are wider than this value, no matter what the molecule is, what would mean that all of the considered molecules are able to permeate through the swollen-state polymer. Finally, this

empirical method leads to infer that the ease of permeation through the gel-phase is ordered as methanol > ethanol > isobutene > 1-propanol > 1-butanol, the same as deduced from the Ogston distribution coefficient.

6.3.2 Resins swollen-state morphology

The role of the swelling phenomena constitutes an important feature related to the molecular permeation through the polymer backbone of a resin and the adsorption on an active site. These processes take place mainly within the swollen polymer, or gel-like phase [45]. It is then of common sense trying to correlate the catalytic performance of a resin with its swollen-state morphology, as well as with its functionalization degree.

With regard to the morphology of the gel phase in the swollen-state, ISEC provides information of the expanded volume in polymer domains of different densities swollen in water. In Figure 6.1, the ISEC pattern corresponding to the ion-exchangers used in this work is shown.

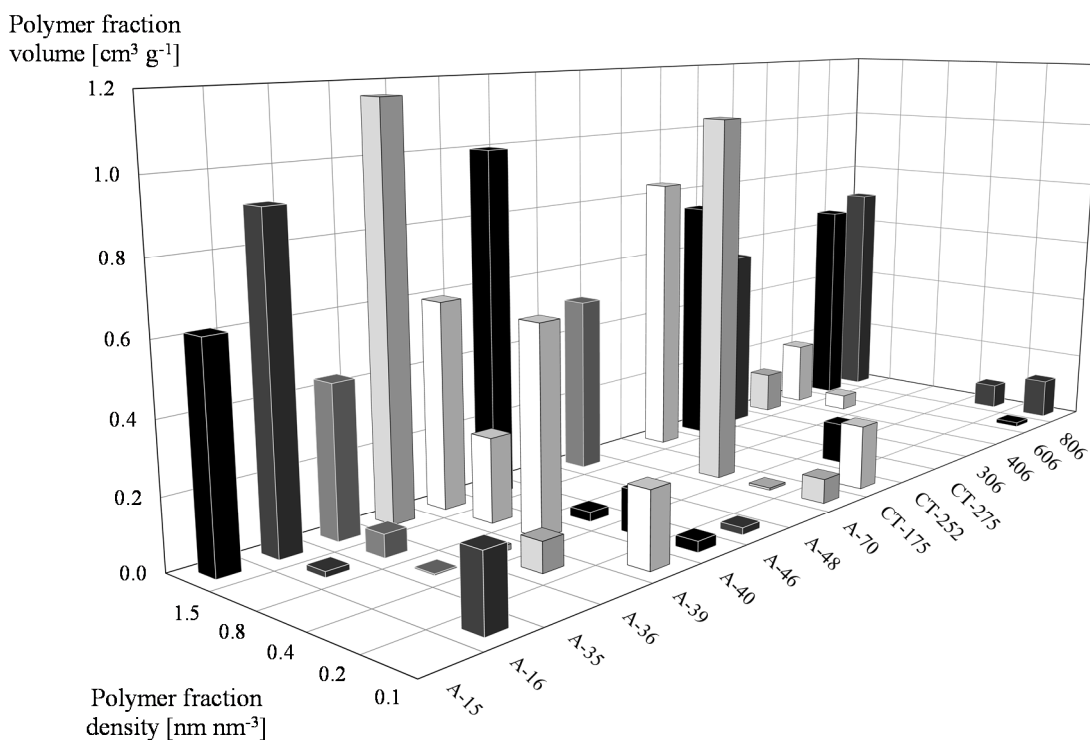


Figure 6.1 ISEC morphological pattern of the gel-phase

It can be considered that the number of acid centers contained in a polymer mass fraction is proportional to its polymer chain length, thus to its characteristic chain density [69]. Figure 6.1 indicates that, in the swollen state, denser polymer fractions are generally more frequent. Actually, the densest volume (1.5 nm nm^{-3}) is present in all but one of the catalysts (A-70 constitutes the sole exception) and it occupies the highest percentage of the total swollen-state volume. In case of sterically demanding reactions, the acid centers contained within the densest polymer domains become less accessible,

and consequently less efficient, than the more expandable ones due to permeation impediments. Nevertheless, their contribution to the catalytic phenomenon might be higher than those of low-density domains, because of the larger number of active sites due to their higher density. Also, medium and high density fractions might allow interaction between reactants and the polymer matrix.

Because of the polar and non-aqueous environment of these reactions, it has been widely accepted that ion-exchangers experience the swelling phenomenon, but also that this swelling does not reach the degree exhibited when submerged in water. It can be assumed that each of the five specific volumes of polymer detected by ISEC will maintain their identity even though the reaction is performed in a somehow less polar organic environment [69]. Then, the ISEC information cannot be directly applicable. Nevertheless, it can also be assumed that the fraction of volume occupied by each polymer fraction in water will have a proportional relation to that occupied in organic, alcoholic media.

6.3.3 Relations between swollen-state morphology and catalytic activity

As seen in Chapter 5, catalysts can be classified into two groups regarding their activity progression as the size of the alcohol grows (Table 5.1). The reactivity of primary alcohols with isobutene followed the order 1-butanol > 1-propanol > ethanol > methanol for resins A-35, A-15, A-36, A-40, A-48, CT-175, CT-252, and CT-275, but for resins A-16, A-39, A-46, A-70, 306, 406, 606, and 806, this order was 1-butanol > 1-propanol > methanol > ethanol. The magnitude of the observed differences between alcohols reactivity, i.e., experimental rates, exceeded that of the experimental error and should, therefore, be considered as significant.

Insight of the properties displayed by these two groups of catalysts reveals that the first one was formed mainly by highly cross-linked, oversulfonated catalysts. Three exceptions can be found, though, since A-15 and CT-175 are conventionally sulfonated resins, and CT-252 is a medium cross-linked catalyst. With regard to the second group of catalysts, none of them was oversulfonated and they were of low, medium, and high cross-linking degree. As described in Chapter 5, the first group of resins presents higher concentration of active sites in the gel phase than the second one. In fact, relative amounts of the lowest density polymer domains are generally higher for this second group of resins than for the first one, as shown in Figure 6.1. Such phenomenological assessment has been used as a classification for the resins: henceforward, resins with reaction rates in the order 1-butanol > 1-propanol > ethanol > methanol will be referred to as group A, whereas those with an order 1-butanol > 1-propanol > methanol > ethanol, as group B.

Due to the different chain density of the polymer fractions, the overall intrinsic reaction rate achieved by a catalyst can be expressed as a sum of contributions of the individual polymer domains, similar to what is proposed in a previous work [69]. For each catalyst, the individual contribution of each polymer domain of a characteristic chain

density was computed as a product of a specific catalytic activity, the acid capacity, and the fraction of volume that it occupies, as follows:

$$r_n = \sum_{i=0.1}^{1.5} r_i = \sum_{i=0.1}^{1.5} \left[TOF_i \cdot [H^+]_n \cdot \left(\frac{V_{sp,i}}{\sum_{j=0.1}^{1.5} V_{sp,j}} \right) \right] \quad (6.3)$$

with

- r_n : intensive reaction rate for the catalyst n [$\text{mol (g}_{\text{cat}} \text{ h)}^{-1}$]
- r_i : contribution to the reaction rate induced by polymer fraction i [$\text{mol (g}_{\text{cat}} \text{ h)}^{-1}$]
- TOF_i : specific activity of the polymer fraction i [$\text{mol (meqH}^+ \text{ h)}^{-1}$]
- $[H^+]_n$: acid capacity of the catalyst n [$\text{meqH}^+ \text{ g}_{\text{cat}}^{-1}$]
- $V_{sp,i}$: volume occupied by fraction i in the water-swollen resin n per gram of catalyst [$\text{cm}^3 \text{ g}_{\text{cat}}^{-1}$]

Specific activity, or turnover frequencies (TOF), are considered to be one of the best ways to compare catalysts on a rational basis and are often found in literature [156]. TOF can be evaluated as the quotient between rate and acid capacity under the assumption that all active sites are accessible to reactants. In this work, the specific activity of the polymer fraction i , TOF_i , was considered to depend on the characteristic chain density. By defining TOF_i , active sites located in different polymer domains are distinguishable and can be compared in terms of their effectiveness, what can be related to the accessibility of reactants towards them.

Equation 6.3 was applied separately to both catalysts groups, A and B. With this procedure, two sets of up to 8 equations (one per catalyst) and two sets of 5 common unknown parameters (corresponding to the specific activity of each polymer fraction, which is equal for catalysts of a same group) are considered. Unknown parameters values were estimated by an optimization mathematical procedure in which the sum of squares of differences between experimental and calculated reaction rate values was minimized.

6.3.3.1 MTBE experiments

As Figure 6.2 shows, MTBE rates calculated by means of Equation 6.3 fit globally well with experimental values, irrespectively of the group of catalysts considered.

Distribution of the computed specific activity values for each characteristic polymer chain density, TOF_i , which is presented in Figure 6.3, indicates differences between TOF_i that have morphological implications. According to this model, a chain concentration of 0.4 nm nm^{-3} provides maximum TOF in group A resins, which would be the polymer fraction working with a higher performance. On the other hand, the highest-performance polymer fraction for group B resins would be that of 0.1 nm nm^{-3} , which corresponds to the most expandable polymer domain.

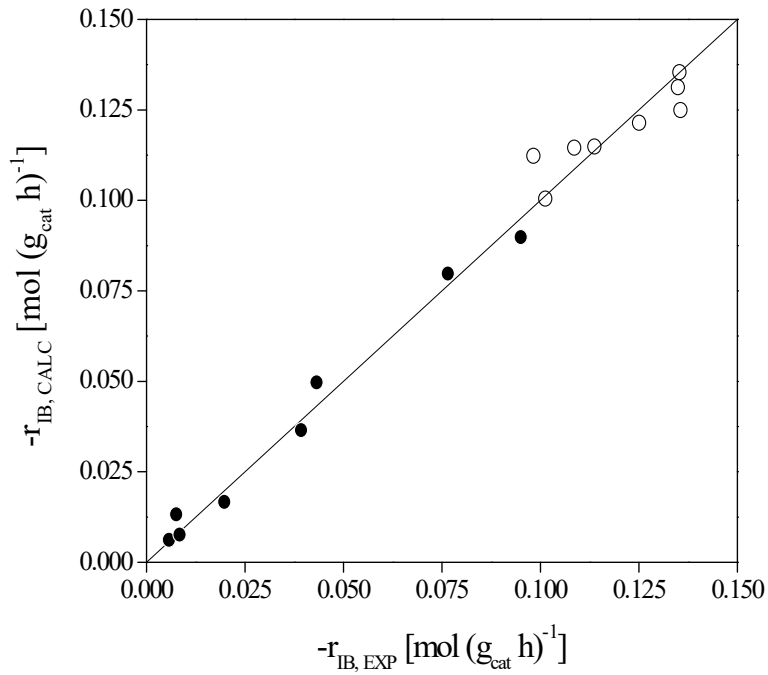


Figure 6.2 Reaction rate fit for the sixteen catalysts in the MTBE reaction. $T = 333 \text{ K}$, $R_{A/O}^{\circ} = 1.0$, $d_p = 0.25\text{-}0.40 \text{ mm}$, $\text{WHSV} > 500 \text{ h}^{-1}$. Group A (open symbols), Group B (solid symbols)

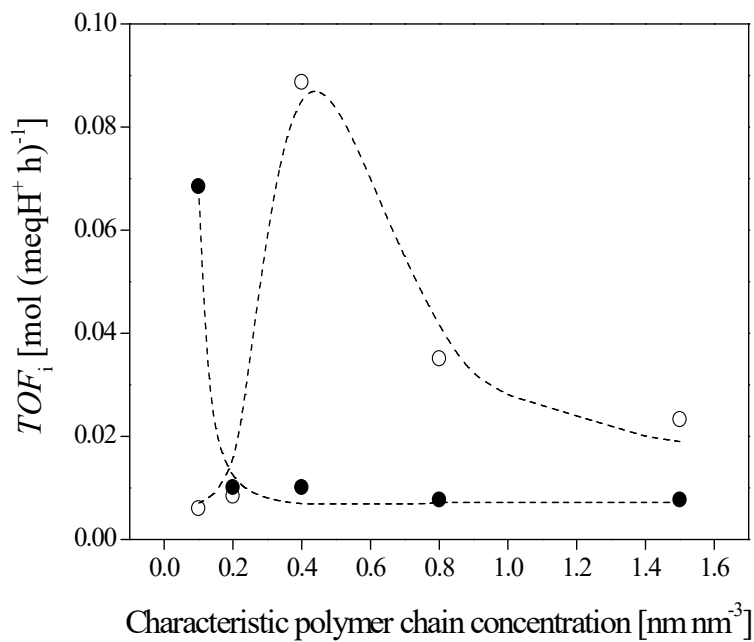


Figure 6.3 TOF distribution for each characteristic polymer chain density for the MTBE experiments. $T = 333 \text{ K}$, $R_{A/O}^{\circ} = 1.0$, $d_p = 0.25\text{-}0.40 \text{ mm}$, $\text{WHSV} > 500 \text{ h}^{-1}$. Group A (open symbols), Group B (solid symbols)

TOF distribution for the MTBE experiments shown in Figure 6.3 should be, at first, handled with some precautions as they are necessarily bound to experimental error. Differences of TOF_i could be, then, non-significant. However, results in Figure 6.3 can be explained in terms of morphological differences between resins and the catalytic activity displayed by them.

Regarding group A resins, TOF_i distribution in Figure 6.3 suggests that active sites located in a polymer volume fraction with a characteristic chain density of 0.4 nm nm^{-3} are the most effective. This can be related to local spatial distribution of active sites within the gel-phase that could allow coordination to multiple active sites. Participation of several groups can stabilize better the reaction intermediate. On the other hand, as low density domains present very dispersed functional groups, reactants cannot adsorb in more than one active site therein at the same time. Thicker polymer fractions ($> 0.8 \text{ nm nm}^{-3}$) would hinder reactants accessibility towards active sites, leading a decrease of the specific activity. According to the gel-phase distribution displayed by group A catalysts (Figure 6.1), domains with 0.4 nm nm^{-3} density represent an actually low fraction of polymer volume. Although in these domains the specific activity might be higher than the rest, their contribution to the overall reaction rate is low.

In relation to group B resins, only the lowest density polymer zone (0.1 nm nm^{-3}) displayed a good specific activity, whereas any density increase leads to a dramatic loss of the active sites effectiveness. In this case, rather than interpreting the results on the basis of an extremely high efficiency of active sites located in the most expandable domain, it seems that they provide wide channels that facilitate the access to denser volume fractions surrounding them. Similar inferences can be found in previous works [69]. The similarly low specific activity values displayed by polymer masses of 0.2, 0.4, 0.8, and 1.5 nm nm^{-3} nominal chain densities may be interpreted as null significant differences between their active sites effectiveness.

6.3.3.2 Generalization of the empirical model

The same procedure was applied to the ETBE experimental data, yielding similar results to those from MTBE data. Figures 6.4 and 6.5 prove this fact.

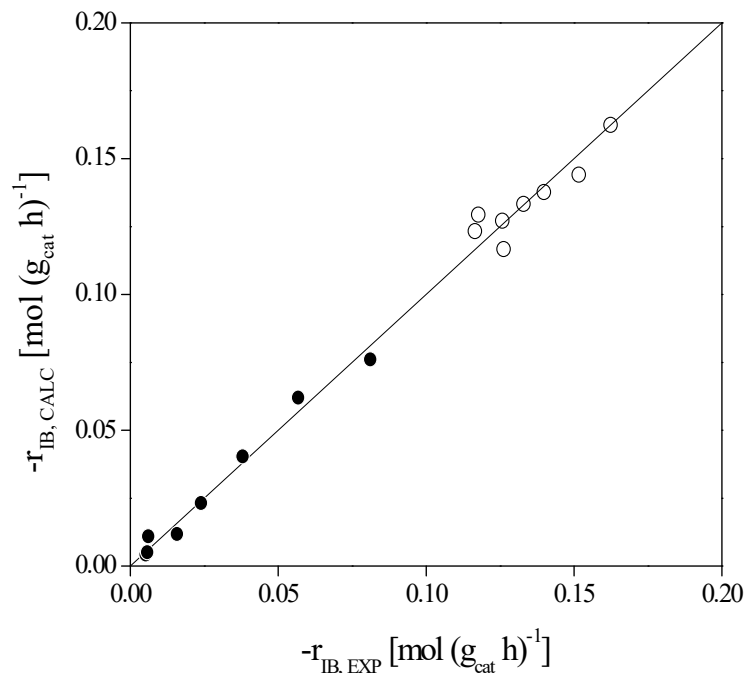


Figure 6.4 Reaction rate fit for the sixteen catalysts in the ETBE reaction. $T = 333 \text{ K}$, $R_{A/O}^{\circ} = 1.0$, $d_p = 0.25\text{-}0.40 \text{ mm}$, $WHSV > 500 \text{ h}^{-1}$. Group A (open symbols), Group B (solid symbols)

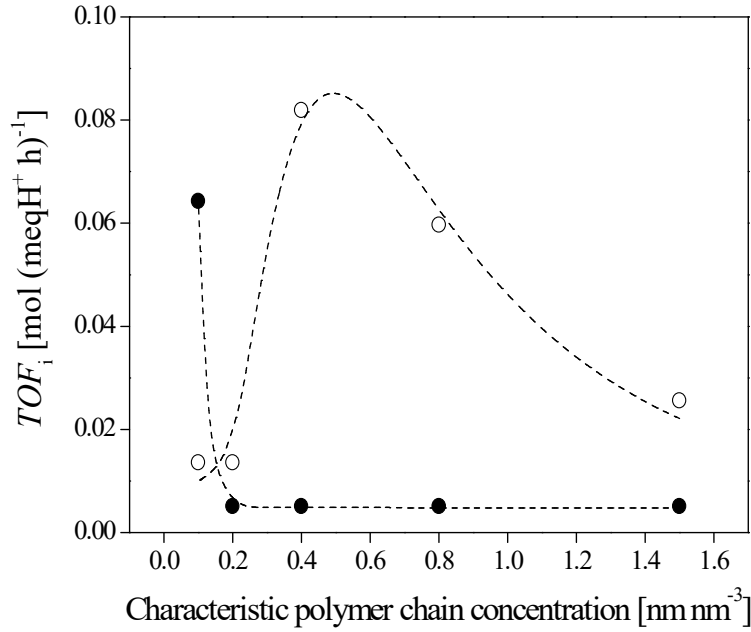


Figure 6.5 TOF distribution for each characteristic polymer chain density for the ETBE experiments. $T = 333 \text{ K}$, $R_{A/O}^{\circ} = 1.0$, $d_p = 0.25\text{-}0.40 \text{ mm}$, $\text{WHSV} > 500 \text{ h}^{-1}$. Group A (open symbols), Group B (solid symbols)

Consequently, it was considered appropriate to develop a generalization of the empirical equation (Equation 6.3) that could be applied to similar reaction schemes. Among the parameters in Equation 6.3, both acid capacity and polymer volume fraction distribution are specific of each studied resin. Therefore, TOF_i are the only parameters with different values for each reaction. As previously discussed, the main difference between the four considered reaction systems was that of the alcohol molecular size, which is inherently related to its degree of penetrability through progressively denser polymer fractions, assessed by means of the Ogston distribution coefficient (Table 6.1).

For such purpose, the parameter TOF_i^R , corresponding to the volume fraction i for the reaction R , was defined relative to the MTBE formation reaction according to Equation 6.4.

$$TOF_i^R = k_R \cdot TOF_i^{MTBE} \cdot \frac{K_{O,i}^{MeOH}}{K_{O,i}^{ROH}} \quad (6.4)$$

with TOF_i^R : specific activity of the polymer fraction i for the reaction R [mol (meqH⁺ h)⁻¹]

k_R : proportionality constant for the reaction R

TOF_i^{MTBE} : specific activity of the polymer fraction i for MTBE [mol (meqH⁺ h)⁻¹]

$K_{O,i}^{MeOH}$: Ogston distribution coefficient of methanol through a polymer fraction i

$K_{O,i}^{ROH}$: Ogston distribution coefficient of a primary linear alcohol through a polymer fraction i

The parameter TOF_i^R , which substitutes TOF_i in Equation 6.3, was considered to be proportional to TOF_i^{MTBE} and to the relation between the Ogston distribution coefficient of a polymer domain, $K_{O,i}$, with methanol and the corresponding one with the considered alcohol. The relation between alcohols Ogston distribution coefficients stands for the relative differences in concentration of these compounds inside the gel-phase, in order to take into consideration the possible partial exclusion of a reactant from a particular polymer zone.

By means of this procedure, 21 equations with 5 parameters related to the polymer domain and 3 proportionality constants related to each reaction other than the MTBE synthesis were considered for group A catalysts. Regarding group B, 32 equations can be gathered with the same number and nature of unknown parameters as in group A. In total, therefore, 53 equations and 16 unknown parameters were considered. Estimation of parameters values proceeded similarly as in the MTBE case. Figure 6.6 shows the results of the simultaneous fit of equations 6.3 and 6.4 to all experimental values.

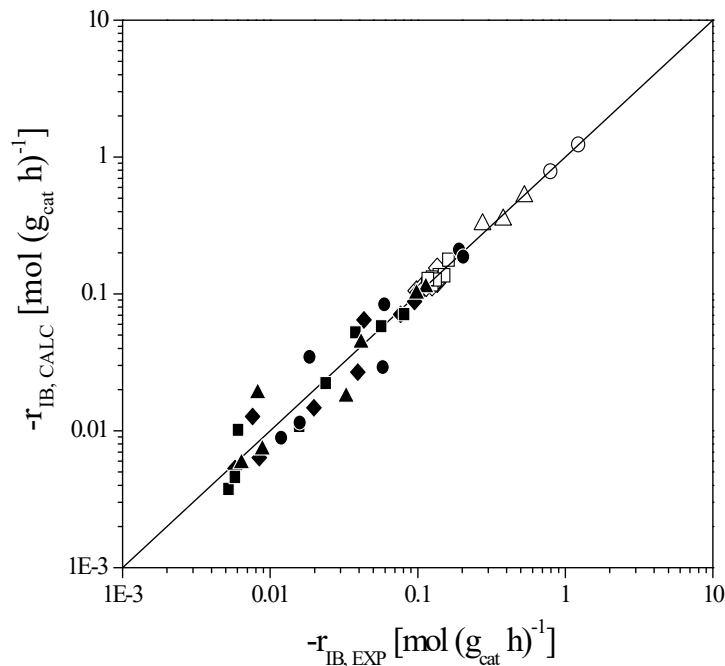


Figure 6.6 Reaction rate fit for the four considered reactions. $T = 333 \text{ K}$, $R_{A/O}^{\circ} = 1.0$, $d_p = 0.25\text{-}0.40 \text{ mm}$, $WHSV > 500 \text{ h}^{-1}$. Open symbols (Group A catalysts): MTBE (\diamond), ETBE (\square), PTBE (Δ) and BTBE (\circ). Solid symbols (Group B catalysts): MTBE (\blacklozenge), ETBE (\blacksquare), PTBE (\blacktriangle) and BTBE (\bullet)

As indicated above, proportionality constants, k_R , related to the considered reaction, were obtained as fitting parameters. Figure 6.7 plots k_R values against the molecular length of the alcohol involved in the reaction R , other than the MTBE synthesis.

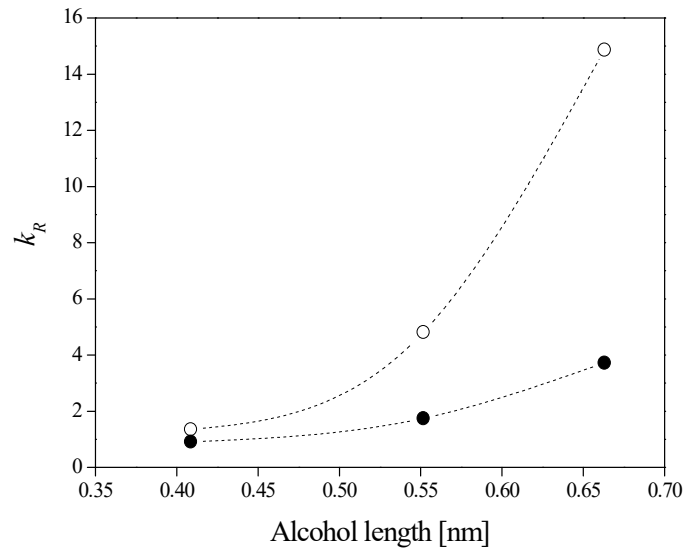


Figure 6.7 k_R values versus alcohol molecular length. $T = 333$ K, $R_{A/O}^o = 1.0$, $d_p = 0.25$ - 0.40 mm, $WHSV > 500$ h^{-1} . Group A (open symbols), Group B (solid symbols)

As seen in Figure 6.7, k_R values for both A and B resins increased exponentially with the alcohol size, which indicates that the effect of the alcohol size on the reaction kinetics is the same for each alcohol irrespectively of the catalyst type. However, relative differences between k_R of each group grew as the molecule length increased. Therefore, it can be inferred that differences between catalyst types may become more important for larger molecules, as observed in Chapter 5.

As indicated in Figure 6.8, polymer fractions of 0.4 and 0.1 $nm\ nm^{-3}$ nominal chain density would provide maximum specific activity for resins of groups A and B, respectively. Since oversulfonated ion-exchangers would be included in group A resins, it can be stated that oversulfonated catalysts composed by a polymer mass of a characteristic chain density around 0.4 $nm\ nm^{-3}$ would be the most active resins in the etherification reactions of isobutene.

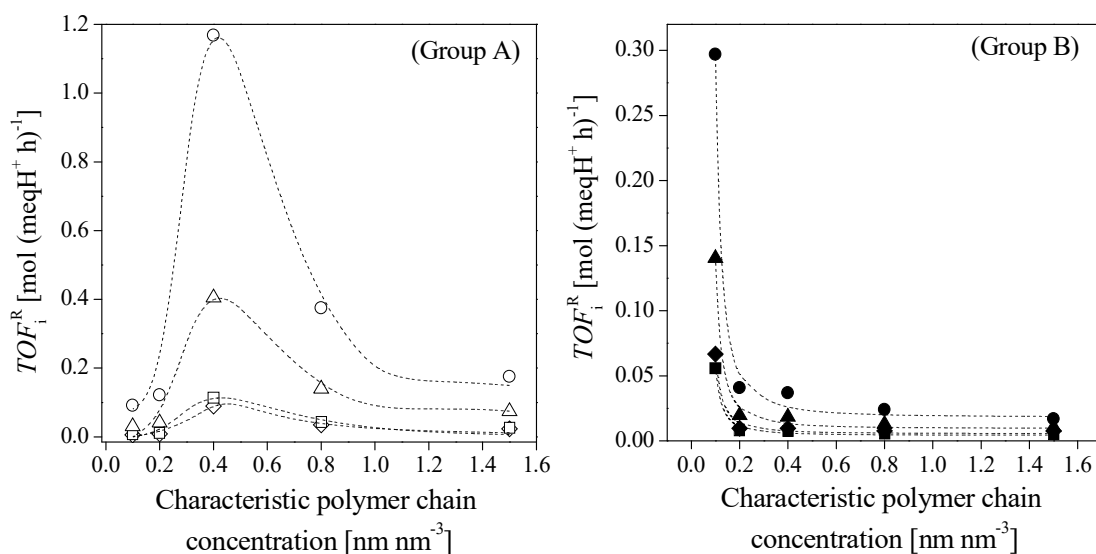


Figure 6.8 TOF distribution for each characteristic polymer chain density. $T = 333$ K, $R_{A/O}^o = 1.0$, $d_p = 0.25$ - 0.40 mm, $WHSV > 500$ h^{-1} . Group A (open symbols): MTBE (\diamond), ETBE (\square), PTBE (Δ) and BTBE (\circ). Group B (solid symbols): MTBE (\blacklozenge), ETBE (\blacksquare), PTBE (\blacktriangle) and BTBE (\bullet)

Regarding the differences between calculated specific activities, TOF_i^R values depicted in Figure 6.8 are generally higher for reactions involving larger molecules (i.e., $TOF_i^{BTBE} > TOF_i^{PTBE} > TOF_i^{ETBE} > TOF_i^{MTBE}$). These differences can be considered negligible between ETBE and MTBE reactions as well as between low TOF_i^R values, assuming some inaccuracy of the model and experimental error. However, a feasible interpretation of the observed differences between maximum values of specific activity in Figure 6.8 (e.g., $TOF_{0.4}^R$ for group A catalysts) would be related to the size of the alcohol and to the local concentration of active sites. Assuming both the Ogston model and the evaluation of the random coil diameter (Equations 6.1 and 6.2), none of the considered reactants present important permeation hindrances through the polymer. Furthermore, reactants chemisorption on active centers leads to enthalpic interactions, which can counterbalance steric impediments that might affect molecules of similar sizes to the equivalent pore diameters of the polymer matrix [157]. Thus, within this range of molecular sizes, large molecules could coordinate to multiple active sites simultaneously easier than small molecules. This could explain the observed order of primary alcohols reactivity with isobutene.

Finally, assuming this empiricism, if different catalysts need to be tested, the first thing to do would be to establish which group the catalysts belong to. For instance, oversulfonated catalysts would probably belong to group A. Then, by comparison of their working-state morphology and acid capacity, an a priori estimation of their activity level could be easily achieved.

6.4 Conclusions

The empirical model presented in this chapter described satisfactorily experimental reaction rates for the methyl *tert*-butyl ether and the ethyl *tert*-butyl ether syntheses, separately. A generalization of the empirical model to reactions of the same nature (the propyl *tert*-butyl ether, and the butyl *tert*-butyl ether syntheses) was successfully achieved by means of the Ogston distribution coefficient.

Regarding active sites effectiveness, higher specific activities were found for active sites located in polymer fractions with a characteristic chain density of 0.4 nm nm^{-3} , for a group of resins that would allow multiple active sites coordination. These resins were A-35, A-15, A-36, A-40, A-48, CT-175, CT-252, and CT-275. A group of resins was found that presented no favored polymer fraction, in terms of the active sites effectiveness therein. Those were A-16, A-39, A-46, A-70, 306, 406, 606, and 806. Highly acidic oversulfonated resins with a polymer fraction of a chain density around 0.4 nm nm^{-3} would be the most active catalysts for the studied reactions.

**7. Simultaneous liquid-phase
etherification of isobutene with ethanol
and 1-butanol over macroreticular acidic
ion-exchange resins**

7.1 Introduction

Accordingly with the current legislation struggle towards the introduction of next generation biofuels, production of biomass-derived compounds for the gasoline pool is encouraged. Among these, ethanol, obtained through fermentative processes, has been largely chosen for this purpose. However, since it has generated concerns in relation to its competition with food supplies, some alternatives are being evaluated. In this sense, 1-butanol has been targeted as a promising alternative: it has experienced a renovated interest from private corporations and its expected production by 2020 is around hundreds of million gallons [11,18,32].

Butanol production at industrial scale can be accomplished by means of bacteria-based fermentation of sugars. Although it was eclipsed during the 1950s by lower-cost petrochemical routes, this is a well-known process that had been in use early in the 20th century in the US, until the 1980s in South Africa and the USSR, and still today in China.

On the other hand, given that a complete substitution of current mainstream gasoline compounds, such as MTBE or ETBE, is not likely to be viable in the short term, integrated processes capable of obtaining both current and alternative oxygenates are of interest. In addition, as seen in previous chapters, BTBE synthesis reaction rates are higher than those of ETBE, which would result in operative savings regarding its industrial production. This fact was also indicated in previous studies [59,60].

ETBE technology is already well established and BTBE production would not add noticeable modifications to the existing ETBE production units. Furthermore, the simultaneous production of these two ethers could be of special interest since, on one hand, it would offer to the manufacturer operating flexibility and adaptability to the market demands and stock disposal, and, on the other hand, it would allow using products from fermentative processes in which both ethanol and 1-butanol are obtained, such as the ABE fermentation (fermentation of grain to obtain acetone, 1-butanol, and ethanol), without further separation of the two alcohols.

Therefore, the aim of this chapter is to study the simultaneous production of ETBE and BTBE. Firstly, a catalyst screening study has been carried out to select the best catalysts and to identify their most relevant properties. Subsequently, the effect of some operating conditions, such as temperature and initial reactants concentration, on reaction rates and side reactions extension has been analyzed. Finally, the performance of the simultaneous etherification has been compared to that of the individual syntheses of both ETBE and BTBE.

7.2 Experimental

7.2.1 Chemicals and catalysts

Reactants were ethanol, 1-butanol and pure isobutene. As reaction products or byproducts, the following compounds were used for analytical procedures: 2-methyl-2-propanol (TBA), 2,4,4-trimethyl-1-pentene (TMP-1), 2,4,4-trimethyl-2-pentene (TMP-2), 2-ethoxy-2-methylpropane (ETBE), and 2-methyl-2-propoxybutane (BTBE).

Six commercial ion-exchange resins were used as catalysts, supplied by Rohm & Haas (Amberlyst™ type) and by Purolite® (namely: A-16, A-35, A-39, A-46, A-70, and CT-275). All resins were macroreticular, acidic, sulfonated polymers of styrene-divinylbenzene. Relevant properties have been listed in Tables 2.2 and 2.3.

7.2.2 Apparatus, procedure and analysis

Experiments were carried out in a batch reactor setup at constant temperature, in the range of 315 to 353 K, and at 2.5 MPa. The initial alcohol/isobutene molar ratio ($R_{A/O}^o$) was varied from 0.5 to 5.5 and the initial ethanol/1-butanol molar ratio ($R_{E/B}^o$) from 0.5 to 2.0. Since catalysts were supplied in wet state, the resins pretreatment consisted in reducing their water content. Additionally, catalyst beads were crushed and sieved in order to obtain desired particle diameters, d_p .

The experimental procedure was as follows: the catalyst load, ranging 0.1-1.0%wt., was introduced into a catalyst injector and pressurized to 2.5 MPa with nitrogen. The corresponding amount of alcohols was introduced into the reactor vessel and the heating and the stirring were switched on. The isobutene was introduced into the reactor, from a pressure burette, impelled by nitrogen by difference of pressures. Once the reactive mixture reached the desired temperature the catalyst was injected. This instant was considered as the starting point of the reaction.

Samples were taken inline from the reaction medium every 32 minutes through a sampling valve that injected 0.2 μ L of pressurized liquid into an Agilent gas chromatograph 6890, equipped with a capillary column (100% dimethylpolysiloxane, 50 m \times 0.20 mm \times 0.50 μ m), coupled with a mass selective detector HP5973N used to identify and quantify the reaction system components. The oven temperature was programmed with a 10 min hold at 333 K followed by a 10 K/min ramp, from 333 to 353 K, and a second hold of 11.5 min at 353 K. The carrier gas (Helium) flow was set to 0.6 mL/min. This system identified and quantified the concentration of reactants, products and byproducts, when formed.

7.2.3 Calculations

Initial reaction rates (r_j^o), conversion of reactant j (X_j), selectivity of reactant j towards product k (S_j^k), and turnover frequency (TOF), have been calculated as follows:

$$r_j^o = \frac{1}{W_{cat}} \left. \frac{dn_j}{dt} \right|_{t=0} \quad (7.1)$$

where W_{cat} is the weight of dry catalyst, n_j is the number of moles of the compound j and t is the time of reaction.

$$X_j = \frac{\text{mole of } j \text{ reacted}}{\text{mole of } j \text{ fed}} \quad (7.2)$$

$$S_j^k = \frac{\text{mole of } j \text{ reacted to produce } k}{\text{mole of } j \text{ reacted}} \quad (7.3)$$

$$TOF = \frac{\text{reaction rate}}{[\text{active site}]} \quad (7.4)$$

7.3 Results and discussion

7.3.1 Catalyst screening

The studied reaction scheme is shown in Figure 7.1. Main reactions are etherification of isobutene (IB) with ethanol (EtOH) and with 1-butanol (1-BuOH) to produce ETBE and BTBE (R1 and R2, respectively). Side reactions are isobutene hydration to give TBA (R3) and isobutene dimerization to give either TMP-1 or TMP-2 (R4). Other possible side reactions, like alcohols dehydration to form linear ethers, or further isobutene oligomerization to produce heavier oligomers, as trimers or tetramers, were not detected.

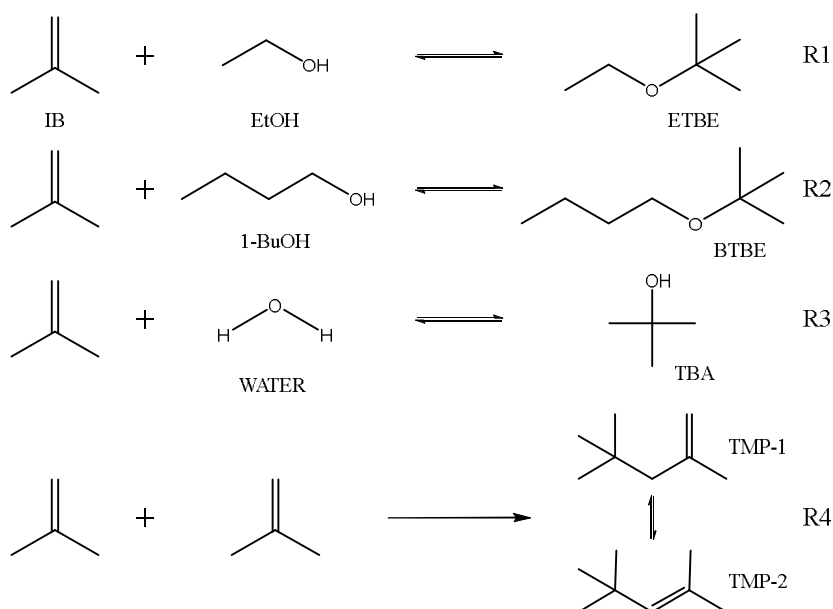


Figure 7.1 Reaction scheme

The catalytic behavior of six commercial acidic macroreticular ion-exchange resins was compared at 333 K. Preliminary experiments were carried out to determine the conditions at which the effect of mass transfer limitations on the overall reaction rates could be neglected. CT-275 and A-39 were selected for these previous runs since these two catalysts were considered to be representative of the range of properties of the tested resins. No significant differences in initial reaction rate values were found for experimental runs carried out with stirring speeds between 500 and 750 rpm, for each catalyst at 333 K. As for the possible effect of internal mass transfer limitations, CT-275 and A-39 beads were crushed and sieved to obtain different ranges of particle sizes, namely 0.08-0.16 mm and 0.25-0.40 mm. Again, no significant differences in the measured reaction rates were observed at 333 K. Therefore, all further experiments were done at 750 rpm and with 0.25-0.40 mm catalyst particles, unless otherwise is indicated.

The initial alcohol/isobutene molar ratio, $R_{A/O}^{\circ}$, was set at 1.0 and the initial ethanol/1-butanol molar ratio, $R_{E/B}^{\circ}$, was varied in the range 0.5-2.0. Since the tested resins presented large differences in terms of activity, the catalyst load was varied accordingly in order to achieve conversion levels far above detection limits. The possible effect of the catalyst load (0.1-1.0%wt.) was considered as negligible, given that previous studies found it non-significant when catalysts loads were lower than 5.5%wt. in similar systems [105].

As it is shown in Figure 7.2, A-35 was the most active catalyst for the two etherification reactions irrespectively of $R_{E/B}^{\circ}$. Initial ETBE reaction rates were hardly affected by reactants composition, whereas BTBE rates strongly diminished when the amount of ethanol increased for all resins. The relative decrease of initial BTBE rates was about 80% from $x_{EtOH}^{\circ} = 0.17$ to $x_{EtOH}^{\circ} = 0.33$ ($R_{E/B}^{\circ} = 0.5$ and $R_{E/B}^{\circ} = 2.0$, respectively). This fact suggests a preferential adsorption of ethanol over 1-butanol that could take place on all the tested catalysts.

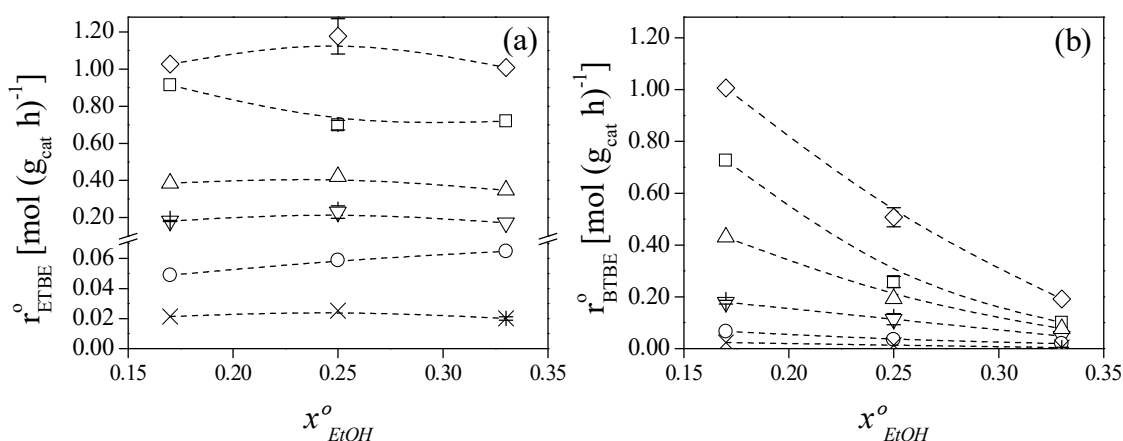


Figure 7.2 Initial ETBE (a) and BTBE (b) reaction rate vs. initial ethanol molar fraction. Error bars refer to the standard uncertainty for replicated experiments. $T = 333$ K, $R_{A/O}^{\circ} = 1.0$, $d_p = 0.25$ - 0.40 mm, 750 rpm. A-35 (\diamond), CT-275 (\square), A-16 (Δ), A-39 (∇), A-70 (\circ) and A-46 (\times)

Resins catalytic activity followed the relative order $A-35 > CT-275 > A-16 > A-39 > A-70 > A-46$. This relative order of activity can be globally explained by the relative order of resins acid capacity, except for resins A-16 and A-39, whose acid capacity is almost coincident, but they have significantly different activity. Like in previous chapters, as shown in Figure 7.3, an almost linear relationship can be observed between the resins activity, in terms of initial reaction rates, and the active sites concentration in the gel-type phase (computed as the ratio between acid capacity, $[H^+]$, and the specific swollen polymer volume, V_{sp} , determined by ISEC [65,66]). From these results, it can be stated that the water-swollen state morphology of the resins is directly related to their actual morphology in the reaction medium. In the ETBE synthesis, the catalytic activity is not affected by the alcohol ratio, $R_{E/B}^{\circ}$. On the contrary, BTBE synthesis is sensitive to the alcohol ratio. At every experimental condition, a clear linear dependence is observed between initial reaction rate and $[H^+]/V_{sp}$.

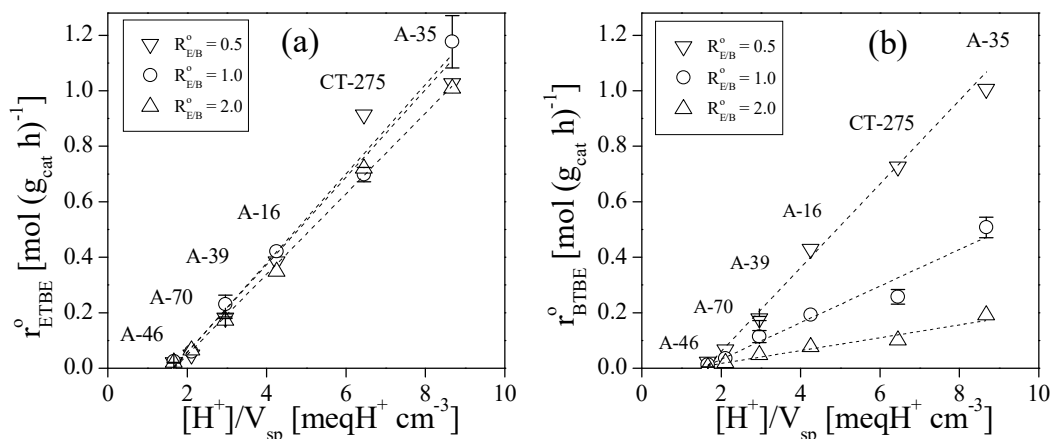


Figure 7.3 Dependence of the initial ETBE (a) and BTBE (b) reaction rate on the acid sites density in the swollen gel phase volume. Error bars refer to the standard uncertainty for replicated experiments. $T = 333 \text{ K}$, $R_{A/O}^0 = 1.0$, $d_p = 0.25\text{-}0.40 \text{ mm}$, 750 rpm

Higher reaction rates are obtained with catalysts that present a high acid capacity and a relatively rigid structure, what suggests that it is important to maintain high active sites concentration in the gel phase and that an excessive swelling of the polymer backbone has a detrimental effect on etherification rates. From a manufacturer standpoint, resins with high acid capacity and crosslinking degree ($>14\%$ DVB) are more prone to exhibit higher catalytic activity. For instance, among the highly crosslinked resins, i.e. A-35, A-46 and CT-275, the higher the acid capacity, the faster the reaction rate, and among the highly acidic resins, i.e. A-16, A-35, A-39 and CT-275, a higher crosslinking degree leads to faster reaction rates.

Given that the activity level of the tested resins is far from being similar, the specific activity, or turnover frequency (TOF), can be used to compare resins activity. TOF^0 has been calculated as the ratio between the initial overall reaction rate and the acid capacity, under the assumption that all active sites are accessible to reactants. Even though such an assumption may not be valid for ion-exchangers in the present reaction medium, TOF can be considered a fair indication of the overall effectiveness of the active sites for each resin and it would include the effect of the active site accessibility. As seen in Figure 7.4 the relative order of specific activity was $A-35 > CT-275 > A-16 > A-39 > A-46 \geq A-70$, irrespectively of $R_{E/B}^0$. This order reinforces the idea that high local concentrations of active sites enhance etherification rates, because A-35 and CT-275 presented superior specific activity. Resins with similar acid capacity, but more flexible structures, i.e. A-39 compared to A-16, were drastically less active. Special attention should be paid to resins A-70 and A-46, since the latter, with a more rigid structure, presented a level of specific activity at least equal to that of A-70, whose acid capacity triples that of A-46.

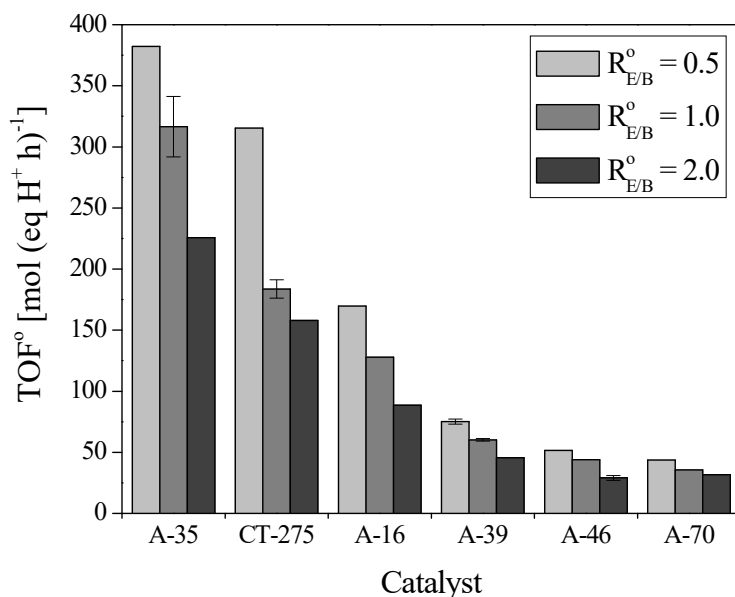


Figure 7.4 TOF° displayed by each catalyst. Error bars refer to the standard uncertainty for replicated experiments. $T = 333\text{ K}$, $R_{A/O}^{\circ} = 1.0$, $d_p = 0.25\text{-}0.40\text{ mm}$, 750 rpm

It is also observed that, for all resins, a higher 1-butanol concentration leads to a higher specific activity. This fact can be explained by assuming that the longer hydrocarbon chain of 1-butanol could interact with the hydrophobic polymer backbone of the resins, whereas the interaction between ethanol and the polymer would be mainly restricted to its hydroxyl group. As a result of the 1-butanol interaction, resins would experience a higher swelling, and a larger number of active sites would become accessible to reactants and, hence, their specific activity would increase.

As for the products distribution, Table 7.1 lists the isobutene selectivity towards products at the end of the experimental runs ($t = 300\text{ min}$). In general, no significant differences in isobutene selectivity towards ethers were detected among the tested catalysts, irrespectively of the initial reactants concentration. As an exception, the least active resin, A-46, presented slightly higher values of selectivity towards ETBE than the other catalysts. Selectivity values towards TBA were null or rather low. The isobutene selectivity towards dimers, when produced, generally increased at higher initial ethanol concentration, except for resin A-39, for which the opposite results were observed. From values in Table 7.1, the most active resin, A-35, presented scarce byproducts formation, which makes A-35 the most appropriate catalyst for the simultaneous etherification.

Table 7.1 Isobutene selectivity towards products and byproducts at $t = 300$ min. Standard uncertainty for replicated experiments is presented

Catalyst	Catalyst load [%wt.]	$R_{E/B}^{\circ}$	Isobutene selectivity towards main products and byproducts, S_{IB}^k [%]				
			ETBE	BTBE	TBA	TMP-1	TMP-2
A-16	0.20	0.5	41.8	56	0	1.7	0.4
		1.0	59.5	38.1	0	1.9	0.5
		2.0	75.5	19.5	0	4	1
A-35	0.15	0.5	39.2	58.9	0	1.5	0.4
		1.0	60.9 ± 1.7	37 ± 1	0.2 ± 0.04	1.5 ± 0.5	0.3 ± 0.1
		2.0	77.6	19.7	0	2.2	0.5
A-39	0.26	0.5	40.8 ± 0.1	48.6 ± 5.5	0	8 ± 4	2 ± 1
		1.0	58 ± 1	35.5 ± 1.7	0.1 ± 0.1	5.3 ± 1.7	1.4 ± 0.5
		2.0	75.6	21.5	0	2.4	0.6
A-46	0.40	0.5	48.4	51.6	0	0	0
		1.0	66.7	33.3	0	0	0
		2.0	82.8 ± 0.9	17.2 ± 0.9	0	0	0
A-70	0.25	0.5	44.8	55.2	0	0	0
		1.0	62.4	37.6	0	0	0
		2.0	77.5	22.5	0	0	0
CT-275	0.15	0.5	41.0	54.2	0	3.8	1
		1.0	64 ± 2	30 ± 2	0.3 ± 0.1	5 ± 2	1.2 ± 0.4
		2.0	73.9	14.3	0	9.2	2.5

The singular behavior of A-39 with respect to higher selectivity towards dimers has to be explained as a basis of its properties. A-39 presents the highest swelling capacity among the tested resins, because of its low amount of DVB. Therefore, A-39 would be more affected by swelling and, as a result, the observed increase of isobutene selectivity towards dimers in A-39 experiments could be explained by the larger number of inner active sites that become accessible at higher 1-butanol concentration, which would have a more pronounced effect in A-39 than in the other catalysts.

7.3.2 Effect of the initial concentration on the simultaneous etherification

To study the effect that different reactants concentration could have on the simultaneous etherification reaction performance, initial reactants composition was varied as follows: at equimolar amount of alcohols ($R_{E/B}^{\circ} = 1.0$), the initial molar ratio alcohol/isobutene ($R_{A/O}^{\circ}$) was varied from 0.5 (excess of isobutene) to 5.5 (large excess of alcohols); and, at stoichiometric initial composition alcohol/isobutene ($R_{A/O}^{\circ} = 1.0$), the initial molar ratio ethanol/1-butanol ($R_{E/B}^{\circ}$) was varied between 0.5 (high initial concentration of 1-butanol) and 2.0 (high initial concentration of ethanol). All further experiments were carried out using A-35 as catalyst, since it has been the most promising catalyst among the tested ones.

Figure 7.5 shows that, for experiments at $R_{E/B}^{\circ} = 1.0$, initial reaction rates increased with increasing the initial isobutene molar fraction, x_{IB}° (which, in the assayed experimental conditions, corresponds to a decrease in $R_{A/O}^{\circ}$). The same behavior can be observed for both

reactions and it agrees with results reported in literature on different alcohol/isobutene systems, in which methanol, ethanol, or 1-butanol were considered [59,136,138].

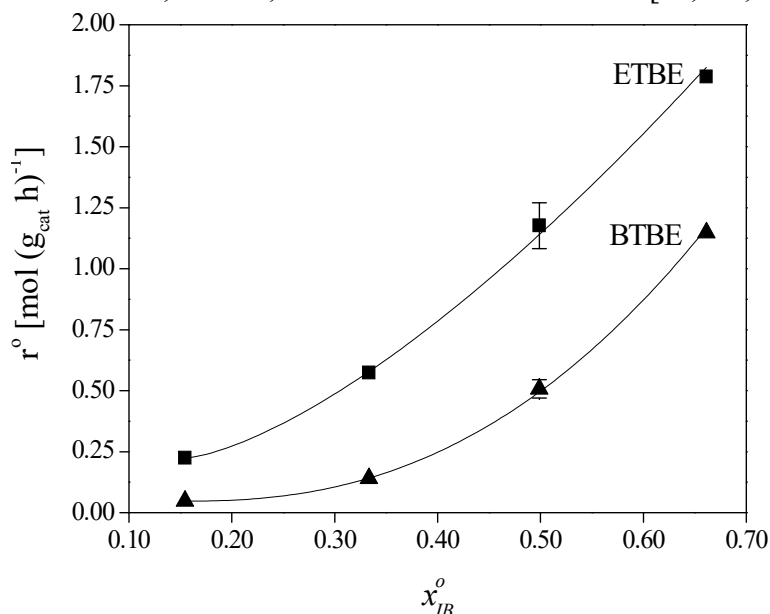


Figure 7.5 Initial etherification rate vs. initial isobutene molar fraction. Error bars refer to the standard uncertainty for replicated experiments. A-35, $R_{E/B}^0 = 1.0$, $T = 333$ K, $d_p = 0.25$ - 0.40 mm, 750 rpm. ETBE (■), BTBE (▲)

As for the influence of the initial alcohols composition on rates, it has been shown in the previous section that ETBE rate was hardly affected, whereas BTBE rate strongly diminished as ethanol concentration increased (Figure 7.2). This fact has been related to a possible preferential adsorption of ethanol over 1-butanol on the catalyst active sites, what hinders BTBE formation. To check it, some adsorption experiments were performed using A-35 at 333 K and atmospheric pressure. 10 mL of commercial size beads, previously pretreated to reduce their water content (catalyst dry weight was about 3.6 g), were introduced into test tubes containing 20 mL of alcohol mixtures, submerged in a thermostatic bath. Five different alcohol mixtures were used, whose initial ethanol/1-butanol ratio, $R_{E/B}^0$, ranged from 8.4 to 0.10. Then, the liquid-phase composition was analyzed by means of repeated GC analyses. The evolution in time of the ethanol/1-butanol molar ratio of the liquid phase is represented in Figure 7.6 for the different mixtures. As seen in the figure, ethanol/1-butanol molar ratios slightly decreased progressively for all $R_{E/B}^0$, what indicates a preferential adsorption of ethanol compared to 1-butanol. These results are in agreement with literature data on the adsorbed concentration of alcohols on the ion-exchange resin AmberlystTM 15 in gas-phase experiments [158] where it was found that the amount of alcohol adsorbed by the resin was higher for alcohols with shorter carbon chains, considering a series of C₁ to C₄ linear primary alcohols (i.e. methanol, ethanol, 1-propanol, and 1-butanol).

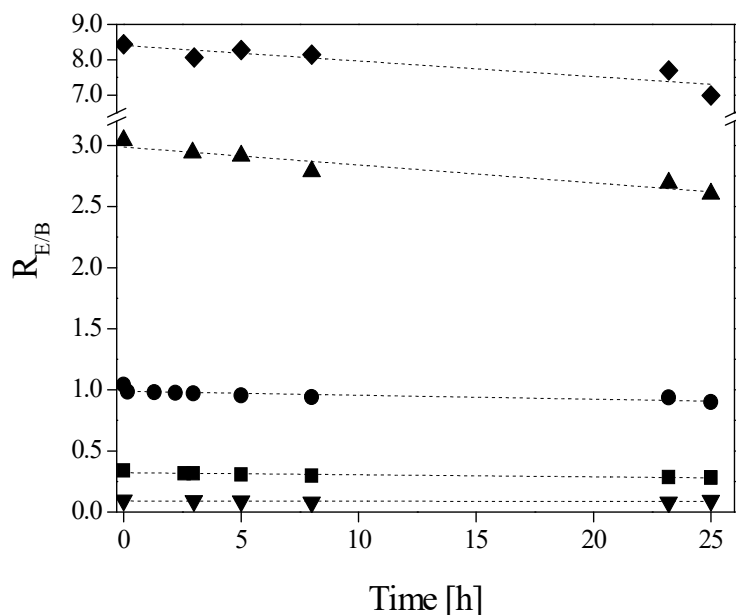


Figure 7.6 Evolution in time of the liquid-phase ethanol/1-butanol molar ratio at $T = 333\text{ K}$ with A-35. $R_{E/B}^{\circ} = 8.4$ (♦), $R_{E/B}^{\circ} = 3.04$ (▲), $R_{E/B}^{\circ} = 1.03$ (●), $R_{E/B}^{\circ} = 0.34$ (■), $R_{E/B}^{\circ} = 0.10$ (▼)

With regard to byproducts formation at $R_{E/B}^{\circ} = 1.0$, dimerization of isobutene was notably favored when isobutene was in excess ($R_{A/O}^{\circ} = 0.5$, which, in the assayed experimental conditions, corresponds to $x_{IB}^{\circ} = 0.66$). Under these conditions and after 300 min, isobutene selectivity values towards TMP-1 and TMP-2 were up to 18 and 5%, respectively. In large excess of alcohols ($R_{A/O}^{\circ} = 5.5$, which, in the assayed experimental conditions, corresponds to $x_{IB}^{\circ} = 0.15$) no dimers were detected. On the other hand, higher amounts of TBA were formed when alcohols were in excess (isobutene selectivity towards TBA was up to 0.8% at $t = 300\text{ min}$ with $R_{A/O}^{\circ} = 5.5$), which can be related to the alcohols water content.

The enhancement of dimers formation when isobutene is in excess is known to be due to the adsorption of isobutene on non-dissociated sulfonic groups, typically associated to a concerted mechanism (general acid catalysis) [58]. In this type of mechanism, the rate-determining step is the surface reaction either between adsorbed molecules or between adsorbed and non-adsorbed molecules, as would be the case of the isobutene dimerization [59,60,62,131]. This mechanism is faster than the ionic one (specific acid catalysis), which is characteristic of large excess of a polar compound, e.g. water and alcohols, and can account for the decrease of etherification rates observed at high $R_{A/O}^{\circ}$.

Main products distribution dependence on initial reactants composition is depicted in Figures 7.7 and 7.8, in terms of isobutene selectivity towards ethers against isobutene conversion for different initial composition of the reactants mixture. As it is seen in Figure 7.7, where results correspond to experiments at $R_{E/B}^{\circ} = 1.0$, the excess of alcohols enhances isobutene selectivity towards ETBE over BTBE. Results at $R_{A/O}^{\circ} = 1.0$, which are shown in Figure 7.8, show that a high concentration of ethanol ($R_{E/B}^{\circ} = 2.0$) favors ETBE production over that of BTBE. In the range of the assayed initial compositions, overall isobutene selectivity towards ethers was about 97% for the highest isobutene

conversion values, except for the experiment at $R_{A/O}^{\circ} = 0.5$ and $R_{E/B}^{\circ} = 1.0$, in which the isobutene selectivity towards ethers dropped to around 80% because of the already commented enhancement of isobutene dimerization.

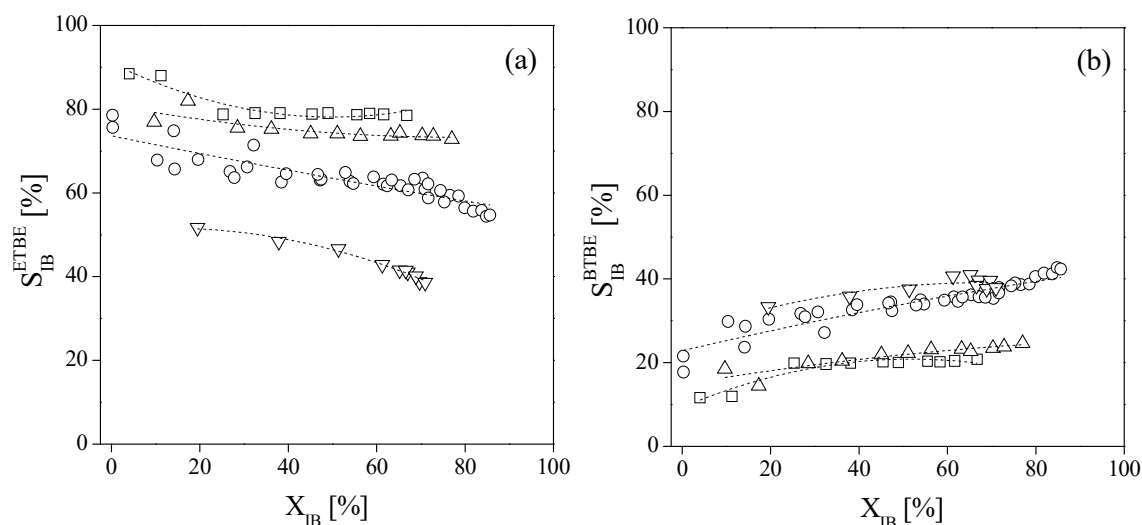


Figure 7.7 Isobutene selectivity towards ETBE (a) and BTBE (b) as a function of isobutene conversion. A-35, $R_{E/B}^{\circ} = 1.0$, $T = 333$ K, $d_p = 0.25$ - 0.40 mm, 750 rpm. $R_{A/O}^{\circ} = 5.5$ (\square), $R_{A/O}^{\circ} = 2.0$ (Δ), $R_{A/O}^{\circ} = 1.0$ (\circ), $R_{A/O}^{\circ} = 0.5$ (∇)

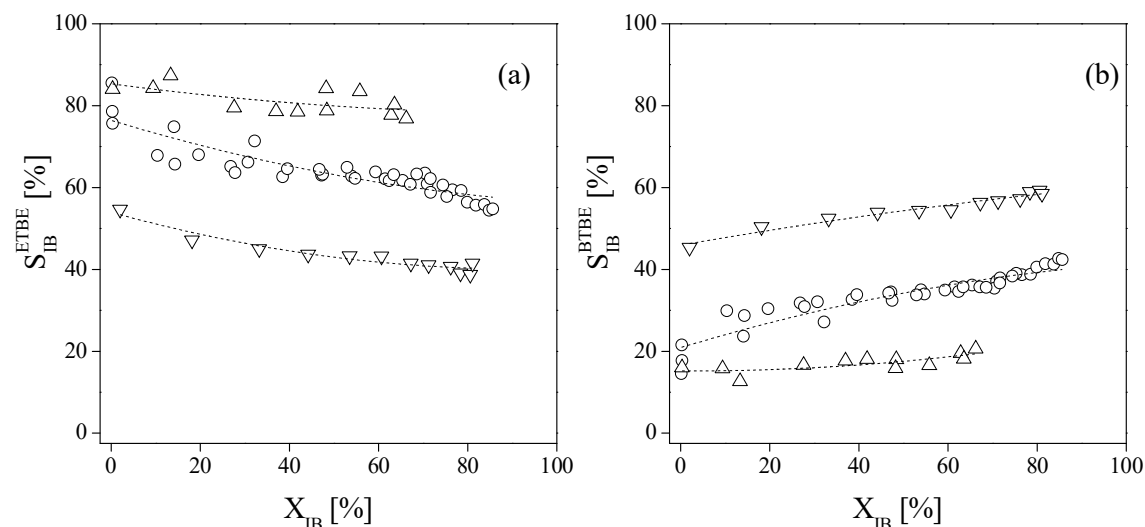


Figure 7.8 Isobutene selectivity towards ETBE (a) and BTBE (b) as a function of isobutene conversion. A-35, $R_{A/O}^{\circ} = 1.0$, $T = 333$ K, $d_p = 0.25$ - 0.40 mm, 750 rpm. $R_{E/B}^{\circ} = 2.0$ (Δ), $R_{E/B}^{\circ} = 1.0$ (\circ), $R_{E/B}^{\circ} = 0.5$ (∇)

From an industrial standpoint, these results point out that the overall performance of the simultaneous etherification can be adapted to the market demands and stock disposal by selecting the reactants composition. For instance, given that byproducts are not desirable, $R_{A/O}^{\circ}$ should be near 1.0 or slightly higher, and if production of one ether is preferred over the other, the corresponding alcohol concentration should be increased. If an increased overall ethers production is required, $R_{E/B}^{\circ}$ should be below 1.0, because BTBE synthesis is more penalized than ETBE at low concentrations of the respective alcohol, in both terms of reaction rate and selectivity.

7.3.3 Effect of temperature on the simultaneous etherification

The effect of temperature on the simultaneous etherification process performance was assessed by carrying out experiments in the temperature range of 315 to 353 K, at $R_{A/O}^{\circ} = 1.0$, $R_{E/B}^{\circ} = 1.0$, and using A-35 as catalyst.

The isobutene selectivity towards ethers at different isobutene conversion levels is depicted in Figure 7.9 as a function of temperature. As it is observed, isobutene selectivity towards ETBE is higher than towards BTBE. Both selectivity values approach as temperature and conversion increase.

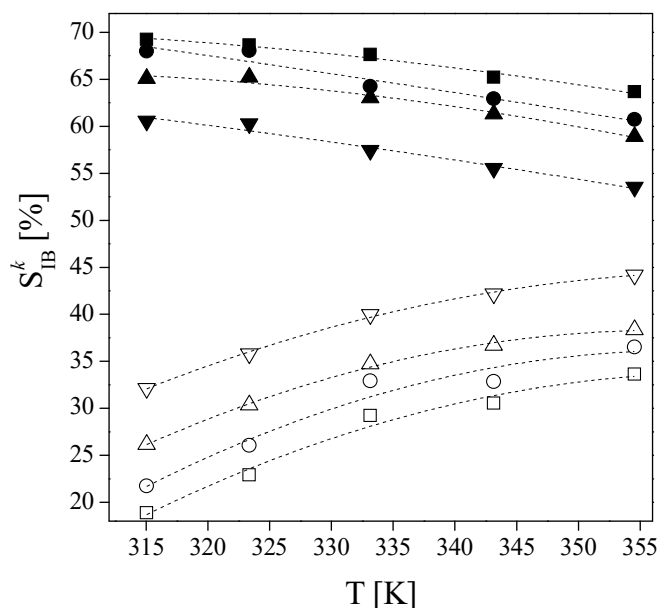


Figure 7.9 Isobutene selectivity towards main products as a function of temperature for a given isobutene conversion level. A-35, $R_{A/O}^{\circ} = 1.0$, $R_{E/B}^{\circ} = 1.0$, $d_p = 0.25\text{-}0.40$ mm, 750 rpm. Solid symbols: S_{IB}^{ETBE} at $X_{IB} = 20\%$ (■), $X_{IB} = 40\%$ (●), $X_{IB} = 60\%$ (▲), and $X_{IB} = 80\%$ (▼); Open symbols: S_{IB}^{BTBE} at $X_{IB} = 20\%$ (□), $X_{IB} = 40\%$ (○), $X_{IB} = 60\%$ (△), $X_{IB} = 80\%$ (▽)

With regard to the sensitivity of etherification rates to temperature variations, the Arrhenius plot of initial etherification reaction rates is shown in Figure 7.10. As seen, rates at the highest assayed temperature (around 353 K) are not aligned with the rest. It indicates that, at 353 K, some transport limitations affect the overall reaction rate. As it can be assumed that there was no significant effect of the external mass transfer, since the stirring speed was large enough (750 rpm), the observed depletion in the Arrhenius plot would indicate that the catalyst bead size used for these experiments ($d_p = 0.25\text{-}0.40$ mm) was large enough for the catalyst to experience non-negligible hindrances due to diffusion through the pores at that temperature. Thus, an additional experiment was performed, using a smaller particle size ($d_p = 0.08\text{-}0.16$ mm) at 353 K, also included in Figure 7.10 as open symbols, which gives reaction rate values aligned with lower-temperature rates, within the margin of experimental error, what confirms the effect of the internal mass transport limitations at 353 K.

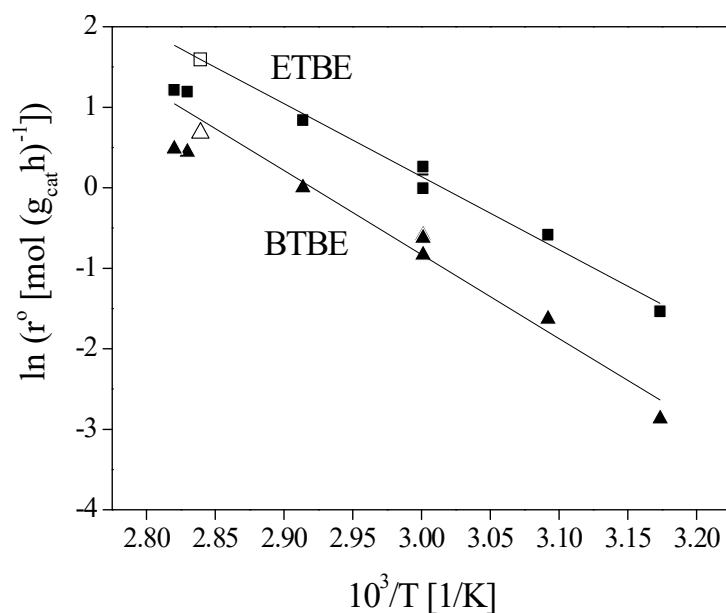


Figure 7.10 Arrhenius plot of the initial etherification rates. Solid lines represent the fit of rate data to straight lines. Open symbols represent rate data using bead size range of 0.08-0.16 mm. A-35, $R_{A/O}^{\circ} = 1.0$, $R_{E/B}^{\circ} = 1.0$, $d_p = 0.25$ -0.40 mm, 750 rpm. ETBE (■), BTBE (▲)

From the slope of the solid lines shown in Figure 7.10, the calculated apparent activation energies in the simultaneous synthesis result in (75 ± 4) kJ mol⁻¹ and (85 ± 7) kJ mol⁻¹ for the ETBE and BTBE syntheses, respectively. ETBE apparent activation energy agrees with literature data, which has been reported to be in the range of 72 to 83 kJ mol⁻¹ using A-35 as catalyst [19]. No reported data for the BTBE synthesis activation energy were found in the open literature.

Given that no information was found regarding BTBE synthesis reaction rate dependence on temperature, some additional experiments were carried out in the temperature range between 303 and 353 K in the BTBE system. Experimental conditions concerning this set of experiments were: $R_{A/O}^{\circ} = 1.0$, A-35 as catalyst, 0.25-0.40 mm beads (the same particle size range was used for comparison purposes), and stirring speed of 750 rpm. Literature rate data regarding ETBE rate dependence on temperature were also retrieved from a previous study aimed at determining the experimental conditions that ensured no significant mass transfer limitations [159]. The logarithm of the isobutene consumption rate for these three systems (i.e., ETBE synthesis, BTBE synthesis, and simultaneous ETBE and BTBE syntheses) is plotted against the inverse temperature in Figure 7.11.

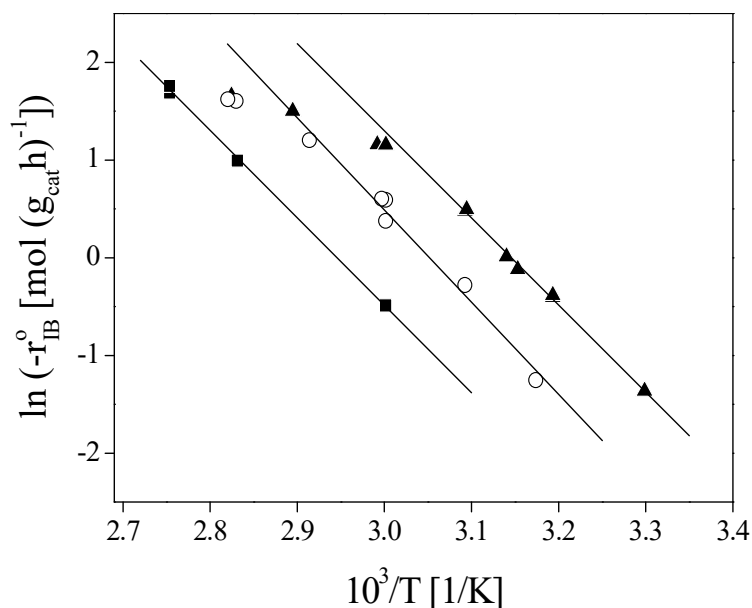


Figure 7.11 Dependence of initial rates on temperature. Solid lines represent the fit of rate data free from mass transfer effects to straight lines. A-35, $d_p = 0.25\text{-}0.40$ mm, 750 rpm, $R_{A/O}^\circ = 1.0$, and $R_{E/B}^\circ = 1.0$ (only simultaneous synthesis). ETBE (■), BTBE (▲), simultaneous synthesis (○)

Results in Figure 7.11 allow inferring that the isobutene consumption rate dependence on temperature is analogous for the three systems, given that the slopes of the straight lines are almost equal. From these slopes, apparent activation energies are (74 ± 1) kJ mol^{-1} and (74 ± 2) kJ mol^{-1} for the individual syntheses of ETBE and BTBE, respectively. Notice that the estimated values of ETBE apparent activation energy in both the simultaneous synthesis and the individual one are the same, within the margin of experimental error, whereas there is a slight increase of the BTBE apparent activation energy in the simultaneous system compared to that of the individual synthesis. This fact could suggest that ETBE synthesis reaction rate would not be affected by the presence of 1-butanol, but that BTBE reaction rate could be influenced in the simultaneous system, possibly due to a change in the number of active sites accessible to 1-butanol promoted by the ethanol presence, compared to those in the individual BTBE synthesis.

Isobutene consumption rate at a given temperature follows the order: BTBE system > simultaneous system > ETBE system, when internal mass transfer effects on overall reaction rates are negligible. At temperatures higher than 333 K, and using A-35 particles of $d_p = 0.25\text{-}0.40$ mm, rate limitations due to internal mass transfer on the BTBE synthesis become non-negligible. Likewise, these effects are significant at temperatures higher than 343 K for the simultaneous system. No significant mass transfer limitations on rates were detected in the ETBE system at temperatures as high as 363 K, using the same catalyst and particle size range.

From these results, efficiency factors using 0.25-0.40 mm beads of A-35 can be calculated as the quotient between actual initial rates and initial rates free from mass transfer effects. Efficiency factors for the BTBE synthesis are about 0.5 and 0.3 at 343

K and 353 K, respectively. For the simultaneous system, efficiency is slightly over 0.6 at 353 K. Within the assayed temperature range, 0.25-0.40 mm particles of A-35 would present efficiency factor values close to unity for the individual synthesis of ETBE at all temperatures. Thus, rate limitations due to diffusion through the pores are more accused in the BTBE synthesis than they are in the ETBE synthesis. Given that the difference between these two systems is the size of the involved compounds, it seems reasonable to assume that BTBE formation is hindered by internal mass transport limitations because of the steric effects caused by either 1-butanol or the resulting ether at those temperatures. Results also point out that mass transport limitations on ETBE rate, when produced simultaneously with BTBE, also arise, whereas these limitations were not observed in the absence of 1-butanol. This fact suggests that the presence of 1-butanol reduces the mass transport within the resin for both 1-butanol and ethanol.

7.3.4 Comparison between simultaneous system and individual syntheses

Finally, the performance of the etherification reaction of each individual synthesis was compared to that of the simultaneous process by means of three analogous experimental runs (one with ethanol, one with 1-butanol, and one with the two alcohols as reactants). Experimental conditions regarding these runs were as follows: $T = 333$ K, A-35 as catalyst, catalyst load = 0.16%wt., $d_p = 0.25$ -0.40 mm, stirring speed = 750 rpm, and $R^{\circ}_{A/O} = 1.0$. Initial concentrations could not be the same, since no diluents were added. Therefore, to maintain the initial alcohol/isobutene molar ratio ($R^{\circ}_{A/O}$) at 1.0, the initial molar ratios were 1:1 (isobutene:alcohol) in the individual syntheses, and 2:1:1 (isobutene:ethanol:1-butanol) in the simultaneous process. Figures 7.12 and 7.13 show the mole evolution in time of the main compounds for the three systems. Figure 7.12a corresponds to the reaction between isobutene and ethanol, and Figure 7.12b to the reaction with 1-butanol. In Figure 7.13, the mole evolution of an experiment with both ethanol and 1-butanol as reactants is presented.

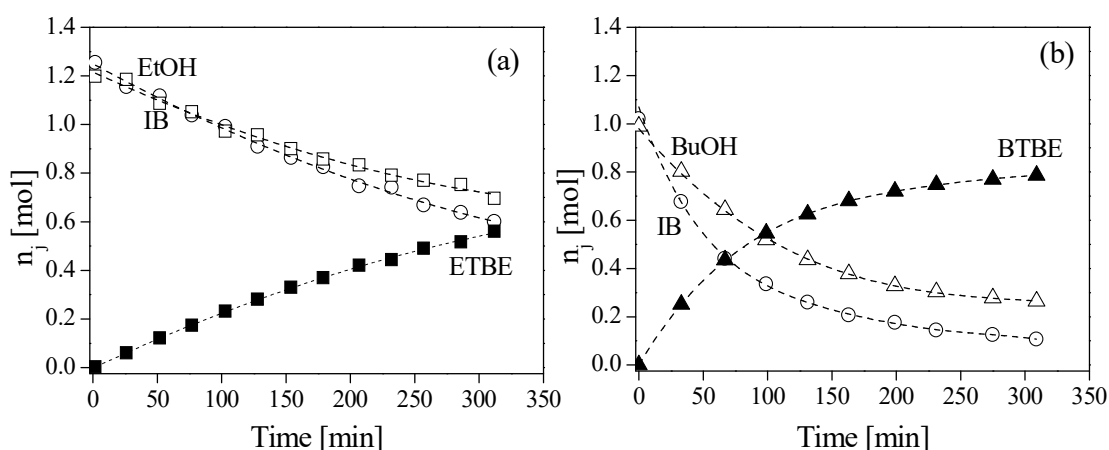


Figure 7.12 Mole evolution in time of the main compounds for ETBE (a) and BTBE (b) individual syntheses. A-35, catalyst load = 0.16%wt., $d_p = 0.25$ -0.40 mm, 750 rpm, $R^{\circ}_{A/O} = 1.0$, $T = 333$ K. IB (\circ), EtOH (\square), BuOH (Δ), ETBE (\blacksquare), BTBE (\blacktriangle)

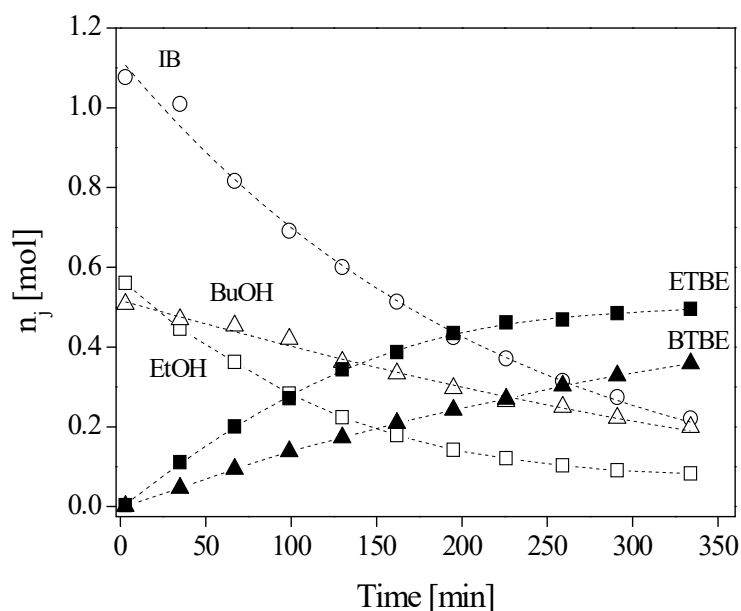


Figure 7.13 Mole evolution in time of the main compounds in the simultaneous syntheses. A-35, catalyst load = 0.16%wt., $d_p = 0.25\text{-}0.40$ mm, 750 rpm, $R_{A/O}^\circ = 1.0$, $R_{E/B}^\circ = 1.0$, $T = 333$ K. IB (\circ), EtOH (\square), BuOH (Δ), ETBE (\blacksquare), BTBE (\blacktriangle)

As it can be seen in Figure 7.12, the individual BTBE production proceeds much faster and in a larger extent than that of ETBE. This fact is consistent with the higher reactivity of larger primary alcohols with isobutene already reported in literature [59,142,160]. In contrast, in the simultaneous system (Figure 7.13), the opposite situation was observed, which can be explained by the previously discussed preferential adsorption of ethanol compared to 1-butanol on the resin active sites.

With regard to the side reactions extension in the studied systems, isobutene selectivity values (Table 7.2) towards ethers and byproducts were almost the same for the two individual syntheses, reaching selectivity values towards ether over 91% in both cases. On the other hand, overall isobutene selectivity towards ethers in the simultaneous system reached values of about 97% at $t = 300$ min, what would imply a significant advantage in industrial operation. The higher overall selectivity towards ethers in the simultaneous process is consistent with a larger number of accessible active sites occupied by alcohol molecules compared to individual syntheses.

Table 7.2 Reactants initial concentration and conversion and selectivity at $t = 300$ min for individual and simultaneous processes. A-35, catalyst load = 0.16%wt., $d_p = 0.25\text{-}0.40$ mm, 750 rpm, $T = 333$ K

Reactants initial concentration [mol L^{-1}]			Reactants conversion and selectivity [%]							
isobutene	ethanol	1-butanol	X_{IB}	X_{EtOH}	X_{BuOH}	S_{IB}^{ETBE}	S_{IB}^{BTBE}	S_{IB}^{TMP-1}	S_{IB}^{TMP-2}	S_{IB}^{TBA}
6.1	6.1		48.9	42.8		91.3		6.8	1.6	0.3
5.1		5.1	88.0		73.6		91.3	6.9	1.7	0.2
5.5	2.8	2.8	76.3	84.6	60.5	57.5	39.3	2.5	0.5	0.2

7.4 Conclusions

Several aspects of the syntheses of ETBE and BTBE by means of the simultaneous etherification of isobutene with ethanol and 1-butanol over acidic macroreticular ion-exchange resins have been studied. From the screening study in which six different ion-exchange resins were tested, A-35 stands out as the most appropriate catalyst for the simultaneous etherification process, because it yields low byproducts formation and high reaction rates.

Experimental reaction rates have been found to increase linearly with the resin active sites concentration in the swollen gel phase volume of the tested resins. Strongly acidic catalysts with high crosslinking degrees achieve faster reaction rates, what implies that some rigidity of the polymer backbone is required to avoid excessive swelling in order to maintain a high active sites density in the catalyst gel phase.

Both ethers formation rates increase at high initial isobutene concentration, but dimers are produced in a larger extent. ETBE reaction rate is hardly affected by variation of the initial alcohols molar ratio, whereas BTBE production rate strongly diminishes when ethanol concentration is higher than that of 1-butanol. A preferential adsorption of ethanol over 1-butanol on the tested resins has been observed.

In the simultaneous etherification process, ETBE and BTBE apparent activation energies are $(75 \pm 4) \text{ kJ mol}^{-1}$ and $(85 \pm 7) \text{ kJ mol}^{-1}$, respectively, and, in the individual processes, $(74 \pm 1) \text{ kJ mol}^{-1}$ and $(74 \pm 2) \text{ kJ mol}^{-1}$, respectively. The apparent activation energy for the ETBE synthesis is not modified by the 1-butanol presence, while that of BTBE synthesis slightly increases by the ethanol presence. Since ethanol adsorbs preferentially on the catalyst, its presence reduces noticeably the BTBE formation rate, below the ETBE formation rate at equal initial molar concentration. Finally, the simultaneous syntheses of ETBE and BTBE present high reactants conversion and selectivity towards the desired products. The simultaneous process produces less byproducts than each of the individual syntheses.

8. Kinetics of the liquid-phase synthesis of alkyl tertiary butyl ethers over AmberlystTM 35

8.1 Introduction

Kinetics of methyl *tert*-butyl ether (MTBE) and ethyl *tert*-butyl ether (ETBE) syntheses has been studied during the past three decades. In the earliest works, kinetic expressions were obtained in terms of concentrations, e.g., [161,100]. Later on, the high non-ideality of olefin-alcohol-ether mixtures was taken into account and activity-based expressions were found to be more appropriate, e.g., [95,162,163]. More recently, rate expressions can be found that include the influence on reaction rate of the interaction between the liquid reaction medium and the catalyst matrix, e.g., [19,136,138,150]. Rate equations for these reactions are usually derived from the Langmuir-Hinshelwood-Hougen-Watson (LHHW) formalism, in which the surface reaction is considered as the rate-determining step. Depending on the assumptions adopted by each author, the kinetic models reported in the literature can differ, for instance, on the number of active sites, or clusters of them, that participate in the rate-determining step or on the compounds that adsorb significantly on the resin active sites.

In this framework, the kinetics of three etherification reaction systems in the liquid-phase has been studied: the individual productions of PTBE and BTBE, and the simultaneous syntheses of ETBE and BTBE (Figure 8.1) over the ion-exchange resin Amberlyst™ 35.

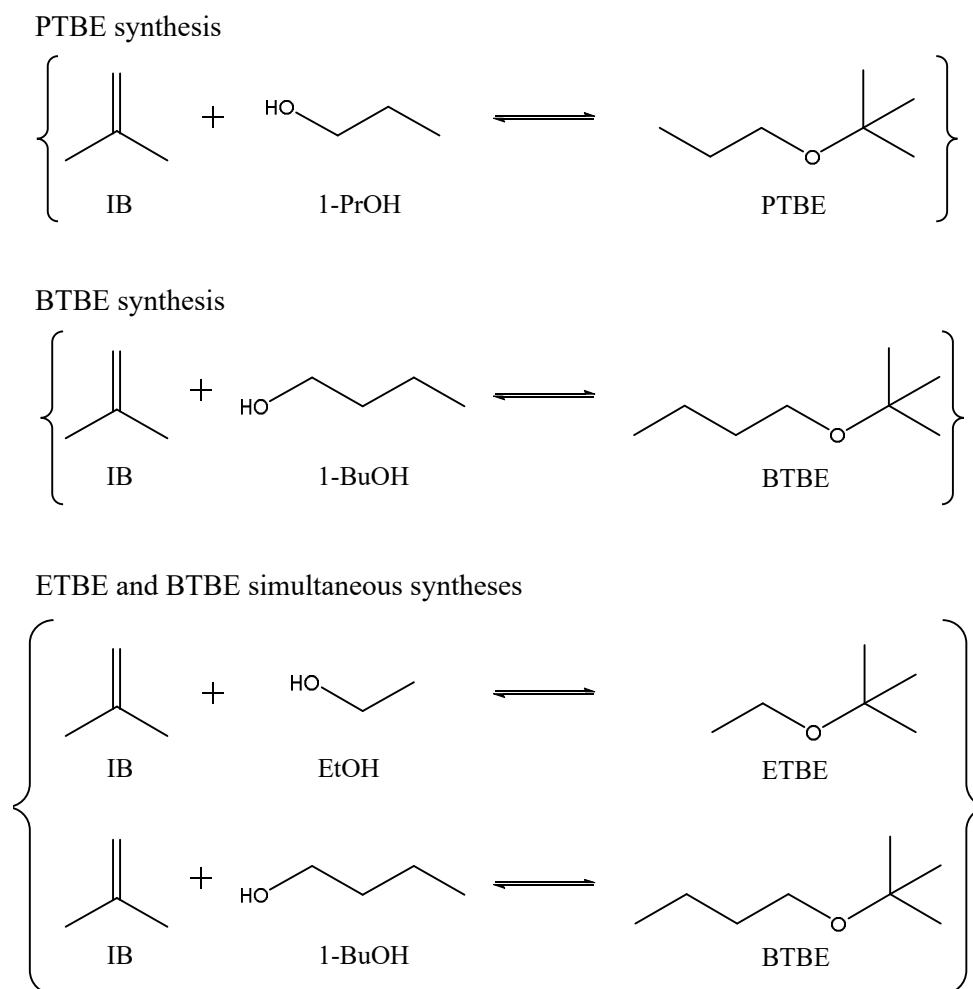


Figure 8.1 Studied reaction systems

The considered reactions involve the addition of one alcohol molecule to one isobutene molecule through the double bond of the olefin, the main difference being the length of the alcohol. In the case of the simultaneous syntheses of ETBE and BTBE, the relative occupancy of active sites by adsorption of both alcohols, with preferential adsorption of ethanol over 1-butanol (see Chapter 7), might affect kinetics and, therefore, it has to be taken into account. The ability of a reactant to access and adsorb on the resin active sites plays a determinant role in the reaction. Obviously, this ability depends on the reactant nature, and also some interaction effect with the other compounds could arise.

To date, no references have been found in the available literature concerning the kinetics of PTBE and BTBE reaction syntheses in the liquid-phase over ion-exchange resins as catalysts, nor of simultaneous syntheses of these ethers. The most relevant related references are the kinetic study of the PTBE gas-phase synthesis by Słomkiewicz [107] and the study of Ancillotti and coworkers regarding the simultaneous production of MTBE and BTBE [59,60], both using Amberlyst™ 15 as the catalyst.

The aim of this chapter is to study the kinetics of these reaction systems. A proposal is presented of a methodology for obtaining a systematic combination of kinetic models and for subsequently comparing fitting results to experimental data.

8.2 Experimental

8.2.1 Chemicals and catalyst

Reactants were ethanol, 1-propanol, 1-butanol, and either 2-methylpropene (isobutene) or the synthetic C₄ mixture as the isobutene source. Some chemical standards were used for chromatographic analysis: 2-methyl-2-propanol (TBA), diethyl ether (DEE), 2,4,4-trimethyl-1-pentene (TMP-1), 2,4,4-trimethyl-2-pentene (TMP-2), 2-ethoxy-2-methylpropane (ETBE), 2-methyl-2-propoxypropane (PTBE), and 1-*tert*-butoxybutane (BTBE).

As catalyst, the ion-exchange resin Amberlyst™ 35 (A-35) was used because, as seen in previous chapters, it was found to be the most active catalyst, among the tested ones, for these reactions. A-35 is a macroreticular, strongly acidic sulfonated polymer of styrene-divinylbenzene. Its physical properties are listed in Table 8.1. Like in previous chapters, the catalyst was pretreated to reduce its water content because it is commercially supplied in wet form. Since specific ranges of catalyst particle size were used, the catalyst beads were crushed and sieved before drying in the atmospheric oven.

Table 8.1 Physical properties of A-35

Catalyst		Amberlyst™ 35
Structure		Macroreticular
Divinylbenzene	[%]	20
Skeletal density, ρ_{sk}	[g / cm ³]	1.542
Acid capacity ^a	[meqH ⁺ / g _{cat}]	5.32
Mean particle diameter, $d_{p,m}$ ^b	[μ m]	623
BET surface area, S_{BET}	[m ² / g _{cat}]	29.0
Swollen-state pore volume, V_g ^c	[cm ³ / g]	0.720
Volume of the swollen polymer phase, V_{SP} ^c	[cm ³ / g]	0.613
Porosity in polar medium, ϕ_p ^d		0.513
Max. temperature operation, T_{max}	[K]	423

^a Titration against standard base. ^b Laser diffraction technique in air. ^c Inverse Steric Exclusion Chromatography technique [65,66].

$$\phi_p = (V_g + V_{SP} - 1/\rho_{sk}) / (V_g + V_{SP})$$

8.2.2 Apparatus, procedure and analysis

Experiments were performed at constant pressure and at the temperature range from 303 to 354 K, using two reactor setups. Most of the experiments were performed in a batch stirred tank reactor setup and some experiments were carried out in a continuously operated fixed-bed catalytic reactor. The initial reactants mixture in batch experiments, and the reactor feed in continuous experiments were free of ether. Kinetic data from the experiments in the fixed-bed reactor were used to validate the kinetic models for the individual syntheses of both PTBE and BTBE. All the experiments were performed using 0.25-0.40 mm catalyst beads, unless indicated otherwise.

8.2.2.1 Batch reactor

In the individual syntheses of PTBE and BTBE, the initial alcohol to isobutene molar ratio, $R_{A/O}^o$, was varied from 1.0 to 2.0. In the simultaneous syntheses of ETBE and BTBE, the initial molar alcohol/isobutene and ethanol/1-butanol ratios ($R_{A/O}^o$ and $R_{E/B}^o$) were both varied from 0.5 to 2.0. Pure isobutene was used as reactant for all the experiments carried out in the batch reactor.

The experimental and analysis procedures for the batch reactor experiments have been described in Chapter 3 for the individual syntheses, and in Chapter 7 for the simultaneous syntheses.

Reaction rates were calculated by differentiating with respect to time empirical functions fitted to the evolution of moles of reactants or products, as follows:

$$r_j = \frac{1}{W_{cat}} \left(\frac{dn_j}{dt} \right) \left[\frac{\text{mol}}{\text{h g}_{cat}} \right] \quad (8.1)$$

where W_{cat} is the weight of dry catalyst, n_j is the number of mole of the compound j and t is the time of reaction.

8.2.2.2 Fixed-bed reactor

Some experiments were performed in the catalytic fixed-bed tubular microreactor operating at constant temperature and under differential conditions. The amount of catalyst in the catalytic bed was selected in order to obtain a low isobutene conversion level at each temperature, so the reactor behaved differentially. To keep the reactor bed as isothermal, the catalyst was diluted with inert silicon carbide of the same particle size range. Inert/catalyst mass ratios were kept under 300, to avoid back-mixing and channeling [159,19]. Either pure isobutene or the C₄ mixture was used as the isobutene source. Reactor feed was free of product, what means a null isobutene conversion level at the reactor inlet. The alcohol to isobutene molar ratio ($R_{A/O}^o$) at the reactor inlet was set to 1.0.

Experimental results were quantified in terms of reaction rate with respect to isobutene, by means of the following expression, which applies to a plug-flow fixed-bed catalytic reactor under differential regime:

$$-r_{IB} = \frac{F_{IB}^o (X_{IB,outlet} - X_{IB,inlet})}{W_{cat}} \quad (8.2)$$

where F_{IB}^o is the isobutene reference molar flow at null conversion, $X_{IB,outlet}$ is the isobutene conversion at the reactor outlet, and $X_{IB,inlet}$, the inlet isobutene conversion, was zero. Isobutene conversion was calculated as follows:

$$X_{IB} = 1 - \frac{F_{IB,outlet}}{F_{IB,inlet}} \quad (8.3)$$

8.3 Results and discussion

8.3.1 Experimental results

To obtain intrinsic kinetics, experimentally measured reaction rates must be free from mass transfer limitations. Internal mass transfer effects could arise with large particle size, and external mass transfer resistance may happen at low fluid velocity at the external catalyst surface, that is, at low stirring speed in the batch reactor, or at low flow rate in the fixed-bed reactor. The presence of mass transfer limitations leads to lower measured reaction rates. In particular, this effect is more noticeable at higher temperature, because of the higher expected chemical reaction rates. Therefore, one way to find out whether mass transfer effects occur is to check if a reduction of the apparent activation energy is observed in experiments carried out under the same conditions, but at increasing temperature. With this purpose, the logarithm of initial reaction rates (for batch reactor experiments) and steady-state reaction rates under differential regime (for fixed-bed reactor experiments) is plotted against the inverse temperature in Figure 8.2. These reaction rates were obtained in experiments with the same reactants composition, i.e., $R_{A/O}^o = 1.0$ and using pure isobutene, for the individual syntheses of both PTBE and

BTBE⁴. Note that, if measured reaction rates are free from mass transfer limitations, their values should agree in both used reactor systems.

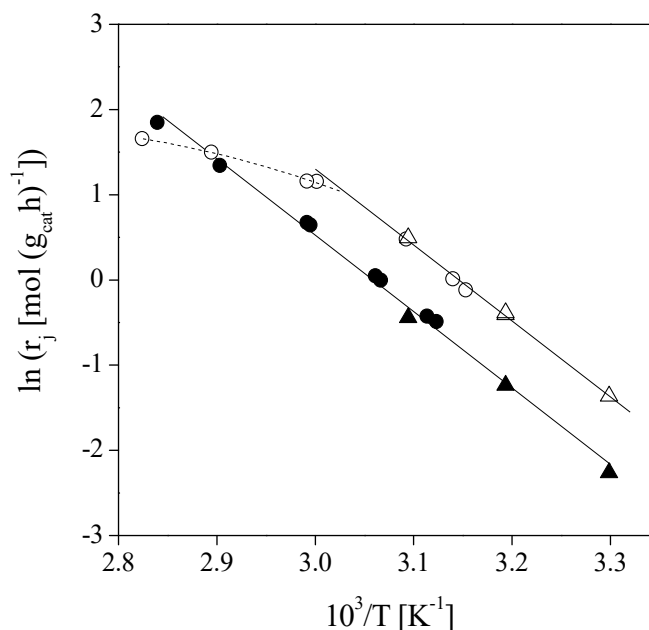


Figure 8.2 Arrhenius plot of reaction rate data. $R_{A/O}^0 = 1.0$, pure isobutene.

Solid symbols: PTBE formation rates from the batch reactor setup (●) and from the fixed-bed reactor setup (▲). Open symbols: BTBE formation rates from the batch reactor setup (○) and from the fixed-bed reactor setup (Δ)

As seen in Figure 8.2, PTBE reaction rate values are distributed around a well-defined straight line, with agreement between results obtained from the batch reactor and the fixed-bed reactor. This fact indicates that PTBE rates were not significantly affected by neither external nor internal diffusion effects, within the margin of experimental error, in the whole assayed range of temperatures. On the contrary, BTBE formation rates drop at temperatures higher than 323 K (at about $10^3/T < 3.1$ K⁻¹ in Figure 8.2), what indicates the effect of mass transfer resistances. This effect was also observed in the simultaneous synthesis of ETBE and BTBE (see section 7.3.3) at temperatures higher than 343 K with catalyst particles in the range of 0.25 to 0.40 mm. Since in an additional experiment at 352 K and using smaller catalyst particles ($d_p = 0.08$ -0.16 mm) this effect disappeared, it can be attributed to internal mass transfer effects, that is, to diffusional limitations within the catalyst particles.

Slopes of the solid straight lines in Figure 8.2 reveal almost identical apparent activation energies for both PTBE and BTBE formation reactions, their values being (75 ± 4) and (74 ± 2) kJ mol⁻¹, respectively. As indicated in Chapter 7, apparent activation energies for ETBE and BTBE formations in their simultaneous syntheses were (75 ± 4) and (85 ± 7) kJ mol⁻¹, respectively. These values are similar to those quoted in literature for

⁴ A list of the considered experimental conditions and main results, in terms of initial reaction rates, for each reaction system can be found in Tables A7, A8, and A9 (Appendix I).

similar reactions over the same catalyst, i.e., syntheses of MTBE (84 kJ mol⁻¹ [159]) and ETBE (between 72 and 83 kJ mol⁻¹ [159,19]).

8.3.2 Systematic kinetic modeling

Experimental intrinsic rate data, free from mass transfer limitations, for each reaction system were used to fit kinetic equations based on the LHHW kinetic formalism. In the case of individual synthesis of PTBE and BTBE, only one kinetic equation is required; in the simultaneous ETBE and BTBE, a system of two kinetic equations, one per reaction, is considered. For each reaction, a large number of different kinetic equations has been proposed by the systematical combination of all possible rate-determining steps, and adsorbed and non-adsorbed species on the catalyst. UNIFAC-Dortmund [85] activities were used rather than concentrations, due to high non-ideality of the reacting mixtures. All proposed equations can be described by the following general expression:

$$\text{reaction rate} = \frac{[\text{kinetic term}][\text{driving force}]}{[\text{adsorption term}]^n} \Psi \quad (8.4)$$

Five parts can be distinguished in the general kinetic expression: the kinetic term, the driving force, the adsorption term, the exponent of the denominator, and Ψ , a factor that accounts for the effect on the catalytic activity due to a possible interaction between the reaction medium and the catalyst, that has been found to enhance the reaction rate prediction in analogous reaction systems [150].

- The kinetic term, which is always present in the kinetic equation, is expected to depend only on temperature, following the Arrhenius law. It can be expressed as follows:

$$[\text{kinetic term}] = k'_i = \exp \left[k'_{i_1} + k'_{i_2} \left(\frac{1}{T} - \frac{1}{\bar{T}} \right) \right] \quad (8.5)$$

where k'_{i_1} and k'_{i_2} are the parameters to be fitted. The mean experimental temperature, \bar{T} , is included in order to reduce the correlation between both parameters. The kinetic term is actually an apparent kinetic coefficient, k'_i , that consists of a product of the intrinsic kinetic constant of the rate determining step, and eventually adsorption equilibrium constants and the chemical equilibrium constant, depending on the considered mechanism.

- The driving force accounts for the distance to the equilibrium position and it is always included in the fitted kinetic expressions. This term decreases as the reaction proceeds towards equilibrium, where it becomes zero. Depending on the considered rate-determining step (i.e., surface reaction, alcohol adsorption, isobutene adsorption, or ether desorption), the driving force can be expressed as follows:

$$\text{Surface reaction: [driving force]} = \left(a_{IB} a_{OH} - \frac{a_E}{K_{Eq_i}} \right) \quad (8.6a)$$

$$\text{Alcohol adsorption: [driving force]} = \left(a_{OH} - \frac{a_E}{K_{Eq_i} a_{IB}} \right) \quad (8.6b)$$

$$\text{Isobutene adsorption: [driving force]} = \left(a_{IB} - \frac{a_E}{K_{Eq_i} a_{OH}} \right) \quad (8.6c)$$

$$\text{Ether desorption: [driving force]} = \left(a_{IB} a_{OH} - \frac{a_E}{K_{Eq_i}} \right) \quad (8.6d)$$

where a_j is the activity of compound j , K_{Eq_i} is the equilibrium constant of reaction i , and the subscripts IB , OH , and E refer, respectively, to isobutene, the corresponding alcohol (1-propanol, 1-butanol, or ethanol), and the resulting ether (PTBE, BTBE, or ETBE).

Equilibrium constants values, K_{Eq_i} , had been obtained from chemical composition at equilibrium (see Chapter 3):

$$\ln K_{Eq_{ETBE}} = \frac{(4860 \pm 210)}{T} - (11.46 \pm 0.60) \quad (8.7)$$

$$\begin{aligned} \ln K_{Eq_{PTBE}} = & 864.31 + \frac{105496}{RT} - \frac{1414.36}{R} \ln T + \\ & \frac{10.9645}{2R} T - \frac{27.836 \times 10^{-3}}{6R} T^2 + \frac{2.089 \times 10^{-5}}{12R} T^3 \end{aligned} \quad (8.8)$$

$$\begin{aligned} \ln K_{Eq_{BTBE}} = & 870.35 + \frac{105348}{RT} - \frac{1425.42}{R} \ln T + \\ & \frac{11.0849}{2R} T - \frac{28.316 \times 10^{-3}}{6R} T^2 + \frac{2.1305 \times 10^{-5}}{12R} T^3 \end{aligned} \quad (8.9)$$

In the particular case of the simultaneous syntheses of ETBE and BTBE, it was considered that each reaction could be limited by a different step. Therefore, all possible combinations of driving forces were taken into account.

- The adsorption term accounts for the relative occupancy of the free and the occupied active sites by the different adsorbed species. The adsorption of byproducts (e.g., isobutene dimers, TMP-1 and TMP-2, and TBA) was not considered in the adsorption term, because they were produced in very small amounts in only some of the experiments (the sum of all byproducts was always less than 8% wt. of the reaction medium). The adsorption term can be expressed as follows:

$$[\text{adsorption term}] = \left(\alpha_I + \sum_{j=IB,OH,E} \alpha_j K_j a_j \right) \quad (8.10)$$

Each summand in the adsorption term refers to the relative distribution of occupancy of the active sites. Parameter α_l corresponds to the vacant active sites, and α_j to the active sites occupied by species j . They can take two possible values: 0, when its relative occupancy is not significant, or 1, when it is significant. For example, $\alpha_l = 0$ would indicate that practically there are not vacant active sites, and $\alpha_{OH} = 1$ would indicate that the contribution of the alcohol adsorption is significant.

In the case that $\alpha_l = 1$, parameters K_j correspond to the actual adsorption equilibrium constant of each species j on the catalyst, $K_{a,j}$. If $\alpha_l = 0$, the adsorption term has been expressed as $\left(a_l + \sum_{j \neq l} \alpha_j K_j a_j \right)$, with $K_j = \frac{K_{a,j}}{K_{a,l}}$. Thus, in this situation, the first summand becomes simply the first significant activity a_j , to avoid the total correlation of its adsorption equilibrium constant and the kinetic constant k'_i , and the parameters K_j become, in fact, a ratio of adsorption equilibrium constants. Based on the thermodynamic dependence of equilibrium constants with temperature, every K_j can be expressed as:

$$K_j = \exp \left[K_{j_l} + K_{j_T} \left(\frac{1}{T} - \frac{1}{T} \right) \right] \quad (8.11)$$

When K_j does not depend significantly on temperature, parameter K_{j_T} should be equal to zero, being K_{j_l} the only parameter to be fitted. Additionally, if ether desorption is considered as the rate-determining step, the ether related summand constant K_j would include the respective reaction equilibrium constant.

For the particular case of the simultaneous syntheses of ETBE and BTBE, the adsorption term in their respective kinetic equations should be the same, because of the same relative occupancy of the free and the occupied active sites at a given moment, irrespectively of the reaction taking place.

- The exponent in the adsorption term, n , which accounts for the number of active sites, or clusters, involved in the reaction, was varied from 1 to 3, because these are considered the most likely values.
- The interaction term, Ψ , is a factor based on the Hildebrand solubility parameter, δ . If the possible effect of the interaction between reaction medium and the catalyst is significant, it should be included in the kinetic equation, otherwise, it is equal to unity. This term was calculated as follows [150,136]:

$$\Psi = \exp \left[\alpha_D \frac{\bar{V}_M \phi_P^2}{RT} (\delta_M - \delta_P)^2 \right] \quad (8.12)$$

Included in this term are the liquid mixture molar volume, \bar{V}_M , the catalyst porosity in swollen-state, ϕ_P , the gas constant, R , the temperature, T , and the

Hildebrand solubility parameter for both the liquid mixture and the catalyst, δ_M and δ_P . In the fitting procedure, α_D can take the value equal to 1 (the reaction medium-catalyst interaction would affect reaction rates), or equal to 0 (no significant interaction).

If the interaction term is included in the kinetic expression, it has been considered that δ_P can either be constant within the temperature range or it can linearly decrease as temperature increases, according to literature [150,136]. In this later case, δ_P has the form:

$$\delta_P = k_{D_I} + k_{D_T} (T - \bar{T}) \quad (8.13)$$

in which both k_{D_I} and k_{D_T} are the fitted parameters, and the mean temperature, \bar{T} , is included to reduce the correlation between both.

The remaining values within the interaction term are already known, calculated from the reaction medium composition (\bar{V}_M and δ_M can be estimated as it is described in [88,89,164] as a function of the species concentration in the reaction medium and the temperature) and the catalyst porosity in a polar medium ($\phi_p = 0.513$ from Table 8.1).

For the individual syntheses of both PTBE and BTBE, 117 different kinetic equations are obtained: there are 14 possible combinations of adsorbed and non-adsorbed species in the adsorption term (which are listed in Table 8.2) and each of the subsequent adsorption constants can be sensitive or not sensitive to temperature variations. Additionally, the interaction term can be included in the kinetic equation ($\Psi \neq 1$) or not included ($\Psi = 1$). Since there are four possible driving forces and three possible values of n , up to 1,404 different kinetic equations can be proposed.

Table 8.2 Possible forms of the adsorption term in kinetic expressions for PTBE and BTBE individual syntheses

no.	Adsorption term	no.	Adsorption term
1	1	8	$(1 + K_E a_E)^n$
2	a_{IB}^n	9	$(a_{IB} + K_E a_E)^n$
3	$(1 + K_{IB} a_{IB})^n$	10	$(1 + K_{IB} a_{IB} + K_E a_E)^n$
4	a_{OH}^n	11	$(a_{OH} + K_E a_E)^n$
5	$(1 + K_{OH} a_{OH})^n$	12	$(1 + K_{OH} a_{OH} + K_E a_E)^n$
6	$(a_{IB} + K_{OH} a_{OH})^n$	13	$(a_{IB} + K_{OH} a_{OH} + K_E a_E)^n$
7	$(1 + K_{IB} a_{IB} + K_{OH} a_{OH})^n$	14	$(1 + K_{IB} a_{IB} + K_{OH} a_{OH} + K_E a_E)^n$

Similarly, for the simultaneous syntheses of ETBE and BTBE, the total number of kinetic equations to consider is 152,064: there are 57 possible adsorption terms and 1,056 equations for each combination of n and each combination of driving forces (Table A10 in Appendix I).

Optimal values of the kinetic equations parameters were obtained using the Levenberg-Marquardt algorithm by minimization of the weighted sum of squared errors (WSSE), defined as:

$$WSSE = \sum_i \left(\frac{r_{exp} - r_{calc}}{w} \right)_i^2 \quad (8.14)$$

where r_{exp} is the experimental reaction rate, r_{calc} is the calculated one, and w is the weight factor. Because reaction rates values differ significantly depending on the experimental temperature, to obtain a best joint fit at all temperatures, w was the mean reaction rate value of each experimental series in the individual syntheses of PTBE and BTBE, and w was the maximum reaction rate value for each reaction in the simultaneous syntheses of ETBE and BTBE.

After all proposed kinetic equations were fitted to the experimental rate data, some criteria were applied to reject the less plausible kinetic models, on a basis of mathematical and physicochemical aspects:

- Expressions containing one or more parameters with relative standard uncertainty above 100% were rejected, since all parameters in a suitable kinetic expression should be significant.
- The temperature-dependent fitted parameter in the apparent kinetic constant, k'_{i_T} , has to be negative in order to produce a positive apparent activation energy.
- As it has been said, K_j is an adsorption equilibrium constant when $\alpha_j = 1$. Thus, in these cases, the temperature-dependent parameter, K_{j_T} , has to be positive, because it is related to the adsorption enthalpy of the species j , $\Delta H_{a,j}^o$, since adsorption is an exothermic process, as:

$$k_{j_T} = -\frac{\Delta H_{a,j}^o}{R} \quad (8.15)$$

In the cases where $\alpha_j = 0$, this restriction does not apply, because K_j is actually a ratio of adsorption equilibrium constants.

- Values of δ_P have to be positive and, in cases where δ_P depends on temperature, this dependence should reflect a slight decrease at increasing temperature, according to literature [136]. Thus, if this temperature dependence is included in the kinetic equation, k_{D_T} must be negative.

8.3.3 Model selection and model averaging

Even after applying the rejection criteria mentioned in the previous subsection 8.3.2, a large number of kinetic models fitted reasonably well the experimental data. A good model should present a low WSSE value. In general, residuals decrease when a larger number of parameters are included in the model. To compare WSSE values among models with different number of parameters, the Akaike Information Criterion (AIC) was used. AIC can be calculated as [165]:

$$AIC = m \left[\ln \left(\frac{WSSE}{m} \right) \right] + 2k \quad (8.16)$$

where m is the number of experimental points and k is the number of fitted parameters in the model plus one. Notice that, with similar levels of WSSE, Akaike favors models that have less parameters. Given that samples were relatively small (m/k was almost always less than 40), AICc was used instead of AIC [166]:

$$AICc = AIC + \frac{2k(k+1)}{m-k-1} \quad (8.17)$$

By defining Δ_i as the difference between AICc of the model i and the minimum AICc of the models with physical-chemical meaning that fit well the experimental data, the selected equations can be ranked from more to less likely models. The equation of the most likely model has a Δ_i value of 0. As a general rule, it is considered: *i*) that equations with Δ_i values lower than 2 are essentially as good as the best one, *ii*) equations with Δ_i values up to 6 should not be discarded, and *iii*) equations with Δ_i values over 10 should be rejected [166,167].

The Akaike weight, $w_{Akaike,i}$, for a given kinetic equation is analogous to the probability that one particular equation is the best model. The Akaike weight is calculated as:

$$w_{Akaike,i} = \frac{\exp\left(-\frac{1}{2}\Delta_i\right)}{\sum_{r=1}^R \exp\left(-\frac{1}{2}\Delta_r\right)} \quad (8.18)$$

Notice that, among a given set of equations, large differences between Δ_i values would result in a high value of $w_{Akaike,i}$ for the “best” equations. On the contrary, similar Δ_i values lead to no clear discrimination between them, with a relatively large uncertainty in model selection. In such situations, a different approach is needed in order to choose one useful kinetic expression: model averaging is, in this case, a more robust procedure choice than individual model selection, because it takes into account the model uncertainty.

In model averaging, two different approaches can be considered: “natural averaging” and “full-model averaging” [167]. In natural averaging, estimates of the parameters contained in the best equation are averaged with those of the other preselected equations that contain them. Therefore, the final averaged model contains the same parameters

than the best equation. In full-model averaging, the resulting averaged equation includes all terms that have been found to be significant in the different candidate equations. When one or more equations do not contain a particular parameter, they simply do not contribute to its average value. However, given the fundamental differences between kinetic models (for instance, the term K_j correspond to adsorption equilibrium constants in models with $\alpha_j = 1$ or to ratios of adsorption equilibrium constants in models with $\alpha_j = 0$), the latter approach is regarded as not appropriate to obtain useful kinetic expressions.

If $\hat{\beta}_{ji}$ is a certain estimated parameter in equation i , the estimated average parameter, $\hat{\beta}_j$, can be calculated as follows [167]:

$$\hat{\beta}_j = \frac{\sum_{i=1}^R w_{Akaike,i} \hat{\beta}_{ji}}{\sum_{i=1}^R w_{Akaike,i}} \quad (8.19)$$

where $w_{Akaike,i}$ is the Akaike weight for equation i . Uncertainties associated to average parameters have then two components, the uncertainty of the fitted parameter in equation i and the model selection uncertainty. Standard uncertainty of estimated $\hat{\beta}_j$ can be calculated by the following expression [167]:

$$se(\hat{\beta}_j) = \sum w_{Akaike,i} \sqrt{var(\hat{\beta}_{ji}) + (\hat{\beta}_{ji} - \hat{\beta}_j)^2} \quad (8.20)$$

8.3.4 Fitting of kinetic data

8.3.4.1 Synthesis of PTBE

Deviations between experimental and calculated PTBE formation rates from the fitting of every kinetic equation are shown in Figure 8.3 as the inverse of minimal WSSE values for each equation, so the lower deviation corresponds to the larger $WSSE^{-1}$ value. Equations containing at least one parameter with a relative standard uncertainty larger than 100% are not shown.

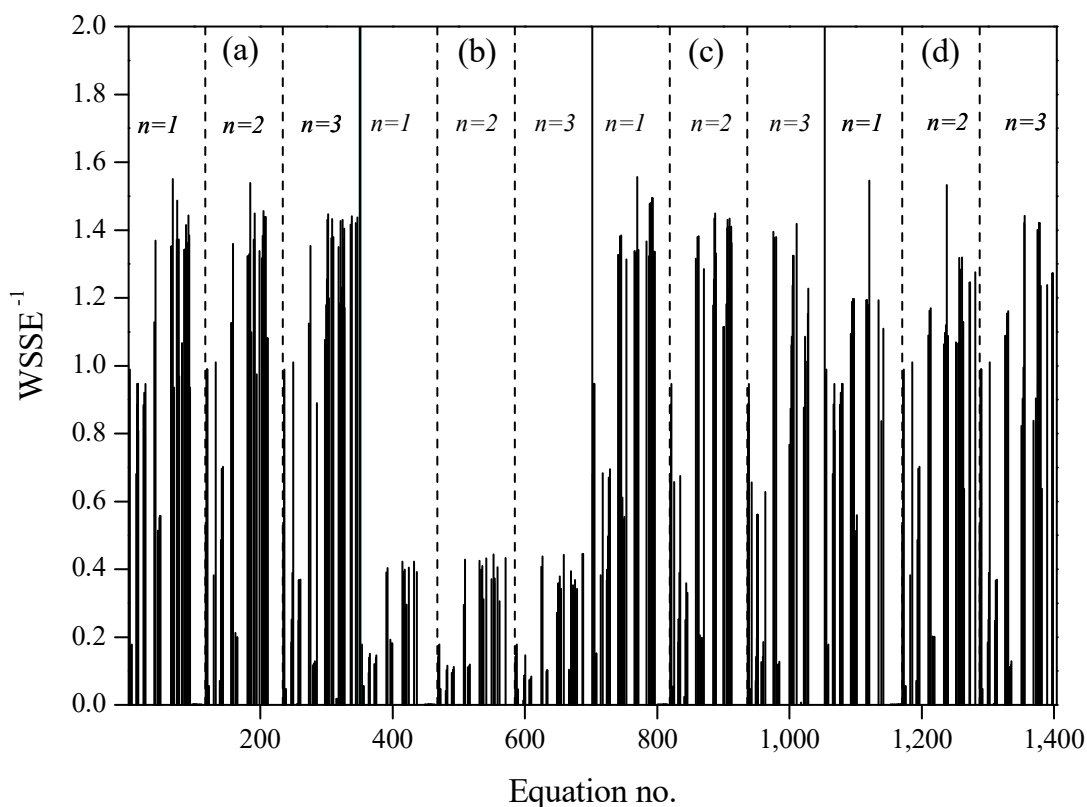


Figure 8.3 Inverse of WSSE values for each equation fitted to PTBE kinetic data, grouped according to the considered rate limiting step: (a) surface reaction (Eq. 8.6a), (b) 1-propanol adsorption (Eq. 8.6b), (c) isobutene adsorption (Eq. 8.6c), and (d) PTBE desorption (Eq. 8.6d)

As seen in Figure 8.3, equations derived from considering 1-propanol adsorption as the rate-limiting step did not fit well the experimental rate data, so they were discarded. Once the above mentioned criteria were applied to the remaining equations, the best ones (i.e., those with $WSSE^{-1}$ values within the upper quartile, that is $WSSE^{-1} \geq 1.19$) were preselected. Then, the number of equations to consider was reduced down to 85. These equations, along with their corresponding fitted parameters values, are listed in Table 8.3 in decreasing order of likelihood, according to their Δ_i values.

Table 8.3 Preselected PTBE kinetic equations

Equation	[kinetic term]		[driving force] ^a	Ads. ^b	[Adsorption term]						[Ψ]		WSSE	Δ _i	
	k' _I	k' _T			isobutene		1-propanol		PTBE		n	δ _p			
					K _{IB_I}	K _{IB_T}	K _{OH_I}	K _{OH_T}	K _{E_I}	K _{E_T}		k _{D_I}			k _{D_T}
770	0.02	-9554	(c)	11					-1.42	-9392	1	16.6		0.642	0
68	0.37	-9038	(a)	11					-1.37	-9056	1	20.5		0.645	1
1,121	-3.46	-13414	(d)	11					-5.21	-13404	1	20.4		0.647	1
185	0.02	-9516	(a)	11					-2.10	-8309	2	16.6		0.650	2
75	26.0	-4864	(a)	12			25.6	3943	25.2		1	20.4		0.672	9
790	556	-9541	(c)	13			556		555	-4595	1	16.1		0.676	10
789	27	-4947	(c)	13			26.5	4544	25.9		1	16.3		0.677	10
793	102	-6879	(c)	13			102	2578	102	-1920	1	16.5		0.670	11
976	0.52	-8267	(c)	8					-0.93		3			0.717	12
205	256	-9520	(a)	13			128		127	-3940	2	15.8		0.687	12
887	-0.48	-10544	(c)	11					-1.69	-7704	2	15.0		0.697	13
302	-0.48	-10525	(a)	11					-2.11	-7322	3	15.0		0.699	13
192	3.68	-4259	(a)	12			1.52	3298	0.75		2	18.5		0.690	13
888	-0.45	-9643	(c)	11					-1.70	-7073	2	15.0	-0.08	0.690	13
303	-0.45	-9623	(a)	11					-2.11	-6718	3	15.0	-0.08	0.691	13
309	2.95	-4844	(a)	12			0.39	2921	-0.27		3	18.7		0.698	15
907	385	-10668	(c)	13			193		191	-7440	2	15.0		0.699	15
322	43	-10676	(a)	13			14.51		12.3	-7563	3	15.0		0.701	15
744	0.50	-8399	(c)	8					0.62		1	19.0		0.724	16
92	680	-9385	(a)	13			680		679	-6090	1	20.2	-0.03	0.693	16
861	0.50	-8404	(c)	8					-0.21		2	19.1		0.725	16
1,011	1.38	-6169	(c)	12			-0.66	4506	-0.60		3	17.1		0.705	16
208	20.13	-6630	(a)	13			10.1	1389	8.87	-1740	2	15.8		0.695	16
978	0.50	-8402	(c)	8					-0.67		3	19.1		0.726	16
88	594	-9386	(a)	13			594		593	-6078	1	19.4		0.707	17
910	55.1	-5601	(c)	13			27.8	2492	26.2	-5037	2	15.0		0.698	17
325	19	-2990	(a)	13			6.36	2528	4.24	-4853	3	15.0		0.699	17
42	0.68	-8017	(a)	8					0.69		1	22.9		0.731	17
784	2.42	-8994	(c)	13			2.19		2.71		1			0.732	18
906	221	-134	(c)	13			111	5133	110		2	15.0		0.712	18
746	0.49	-8466	(c)	8					0.60		1	19.6	-0.03	0.722	18
863	0.48	-8473	(c)	8					-0.23		2	19.7	-0.03	0.724	18
980	0.48	-8471	(c)	8					-0.69		3	19.7	-0.03	0.725	18
339	3.07	-4762	(a)	14	-3.16	21937	0.43	2653	-0.28		3	18.1		0.694	18
159	0.68	-8017	(a)	8					-0.16		2	22.9		0.736	19
766	0.13	-9000	(c)	11					0.37		1			0.747	19
308	1.91	-8408	(a)	12				-0.49	-0.33		3	19.7		0.727	19
337	1.68	-7662	(a)	14	-2.91	20095	-0.92		-0.53		3	20.0		0.706	19
276	0.68	-8010	(a)	8					-0.62		3	22.9		0.739	19
74	1.08	-8221	(a)	12				-0.52	1.03		1	22.1		0.729	19
191	1.51	-8284	(a)	12				-0.49	0.15		2	20.9		0.729	19
66	0.48	-8435	(a)	11				0.20			1	19.6		0.740	19
909	95.8	-128	(c)	13			48.2	5030	46.9		2	15.0	-0.05	0.709	20
742	0.40	-9000	(c)	8					0.40		1			0.754	20
204	86.1	-6479	(a)	13			43.0	1407	42.2		2	16.0		0.723	20
913	0.61	-9000	(c)	14	-5.09			-2.01	-0.26		2			0.734	20
772	0.46	-9000	(c)	12				-2.56	0.47		1			0.745	20
181	0.14	-9000	(a)	11					-0.47		2			0.756	21
345	1.92	-7983	(a)	14	-2.94	23217	-0.57		-0.50		3	20.6	-0.07	0.704	21
311	2.17	-8555	(a)	12				-0.22	-0.29		3	19.7	-0.04	0.725	21
199	6.31	-9000	(a)	13				3.05	2.63		2			0.747	21
347	3.39	-4534	(a)	14	-3.14	22312	0.63	2573	-0.21		3	18.4	-0.05	0.696	21
859	0.40	-9000	(c)	8	-0.42						2			0.760	21
77	1.05	-8249	(a)	12				-0.59	0.98		1	22.3	-0.01	0.729	21
911	638	-10661	(c)	13				319	318	-7442	2	15.0	-0.05	0.718	21
768	0.07	-8997	(c)	11					0.26		1	15.7		0.750	21
889	0.66	-9000	(c)	11				-1.58	-0.21		2			0.751	22
912	569	-5601	(c)	13			285	2488	283	-5043	2	15.0	-0.04	0.709	22
327	603	-2990	(a)	13			201	2498	199	-4942	3	15.0	-0.05	0.712	22
183	0.07	-8981	(a)	11					-0.62		2	15.7		0.755	22
1,006	0.91	-9000	(c)	12				-1.33	-0.53		3			0.755	22
86	14.4	-8709	(a)	13				14.0	14.3		1	20.2		0.745	23

Table 8.3 (continued)

Equation	[kinetic term]		[driving force] ^a	[Adsorption term]							[Ψ]		WSSE	Δ_i		
	k'_I	k'_T		Ads. ^b	isobutene		1-propanol		PTBE		δ_P					
					K_{IB_I}	K_{IB_T}	K_{OH_I}	K_{OH_T}	K_{E_I}	K_{E_T}	n	K_{D_I}			K_{D_T}	
769	0.10	-8734	(c)	11					0.21			1	16.6	-0.06	0.747	23
796	0.48	-9000	(c)	14	-4.87		-2.5		0.46			1			0.749	23
326	613	-10674	(a)	13			204		202	-7563		3	15.1	-0.06	0.729	24
754	0.42	-9000	(c)	10	-5.01				0.37			1			0.762	24
319	9.53	-2110	(a)	13			3.28	2936	1.50	-3780		3			0.741	24
184	0.10	-8712	(a)	11					-0.66			2	16.6	-0.06	0.752	24
93	542	-8996	(a)	13			542	146	542	-1754		1	20.4	-0.03	0.723	25
87	356	-7826	(a)	13			355	1286	355			1	19.7		0.745	25
788	13	-9186	(c)	13			13.3		13.71			1	16.7		0.756	25
90	627	-7817	(a)	13			627	1293	627			1	20.2	-0.02	0.735	25
203	28	-9190	(a)	13			13.8		13.3			2	16.4		0.759	25
91	364	-8997	(a)	13			364	148	364	-1721		1	19.4		0.740	26
871	0.43	-9000	(c)	10	-5.08				-0.47			2			0.778	27
301	-0.36	-8373	(a)	11					-0.93			3	15.0	-0.14	0.797	33
886	-0.36	-8394	(c)	11					-0.45			2	15.0	-0.14	0.798	33
1,117	-3.28	-12415	(d)	11					-3.31			1			0.839	36
1,005	-0.85	-8616	(c)	11					-1.59	-5206		3	15.0	-0.23	0.809	37
304	1.77	-9000	(c)	12			-0.49		-0.61			3			0.834	38
323	33	-9448	(c)	13			11.11		10.3			3	15.0	-0.08	0.814	38
908	26.0	-9461	(c)	13			13.2		12.8			2	15.0	-0.08	0.814	38
1,135	23	-12414	(d)	13			25.8		22.5			1			0.839	38
1,097	-3.10	-12421	(d)	8					-2.72			1	22.7	-0.06	0.835	40
1,029	168	-396	(c)	13			56.3	2711	54.9	-1404		3	15.0	-0.23	0.815	43

^a Considered driving force as indicated in Figure 8.3, i.e., (a) surface reaction (Eq. 8.6a), (c) isobutene adsorption (Eq. 8.6c), and (d) PTBE desorption (Eq. 8.6d). ^b Adsorption term type as indicated in Table 8.2, i.e., Ads. 8: $(1 + K_E a_E)^n$, Ads. 10: $(1 + K_{IB} a_{IB} + K_E a_E)^n$, Ads. 11: $(a_{OH} + K_E a_E)^n$, Ads. 12: $(1 + K_{OH} a_{OH} + K_E a_E)^n$, Ads. 13: $(a_{IB} + K_{OH} a_{OH} + K_E a_E)^n$, and Ads. 14: $(1 + K_{IB} a_{IB} + K_{OH} a_{OH} + K_E a_E)^n$

Some global information can be inferred by considering the frequency of appearance of a particular term in kinetic equations listed in Table 8.3. For instance, with regard to the adsorbed and non-adsorbed species on the catalyst active sites, both PTBE and 1-propanol are likely to be adsorbed, since most of the preselected models include these two compounds in the adsorption term (all the selected models include PTBE and 82% include 1-propanol). On the other hand, less than a half of equations consider that isobutene is adsorbed in significant amounts (47% of the models). The assumption that the number of vacant active sites is negligible ($\alpha_I = 0$) is consistent with more than half the equations (60%). Furthermore, the term Ψ is included in most equations (79%), which indicates that the influence on reaction rates of the interaction between the catalyst and the reaction medium should be considered as significant.

With regard to the considered driving forces among the preselected equations, 48% of them derive from models based on assuming that the surface reaction step is the rate-determining step, 47% consider isobutene adsorption to be rate-determining, and only 5% consider ether desorption. Accordingly, it seems probable that the rate-determining step for the PTBE synthesis reaction rate is either the surface reaction or the isobutene adsorption steps.

As for Δ_i values, the first four equations in Table 8.3 (equations #770, #68, #1,121, and #185) clearly stand out as the most plausible ones. Notice that values of Δ_i in the table indicate a very low model selection uncertainty for the PTBE kinetics, which indicates that selection of a single equation is, in this case, a better option than model averaging.

The four mentioned equations are very similar among them, and they are consistent with the above mentioned global considerations (Table 8.4). The main difference is the considered driving force: the rate-determining step would be isobutene adsorption, according to equation #770, the surface reaction for equations #68 and #185, and the ether desorption for equation #1,121.

Table 8.4 Equations #770, #68, #1,121, and #185 for PTBE kinetics

Equation	Kinetic expression	Parameters values	E'_a [kJ mol ⁻¹]
770	$r_{PTBE} = \frac{k'_{PTBE} \left(a_{IB} - \frac{a_E}{a_{OH} K_{EqPTBE}} \right)}{a_{OH} + K_E a_E} \exp \left[\frac{\bar{V}_M \phi_p^2}{RT} (\delta_M - \delta_p)^2 \right]$	$k'_{PTBE} \left[\frac{mol}{g_{cat} h} \right] = \exp \left[(0.016 \pm 0.014) - (9.55 \pm 0.08) \cdot 10^3 \left(\frac{1}{T} - \frac{1}{327.7} \right) \right]$ $K_E = \exp \left[-(1.42 \pm 0.07) - (9.4 \pm 0.3) \cdot 10^3 \left(\frac{1}{T} - \frac{1}{327.7} \right) \right]$ $\delta_p \left[MPa^{1/2} \right] = (16.6 \pm 0.4)$	79.4 ± 0.7
68	$r_{PTBE} = \frac{k'_{PTBE} \left(a_{IB} a_{OH} - \frac{a_E}{K_{EqPTBE}} \right)}{a_{OH} + K_E a_E} \exp \left[\frac{\bar{V}_M \phi_p^2}{RT} (\delta_M - \delta_p)^2 \right]$	$k'_{PTBE} \left[\frac{mol}{g_{cat} h} \right] = \exp \left[(0.366 \pm 0.014) - (9.04 \pm 0.08) \cdot 10^3 \left(\frac{1}{T} - \frac{1}{327.7} \right) \right]$ $K_E = \exp \left[-(1.37 \pm 0.07) - (9.1 \pm 0.4) \cdot 10^3 \left(\frac{1}{T} - \frac{1}{327.7} \right) \right]$ $\delta_p \left[MPa^{1/2} \right] = (20.5 \pm 0.3)$	75.1 ± 0.7
1,121	$r_{PTBE} = \frac{k'_{PTBE} \left(a_{IB} a_{OH} - \frac{a_E}{K_{EqPTBE}} \right)}{a_{OH} + K_{EqPTBE} K_E a_E} \exp \left[\frac{\bar{V}_M \phi_p^2}{RT} (\delta_M - \delta_p)^2 \right]$	$k'_{PTBE} \left[\frac{mol}{g_{cat} h} \right] = \exp \left[-(3.460 \pm 0.014) - (13.4 \pm 0.08) \cdot 10^3 \left(\frac{1}{T} - \frac{1}{327.7} \right) \right]$ $K_E = \exp \left[-(5.21 \pm 0.07) - (13.4 \pm 0.4) \cdot 10^3 \left(\frac{1}{T} - \frac{1}{327.7} \right) \right]$ $\delta_p \left[MPa^{1/2} \right] = (20.4 \pm 0.3)$	111.5 ± 0.7
185	$r_{PTBE} = \frac{k'_{PTBE} \left(a_{IB} a_{OH} - \frac{a_E}{K_{EqPTBE}} \right)}{(a_{OH} + K_E a_E)^2} \exp \left[\frac{\bar{V}_M \phi_p^2}{RT} (\delta_M - \delta_p)^2 \right]$	$k'_{PTBE} \left[\frac{mol}{g_{cat} h} \right] = \exp \left[(0.019 \pm 0.014) - (9.52 \pm 0.08) \cdot 10^3 \left(\frac{1}{T} - \frac{1}{327.7} \right) \right]$ $K_E = \exp \left[-(2.10 \pm 0.06) - (8.3 \pm 0.3) \cdot 10^3 \left(\frac{1}{T} - \frac{1}{327.7} \right) \right]$ $\delta_p \left[MPa^{1/2} \right] = (16.6 \pm 0.4)$	79.1 ± 0.7

At this point, the following considerations have been taken into account: (i) equations containing parameters with lower relative standard uncertainties are preferred –in this sense, the relative standard uncertainty of the parameter k' , in both equations #68 and #1121 is significantly lower than in both equations #770 and #185–, (ii) as seen in Table 8.4, the apparent activation energy calculated from equation #1121 is much higher than the experimentally obtained value, and (iii) it seems unlikely that the rate-determining step is the ether desorption. Therefore, equation #68 was selected as the most appropriate one to describe the PTBE kinetics. The fit of equation #68 to the experimental reaction rate data, and the distribution of residuals are shown in Figure 8.4.

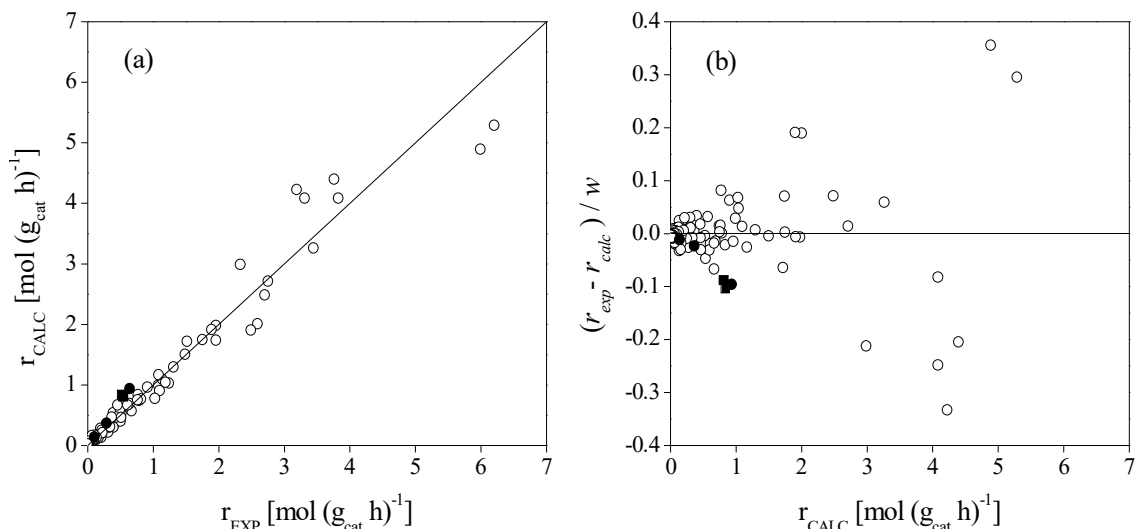


Figure 8.4 Comparison between experimental and calculated PTBE reaction rates from equation #68 (a), and residuals distribution (b). Experimental rates obtained in the batch reactor (○), in the fixed-bed reactor using the C₄ as isobutene source (●), and in the fixed-bed reactor using pure isobutene (■)

Parameters in the adsorption term are related to the ratio between PTBE and 1-propanol adsorption equilibrium constants, as follows:

$$K_E = \frac{K_{a,PTBE}}{K_{a,1-PrOH}} \quad (8.21)$$

where $K_{a,PTBE}$ and $K_{a,1-PrOH}$ are the PTBE and 1-propanol adsorption equilibrium constants, respectively. According to the fitted parameters values of K_E , the ratio between adsorption constants would be sensitive to temperature variation. This could indicate that the heat of adsorption of each compound on the catalyst active sites is different. This parameter is related to the adsorption thermodynamic properties, as follows:

$$\ln K_E = -\frac{\Delta H_{a,PTBE}^o - \Delta H_{a,1-PrOH}^o}{RT} + \frac{\Delta S_{a,PTBE}^o - \Delta S_{a,1-PrOH}^o}{R} \quad (8.22)$$

Based on the above expression, differences of enthalpy and entropy changes of adsorption between PTBE and 1-propanol can be computed for equation #68 (Table 8.5). From values in Table 8.5, 1-propanol adsorption on the resin would be more exothermic than PTBE adsorption. However, these results should be taken as a clue, but not as an evidence, because no reported experimental data has been found regarding the liquid-phase adsorption of the involved compounds on Amberlyst™ 35. Moreover, strong discrepancies can be found in results quoted in the literature regarding the adsorption of different alcohols, alkenes, and ethers on ion-exchange resins, e.g., [168,169]. In these studies, which investigated the gas-phase adsorption of different compounds on a similar catalyst, Amberlyst™ 15, values of -8.3 or -43.5 kJ mol⁻¹ were reported for the ethanol adsorption enthalpy, depending on the author. It should be mentioned that the temperature ranges selected in the two studies probably had a significant influence on the obtained results. On the other hand, isobutene adsorption

enthalpy values reported in both works were quite similar, i.e., -54.2 and -60.2 kJ mol⁻¹, what indicates that this is a more reliable value [168,169].

Table 8.5 Adsorption thermodynamic relations calculated from the selected PTBE kinetic equation. Standard uncertainties are indicated

Thermodynamic relations	Equation #68
Enthalpy of adsorption, [kJ mol ⁻¹]	$\Delta H_{a,PTBE}^{\circ} - \Delta H_{a,I-PrOH}^{\circ}$
Entropy of adsorption, [J (mol K) ⁻¹]	$\Delta S_{a,PTBE}^{\circ} - \Delta S_{a,I-PrOH}^{\circ}$
	75 ± 3
	218 ± 5

8.3.4.2 Synthesis of BTBE

Analogously to the previous section, results from fitting the kinetic equations to the BTBE synthesis rate data are shown in Figure 8.5 as the inverse of WSSE values for each equation (excluding those containing at least one parameter with a relative standard uncertainty above 100%).

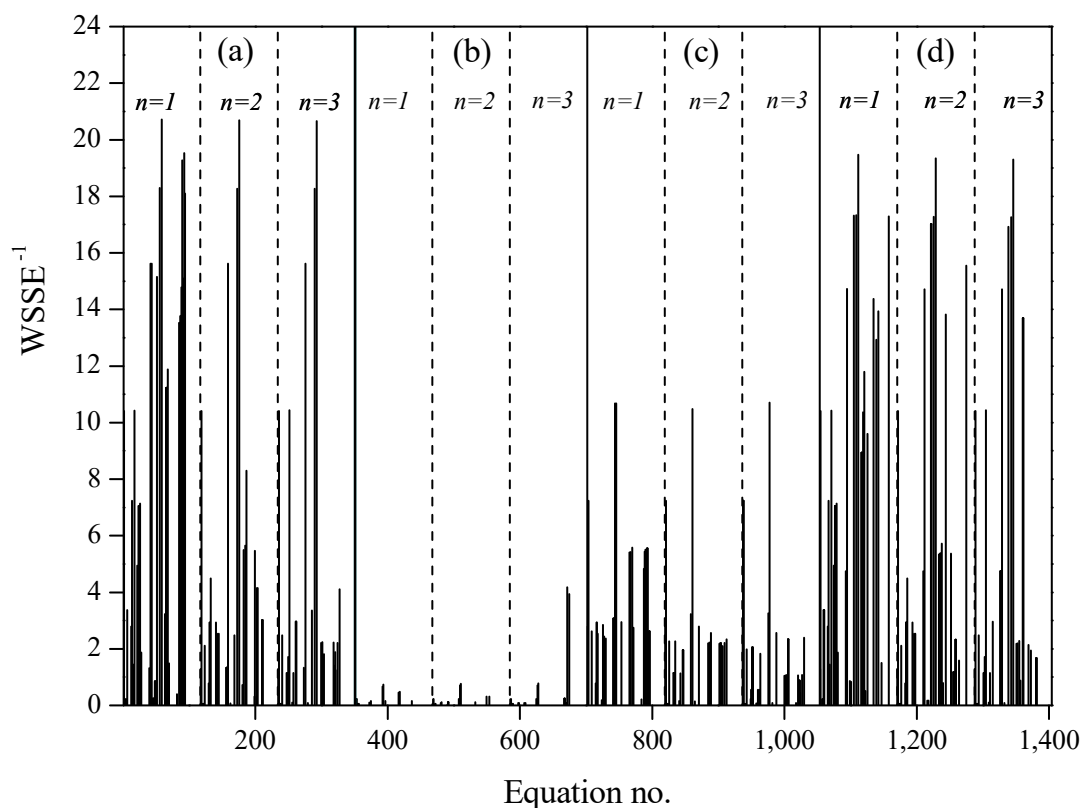


Figure 8.5 Inverse of WSSE values for each equation applied to BTBE kinetic data, grouped according the considered rate limiting step: (a) surface reaction (Eq. 8.6a), (b) 1-butanol adsorption (Eq. 8.6b), (c) isobutene adsorption (Eq. 8.6c), and (d) BTBE desorption (Eq. 8.6d)

As seen in Figure 8.5, equations derived from considering that either the surface reaction or the ether desorption steps are the rate-determining steps of the BTBE synthesis reaction provided a better fit to the experimental reaction rate data. The best

remaining equations, after applying the discrimination criteria based on the WSSE⁻¹ value, that is, models with WSSE⁻¹ ≥ 5.56, are shown in Table 8.6.

Table 8.6 Preselected BTBE kinetic equations

Equation	[kinetic term]		[driving force] ^a	[Adsorption term]							[Ψ]		WSSE	Δ _i		
	k' _I	k' _T		Ads. ^b	isobutene		1-butanol		BTBE			δ _p				
					K _{IB_I}	K _{IB_T}	K _{OH_I}	K _{OH_T}	K _{E_I}	K _{IB_T}	n	k _{D_I}			k _{D_T}	
59	2.06	-10238	(a)	10	-0.57					-0.18		1	16.5	-0.24	0.048	0
176	2.06	-10263	(a)	10	-1.38					-1.03		2	16.4	-0.24	0.048	0
293	2.05	-10272	(a)	10	-1.84					-1.49		3	16.4	-0.24	0.048	0
1,112	-1.60	-14657	(d)	10	-0.54					-4.15		1	16.6	-0.24	0.051	3
1,105	-1.47	-13800	(d)	10	-0.08					-3.87		1			0.058	3
56	1.83	-9172	(a)	10	-1.11					-0.55		1	18.7		0.055	3
290	1.82	-9161	(a)	10	-2.34					-1.80		3	18.8		0.055	3
173	1.81	-9151	(a)	10	-1.92					-1.36		2	18.8		0.055	3
1,229	-1.61	-14686	(d)	10	-1.37					-5.01		2	16.6	-0.24	0.052	3
1,346	-1.62	-14697	(d)	10	-1.82					-5.47		3	16.6	-0.24	0.052	3
94	2.70	-9000	(a)	14	0.31		0.33			0.62		1			0.055	3
1,222	-1.49	-13814	(d)	10	-0.98					-4.79		2			0.059	4
1,339	-1.50	-13820	(d)	10	-1.45					-5.26		3			0.059	4
1,109	-1.83	-13527	(d)	10	-1.06					-4.52		1	18.8		0.058	5
1,226	-1.84	-13526	(d)	10	-1.85					-5.32		2	18.8		0.058	6
1,343	-1.84	-13525	(d)	10	-2.28					-5.76		3	18.8		0.058	6
90	2.11	-14482	(a)	13			0.33	-13459		0.31		1	15.8	-0.39	0.052	6
159	1.45	-9094	(a)	8						-1.71		2	21.2		0.064	8
276	1.45	-9092	(a)	8						-2.12		3	21.2		0.064	8
42	1.45	-9100	(a)	8						-0.98		1	21.2		0.064	8
93	2.19	-14659	(a)	13			0.46	-12661		0.46	-1863	1	15.4	-0.40	0.051	9
52	2.25	-9000	(a)	12	0.06					0.31		1			0.066	9
1,095	-2.23	-13493	(d)	8						-4.97		1	21.3		0.068	10
1,212	-2.23	-13489	(d)	8						-5.70		2	21.3		0.068	10
1,329	-2.23	-13488	(d)	8						-6.12		3	21.3		0.068	10
1,135	-0.83	-13331	(d)	13				1.44		-3.38		1			0.070	11
1,158	-1.71	-11138	(d)	14	-0.61	5085		-1.89	2967	-3.79		1	19.3		0.058	14
89	2.93	-8999	(a)	13				1.56		0.67		1	15.0	-0.16	0.068	16
1,244	-2.26	-13026	(d)	12				-2.87		-5.50		2	22.0		0.072	16
1,361	-2.25	-12997	(d)	12				-3.12		-5.91		3	22.0		0.073	16
86	3.01	-9211	(a)	13				1.67		0.67		1	15.0		0.074	17
92	3.00	-9082	(a)	13				1.64		1.10	-5473	1	15.0	-0.17	0.066	17
1,142	-0.83	-13298	(d)	13				1.45		-3.39		1	15.2	-0.18	0.072	18
88	3.08	-9289	(a)	13				1.75		1.11	-5708	1	15.0		0.073	19
87	2.80	-11676	(a)	13				1.42	-3476	0.48		1	15.0		0.073	19
1,139	-0.66	-13518	(d)	13				1.66		-3.32		1	15.3		0.077	19
1,275	-1.73	-11606	(d)	14	-1.49	3071		-2.20	1111	-4.78		2	19.5		0.064	19
91	2.90	-12033	(a)	13				1.53	-3813	0.90	-5211	1	15.2		0.071	21
66	1.15	-9160	(a)	11						-1.57		1	17.0		0.089	23
68	1.15	-9272	(a)	11						-0.53	-15881	1	16.9		0.084	23
1,121	-2.52	-13649	(d)	11						-4.20	-19910	1	17.0		0.085	23
2	1.57	-9731	(a)	1								1	20.0		0.096	24
119	1.57	-9731	(a)	1								2	20.0		0.096	24
236	1.57	-9731	(a)	1								3	20.0		0.096	24
1,055	1.57	-9731	(d)	1								1	20.0		0.096	24
1,172	1.57	-9731	(d)	1								2	20.0		0.096	24
1,289	1.57	-9731	(d)	1								3	20.0		0.096	24
978	1.15	-9212	(c)	1						-2.13		3	16.9		0.093	25
744	1.15	-9224	(c)	1						-0.98		1	16.9		0.094	25
861	1.12	-8906	(c)	8						-1.65		2	17.6		0.095	26
252	1.60	-9837	(a)	5				-5.11				3	19.7		0.096	26
1,305	1.60	-9837	(d)	5				-5.11				3	19.7		0.096	26
18	1.61	-9796	(a)	5				-3.21				1	19.8		0.096	26
1,071	1.61	-9796	(d)	5				-3.21				1	19.8		0.096	26
1,119	-2.57	-13127	(d)	11						-5.47		1	18.1		0.096	26
1,117	-2.46	-14377	(d)	11						-5.60		1			0.112	31
187	4.21	-9000	(a)	12				1.46		-0.2		2			0.121	37
14	1.16	-9673	(a)	4								1	16.2		0.138	41

Table 8.6 (continued)

Equation	[kinetic term]		[driving force] ^a	Ads. ^b	[Adsorption term]						[Ψ]		WSSE	Δ _i	
	k' ₁	k' _T			isobutene		1-butanol		BTBE		δ _p				
					K _{IB₁}	K _{IB_T}	K _{OH₁}	K _{OH_T}	K _{E₁}	K _{IB_T}	n	k _{D₁}			k _{D_T}
1,067	1.16	-9673	(d)	4							1	16.2		0.138	41
704	1.16	-9673	(c)	1							1	16.2		0.138	41
821	1.16	-9673	(c)	1							2	16.2		0.138	41
938	1.16	-9673	(c)	1							3	16.2		0.138	41
24	25.5	-9254	(a)	6				24.4			1	16.8		0.142	44
1,077	25.5	-9254	(d)	6				24.4			1	16.8		0.142	44
26	20.7	-8426	(a)	6				19.6	1088		1	16.7		0.140	46
1,079	20.7	-8426	(d)	6				19.6	1088		1	16.7		0.140	46
1,238	-3.11	-12741	(d)	11				-4.88	-13550		2	15.0		0.175	56
185	0.56	-8290	(a)	11				-1.23	-9007		2	15.0		0.177	57
770	0.56	-8291	(c)	11				-0.42	-9846		1	15.0		0.179	58

^a Considered driving force as indicated in Figure 8.3 and 8.5, i.e., (a) surface reaction (Eq. 8.6a), (c) isobutene adsorption (Eq. 8.6c), and (d) PTBE desorption (Eq. 8.6d). ^b Adsorption term type as indicated in Table 8.3, i.e., Ads. 1: 1, Ads. 4: a_{OH}^n , Ads. 5: $(1 + K_{OH}a_{OH})^n$, Ads. 6: $(a_{IB} + K_{OH}a_{OH})^n$, 8: $(1 + K_E a_E)^n$, Ads. 10: $(1 + K_{IB}a_{IB} + K_E a_E)^n$, Ads. 11: $(a_{OH} + K_E a_E)^n$, Ads. 12: $(1 + K_{OH}a_{OH} + K_E a_E)^n$, Ads. 13: $(a_{IB} + K_{OH}a_{OH} + K_E a_E)^n$, and Ads. 14: $(1 + K_{IB}a_{IB} + K_{OH}a_{OH} + K_E a_E)^n$.

Following the same procedure as in the previous section, prior to selecting the most appropriate expression to describe the BTBE synthesis kinetics, the preselected equations in Table 8.6 were analyzed to infer some global information: the interaction term, Ψ, is likely to be significant, since it is included in 88% of the preselected equations; BTBE should be considered to be adsorbed on the catalyst active sites in significant amounts, given that most equations include it in the adsorption term (72%); the number of vacant active sites is likely to be significant ($\alpha_D = 1$), because it is included in more than a half of the equations (64%); on the other hand, no conclusive information can be obtained regarding isobutene and 1-butanol adsorption on the catalyst active sites, since only about half the equations include isobutene and/or 1-butanol in the adsorption term (49% and 51%, respectively).

As for the considered driving forces, 45% of the equations are derived from assuming the surface reaction as the rate-determining step, 45% are based on considering the ether desorption as rate-determining, and 10% assume isobutene adsorption step as the rate-determining step. Notice that, similarly to the PTBE case, the surface reaction is likely to be the rate-determining step but that, unlike in the PTBE case, the odds that ether desorption is the rate-determining step are just as high. These results could be related to possible transport hindrances of the formed BTBE through the catalyst matrix, perhaps due to its larger molecular size. This said, the assumption that the surface reaction is the rate-determining step seems to be more appropriate because of the following considerations: (i) the form of the driving force terms, when assuming that either the surface reaction or the ether desorption as the rate-determining steps, match up and, as a consequence, it is hard to distinguish among both possibilities; (ii) all literature references regarding similar reaction systems assume that the surface reaction is the rate-determining step, e.g., [95,131,138,163]; and (iii) under the same level of probability, the simplest explanation of the actual mechanism, the surface reaction as the rate-determining step, is preferred.

According to the fitting results, the best set of equations to describe BTBE kinetics would present an adsorption term of the form $(1 + K_{IB} a_{IB} + K_E a_E)^n$, which would indicate that the amount of adsorbed 1-butanol is not significant compared to other adsorbed compounds, and that a significant proportion of the catalyst active sites would be unoccupied. This fact could indicate that 1-butanol adsorption is strongly hindered, perhaps due to diffusion limitations through the catalyst matrix. However, alcohol molecules have been reported to be adsorbed on resins active sites in much larger amounts than both alkenes and ethers [168,169] and, therefore, it is often regarded as unlikely that, in the presence of alcohol molecules, other compounds would be adsorbed in significantly higher amounts. Likewise, it is considered as improbable that the number of vacant active sites could be significant when alcohol molecules are present in liquid-phase reaction media. Therefore, despite their relatively worst fitting to rate data, equations already proposed in the literature should be considered as well. Actually, it should be noticed that, among the preselected equations in Table 8.6, there is very little difference between them in terms of both WSSE and Δ_i values, what would indicate that the model selection uncertainty is, in this case, rather important.

The first three equations in Table 8.6 (equations #59, #176, and #293) are the same, except for the different values of the exponent in the adsorption term ($n = 1, 2,$ and $3,$ respectively). BTBE synthesis reaction rates calculated by these kinetic equations are plotted against experimental values in Figures 8.6, 8.7, and 8.8, respectively. As seen, no differences can be appreciated between them in terms of their fitting to experimental rate values.

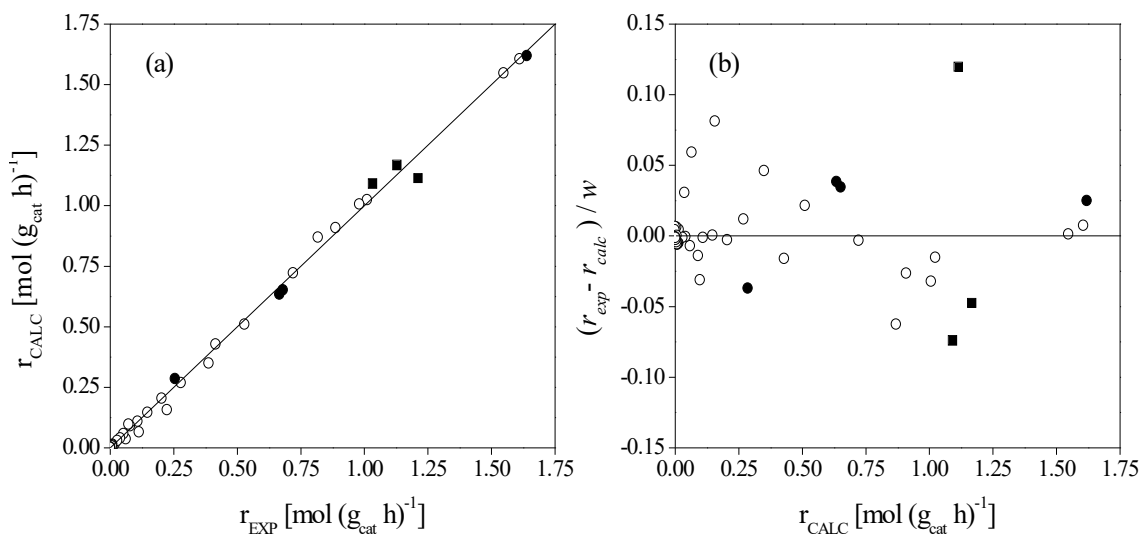


Figure 8.6 Comparison between experimental and calculated BTBE reaction rates from equation #59 (a), and residuals distribution (b). Experimental reaction rates were obtained in the batch reactor (\circ), in the fixed-bed reactor using the C_4 as isobutene source (\bullet), and in the fixed-bed reactor using pure isobutene (\blacksquare)

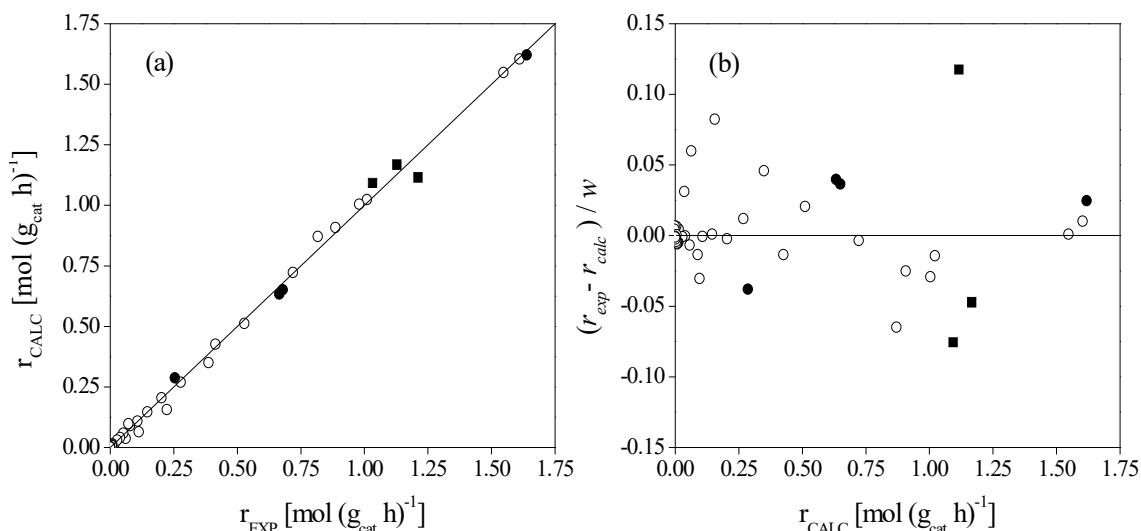


Figure 8.7 Comparison between experimental and calculated BTBE reaction rates from equation #176 (a), and residuals distribution (b). Experimental reaction rates were obtained in the batch reactor (○), in the fixed-bed reactor using the C₄ as isobutene source (●), and in the fixed-bed reactor using pure isobutene (■)

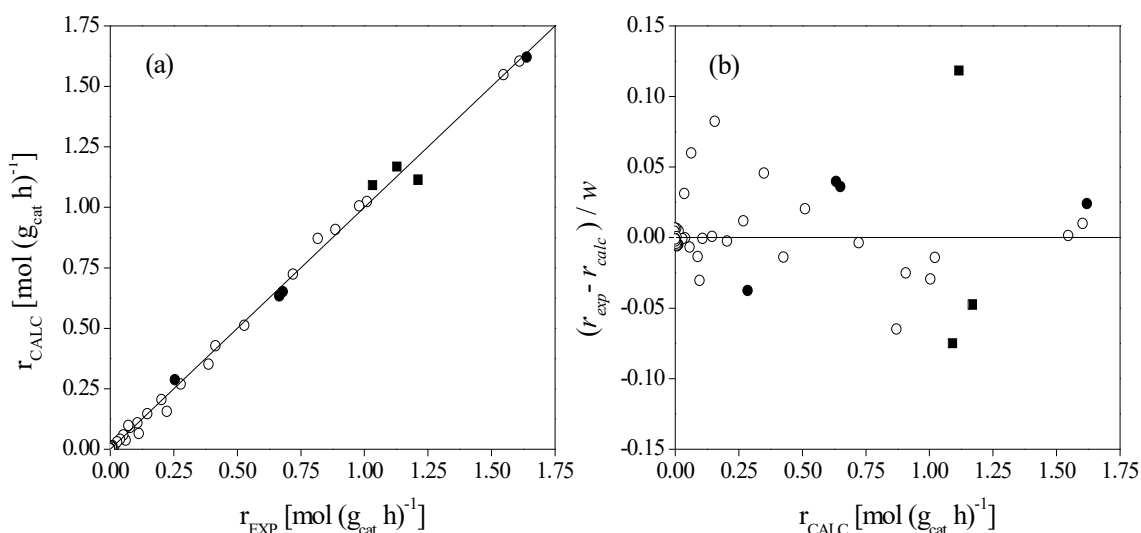


Figure 8.8 Comparison between experimental and calculated BTBE reaction rates from equation #293 (a), and residuals distribution (b). Experimental reaction rates were obtained in the batch reactor (○), in the fixed-bed reactor using the C₄ as isobutene source (●), and in the fixed-bed reactor using pure isobutene (■)

Values of the parameters in the three considered equations reveal very little differences among models. For instance, calculated apparent activation energies are (85.1 ± 0.8) , (85.3 ± 0.3) , and (85.4 ± 0.8) kJ mol⁻¹ for equations #59, #176, and #293, respectively. These are larger values than the experimentally determined from the temperature dependence of initial reaction rates (i.e., 74 ± 2 kJ mol⁻¹), but they cannot be considered as unrealistic, according to activation energies values quoted in the literature for similar reactions, e.g., [19,138,159].

Parameters in the adsorption term of these equations correspond actually to individual adsorption equilibrium constants of the involved compounds. According to all three equations, the BTBE adsorption equilibrium constant would be slightly larger than that of isobutene (about 1.5 times greater), which would agree literature data on similar systems [57,168]. None of the adsorption constants showed significant dependence on temperature within the assayed temperature range. Thus, enthalpy changes of adsorption would be lower than their uncertainty from kinetic experiments. However, Gibbs free energy changes of adsorption, $\Delta G_{a,j}^o$, can be computed as follows:

$$\ln K_{a,j} = -\frac{\Delta G_{a,j}^o}{RT} \quad (8.23)$$

Calculated $\Delta G_{a,j}^o$ values, which are listed in Table 8.7, are positive. These results are not consistent with the adsorption of isobutene and BTBE, being a spontaneous process, and, therefore, equations #59, #176, and #293 should be discarded.

Table 8.7 Free energy change of adsorption, $\Delta G_{a,j}^o$, calculated from equations #59, #176, and #293 for the BTBE synthesis. Standard uncertainties are indicated

Equation	$\Delta G_{a,IB}^o$ ^a [kJ mol ⁻¹]	$\Delta G_{a,BTBE}^o$ ^a [kJ mol ⁻¹]
59	1.55 ± 0.07	0.5 ± 0.3
176	3.77 ± 0.07	2.8 ± 0.3
293	5.02 ± 0.07	4.1 ± 0.3

^a At \bar{T} = 328.6 K

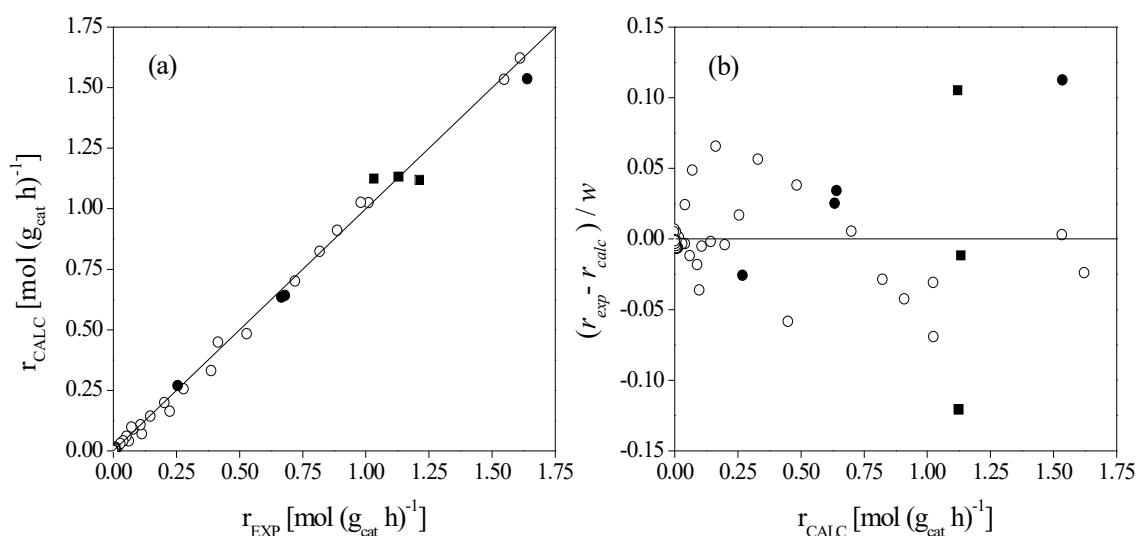
Given that the equations that presented the best fit to experimental rate data are not consistent, other expressions must be found to describe BTBE kinetics. The next step is to consider equations with a relative good fit and that assume no significant vacant active sites in the catalyst (Table 8.6): equations #90, #93, #1135, #89, #86, #92, #1142, #88, #87, #1139, and #91. They present, essentially, the same adsorption term, except for the combination of temperature-dependent parameters. Among these, equations #90 and #93 can be discarded, because they lead to estimated apparent activation energies larger than 120 kJ mol⁻¹, and equations #1135, #1142, and #1139 can be rejected, because they are based on models where the ether desorption as the rate-determining step is assumed.

Parameters values for the remaining equations among this particular subset are listed in Table 8.8. Since it is not possible to discriminate among them in terms of the goodness of their fit to the experimental rate data, and because they are very similar and differences can be attributed to model uncertainty, it was considered as more appropriate to build an average model, rather than selecting one single equation. Averaged parameters values are also shown in Table 8.8, along with the resulting thermodynamic relations. BTBE reaction rates calculated by the average equation are plotted against experimental reaction rate values in Figure 8.9, along with the corresponding residuals distribution.

Table 8.8 Equations #89, #86, #92, #88, #87, #91, and resulting averaged equation for the BTBE synthesis reaction kinetics

Equation:	
$r_{BTBE} = \frac{k'_{BTBE} \left(a_{IB} a_{OH} - \frac{a_E}{K_{Eq_{BTBE}}} \right)}{a_{IB} + K_{OH} a_{OH} + K_E a_E} \exp \left[\frac{V_M \phi_P^2}{RT} (\delta_M - \delta_P)^2 \right]$	
Equation	Parameters values
89	$k'_{BTBE} \left[\frac{mol}{g_{cat} h} \right] = \exp \left[(2.929 \pm 0.008) - (9.00 \pm 0.11) \cdot 10^3 \left(\frac{1}{T} - \frac{1}{328.6} \right) \right]$ $K_{OH} = \exp [1.558 \pm 0.010]$ $K_E = \exp [0.67 \pm 0.13]$ $\delta_p \left[MPa^{1/2} \right] = (15.0 \pm 0.6) - (0.16 \pm 0.06)(T - 328.6)$
88	$k'_{BTBE} \left[\frac{mol}{g_{cat} h} \right] = \exp \left[(3.081 \pm 0.008) - (9.29 \pm 0.12) \cdot 10^3 \left(\frac{1}{T} - \frac{1}{328.6} \right) \right]$ $K_{OH} = \exp [1.755 \pm 0.010]$ $K_E = \exp \left[(1.11 \pm 0.15) - (6 \pm 2) \cdot 10^3 \left(\frac{1}{T} - \frac{1}{328.6} \right) \right]$ $\delta_p \left[MPa^{1/2} \right] = 15.0 \pm 0.3$
86	$k'_{BTBE} \left[\frac{mol}{g_{cat} h} \right] = \exp \left[(3.009 \pm 0.008) - (9.21 \pm 0.12) \cdot 10^3 \left(\frac{1}{T} - \frac{1}{328.6} \right) \right]$ $K_{OH} = \exp [1.674 \pm 0.010]$ $K_E = \exp [0.67 \pm 0.14]$ $\delta_p \left[MPa^{1/2} \right] = 15.0 \pm 0.3$
87	$k'_{BTBE} \left[\frac{mol}{g_{cat} h} \right] = \exp \left[(2.804 \pm 0.008) - (11.68 \pm 0.12) \cdot 10^3 \left(\frac{1}{T} - \frac{1}{328.6} \right) \right]$ $K_{OH} = \exp \left[(1.418 \pm 0.011) - (3.48 \pm 0.17) \cdot 10^3 \left(\frac{1}{T} - \frac{1}{328.6} \right) \right]$ $K_E = \exp [(0.48 \pm 0.12)]$ $\delta_p \left[MPa^{1/2} \right] = 15.0 \pm 0.3$
92	$k'_{BTBE} \left[\frac{mol}{g_{cat} h} \right] = \exp \left[(3.003 \pm 0.008) - (9.08 \pm 0.11) \cdot 10^3 \left(\frac{1}{T} - \frac{1}{328.6} \right) \right]$ $K_{OH} = \exp [1.643 \pm 0.010]$ $K_E = \exp \left[(1.10 \pm 0.13) - (5.5 \pm 1.8) \cdot 10^3 \left(\frac{1}{T} - \frac{1}{328.6} \right) \right]$ $\delta_p \left[MPa^{1/2} \right] = (15.0 \pm 0.6) - (0.17 \pm 0.06)(T - 328.6)$
91	$k'_{BTBE} \left[\frac{mol}{g_{cat} h} \right] = \exp \left[(2.899 \pm 0.008) - (12.03 \pm 0.12) \cdot 10^3 \left(\frac{1}{T} - \frac{1}{328.6} \right) \right]$ $K_{OH} = \exp \left[(1.529 \pm 0.011) - (3.81 \pm 0.16) \cdot 10^3 \left(\frac{1}{T} - \frac{1}{328.6} \right) \right]$ $K_E = \exp \left[(0.90 \pm 0.12) - (5.2 \pm 1.6) \cdot 10^3 \left(\frac{1}{T} - \frac{1}{328.6} \right) \right]$ $\delta_p \left[MPa^{1/2} \right] = 15.2 \pm 0.3$
Averaged model parameters	
$k'_{BTBE} \left[\frac{mol}{g_{cat} h} \right] = \exp \left[(2.98 \pm 0.05) - (9.10 \pm 0.16) \cdot 10^3 \left(\frac{1}{T} - \frac{1}{328.6} \right) \right]$ $K_{OH} = \exp [1.62 \pm 0.06]$ $K_E = \exp [0.8 \pm 0.2]$ $\delta_p \left[MPa^{1/2} \right] = (15.0 \pm 0.5) - (0.17 \pm 0.04)(T - 328.6)$	
Calculated properties	
E'_a [kJ mol ⁻¹]	76 ± 1
$\Delta G_{a, I-BuOH}^o - \Delta G_{a, IB}^o$ [kJ mol ⁻¹]	-4.43 ± 0.17
$\Delta G_{a, BTBE}^o - \Delta G_{a, IB}^o$ [kJ mol ⁻¹]	-2.2 ± 0.6

^a At $\bar{T} = 328.6$ K

**Figure 8.9** Comparison between experimental and calculated BTBE reaction rates obtained with the equation averaged from equations #89, #86, #92, #88, #87, and #91 (a), and residuals

distribution (b). Experimental rates were obtained in the batch reactor (○), in the fixed-bed reactor using the C₄ as isobutene source (●), and in the fixed-bed reactor using pure isobutene (■). As it can be seen in Figure 8.9, the averaged equation describes rather well the experimental rate data variation. In contrast to equations #59, #176, #293, parameters in the adsorption term of the averaged equation would indicate that 1-butanol adsorption constant is five times greater than that of isobutene. On the other hand, similarly as calculated from equations #59, #176, and #293, the present model indicates that BTBE adsorption equilibrium constant doubles that of isobutene.

At this point, it was considered appropriate to analyze also equations #66 and #68, which are based on assuming that the amount of adsorbed isobutene on the catalyst active sites would not be significant in comparison to the other compounds, because of the already commented uncertainty regarding model selection for the BTBE synthesis, and the physicochemical similarities between BTBE and PTBE systems. Notice that equation #68 had been selected as the most suitable one to describe PTBE kinetics and that equation #66 is analogous to #68 (i.e., the difference between these two expressions is the ratio between BTBE and 1-butanol adsorption equilibrium constants, which is sensitive to temperature within the assayed range for equation #68 and non-sensitive for equation #66).

Similarly to the previous case (equations #89, #86, #92, #88, #87, #91), parameters values for this model were averaged from equations #66 and #68. The resulting kinetic equation, estimated parameters values, and thermodynamic relations are shown in Table 8.9. As seen in Figure 8.10, the present equation also describes rather well experimental reaction rates.

Table 8.9 Averaged equation from equations #66 and #68, estimated parameters values, and thermodynamic relations for the BTBE synthesis reaction

Equation: $r_{BTBE} = \frac{k'_{BTBE} \left(a_{IB} a_{OH} - \frac{a_E}{K_{Eq_{BTBE}}} \right)}{a_{OH} + K_E a_E} \exp \left[\frac{\bar{V}_M \phi_P^2}{RT} (\delta_M - \delta_P)^2 \right]$			
Averaged model parameters		Thermodynamic relations	
$k'_{BTBE} \left[\frac{mol}{g_{cat} h} \right] = \exp \left[(1.151 \pm 0.010) - (9.22 \pm 0.14) \cdot 10^3 \left(\frac{1}{T} - \frac{1}{328.6} \right) \right]$	E'_a [kJ mol ⁻¹]	76.6 ± 1.1	
$K_E = \exp[-(1.1 \pm 0.6)]$	$\Delta G_{a,BTBE}^o - \Delta G_{a,1-BuOH}^o$ ^a	2.9 ± 1.5	
$\delta_P \left[MPa^{1/2} \right] = 17.0 \pm 0.3$	[kJ mol ⁻¹]		

^a At $\bar{T} = 328.6$ K

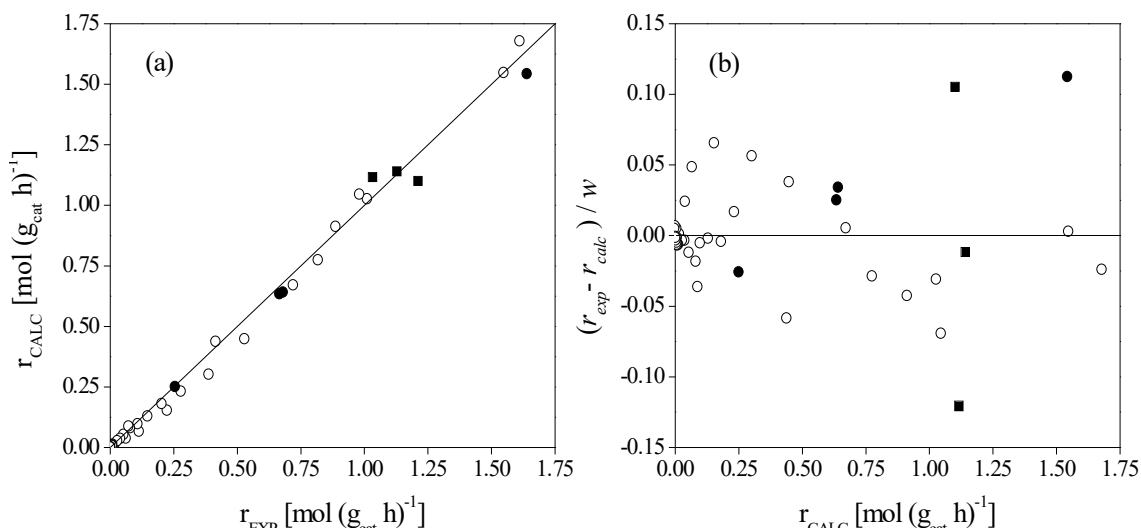


Figure 8.10 Comparison between experimental and calculated BTBE reaction rates obtained with the equation averaged from equations #66 and #68 (a), and residuals distribution (b). Experimental rates were obtained in the batch reactor (\circ), in the fixed-bed reactor using the C_4 as isobutene source (\bullet), and in the fixed-bed reactor using pure isobutene (\blacksquare)

The parameter K_E in the adsorption term of the present equation accounts for the ratio of BTBE to 1-butanol adsorption equilibrium constants. According to the calculated value of K_E , 1-butanol would adsorb preferentially compared to BTBE (about 3 times greater) on the active sites.

Finally, the two averaged equations were fitted to the experimental BTBE reaction rate data affected by diffusion effects. To do so, the optimal values of the apparent kinetic coefficients were calculated by minimization of WSSE for each individual experiment affected by diffusion limitations. The rest of parameters were not altered because the adsorption of the different chemical compounds is not expected to depend on mass transfer effects. Fitted values and minimal WSSE are presented in Table 8.10 for each experiment.

Table 8.10 Fitted values for the apparent kinetic constant, minimal WSSE, and effectiveness factor (η) for each individual experiment affected by mass transfer limitations in the synthesis of BTBE

$R^{\circ}_{A/O}$	T [K]	Equation averaged from equations #89, #86, #92, #88, #87, and #91			Equation averaged from equations #66 and #68		
		k'_{BTBE} [mol (g _{cat} h) ⁻¹]	WSSE	η [%]	k'_{BTBE} [mol (g _{cat} h) ⁻¹]	WSSE	η [%]
1.0	333	25.5	0.011	89	3.97	0.064	86
1.0	334	24.3	0.009	77	4.29	0.006	85
1.0	343	29.3	0.022	45	5.00	0.056	47
1.2	345	39.8	0.157	53	7.25	0.128	58
1.0	354	36.8	0.140	26	7.82	0.392	33
2.0	354	13.3	0.211	9	3.42	0.224	15

The effectiveness factors, η , listed in Table 8.10 were computed as the ratio between the apparent kinetic coefficient, k'_{BTBE} , for each diffusion-limited experiment and that from the corresponding average equation at the same temperature, which can be considered free from mass transfer effects. From the values of η in the table, the effectiveness

factor decreases as temperature increases, as expected. No clear trend is observed regarding the effect of $R^{\circ}_{A/O}$ on η .

BTBE synthesis reaction rates calculated by the two averaged equations are plotted against all experimental values (i.e., reaction rate values, both affected and non-affected by mass transfer limitations) in Figures 8.11 and 8.12. As it can be seen, the two averaged equations underestimate low reaction rate values. The averaged equation built from equations #66 and #68 leads to a somewhat more normal distribution of residuals, which indicates that this equation would be more adequate to describe the BTBE synthesis reaction kinetics.

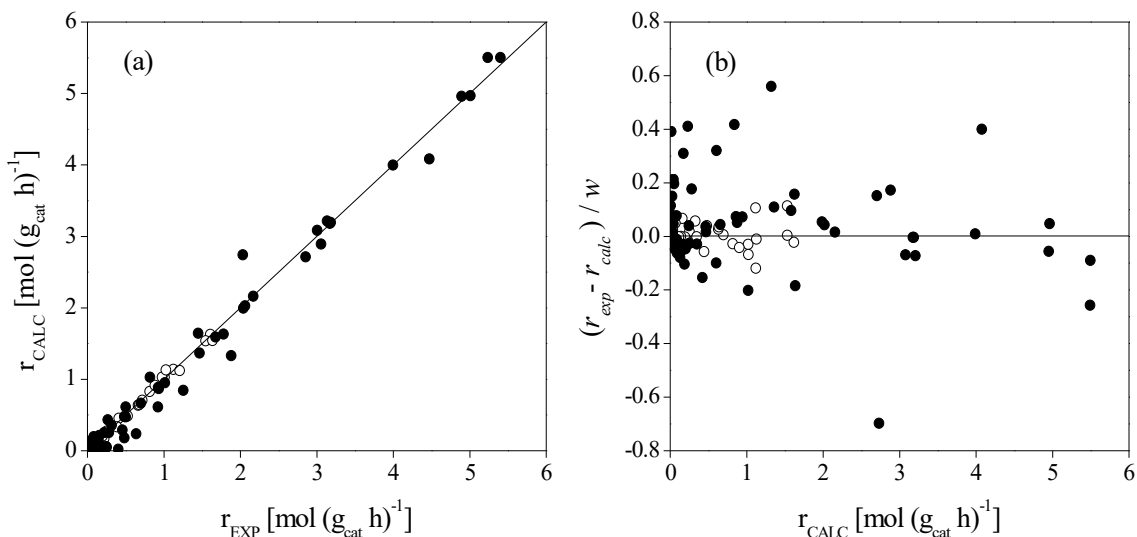


Figure 8.11 Comparison between experimental and calculated BTBE reaction rates obtained with the equation averaged from equations #89, #86, #92, #88, #87 and #91 (a), and residuals distribution (b). Experimental rates were free of mass transfer limitations (\circ), or affected by mass transfer limitations (\bullet)

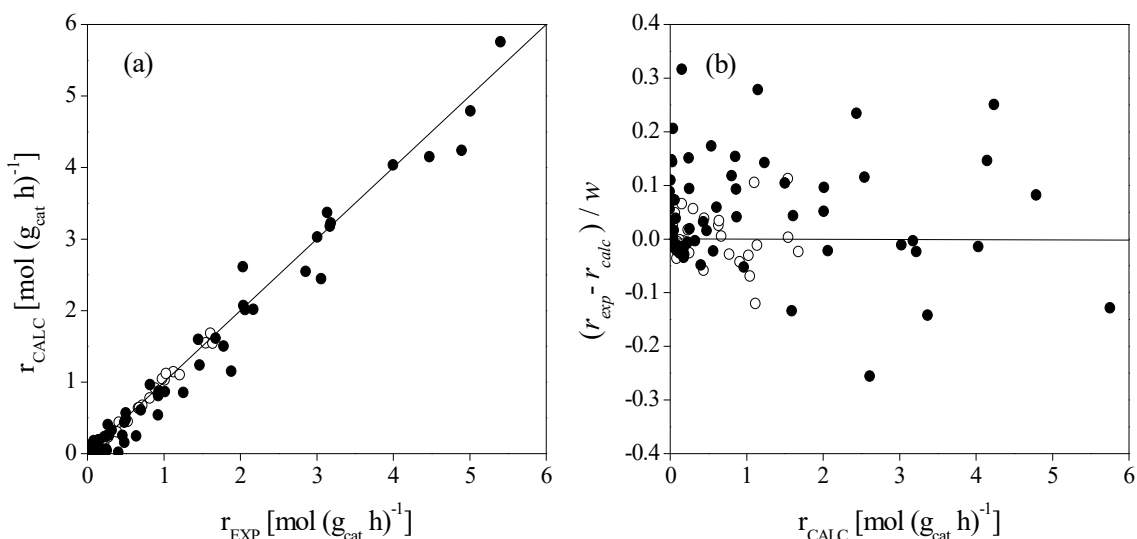


Figure 8.12 Comparison between experimental and calculated BTBE reaction rates obtained with the equation averaged from equations #66 and #68 (a), and residuals distribution (b). Experimental rates were free of mass transfer limitations (\circ), or affected by mass transfer limitations (\bullet)

8.3.4.3 Simultaneous syntheses of ETBE and BTBE

Given the number of considered equations, in the case of the simultaneous syntheses of ETBE and BTBE, and for the sake of clarity, an additional classification of models was established: equations with $\alpha_I = 1$ will be henceforward referred to as type I equations, whereas those with $\alpha_I = 0$ will be type II. 101,520 type I equations and 50,544 type II equations were considered.

Once the equations were fitted to experimental reaction rate data free from mass transfer effects and the earlier mentioned rejecting criteria (section 8.3.2) were applied, 4,264 type I and 14,249 type II equations were obtained. Like in previous sections, the inverse of WSSE values for each equation is shown in Figure 8.13.

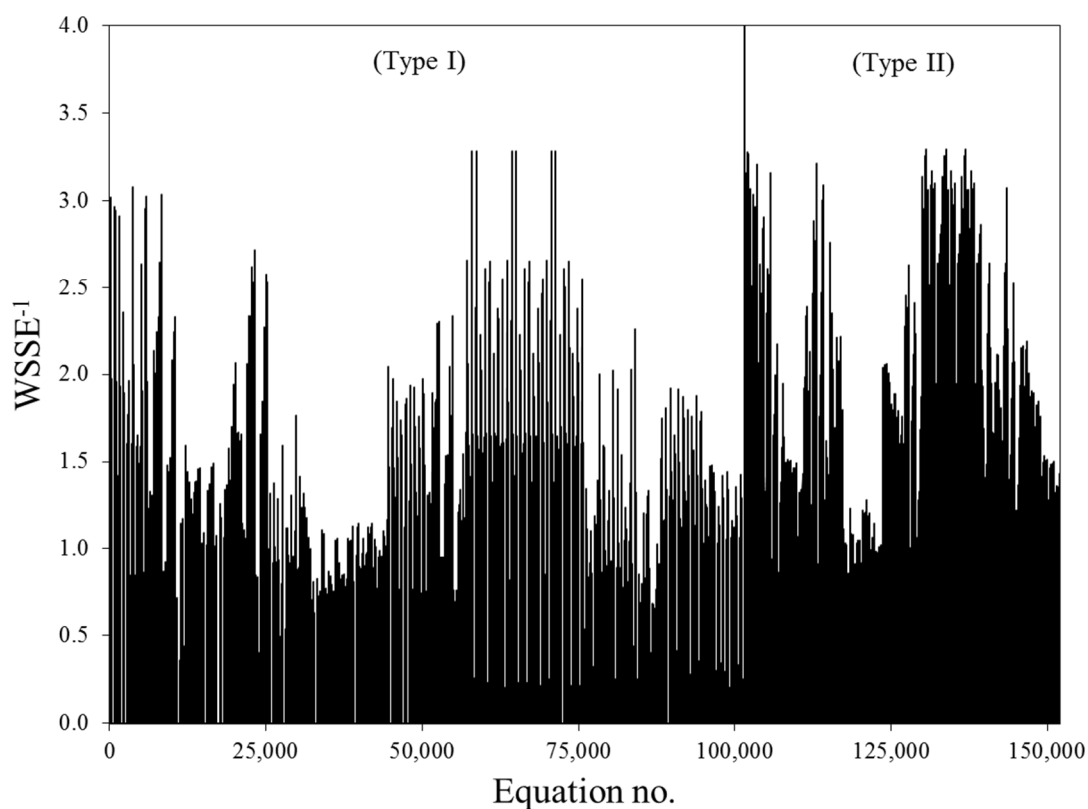


Figure 8.13 Inverse of WSSE values for each fitted equation in the simultaneous syntheses of ETBE and BTBE

The set of equations that presented a better fit to the experimental reaction rates was preselected (i.e., equations that produced $WSSE^{-1} \geq 1.31$) and discussed. All preselected equations include the interaction term, Ψ , what indicates that it should be included in the final kinetic model. With respect to the adsorption term, the frequency of appearance of each of the considered species is as follows: ethanol is included in 94% of the preselected equations, ETBE in 75%, 1-butanol in 70%, BTBE in 59%, and isobutene in 58%. Most of the preselected equations (87%) correspond to type II equations, which is consistent with assuming that the number of vacant active sites is not significant ($\alpha_D = 0$).

Regarding which step should be considered as the rate-determining one, 61% of the preselected equations consider that at least one of the reactions is controlled by the ether desorption step, whereas 56% are based on assuming that the surface reaction step is rate-determining for, at least, one of the reactions. Adsorption of one of the alcohols, or isobutene adsorption would be the rate-determining steps for 23% and 15% of the preselected equations, respectively. Notice that, like in the BTBE system, no conclusive results can be obtained regarding the selection of the rate-determining step, because the assumption that the rate-determining step is either the ethers desorption or the surface reactions lead to the same form of the driving force term in the kinetic equation. At this point, the surface reaction step was chosen as the rate-determining step, because, on one hand, it was considered a more feasible assumption and, on the other hand, the apparent activation energies calculated with the corresponding equations were, globally, closer to the estimated values obtained from initial reaction rates.

The equations and fitted parameters values shown in Table 8.11 correspond to the best equations (i.e., those with $\Delta_i < 10$) belonging to the subset of type II equations, which assume the surface reaction step as the rate-determining step.

From Table 8.11, the most likely equations to describe the kinetics of the simultaneous syntheses of ETBE and BTBE are similar to those found for the individual syntheses of PTBE and BTBE. These equations are consistent with a kinetic model in which both alcohols and one ether are adsorbed on the resin active sites in significant amounts.

On the other hand, kinetic expressions with an adsorption term of the form $(a_{IB} + k_{EtOH} a_{EtOH} + k_{BuOH} a_{BuOH} + k_{ETBE} a_{ETBE})^{n_i}$ should also be considered, since they are the most frequent ones in Table 8.11. As these expressions are essentially the same, except for the temperature dependence of the ratios of adsorption equilibrium constants, an averaged equation could be more appropriate to describe kinetics.

Table 8.11 Most relevant kinetic equations for the simultaneous syntheses of ETBE and BTBE

Equation	Kinetic coefficient terms				Ads. ^a	Adsorption term								Interaction term		WSSE	Δ_i		
	k'_{ETBE_I}	k'_{ETBE_T}	k'_{BTBE_I}	k'_{BTBE_T}		K_{EtOH_I}	K_{EtOH_T}	K_{BuOH_I}	K_{BuOH_T}	K_{ETBE_I}	K_{ETBE_T}	K_{BTBE_I}	K_{BTBE_T}	n_{ETBE}	n_{BTBE}			k_{D_I}	k_{D_T}
101,607	-0.318	-10162	-0.787	-8616	20			-2.36	-10859	0.21			1	1	26.0		0.313	0.0	
101,975	2.60	-10516	4.12	-11106	8	2.58		1.51	-6841	2.68			1	2	25.5		0.310	0.9	
102,164	-0.059	-10451	-1.22	-11006	24			-1.02	-6306	-0.07	1264	-2.24	1	2	25.4		0.306	1.6	
101,977	3.20	-12118	5.18	-14272	8	3.07	-1767	2.08	-8263	3.12			1	2	24.7		0.307	1.6	
101,958	-0.045	-10709	-1.23	-11624	20			-1.04	-6704	-0.07			1	2	25.2		0.317	1.8	
102,160	-0.074	-10743	-1.27	-11567	24			-1.12	-6941	-0.23		-1.76	1	2	25.2		0.312	2.1	
101,568	-0.379	-8445	-0.891	-7257	19					0.15			1	1	26.0		0.329	2.8	
101,987	2.55	-14392	4.00	-14804	8	2.49		1.45	-7002	2.66	4406		1	2	25.5	-0.28	0.305	3.3	
101,974	2.32	-9433	3.64	-8850	8	2.31	-1438	1.35		2.55			1	2	25.9		0.322	6.7	
101,973	2.30	-8458	3.58	-7227	8	2.33		1.24		2.49			1	2	26.0		0.330	7.8	
101,980	4.22	-7578	7.10	-5363	8	4.09	2721	2.88	-4039	4.02	4574		1	2	24.1		0.316	8.6	
101,976	4.16	-8569	7.07	-6988	8	4.03		3.06		3.98	1322		1	2	24.2		0.329	9.5	
101,957	0.069	-8569	-1.12	-7379	20			-1.03		-0.17			1	2	24.4		0.340	9.9	
101,579	4.33	-14749	3.86	-13131	6	4.70	-6343			4.96	-5518		1	1	26.0		0.330	10.1	
101,734	-0.404	-8612	-0.918	-7532	23					0.12		-14.1	-70413	1	1	26.0		0.336	10.6
103,624	2.74	-6919	3.358	-1632	16	1.42	9669	0.63		1.60	7209	0.34	15456	2	3	26.0	-0.53	0.312	11.4
101,610	-0.186	-8812	-0.679	-7577	20			-1.89		0.10			1	1	25.5	-0.03	0.339	11.9	

^a Adsorption term type as indicated in Table A10, i.e., Ads. 6: $(a_{IB} + K_{EtOH} a_{EtOH} + K_{ETBE} a_{ETBE})^{n_i}$, Ads. 8: $(a_{IB} + K_{EtOH} a_{EtOH} + K_{BuOH} a_{BuOH} + K_{ETBE} a_{ETBE})^{n_i}$, Ads. 16: $(a_{IB} + K_{EtOH} a_{EtOH} + K_{BuOH} a_{BuOH} + K_{ETBE} a_{ETBE} + K_{BTBE} a_{BTBE})^{n_i}$, Ads. 19: $(a_{EtOH} + K_{ETBE} a_{ETBE})^{n_i}$, Ads. 20: $(a_{EtOH} + K_{BuOH} a_{BuOH} + K_{ETBE} a_{ETBE})^{n_i}$, Ads. 23: $(a_{EtOH} + K_{ETBE} a_{ETBE} + K_{BTBE} a_{BTBE})^{n_i}$, and Ads. 24: $(a_{EtOH} + K_{BuOH} a_{BuOH} + K_{ETBE} a_{ETBE} + K_{BTBE} a_{BTBE})^{n_i}$

The fit to experimental rate data and residuals distribution for both equations #101,607 and the averaged equation are shown in Figures 8.14 and 8.15, respectively. Equation parameters and thermodynamic relations are listed in Table 8.12.

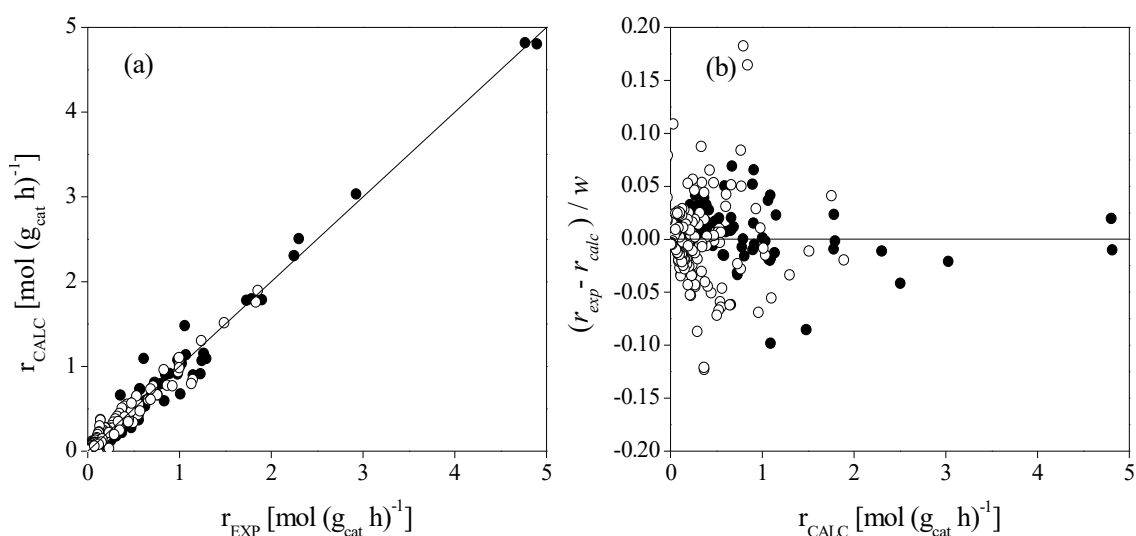


Figure 8.14 Comparison between experimental and calculated ETBE and BTBE reaction rates from equation #101,607 (a), and residuals distribution (b). ETBE rates (●), BTBE rates (○)

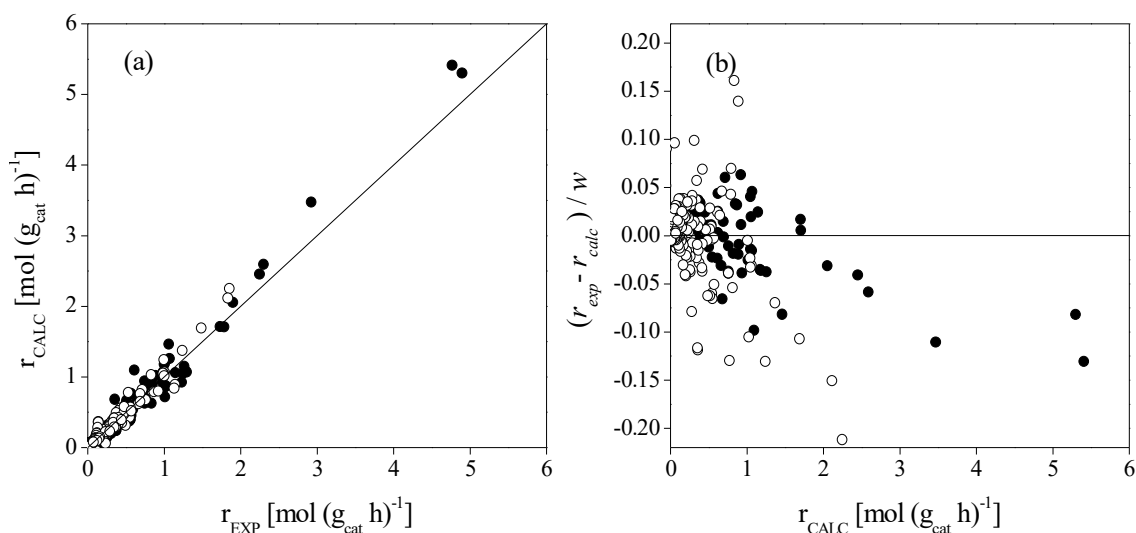


Figure 8.15 Comparison between experimental and calculated ETBE and BTBE reaction rates estimated by the averaged equation (a), and residuals distribution (b). ETBE rates (●), BTBE rates (○)

From Figures 8.14 and 8.15, the fit of equation #101,607 to the experimental reaction rate data is better than that of the averaged equation. Furthermore, apparent activation energies calculated from the averaged equation are rather high in comparison to the experimental values (Table 8.12). Therefore, equation #101,607 has been selected as the most appropriate expression to describe the kinetics of the simultaneous production of ETBE and BTBE.

Table 8.12 Kinetic equations parameters, and thermodynamic relations for the simultaneous syntheses of ETBE and BTBE

Equation 101,607		Averaged equation	
$r_{ETBE} = \frac{k'_{ETBE} \left(a_{IB} a_{EtOH} - \frac{a_{ETBE}}{K_{Eq_{ETBE}}} \right) \exp \left[\frac{\bar{V}_M \phi_P^2}{RT} (\delta_M - \delta_P)^2 \right]}{a_{EtOH} + K_{I-BuOH} a_{I-BuOH} + K_{ETBE} a_{ETBE}}$		$r_{ETBE} = \frac{k'_{ETBE} \left(a_{IB} a_{EtOH} - \frac{a_{ETBE}}{K_{Eq_{ETBE}}} \right) \exp \left[\frac{\bar{V}_M \phi_P^2}{RT} (\delta_M - \delta_P)^2 \right]}{a_{IB} + K_{EtOH} a_{EtOH} + K_{I-BuOH} a_{I-BuOH} + K_{ETBE} a_{ETBE}}$	
$r_{BTBE} = \frac{k'_{BTBE} \left(a_{IB} a_{I-BuOH} - \frac{a_{BTBE}}{K_{Eq_{BTBE}}} \right) \exp \left[\frac{\bar{V}_M \phi_P^2}{RT} (\delta_M - \delta_P)^2 \right]}{a_{EtOH} + K_{I-BuOH} a_{I-BuOH} + K_{ETBE} a_{ETBE}}$		$r_{BTBE} = \frac{k'_{BTBE} \left(a_{IB} a_{I-BuOH} - \frac{a_{BTBE}}{K_{Eq_{BTBE}}} \right) \exp \left[\frac{\bar{V}_M \phi_P^2}{RT} (\delta_M - \delta_P)^2 \right]}{(a_{IB} + K_{EtOH} a_{EtOH} + K_{I-BuOH} a_{I-BuOH} + K_{ETBE} a_{ETBE})^2}$	
Equation parameters			
$k'_{ETBE} \left[\frac{\text{mol}}{\text{g}_{\text{cat}} \text{h}} \right] = \exp \left[-(0.32 \pm 0.04) - (10.2 \pm 0.3) \cdot 10^3 \left(\frac{1}{T} - \frac{1}{333.6} \right) \right]$		$k'_{ETBE} \left[\frac{\text{mol}}{\text{g}_{\text{cat}} \text{h}} \right] = \exp \left[(2.8 \pm 0.3) - (11.5 \pm 1.3) \cdot 10^3 \left(\frac{1}{T} - \frac{1}{333.6} \right) \right]$	
$k'_{BTBE} \left[\frac{\text{mol}}{\text{g}_{\text{cat}} \text{h}} \right] = \exp \left[-(0.79 \pm 0.02) - (8.62 \pm 0.19) \cdot 10^3 \left(\frac{1}{T} - \frac{1}{333.6} \right) \right]$		$k'_{BTBE} \left[\frac{\text{mol}}{\text{g}_{\text{cat}} \text{h}} \right] = \exp \left[-(4.5 \pm 0.5) - (12.5 \pm 1.9) \cdot 10^3 \left(\frac{1}{T} - \frac{1}{333.6} \right) \right]$	
$K_{I-BuOH} = \exp \left[-(2.36 \pm 0.11) - (10.9 \pm 0.8) \cdot 10^3 \left(\frac{1}{T} - \frac{1}{333.6} \right) \right]$		$K_{EtOH} = \exp \left[(2.7 \pm 0.3) \right]$	
$K_E = \exp \left[(0.21 \pm 0.07) \right]$		$K_{I-BuOH} = \exp \left[(1.7 \pm 0.3) - (7.3 \pm 0.7) \cdot 10^3 \left(\frac{1}{T} - \frac{1}{333.6} \right) \right]$	
$\delta_P \left[\text{MPa}^{1/2} \right] = 25.99 \pm 0.10$		$K_{ETBE} = \exp \left[(0.21 \pm 0.07) \right]$	
		$\delta_P \left[\text{MPa}^{1/2} \right] = 25.2 \pm 0.4$	
Thermodynamic relations			
$E'_{a,ETBE} \text{ [kJ mol}^{-1}\text{]} = 84 \pm 3$		$E'_{a,ETBE} \text{ [kJ mol}^{-1}\text{]} = 95 \pm 10$	
$E'_{a,BTBE} \text{ [kJ mol}^{-1}\text{]} = 72 \pm 2$		$E'_{a,BTBE} \text{ [kJ mol}^{-1}\text{]} = 104 \pm 15$	
$\Delta H_{a,I-BuOH}^{\circ} - \Delta H_{a,EtOH}^{\circ} \text{ [kJ mol}^{-1}\text{]} = 90 \pm 6$		$\Delta G_{a,EtOH}^{\circ} - \Delta G_{a,IB}^{\circ} \text{ [kJ mol}^{-1}\text{]} = -7.6 \pm 0.7$	
$\Delta S_{a,I-BuOH}^{\circ} - \Delta S_{a,EtOH}^{\circ} \text{ [kJ mol}^{-1}\text{]} = 251 \pm 11$		$\Delta H_{a,I-BuOH}^{\circ} - \Delta H_{a,IB}^{\circ} \text{ [kJ mol}^{-1}\text{]} = 61 \pm 6$	
$\Delta G_{a,ETBE}^{\circ} - \Delta G_{a,EtOH}^{\circ} \text{ [kJ mol}^{-1}\text{]} = -0.57 \pm 0.19$		$\Delta S_{a,I-BuOH}^{\circ} - \Delta S_{a,IB}^{\circ} \text{ [kJ mol}^{-1}\text{]} = 197 \pm 10$	
		$\Delta G_{a,ETBE}^{\circ} - \Delta G_{a,IB}^{\circ} \text{ [kJ mol}^{-1}\text{]} = -7.9 \pm 0.6$	

a At $\bar{T} = 333.6$ K

Like in the previous section, the candidate equation was fitted to the experimental reaction rate data affected by transport limitations (i.e., those obtained in experiments at temperature higher than 343 K with catalyst particle size within the range of 0.25 to 0.40 mm). Optimal values of the apparent kinetic coefficients, calculated by minimization of WSSE for each individual experiment, are listed in Table 8.13, along with the corresponding WSSE value, and the resulting effectiveness factor (η). Equation #101,607 fits satisfactorily the experimental reaction rate data affected by mass transfer effects (Figure 8.16).

Table 8.13 Fitted values for the apparent kinetic coefficients, minimal WSSE, and effectiveness factor (η) for each individual experiment affected by mass transfer limitations in the simultaneous syntheses of ETBE and BTBE

Equation 101,607							
R ^o _{A/O}	R ^o _{E/B}	T [K]	k'_{ETBE} [mol (g _{cat} h) ⁻¹]	k'_{BTBE} [mol (g _{cat} h) ⁻¹]	WSSE	η_{ETBE} [%]	η_{BTBE} [%]
1.0	1.0	353	2.57	1.51	0.012	64	78
1.0	1.0	355	2.68	1.62	0.003	61	77

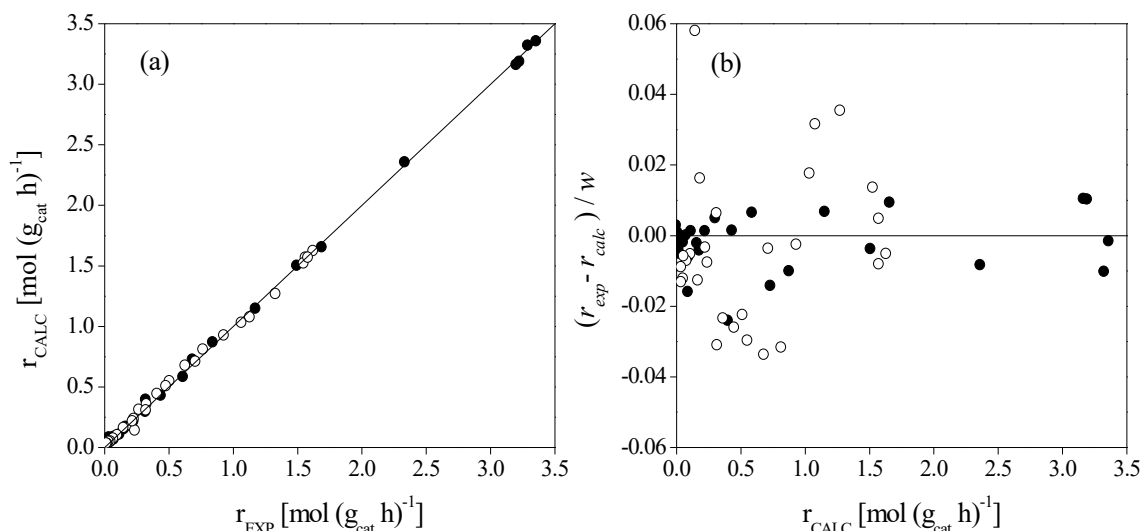


Figure 8.16 Comparison between experimental and calculated ETBE and BTBE reaction rates from equation #101,607 affected by mass transfer limitations (a), and residuals distribution (b).
ETBE rates (●), BTBE rates (○)

8.3.5 Comparison of kinetic equations

Irrespectively of the reaction system, the obtained equations are consistent with ER mechanisms, with the surface reaction being the rate-determining step. One molecule of alcohol, adsorbed on one active site, would react with one isobutene molecule from solution to produce one adsorbed molecule of the corresponding ether. These results are consistent with previous works on similar reaction systems (e.g., MTBE [162] and ETBE [138] syntheses). The fact that all of the obtained equations are consistent with the same kinetic mechanism adds reliability to the present results.

For comparative purposes, the logarithm of the obtained apparent kinetic coefficients are plotted against the inverse temperature in Figure 8.17, and compared with some literature values for the ETBE synthesis [19,138]. With regard to literature references, González [19] studied the ETBE kinetics on A-35 using an industrial C₄ cut as the isobutene source, and the work by Fité et al. [138] studied the ETBE kinetics over the ion-exchange resin Lewatit K2631 using pure isobutene. In fact, since none of these two works obtained the same kinetic model (nor operated under the same conditions) as the ones from the present work, no fully consistent comparison can be provided. Therefore, the comparison in Figure 8.17 should be considered a mere indication of the differences between present and previously reported results.

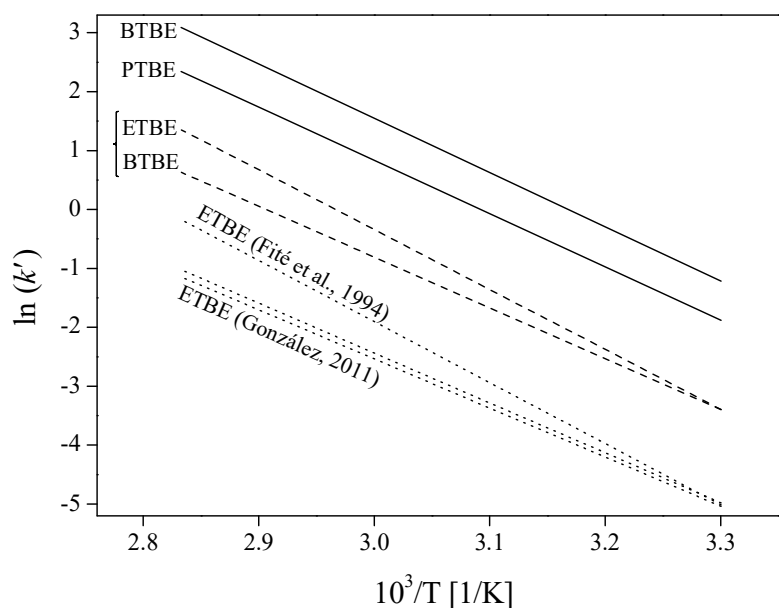


Figure 8.17 Arrhenius plot of the obtained apparent kinetic coefficients for the individual syntheses of PTBE and BTBE (—), for the simultaneous syntheses of ETBE and BTBE (— — —) and for the ETBE individual synthesis from literature ($\cdot \cdot \cdot$) [19,138]

From Figure 8.17, the individual synthesis of BTBE is the fastest reaction, that of PTBE is about the half and rate values for the simultaneous system are, at least, five times smaller. Both BTBE and PTBE rates present a similar sensitivity to temperature variation. With regards to the simultaneous syntheses of ETBE and BTBE, Figure 8.17 shows different sensitivity to temperature variation. As a consequence, the difference between ETBE and BTBE rates in the simultaneous system is almost null at low temperatures (at 303 K, $k'_{ETBE} \approx k'_{BTBE}$) but quite important at high temperatures (at 353 K, $k'_{ETBE} > 2k'_{BTBE}$). Globally, these results are in agreement with the experimentally observed reaction rates variation.

Also from Figure 8.17, the BTBE synthesis performance with and without ethanol presence can be compared. On one hand, it is noticeable that the BTBE apparent kinetic constant is reduced by the presence of ethanol. This can be explained by assuming that, since ethanol presents a higher affinity for the resin than 1-butanol, the resin active sites would be preferentially occupied by ethanol molecules, as discussed in the previous chapter. Therefore, the number of active sites accessible to 1-butanol would be lower in the presence of ethanol. On the other hand, according to the obtained models, BTBE apparent kinetic coefficients in both the individual and the simultaneous systems would present a similar sensitivity with temperature, what would indicate that the effect of ethanol on BTBE kinetics is not temperature-influenced.

With respect to the performance of ETBE, present results in the simultaneous synthesis system cannot be compared to those by González and by Fité et al. However, it would seem that the ETBE apparent kinetic coefficient could be increased by the presence of 1-butanol. If confirmed, it could be explained by assuming that (i) the presence of 1-butanol would not pose significant hindrances to the ethanol adsorption on the active

sites (because of its preferential adsorption over 1-butanol) and, consequently, the amount of adsorbed ethanol could be similar, if not the same, in both the individual and the simultaneous systems; and (ii) the presence of 1-butanol involves some decrease of the reaction medium polarity, which would entail an increase of the proton donor-acceptor strength of the available active sites. Thus, a similar number of active sites could be accessible to ethanol which would be less dissociated and, as a result, the ETBE synthesis reaction could be faster.

According to an ER mechanism, the obtained apparent kinetic coefficients can be related to the kinetic constant for each synthesis reaction, and to the corresponding adsorption constants, as follows:

$$\text{PTBE synthesis: } k'_{PTBE} = k_{PTBE} \frac{K_{a,1-PrOH}}{K_{a,1-PrOH}} = k_{PTBE} \quad (8.24)$$

$$\text{BTBE synthesis: } k'_{BTBE} = k_{BTBE} \frac{K_{a,1-BuOH}}{K_{a,1-BuOH}} = k_{BTBE} \quad (8.25)$$

$$\text{Simultaneous syntheses: } \left\{ \begin{array}{l} \text{ETBE: } k'_{ETBE} = k_{ETBE} \frac{K_{a,EtOH}}{K_{a,EtOH}} = k_{ETBE} \\ \text{BTBE: } k'_{BTBE} = k_{BTBE} \frac{K_{a,1-BuOH}}{K_{a,EtOH}} \end{array} \right. \quad (8.26)$$

$$\left. \begin{array}{l} \text{ETBE: } k'_{ETBE} = k_{ETBE} \frac{K_{a,EtOH}}{K_{a,EtOH}} = k_{ETBE} \\ \text{BTBE: } k'_{BTBE} = k_{BTBE} \frac{K_{a,1-BuOH}}{K_{a,EtOH}} \end{array} \right\} \quad (8.27)$$

where k_i is the actual kinetic constant for reaction i .

As seen in Equations 8.24 to 8.27, the apparent kinetic coefficients of PTBE, BTBE and ETBE synthesis reactions are the actual kinetic constants for each reaction. According to this, the actual activation energies of these synthesis reactions are, respectively, (75.1 ± 0.7), (76.6 ± 1.1), and (84 ± 3) kJ mol^{-1} . In the particular case of the BTBE synthesis in the simultaneous system, the apparent activation energy can be expressed as:

$$E'_{a,BTBE} = E_{a,BTBE} + \Delta H_{a,1-BuOH}^{\circ} - \Delta H_{a,EtOH}^{\circ} \quad (8.27)$$

Assuming that the actual activation energy for the BTBE synthesis reaction is the same as in the individual system, the difference of alcohols heats of adsorption can be estimated from Equation 8.27, its value being of about -5 kJ mol^{-1} . Because of the lack of experimental data, this value can be taken as a good estimate of the actual difference between 1-butanol and ethanol enthalpies of adsorption on A-35. Similar values can be estimated for methanol, ethanol and 1-propanol adsorption enthalpy differences on Amberlyst™ 15 (Table 8.14) [169]. On the contrary, the calculated difference of adsorption enthalpies from the coefficients of the fitted kinetic equation for the BTBE synthesis in the simultaneous system (its value being 90 kJ mol^{-1} , as shown in Table 8.12) seems not reliable, what can be attributed to the mathematical fitting in which a considerable number of parameters are involved, with a large uncertainty.

Table 8.14 Quoted adsorption enthalpies in the gas-phase, $\Delta H_a^\circ(g)$, for methanol, ethanol and 1-propanol on Amberlyst™ 15, enthalpy of vaporization, $\Delta H_a^\circ(vap)$, and calculated adsorption enthalpies in the liquid-phase, $\Delta H_a^\circ(l)$

Property	Compound			Reference
	MeOH	EtOH	1-PrOH	
$\Delta H_a^\circ(g)$ [kJ mol ⁻¹]	-39.7	-43.5	-50.5	Słomkiewicz (2006) [169]
$\Delta H_a^\circ(vap)$ [kJ mol ⁻¹]	37.6	42.3	47	NIST Chemistry WebBook [170]
$\Delta H_a^\circ(l)$ [kJ mol ⁻¹] ^a	-2.1	-1.2	-3.5	–

^a Calculated as $\Delta H_a^\circ(l) = \Delta H_a^\circ(g) + \Delta H_a^\circ(vap)$

8.4 Conclusions

The kinetics of three analogous liquid-phase reaction syntheses over Amberlyst™ 35 has been evaluated. A large number of combinations of kinetic equations, each obtained from the Langmuir-Hinshelwood-Hougen-Watson and Rideal-Eley formalisms, has been systematically proposed and fitted to experimental reaction rates free from mass transfer limitations. Among the used kinetic equations, different rate-determining steps have been considered. Likewise, all possible combinations of adsorbed and non-adsorbed species on the catalyst have been taken into account, as well as the possible influence on reaction rates of the interaction between the catalyst and the reaction medium.

The resulting kinetic models for each etherification reaction are consistent with an Eley-Rideal mechanism in which one molecule of alcohol is adsorbed on the catalyst, where it reacts with one non-adsorbed isobutene molecule to form one adsorbed ether molecule. The obtained models describe satisfactorily the observed reaction rates for the three reaction systems, including those affected by mass-transfer limitations. Some relations between thermodynamic properties of adsorption have been estimated from the fitted parameters values and compared to literature references, when available.

9. Summary and future lines of research

9.1 Summary of the main conclusions

Syntheses of MTBE, ETBE, PTBE, and BTBE, obtained by isobutene etherification with methanol, ethanol, 1-propanol, and 1-butanol, respectively, using ion-exchange resins as catalysts have been explored. The studied reactions constitute an analogous series of reactions in which a variation of the reaction medium properties arises due to the length of the involved compounds. In the present PhD thesis, the study of several aspects regarding this type of reactions has been accomplished. Given the different focuses set in the studies included in this work, main conclusions can be grouped into five sections, accordingly with the main goals presented in Chapter 1.

9.1.1 Conclusions regarding the chemical equilibrium of alkyl *tert*-butyl ethers syntheses

The chemical equilibrium study regarding the four reactions has allowed determining their thermodynamic state functions. From the experimental results, the thermochemical data of formation for the produced ethers has been estimated. As expected, the thermodynamics of the involved reactions have been proven to be independent of the used catalyst and reactor operation mode. All four chemical reactions are reversible, exothermic, and present no significant differences regarding their equilibrium limitations.

The liquid-phase standard enthalpy changes of the studied reaction syntheses have been estimated considering that the enthalpy change of reaction is either independent on temperature or a function of temperature. Enthalpies of PTBE and BTBE are more sensitive to temperature variations than those of MTBE and ETBE.

9.1.2 Conclusions regarding the byproducts formation in the ETBE synthesis

All side reactions taking place along with the ETBE formation have been studied at operating conditions that enhance them. All the side reactions are strongly favored by high temperatures, what means that their kinetics is strongly affected by temperature. On the other hand, the main effect of the initial reactants composition on the byproducts formation is that it affects the nature of the side reactions that are favored. An excess of isobutene in the reactants mixture enhances the formation of isobutene dimers and ethyl *sec*-butyl ether, whereas an excess of ethanol promotes the formation of diethyl ether and *tert*-butyl alcohol. According to the literature data on this subject dealing with similar reaction systems, it seems reasonable to assume that these conclusions can be extended to the possible byproducts formation in all four reaction systems studied throughout this PhD.

9.1.3 Conclusions regarding the effect of the reaction media on reaction rates and the relations between catalysts properties and resins catalytic behavior

The catalytic performance of sixteen ion-exchange resins in the syntheses of MTBE, ETBE, PTBE, and BTBE has been studied. Globally, etherification reactions rates present an upward gradation as the alcohol is larger (1-butanol > 1-propanol > ethanol ~ methanol).

In all cases, resins acid capacity and specific volume of the swollen polymer gel phase have been identified as the most relevant properties to determine each resin catalytic activity. Therefore, highly-acidic resins with a rigid morphology are the most active catalysts in the present reaction systems.

An empirical model, based on the distribution of polymer fractions within the resins gel-type phase, has been proposed which describes satisfactorily the experimental reaction rates for the MTBE and the ETBE syntheses, separately. A generalization of the empirical model to include the PTBE and the BTBE syntheses has been successfully achieved by means of the Ogston distribution coefficient. According to the proposed model, active sites located in polymer fractions with a characteristic chain density of 0.4 nm nm^{-3} would present a higher specific activity, for a group of resins that would allow multiple active sites coordination. A second group of catalysts has been distinguished, for which no favored polymer fraction has been found, in terms of the active sites effectiveness therein.

9.1.4 Conclusions regarding the isobutene etherification with ethanol and 1-butanol to produce ETBE and BTBE

The simultaneous etherification of isobutene with ethanol and 1-butanol, using ion-exchange resins as catalysts, to obtain ETBE and BTBE, respectively, has been studied. Three focuses have been set: a catalytic screening, an assessment of the effect of some operating conditions on the reaction performance, and a comparison of the simultaneous process with each individual synthesis.

According to the screening study, strongly acidic catalysts with high crosslinking degrees achieve faster rates. Accordingly, A-35 is the most appropriate catalyst, among the tested ones, for the simultaneous etherification process because it yields high reaction rates and low byproducts formation.

An increase of the isobutene initial concentration enhances both ethers formation rates. With regards to the alcohols initial concentration, BTBE production rate strongly diminishes when ethanol concentration is higher than that of 1-butanol. On the contrary, ETBE formation rate is not significantly affected by the alcohols concentration in the reactants mixture. A preferential adsorption of ethanol over 1-butanol on the tested resins has been observed.

Finally, the simultaneous syntheses of ETBE and BTBE present high reactants conversion and selectivity towards the desired products. The simultaneous process produces less byproducts than each of the individual syntheses.

9.1.5 Conclusions regarding the kinetics of the liquid-phase synthesis of alkyl *tert*-butyl ethers over Amberlyst™ 35

The kinetics of the individual syntheses of PTBE and BTBE and that of the simultaneous syntheses of ETBE and BTBE has been evaluated. In all cases, Amberlyst™ 35 has been used as the catalyst. Combinations of kinetic equations, obtained from the Langmuir-Hinshelwood-Hougen-Watson and Rideal-Eley formalisms, have been systematically proposed and fitted to experimental reaction rates free from mass transfer limitations.

The resulting kinetic models for each etherification reaction are consistent with an Eley-Rideal mechanism in which one molecule of alcohol is adsorbed on the catalyst, where it reacts with one isobutene molecule from solution to form one adsorbed ether molecule that, finally, desorbs. The obtained models describe satisfactorily the observed reaction rates for the three reaction systems, including those affected by mass-transfer limitations.

9.2 Future lines of research

The present PhD thesis is a contribution to the study of the catalytic reaction processes involved in the synthesis of alkyl *tert*-butyl ethers, which are among the most important fuel ethers to be used as gasoline additives. Hopefully, in the light of the results hereby presented, some future works will be addressed to this subject. If so, the following future research guidelines are proposed:

1. To carry out similar studies focused on the synthesis of other interesting ethers, such as those obtained by etherification of isoamylenes.
2. To further explore integrated processes by which different compounds could be synthesized and purified in the same unit, i.e., simultaneous etherification reactions in reactive distillation units.
3. To manufacture tailored catalysts which could present the set of morphological properties that, according to the results of this PhD, enhance these ethers formation rate. From this, present results could be either confirmed or refused and, more interestingly, if confirmed, important improvements could be brought to alkyl *tert*-butyl ethers industrial production.
4. To carry out cost-benefit studies regarding the introduction of 1-propanol and/or 1-butanol as reactants to obtain the corresponding ethers –either as individual processes or in any combination of simultaneous operation– to be used as additives to the gasoline pool. Such studies should also be addressed to the manufacture processes of potential new catalysts.
5. To study the viability of new biological routes to synthesize secondary, or branched, alcohols to be used as reactants for the etherification of olefins.
6. Likewise, it would be interesting to develop cost-effective synthesis routes that could obtain gasoline additives entirely from renewable, non-edible, feedstocks.
7. Finally, it is the author's belief that operando characterization techniques are needed in order to provide crucial information regarding the morphological properties of ion-exchange resins in actual reaction media.

List of publications, work in progress and conference contributions

List of publications

Authors: J.H. Badia, C. Fité, R. Bringué, E. Ramírez, F. Cunill
Title: Byproducts formation in the ethyl *tert*-butyl ether (ETBE) synthesis reaction on macroreticular acid ion-exchange resins
Journal: Applied Catalysis A: General
Volume: 468 **Pages:** 384-394 **Date:** November 2013
DOI: 10.1016/j.apcata.2013.09.012

Authors: J.H. Badia, C. Fité, R. Bringué, M. Iborra, F. Cunill
Title: Catalytic activity and accessibility of acidic ion-exchange resins in liquid phase etherification reactions
Journal: Topics in Catalysis
Volume: 58 **Issue:** 14 **Pages:** 919-932 **Date:** October 2015
DOI: 10.1007/s11244-015-0460-3

Authors: J.H. Badia, C. Fité, R. Bringué, E. Ramírez, F. Cunill
Title: Thermodynamic analysis of the experimental equilibria for the liquid-phase etherification of isobutene with C₁ to C₄ linear primary alcohols
Journal: Journal of Chemical & Engineering Data
Volume: 61 **Pages:** 1054-1064 **Date:** February 2016
DOI: 10.1021/acs.jced.5b00557

Authors: J.H. Badia, C. Fité, R. Bringué, E. Ramírez, M. Iborra
Title: Relevant properties for catalytic activity of sulfonic ion-exchange resins in etherification of isobutene with linear primary alcohols
Journal: Journal of Industrial and Engineering Chemistry
Volume: 42 **Pages:** 36-45 **Date:** October 2016
DOI: 10.1016/j.jiec.2016.07.025

Work in progress

Authors: J.H. Badia, C. Fité, R. Bringué, E. Ramírez, J. Tejero
Title: Liquid-phase etherification of isobutene with ethanol and 1-butanol over acidic macroreticular ion-exchange resins: catalyst screening and effect of operating conditions
Publication status: first manuscript to be submitted to Applied Catalysis A: General

Conference contributions

Authors: J.H. Badia, R. González, C. Fité, F. Cunill, K.D. Topp

Title: Deactivation of ion-exchange catalysts by acetonitrile and methylamine

Contribution type: oral

Conference: 14th Nordic Symposium on Catalysis

Date and location: Marienlyst (Denmark), 29-31 August 2010

Authors: J.H. Badia, C. Fité, R. Bringué, E. Ramírez, J. Guilera, F. Cunill

Title: Byproducts formation in the ETBE synthesis reaction

Contribution type: poster

Conference: 10th Congress on Catalysis Applied to Fine Chemicals

Date and location: Turku/Åbo (Finland), 16-19 June 2013

Authors: J.H. Badia, C. Fité, R. Bringué, M. Iborra, F. Cunill

Title: Relations between morphology and catalytic activity of macroreticular acidic ion-exchanger catalysts for the syntheses of oxygenates for the gasoline pool

Contribution type: poster

Conference: 16th Nordic Symposium on Catalysis

Date and location: Oslo (Norway), 15-17 June 2014

Authors: J.H. Badia, C. Fité, R. Bringué, E. Ramírez, M. Iborra

Title: Effect of the alcohol size in the etherification of isobutene with linear alcohols catalyzed by macroreticular acidic ion-exchangers

Contribution type: oral

Conference: II International Congress of Chemical Engineering

Date and location: Madrid (Spain), 1-4 July 2014

Authors: R. Soto, C. Fité, E. Ramírez, J.H. Badia, R. Bringué

Title: Empirical kinetic model for the simultaneous liquid-phase etherification of isobutene and isoamylenes with ethanol over Amberlyst™ 35

Contribution type: poster

Conference: II International Congress of Chemical Engineering

Date and location: Madrid (Spain), 1-4 July 2014

Authors: J.H. Badia, C. Fité, R. Bringué, E. Ramírez, J. Tejero

Title: Efecto de la transferencia interna de material sobre la velocidad de reacción en la eterificación simultánea en fase líquida de isobuteno con etanol y 1-butanol sobre Amberlyst-35

Contribution type: oral

Conference: Reunión de la Sociedad Española de Catálisis, SECAT'15

Date and location: Barcelona (Spain), 13-15 July 2015

Authors: J.H. Badia, C. Fité, R. Bringué, E. Ramírez, F. Cunill

Title: Etherification of isobutene with C₁ to C₄ linear primary alcohols in liquid-phase: experimental equilibrium and thermodynamic analysis

Contribution type: poster

Conference: 12th European Congress on Catalysis – EuropaCat-XI

Date and location: Kazan (Russia), 30 August to 4 September 2015

Authors: J.H. Badia, C. Fité, R. Bringué, E. Ramírez, J. Tejero

Title: Simultaneous liquid-phase etherification of isobutene with ethanol and 1-butanol on macroreticular ion-exchange resins

Contribution type: oral

Conference: 10th European Congress of Chemical Engineering

Date and location: Nice (France), 27 September to 1 October 2015

Authors: M. Iborra, E. Ramírez, J.H. Badia, R. Bringué

Title: Implementación del aula invertida en la asignatura Informática Aplicada del grado de Ingeniería Química de la Universidad de Barcelona

Contribution type: oral

Conference: IX Congreso Internacional de Docencia Universitaria e Innovación

Date and location: Bellaterra (Spain), 5-7 July 2016,

Authors: J.H. Badia, C. Fité, R. Bringué, J. Tejero, F. Cunill

Title: Kinetic study of the simultaneous liquid-phase etherification of isobutene with ethanol and 1-butanol over AmberlystTM 35

Contribution type: oral

Conference: IEX 2016

Date and location: Cambridge (United Kingdom), 6-8 July 2016,

Authors: J.H. Badia, R. Bringué, C. Fité, M. Iborra, R. Soto, F. Cunill

Title: Kinetics of the liquid-phase syntheses of propyl *tert*-butyl ether (PTBE) and butyl *tert*-butyl ether (BTBE) over AmberlystTM 35

Contribution type: poster

Conference: 22nd International Congress of Chemical and Process Engineering, CHISA 2016

Date and location: Prague (Czech Republic), 28-31 August 2016

Appendices

Appendix I Additional information

Table A1 Measured reaction medium composition (major compounds) in the MTBE synthesis reaction and calculated mass-action ratios, Γ_x , Γ_γ and Γ_a , for each experimental run. Experiments were carried out in the liquid phase at 1.5 MPa in the fixed-bed tubular reactor at $R^o_{A/O} = 1.03$ and at different LHSV values. Standard uncertainties of mass-action ratios for each experimental run have been estimated by means of the Monte-Carlo method [171] with 1000 generated points applied to the chromatographic analysis results. (Chapter 3)

T [K]	Catalyst	LHSV [h ⁻¹]	Mass fraction, $w \times 10^3$					Γ_x	$\Gamma_\gamma \times 10^3$	Γ_a
			isobutane	<i>trans</i> -2-butene	isobutene	methanol	MTBE			
323	A-15	2.4	416 ± 3	297 ± 2	4.04 ± 0.03	28.0 ± 0.3	254 ± 2	746 ± 10 ^a	107.5 ± 0.6 ^a	80.1 ± 1.0 ^a
		4.4	394 ± 3	317 ± 2	6.36 ± 0.05	29.9 ± 0.3	253 ± 2	443 ± 6	110.3 ± 0.6	48.8 ± 0.6
		9.0	403 ± 3	303 ± 2	15.69 ± 0.12	32.0 ± 0.3	246 ± 2	164 ± 2	112.6 ± 0.6	18.5 ± 0.2
	A-35	2.4	417 ± 3	298 ± 2	4.15 ± 0.03	28.6 ± 0.3	252 ± 2	706 ± 10 ^a	108.2 ± 0.6 ^a	76.3 ± 0.9 ^a
		4.7	403 ± 3	307 ± 2	6.13 ± 0.05	29.0 ± 0.3	254 ± 2	475 ± 6	109.1 ± 0.6	51.8 ± 0.6
		9.0	395 ± 3	315 ± 2	8.11 ± 0.06	30.5 ± 0.3	251 ± 2	338 ± 5	111.0 ± 0.6	37.6 ± 0.5
343	A-15	2.3	392 ± 3	320 ± 2	10.31 ± 0.08	32.4 ± 0.3	245 ± 2	246 ± 3 ^a	124.0 ± 0.6 ^a	30.5 ± 0.4 ^a
		2.4	421 ± 3	294 ± 2	8.18 ± 0.06	31.4 ± 0.3	245 ± 2	319 ± 4 ^a	122.5 ± 0.6 ^a	39.1 ± 0.5 ^a
		2.4	420 ± 3	294 ± 2	8.56 ± 0.07	31.0 ± 0.3	247 ± 2	311 ± 4 ^a	122.2 ± 0.6 ^a	38.0 ± 0.5 ^a
		6.4	403 ± 3	305 ± 2	15.05 ± 0.12	33.1 ± 0.3	243 ± 2	164 ± 2	124.7 ± 0.6	20.4 ± 0.3
		15.0	404 ± 3	303 ± 2	18.21 ± 0.14	34.8 ± 0.3	239 ± 2	127 ± 2	126.5 ± 0.6	16.1 ± 0.2
	A-35	2.4	408 ± 3	303 ± 2	9.69 ± 0.08	30.7 ± 0.3	249 ± 2	279 ± 4 ^a	122.1 ± 0.6 ^a	34.1 ± 0.4 ^a
		2.4	416 ± 3	296 ± 2	10.30 ± 0.08	31.2 ± 0.3	247 ± 2	257 ± 3 ^a	122.5 ± 0.6 ^a	31.4 ± 0.4 ^a
		4.7	401 ± 3	308 ± 2	13.08 ± 0.10	32.6 ± 0.3	245 ± 2	193 ± 3	124.3 ± 0.6	24.0 ± 0.3
		4.7	397 ± 3	312 ± 2	12.21 ± 0.09	32.5 ± 0.3	246 ± 2	208 ± 3	124.3 ± 0.6	25.8 ± 0.3
		6.4	391 ± 3	317 ± 2	12.71 ± 0.10	32.7 ± 0.3	246 ± 2	198 ± 3	124.5 ± 0.6	24.7 ± 0.3
		9.0	395 ± 3	314 ± 2	13.61 ± 0.11	33.2 ± 0.3	244 ± 2	181 ± 2	125.0 ± 0.6	22.7 ± 0.3
		20.1	398 ± 3	310 ± 2	15.98 ± 0.12	34.0 ± 0.3	242 ± 2	149 ± 2	125.8 ± 0.6	18.8 ± 0.2

^a Mass action ratio at equilibrium, which corresponds to the equilibrium constant

Table A2 Measured reaction medium composition (major compounds) in the ETBE synthesis reaction and calculated mass-action ratios, Γ_x , Γ_γ and Γ_a , for each experimental run. Experiments were carried out in the liquid phase at 1.5 MPa in the fixed-bed tubular reactor at $R_{A/O}^o = 1.10$ and at different LHSV values. Standard uncertainties of mass-action ratios for each experimental run have been estimated by means of the Monte-Carlo method [171] with 1000 generated points applied to the chromatographic analysis results. (Chapter 3)

T [K]	Catalyst	LHSV [h ⁻¹]	Mass fraction, $w \times 10^3$					Γ_x	$\Gamma_\gamma \times 10^3$	Γ_a
			isobutane	<i>trans</i> -2-butene	isobutene	ethanol	ETBE			
313	A-35	1.8	341 ± 4	316 ± 4	8.95 ± 0.14	21.2 ± 0.4	313 ± 2	635 ± 14 ^a	93.9 ± 0.7 ^a	59.6 ± 1.1 ^a
	CT-275	1.8	339 ± 4	318 ± 4	9.21 ± 0.14	21.5 ± 0.4	312 ± 2	607 ± 13 ^a	94.2 ± 0.7 ^a	57.2 ± 1.0 ^a
	K2620	1.8	326 ± 4	334 ± 4	9.88 ± 0.15	20.5 ± 0.4	310 ± 2	589 ± 13 ^a	92.8 ± 0.7 ^a	54.6 ± 1.0 ^a
333	A-35	1.9	337 ± 4	318 ± 4	16.2 ± 0.2	32.8 ± 0.5	297 ± 2	217 ± 5 ^a	124.1 ± 0.9 ^a	26.9 ± 0.5 ^a
		6.1	339 ± 4	317 ± 4	16.4 ± 0.3	30.3 ± 0.5	297 ± 2	231 ± 5	121.0 ± 0.9	28.0 ± 0.5
		10.3	342 ± 4	316 ± 4	17.3 ± 0.3	27.6 ± 0.5	297 ± 2	240 ± 5	117.4 ± 0.8	28.2 ± 0.5
		15.4	335 ± 4	319 ± 4	16.6 ± 0.3	34.2 ± 0.6	295 ± 2	202 ± 4	125.7 ± 0.9	25.4 ± 0.4
	CT-275	1.9	344 ± 4	316 ± 4	18.1 ± 0.3	26.9 ± 0.5	295 ± 2	235 ± 5 ^a	116.1 ± 0.8 ^a	27.3 ± 0.5 ^a
		6.2	345 ± 4	313 ± 4	17.4 ± 0.3	27.5 ± 0.5	297 ± 2	240 ± 5	117.2 ± 0.8	28.2 ± 0.5
	K2620	1.9	345 ± 4	312 ± 4	17.2 ± 0.3	29.2 ± 0.5	296 ± 2	229 ± 5 ^a	119.3 ± 0.8 ^a	27.4 ± 0.5 ^a
		6.2	341 ± 4	314 ± 4	16.7 ± 0.3	30.1 ± 0.5	298 ± 2	229 ± 5	120.7 ± 0.9	27.7 ± 0.5
		15.5	340 ± 4	313 ± 4	17.1 ± 0.3	34.9 ± 0.6	295 ± 2	192 ± 4	126.5 ± 0.9	24.2 ± 0.4
353	A-35	2.0	371 ± 4	330 ± 4	44.6 ± 0.6	24.4 ± 0.4	230 ± 2	85 ± 2 ^a	124.1 ± 0.6 ^a	10.5 ± 0.2 ^a
		2.0	352 ± 4	316 ± 4	32.4 ± 0.5	42.4 ± 0.7	258 ± 2	74 ± 2 ^a	150.3 ± 1.0 ^a	11.2 ± 0.2 ^a
		2.0	344 ± 4	325 ± 4	33.5 ± 0.5	40.1 ± 0.7	258 ± 2	76 ± 2 ^a	147.5 ± 1.0 ^a	11.2 ± 0.2 ^a
		2.0	353 ± 4	328 ± 4	35.4 ± 0.6	35.0 ± 0.6	249 ± 2	80 ± 2 ^a	140.0 ± 0.9 ^a	11.2 ± 0.2 ^a
	CT-275	2.0	354 ± 4	322 ± 4	34.4 ± 0.5	36.7 ± 0.6	253 ± 2	79 ± 2 ^a	142.6 ± 0.9 ^a	11.3 ± 0.2 ^a
	K2620	2.0	346 ± 4	326 ± 4	33.4 ± 0.5	38.7 ± 0.7	256 ± 2	78 ± 2 ^a	145.5 ± 1.0 ^a	11.4 ± 0.2 ^a

^a Mass action ratio at equilibrium, which corresponds to the equilibrium constant

Table A3 Measured reaction medium composition (major compounds) in the ETBE synthesis reaction and calculated equilibrium constants, K_x , K_y and K , for each experimental run. Experiments were carried out in the liquid phase at 2.0 MPa in the batch stirred tank reactor from mixtures of different $R^\circ_{A/O}$. Standard uncertainties of the equilibrium constants for each experimental run have been estimated by means of the Monte-Carlo method [171] with 1000 generated points applied to the chromatographic analysis results. (Chapter 3)

T [K]	Catalyst	$R^\circ_{A/O}$	Mass fraction, $w \times 10^3$					K_x	$K_y \times 10^3$	K
			isobutane	<i>trans</i> -2-butene	isobutene	ethanol	ETBE			
323	A-35	0.64	331 ± 8	318 ± 8	28.6 ± 0.7	7.3 ± 0.2	228 ± 4	418 ± 15	76.4 ± 0.8	31.9 ± 1.0
		1.17	290 ± 7	280 ± 7	23.7 ± 0.6	18.9 ± 0.5	385 ± 6	318 ± 11	112.5 ± 1.4	35.8 ± 1.1
		2.40	240 ± 6	232 ± 6	6.9 ± 0.2	174 ± 4	344 ± 5	114 ± 4	311 ± 5	35.3 ± 0.9
343	A-35	0.63	319 ± 6	307 ± 5	51.1 ± 0.8	14.6 ± 0.3	251 ± 3	129 ± 3	109.7 ± 0.7	14.2 ± 0.3
		1.15	297 ± 4	277 ± 4	42.0 ± 0.6	31.7 ± 0.4	332 ± 3	94 ± 2	144.6 ± 0.9	13.6 ± 0.2
		2.24	249 ± 3	235 ± 3	16.8 ± 0.2	175 ± 2	317 ± 2	42.9 ± 0.6	319 ± 2	13.7 ± 0.2
		2.39	243 ± 3	239 ± 4	17.4 ± 0.3	179 ± 2	317 ± 2	40.6 ± 0.7	323 ± 2	13.1 ± 0.2
		2.32	247 ± 3	242 ± 3	17.1 ± 0.2	175 ± 2	317 ± 2	42.2 ± 0.7	317 ± 2	13.4 ± 0.2
363	A-35	1.12	299 ± 4	278 ± 4	57.2 ± 0.7	50.9 ± 0.6	282 ± 2	37.6 ± 0.6	185.0 ± 1.1	6.96 ± 0.10
		1.09	308 ± 5	289 ± 4	57.8 ± 0.9	47.8 ± 0.6	253 ± 2	35.8 ± 0.7	176.0 ± 1.2	6.30 ± 0.11
		1.07	300 ± 4	287 ± 4	58.5 ± 0.9	51.7 ± 0.7	270 ± 2	34.9 ± 0.7	183.6 ± 1.2	6.40 ± 0.10
	CT-275	0.63	291 ± 4	273 ± 3	55.9 ± 0.7	53.3 ± 0.6	288 ± 2	37.3 ± 0.6	190.8 ± 1.1	7.12 ± 0.10
383	A-35	1.14	272 ± 4	248 ± 4	69.4 ± 0.9	74.9 ± 0.8	174.0 ± 1.3	13.0 ± 0.2	241.8 ± 1.3	3.15 ± 0.05
		2.23	218 ± 5	197 ± 5	51.7 ± 1.0	172 ± 3	204 ± 2	9.1 ± 0.2	366 ± 3	3.34 ± 0.07
		2.25	214 ± 4	208 ± 4	51.8 ± 0.8	207 ± 2	227 ± 2	8.7 ± 0.2	390 ± 3	3.38 ± 0.05
		2.39	234 ± 3	214 ± 3	51.4 ± 0.6	187 ± 2	209.3 ± 1.4	8.91 ± 0.13	367 ± 2	3.27 ± 0.04
	CT-275	1.21	189 ± 3	190 ± 3	44.4 ± 0.6	225 ± 2	211 ± 2	8.6 ± 0.2	420 ± 3	3.62 ± 0.06

Table A4 Measured reaction medium composition at equilibrium in the PTBE synthesis reaction and calculated equilibrium constants, K_x , K_y and K , for each experimental run. Experiments were carried out in the liquid phase at 2.0 MPa in a stirred-tank batch reactor from mixtures of different initial alcohol to olefin molar ratios, $R_{A/O}^o$, and using A-35 as catalyst. Standard uncertainties of the equilibrium constants have been estimated for each value by means of the Monte-Carlo method [171] with 1000 generated points applied to the chromatographic analysis results. (Chapter 3)

T [K]	$R_{A/O}^o$	Mass fraction, $w \times 10^3$						K_x	$K_y \times 10^3$	K
		isobutene	1-propanol	PTBE	TBA	TMP-1	TMP-2			
320.2	1.01	39.1 ± 0.6	33.7 ± 0.5	920.3 ± 1.1	6.94 ± 0.17	0	0 ± 0	188 ± 5	309.0 ± 0.8	58 ± 2
321.2	1.01	24.4 ± 0.3	63.4 ± 0.7	907.2 ± 1.0	4.97 ± 0.09	0	0 ± 0	159 ± 3	363.0 ± 1.1	57.9 ± 1.1
323.2	2.00	8.36 ± 0.10	350 ± 3	637 ± 3	0.99 ± 0.02	3.11 ± 0.04	0.518 ± 0.008	72.7 ± 1.4	701 ± 3	51.0 ± 0.9
325.7	1.06	26.5 ± 0.3	78.0 ± 0.7	884.0 ± 0.9	3.02 ± 0.04	7.18 ± 0.08	1.40 ± 0.02	118 ± 2	387.0 ± 1.0	45.7 ± 0.7
333.9	1.01	34.4 ± 0.6	74.1 ± 1.1	880 ± 2	1.34 ± 0.03	8.708 ± 0.147	1.86 ± 0.04	95 ± 3	388.9 ± 1.4	37.1 ± 0.9
344.5	1.04	42.7 ± 0.6	101.5 ± 1.5	842 ± 2	0.79 ± 0.02	10.4 ± 0.2	2.28 ± 0.05	55.3 ± 1.4	439 ± 2	24.3 ± 0.6
352.0	2.00	25.6 ± 0.3	358 ± 3	614 ± 3	0.658 ± 0.012	1.222 ± 0.015	0 ± 0	22.8 ± 0.4	712 ± 2	16.2 ± 0.3
352.2	1.02	57.9 ± 0.7	110.1 ± 1.4	823 ± 2	0.81 ± 0.02	6.82 ± 0.10	1.53 ± 0.03	37.6 ± 0.9	454.8 ± 1.4	17.1 ± 0.4

Table A5 Measured reaction medium composition at equilibrium in the BTBE synthesis reaction and calculated equilibrium constants, K_x , K_y and K , for each experimental run. Experiments were carried out in the liquid phase at 2.0 MPa in a stirred-tank batch reactor from mixtures of different initial alcohol to olefin molar ratios, $R_{A/O}^o$, and using A-35 as catalyst. Standard uncertainties of the equilibrium constants have been estimated for each value by means of the Monte-Carlo method [171] with 1000 generated points applied to the chromatographic analysis results. (Chapter 3)

T [K]	$R_{A/O}^o$	Mass fraction, $w \times 10^3$						K_x	$K_y \times 10^3$	K
		isobutene	1-butanol	BTBE	TBA	TMP-1	TMP-2			
317.2	1.01	21.5 ± 0.4	72.8 ± 1.3	902 ± 2	3.25 ± 0.10	0.410 ± 0.008	0.519 ± 0.008	153 ± 5	396 ± 2	60.7 ± 1.6
323.4	1.01	24.1 ± 0.3	87.7 ± 1.3	880 ± 2	1.37 ± 0.03	5.89 ± 0.10	1.241 ± 0.015	112 ± 3	423 ± 2	47.5 ± 1.1
334.3	1.00	37.6 ± 0.5	95.2 ± 1.3	858 ± 2	1.06 ± 0.02	6.84 ± 0.10	1.55 ± 0.02	66 ± 2	443 ± 2	29.3 ± 0.6
343.5	1.20	36.9 ± 0.7	189 ± 4	769 ± 4	1.18 ± 0.04	2.85 ± 0.06	0.662 ± 0.011	32.4 ± 1.1	576 ± 4	18.7 ± 0.6
345.5	1.03	41.1 ± 0.5	159 ± 2	792 ± 2	1.27 ± 0.03	5.50 ± 0.08	1.278 ± 0.013	35.1 ± 0.8	540 ± 2	19.0 ± 0.4
353.9	2.01	23.8 ± 0.3	437 ± 4	536 ± 4	0.87 ± 0.02	1.79 ± 0.02	0.402 ± 0.004	17.2 ± 0.3	816 ± 2	14.1 ± 0.2
354.1	1.00	65.2 ± 0.8	128 ± 2	793 ± 2	1.38 ± 0.03	10.0 ± 0.2	2.49 ± 0.03	27.6 ± 0.6	499 ± 2	13.8 ± 0.3

Table A6 Experimental conditions and reactants conversion at the final reaction time for the study on the ETBE synthesis byproducts formation (Chapter 4). Catalyst load = 10%wt., $d_p = 0.25\text{-}0.40$ mm, 500 rpm

Catalyst	T [K]	$R_{A/O}^o$ ^a	X_{IB} ^b [%]	X_{EtOH} ^b [%]	
A-35	323	0.5	88	93	
		1.0	90	90	
		2.0	97	47	
	343	0.5		94	88
				82	75
				79	87
		1.0		78	83
				82	82
				92	46
	2.0		91	44	
			91	45	
			83	74	
	363	0.5		84	70
				76	73
		1.0		75	72
			74	71	
2.0			86	64	
			90	92	
383	0.5		89	92	
			89	92	
			90	94	
	1.0		74	71	
			73	53	
			72	52	
2.0		72	53		
		72	53		
		78	75		
CT-275	363	0.5	78	75	
	383	0.5	75	50	
		1.0	85	87	

^a $R_{A/O}^o$ is here referred to nominal initial alcohol/isobutene molar ratio. ^b Conversion values at the final reaction time (t = 300 min)

Table A7 Experimental conditions and initial reaction rates for the synthesis of PTBE using 0.25-0.40 mm A-35 particles as catalyst (Chapter 8)

Setup	Isobutene source ^a	T [K]	$R_{A/O}^{\circ}$ ^b	Initial reaction rate, r° [mol (g _{cat} h) ⁻¹] ^c		
				PTBE	1-PrOH	IB
Batch reactor	IB	320	1.0	0.61	-0.48	-0.62
		321	1.0	0.76	-0.84	-0.76
		323	2.0	0.52	-0.44	-0.53
		326	1.1	1.15	-0.96	-1.57
		326	1.0	1.23	-1.11	-1.51
		334	1.0	2.59	-2.77	-2.10
		334	1.0	1.96	-2.05	-1.97
		344	1.0	3.83	-3.90	-3.86
		352	2.0	3.23	-2.79	-4.37
		352	1.0	6.05	-6.20	-6.18
Fixed-bed reactor	IB	303	1.0			-0.10
		313	1.0			-0.29
		323	1.0			-0.64
	C4	333	1.0			-0.52
		333	1.0			-0.54

^a IB: pure isobutene; C4: C₄ mixture. ^b $R_{A/O}^{\circ}$ is referred to the initial alcohol to isobutene molar ratio for the experiments carried out in the batch reactor and to the fed molar ratio for the fixed-bed reactor. ^c r° was calculated either as reaction rate at t_0 for the experiments carried out in the batch reactor or as the steady-state reaction rate under differential regime for the fixed-bed reactor

Table A8 Experimental conditions and initial reaction rates for the synthesis of BTBE using 0.25-0.40 mm A-35 particles as catalyst (Chapter 8)

Setup	Isobutene source ^a	T [K]	$R_{A/O}^{\circ}$ ^b	Initial reaction rate, r° [mol (g _{cat} h) ⁻¹] ^c			Observations
				BTBE	1-BuOH	IB	
Batch reactor	IB	317	1.0	0.89	-0.61	-0.72	
		318	1.0	1.01	-0.83	-1.10	
		323	1.0	1.61	-1.33	-1.60	
		333	1.0	3.17	-2.00	-3.79	Mass-transfer limitations detected
		334	1.0	3.19	-3.68	-2.08	Mass-transfer limitations detected
		343	1.2	5.41	-3.80	-5.62	Mass-transfer limitations detected
		345	1.0	4.48	-2.73	-5.24	Mass-transfer limitations detected
		354	2.0	2.06	-1.88	-2.70	Mass-transfer limitations detected
		354	1.0	5.23	-6.52	-4.61	Mass-transfer limitations detected
		Fixed-bed reactor	IB	303	1.0		
313	1.0					-0.67	
313	1.0					-0.68	
323	1.0					-1.64	
C4	333		1.0			-1.14	
		333	1.0			-1.01	
		333	1.0			-1.23	

^a IB: pure isobutene; C4: C₄ mixture. ^b $R_{A/O}^{\circ}$ is referred to the initial alcohol to isobutene molar ratio for the experiments carried out in the batch reactor and to the fed molar ratio for the fixed-bed reactor. ^c r° was calculated either as reaction rate at t_0 for the experiments carried out in the batch reactor or as the steady-state reaction rate under differential regime for the fixed-bed reactor

Table A9 Experimental conditions and initial reaction rates for the simultaneous syntheses of ETBE and BTBE using A-35 as catalyst (Chapter 8)

T [K]	$R_{A/O}^o$ ^a	$R_{E/B}^o$ ^b	Initial reaction rate, r^o [mol (g _{cat} h) ⁻¹]				Observations ^c
			ETBE	BTBE	EtOH	1-BuOH	
315	1.0	1.0	0.21	0.05	-0.22	-0.06	
323	1.0	1.0	0.55	0.19	-0.65	-0.17	
333	1.0	1.0	1.25	0.55	-1.49	-0.63	
333	1.0	1.0	1.29	0.53	-1.34	-0.48	
333	1.0	1.0	0.99	0.43	-1.14	-0.43	
333	1.0	0.5	1.03	1.01	-1.03	-0.89	
333	1.0	2.0	1.01	0.19	-0.90	-0.21	
333	2.0	1.0	0.57	0.14	-0.45	-0.07	
333	0.5	1.0	1.79	1.15	-1.78	-1.29	
343	1.0	1.0	2.30	1.00	-2.68	-1.06	
353	1.0	1.0	3.29	1.56	-3.37	-1.56	Mass-transfer limitations detected
354	1.0	1.0	3.35	1.62	-3.29	-1.45	Mass-transfer limitations detected
352	1.0	1.0	4.90	1.85	-4.96	-1.77	$d_p = 0.08-0.16$ mm

^a $R_{A/O}^o$: initial alcohol to isobutene molar ratio. ^b $R_{E/B}^o$: initial ethanol to 1-butanol molar ratio.

^c Catalyst particle diameter range (d_p) was 0.25-0.40 mm unless indicated otherwise.

Table A10 Possible forms of the adsorption term in kinetic expressions for the simultaneous syntheses of ETBE and BTBE (Chapter 8)

no.	Adsorption term	no.	Adsorption term
1	$a_{IB}^{n_i}$	29	1
2	$(a_{IB} + K_{EiOH} a_{EiOH})^{n_i}$	30	$(1 + K_{IB} a_{IB})^{n_i}$
3	$(a_{IB} + K_{BuOH} a_{BuOH})^{n_i}$	31	$(1 + K_{IB} a_{IB} + K_{EiOH} a_{EiOH})^{n_i}$
4	$(a_{IB} + K_{EiOH} a_{EiOH} + K_{BuOH} a_{BuOH})^{n_i}$	32	$(1 + K_{IB} a_{IB} + K_{BuOH} a_{BuOH})^{n_i}$
5	$(a_{IB} + K_{ETBE} a_{ETBE})^{n_i}$	33	$(1 + K_{IB} a_{IB} + K_{EiOH} a_{EiOH} + K_{BuOH} a_{BuOH})^{n_i}$
6	$(a_{IB} + K_{EiOH} a_{EiOH} + K_{ETBE} a_{ETBE})^{n_i}$	34	$(1 + K_{IB} a_{IB} + K_{ETBE} a_{ETBE})^{n_i}$
7	$(a_{IB} + K_{BuOH} a_{BuOH} + K_{ETBE} a_{ETBE})^{n_i}$	35	$(1 + K_{IB} a_{IB} + K_{EiOH} a_{EiOH} + K_{ETBE} a_{ETBE})^{n_i}$
8	$(a_{IB} + K_{EiOH} a_{EiOH} + K_{BuOH} a_{BuOH} + K_{ETBE} a_{ETBE})^{n_i}$	36	$(1 + K_{IB} a_{IB} + K_{BuOH} a_{BuOH} + K_{ETBE} a_{ETBE})^{n_i}$
9	$(a_{IB} + K_{BTBE} a_{BTBE})^{n_i}$	37	$(1 + K_{IB} a_{IB} + K_{EiOH} a_{EiOH} + K_{BuOH} a_{BuOH} + K_{ETBE} a_{ETBE})^{n_i}$
10	$(a_{IB} + K_{EiOH} a_{EiOH} + K_{BTBE} a_{BTBE})^{n_i}$	38	$(1 + K_{IB} a_{IB} + K_{BTBE} a_{BTBE})^{n_i}$
11	$(a_{IB} + K_{BuOH} a_{BuOH} + K_{BTBE} a_{BTBE})^{n_i}$	39	$(1 + K_{IB} a_{IB} + K_{EiOH} a_{EiOH} + K_{BTBE} a_{BTBE})^{n_i}$
12	$(a_{IB} + K_{EiOH} a_{EiOH} + K_{BuOH} a_{BuOH} + K_{BTBE} a_{BTBE})^{n_i}$	40	$(1 + K_{IB} a_{IB} + K_{BuOH} a_{BuOH} + K_{BTBE} a_{BTBE})^{n_i}$
13	$(a_{IB} + K_{ETBE} a_{ETBE} + K_{BTBE} a_{BTBE})^{n_i}$	41	$(1 + K_{IB} a_{IB} + K_{EiOH} a_{EiOH} + K_{BuOH} a_{BuOH} + K_{BTBE} a_{BTBE})^{n_i}$
14	$(a_{IB} + K_{EiOH} a_{EiOH} + K_{ETBE} a_{ETBE} + K_{BTBE} a_{BTBE})^{n_i}$	42	$(1 + K_{IB} a_{IB} + K_{ETBE} a_{ETBE} + K_{BTBE} a_{BTBE})^{n_i}$
15	$(a_{IB} + K_{BuOH} a_{BuOH} + K_{ETBE} a_{ETBE} + K_{BTBE} a_{BTBE})^{n_i}$	43	$(1 + K_{IB} a_{IB} + K_{EiOH} a_{EiOH} + K_{ETBE} a_{ETBE} + K_{BTBE} a_{BTBE})^{n_i}$
16	$(a_{IB} + K_{EiOH} a_{EiOH} + K_{BuOH} a_{BuOH} + K_{ETBE} a_{ETBE} + K_{BTBE} a_{BTBE})^{n_i}$	44	$(1 + K_{IB} a_{IB} + K_{BuOH} a_{BuOH} + K_{ETBE} a_{ETBE} + K_{BTBE} a_{BTBE})^{n_i}$
17	$a_{EiOH}^{n_i}$	45	$(1 + K_{IB} a_{IB} + K_{EiOH} a_{EiOH} + K_{BuOH} a_{BuOH} + K_{ETBE} a_{ETBE} + K_{BTBE} a_{BTBE})^{n_i}$
18	$(a_{EiOH} + K_{BuOH} a_{BuOH})^{n_i}$	46	$(1 + K_{EiOH} a_{EiOH})^{n_i}$
19	$(a_{EiOH} + K_{ETBE} a_{ETBE})^{n_i}$	47	$(1 + K_{EiOH} a_{EiOH} + K_{BuOH} a_{BuOH})^{n_i}$
20	$(a_{EiOH} + K_{BuOH} a_{BuOH} + K_{ETBE} a_{ETBE})^{n_i}$	48	$(1 + K_{EiOH} a_{EiOH} + K_{ETBE} a_{ETBE})^{n_i}$
21	$(a_{EiOH} + K_{BTBE} a_{BTBE})^{n_i}$	49	$(1 + K_{EiOH} a_{EiOH} + K_{BuOH} a_{BuOH} + K_{ETBE} a_{ETBE})^{n_i}$
22	$(a_{EiOH} + K_{BuOH} a_{BuOH} + K_{BTBE} a_{BTBE})^{n_i}$	50	$(1 + K_{EiOH} a_{EiOH} + K_{BTBE} a_{BTBE})^{n_i}$
23	$(a_{EiOH} + K_{ETBE} a_{ETBE} + K_{BTBE} a_{BTBE})^{n_i}$	51	$(1 + K_{EiOH} a_{EiOH} + K_{BuOH} a_{BuOH} + K_{BTBE} a_{BTBE})^{n_i}$
24	$(a_{EiOH} + K_{BuOH} a_{BuOH} + K_{ETBE} a_{ETBE} + K_{BTBE} a_{BTBE})^{n_i}$	52	$(1 + K_{EiOH} a_{EiOH} + K_{ETBE} a_{ETBE} + K_{BTBE} a_{BTBE})^{n_i}$
25	$a_{BuOH}^{n_i}$	53	$(1 + K_{EiOH} a_{EiOH} + K_{BuOH} a_{BuOH} + K_{ETBE} a_{ETBE} + K_{BTBE} a_{BTBE})^{n_i}$
26	$(a_{BuOH} + K_{ETBE} a_{ETBE})^{n_i}$	54	$(1 + K_{BuOH} a_{BuOH})^{n_i}$
27	$(a_{BuOH} + K_{BTBE} a_{BTBE})^{n_i}$	55	$(1 + K_{BuOH} a_{BuOH} + K_{ETBE} a_{ETBE})^{n_i}$
28	$(a_{BuOH} + K_{ETBE} a_{ETBE} + K_{BTBE} a_{BTBE})^{n_i}$	56	$(1 + K_{BuOH} a_{BuOH} + K_{BTBE} a_{BTBE})^{n_i}$
		57	$(1 + K_{BuOH} a_{BuOH} + K_{ETBE} a_{ETBE} + K_{BTBE} a_{BTBE})^{n_i}$

Appendix II Estimation methods

A general description of the methods used through this PhD thesis to estimate properties is provided in this section.

- Joback method for the estimation of various properties

The Joback method allows estimating several properties considering the contributions of certain groups within a molecule to the particular property [89]. Critical properties (temperature, pressure, and volume) and enthalpy change of formation and have been estimated by Joback method. The following equations were used for that purpose:

$$\text{Critical temperature: } T_C = T_b \left[0.584 + 0.965 \left(\sum_k N_k (tck) \right) - \left(\sum_k N_k (tck) \right)^2 \right]^{-1} \quad (\text{A1})$$

$$\text{Critical pressure: } P_C = \left[0.113 + 0.0032 N_{atoms} - \sum_k N_k (pck) \right]^{-1} \quad (\text{A2})$$

$$\text{Critical volume: } V_C = 17.5 + \sum_k N_k (vck) \quad (\text{A3})$$

$$\text{Enthalpy change of formation: } \Delta H_f^\circ (298 \text{ K}) = 68.29 + \sum_k N_k (hfk) \quad (\text{A4})$$

where N_k is the number of groups of the type k in the molecule, and tck , pck , vck , and hfk are the contributions for the group labeled k to the corresponding estimated property. N_{atoms} , in Equation A2, is the number of atoms in the considered molecule. Values used in this thesis are listed in Table A11.

Table A11 Joback group contributions for different properties [89]

Group	tck [K]	pck [bar]	vck [cm ³ mol ⁻¹]	hfk [kJ mol ⁻¹]
-CH ₃	0.0141	-0.0012	65	-76.45
-CH ₂	0.0189	0.000	56	-20.64
-C	0.0067	0.0043	27	82.23
-OH	0.0741	0.0112	28	-208.04
-O	0.0168	0.0015	18	-132.22

In the case of the enthalpy change of formation, it is important to notice that the value given by Equation A4 is referred to gas-phase. To obtain liquid-phase enthalpy changes of formation, the enthalpy of vaporization at 298 K (estimated by the Watson method) was subtracted from the value obtained with Equation A4.

- Modified Benson method for the estimation of the enthalpy change and entropy of formation

Liquid-phase enthalpy change and entropy of formation can be estimated by a group-contribution method similar to the previous one, using Equations A5 and A6, respectively, as follows:

$$\Delta H_f^\circ(298\text{ K}) = \sum_k n_k \Delta H_{fk}^\circ \quad (\text{A5})$$

$$S^\circ(298\text{ K}) = \sum_k n_k S_k^\circ \quad (\text{A6})$$

where n_k is the number of the k groups of in the molecule, and $\Delta_f H_k^\circ$ and S_k° are the contribution for the group labeled k to the enthalpy and entropy changes of formation, respectively. Used values are listed in Table A12.

Table A12 Modified Benson method group contributions for enthalpy and entropy changes of formation [91]

Group	$\Delta_f H_{j, \text{LIQ}}^\circ$ [kJ mol ⁻¹]	$S_{j, \text{LIQ}}^\circ$ [J (mol K) ⁻¹]
C-(H) ₃ (C)	-47.61	83.3
C-(H) ₂ (C) ₂	-25.73	32.38
-CH ₃ corr. (tertiary)	-2.18	
C _d -(H) ₂	21.75	86.19
C _d -(C) ₂	39.16	-29.83
C-(H) ₂ (O) (C)	-35.8	32.59
C-(O) (C) ₃ ether	0.79	-94.68
O-(H) (C)	-191.5	43.89
O-(C) ₂	-110.83	26.78

- Missenard method for the estimation of molar heat capacity

This method, which is also a group-contribution method, can only be applied to molecules without double bonds (hence excluding isobutene). By using the following expression, liquid-phase molar heat capacity at a given temperature can be estimated:

$$C_{PL}(T) = \sum_k n_k (C_{PL}(T))_k \quad (\text{A7})$$

where n_k is the number of the k groups of in the molecule, and $(C_{PL}(T))_k$ is the contribution to the molar heat capacity for the group k at the temperature T . Used values are listed in Table A13.

Table A13 Missenard method group contributions for molar heat capacity [88]

Group	$(C_{PL}(T))_k [\text{J (mol K)}^{-1}]$					
	Temperature [K]					
	248	273	298	323	348	373
CH ₃ -	38.5	40	41.6	43.5	45.8	48.3
-CH ₂ -	27.2	28	28.2	29.1	29.9	31
-C-	8.4	8.4	8.4	8.4	8.4	8.4
OH	27.2	34	43.9	52.3	61.7	71.1
-O-	28.9	29	29.7	30.1	30.5	31

- Růžicka-Domalski method for the estimation of molar heat capacity

This group-contribution method can be used to estimate liquid-phase molar heat capacities from the melting point to the boiling point, by using the following expressions [89]:

$$C_{PL} = R \left[A + B \frac{T}{100} + D \left(\frac{T}{100} \right)^2 \right] \quad (\text{A8})$$

where R is the gas constant in J (mol K)^{-1} and T is the temperature in K. Parameters A , B , and D are calculated as:

$$A = \sum_k n_k a_k \quad B = \sum_k n_k b_k \quad D = \sum_k n_k d_k \quad (\text{A9})$$

where n_k is the number of the k groups, and a_k , b_k , and d_k are tabulated coefficients that account for the contribution of the group k to the molar heat capacity. Used values are listed in Table A14.

Table A14 Růžicka-Domalski method group contributions for molar heat capacity [89]

Group	a_i	b_i	d_i
C—(3H,C)	3.8452	-0.33997	0.19489
C—(2H,2C)	2.7972	-0.05497	0.10679
=C—(2C)	1.957	-0.31938	0.11911
=C—(2H)	4.1763	-0.47392	0.099928
C—(3C,O) (ether, ester)	-3.3182	2.6317	-0.44354
C—(3H,C=) \equiv C—(3H,C)	3.8452	-0.33997	0.19489
C—(3H,O) \equiv C—(3H,C)	3.8452	-0.33997	0.19489
C—(2H,C,O)	1.4596	1.4657	-0.2714
O—(2C)	5.0312	-1.5718	0.3786
O—(H,C)	12.952	-10.145	2.6261

- Modified Watson equation for the estimation of the enthalpy of vaporization

The following expression was used to estimate the enthalpy of vaporization, ΔH_{vap} , of the studied compounds [172]:

$$\Delta H_{vap} = A \left(1 - \frac{T}{T_C} \right)^n \quad (\text{A10})$$

where A and n are tabulated coefficients for each compound, T is the temperature in K, and T_C is the critical temperature. Used values are listed in Table A15 along with the CAS registry number for each involved compound.

Table A15 Coefficients for the modified Benson equation [172]

Compound	CAS no	A	n	T_C
isobutene	115-11-7	32.9500	0.3890	417.90
isobutane	75-28-5	31.9538	0.3920	408.14
<i>trans</i> -2-butene	624-64-6	33.2000	0.3640	428.63
<i>cis</i> -2-butene	590-18-1	34.4904	0.3830	435.58
methanol	67-56-1	52.7227	0.3770	512.58
ethanol	64-17-5	60.8036	0.3800	513.92
1-propanol	71-23-8	70.1792	0.4510	536.78
1-butanol	71-36-3	63.0242	0.3180	563.05
methyl <i>tert</i> -butyl ether	1634-04-4	45.0276	0.4340	497.10
ethyl <i>tert</i> -butyl ether	637-92-3	44.6175	0.3800	516.67
propyl <i>tert</i> -butyl ether	29072-93-3	45.9484	0.3800	558.21
butyl <i>tert</i> -butyl ether	1000-63-1	-	-	-
<i>tert</i> -butyl alcohol	75-65-0	77.3200	0.5650	506.21
2,4,4-trimethyl-1-pentene	107-39-1	48.9377	0.4040	553.00
2,4,4-trimethyl-2-pentene	107-40-4	52.7700	0.4440	558.00

As seen in Table A15, no data was found regarding the estimation of the enthalpy of vaporization for butyl *tert*-butyl ether by means of the present method. For this reason, the following expression, also based on the modified Benson equation, was used instead for this compound [19]:

$$\Delta H_{vap} = \Delta H_{vap}^{T_b} \left(\frac{1 - T/T_C}{1 - T_b/T_C} \right)^{0.375} \quad (\text{A11})$$

where $\Delta H_{vap}^{T_b}$ is the enthalpy of vaporization at the boiling temperature ($T_b = 397$ K) and T_C is the critical temperature ($T_C = 576.1$ K).

The value of $\Delta H_{vap}^{T_b}$, was estimated by the Pitzer corresponding-states correlation, expressed as [89]:

$$\frac{\Delta H_{\text{vap}}}{RT_C} = 7.08(1 - T_r)^{0.354} + 10.95\omega(1 - T_r)^{0.456} \quad (\text{A12})$$

where T_r is the reduced temperature (T/T_C) and ω is the acentric factor ($\omega = 0.380$). The acentric factor at $T_r = 0.7$ is calculated with the reduced vapor pressure, P_{vr} (estimated by the method of Gómez-Thodos), as [88]:

$$\omega = -\ln P_{vr} - 1 \quad (\text{A13})$$

- Method of Gómez-Thodos for the estimation of the reduced vapor pressure

The following relations were used to estimate the reduced vapor pressure, P_{vr} [88]:

$$\ln P_{vr} = \beta \left(\frac{1}{T_r^m - 1} \right) + \gamma (T_r^7 - 1) \quad (\text{A14})$$

$$\gamma = ah + b\beta \quad (\text{A15})$$

$$a = \frac{1 - 1/T_{br}}{T_{br}^7 - 1} \quad (\text{A16})$$

$$b = \frac{1 - 1/T_{br}^7}{T_{br}^7 - 1} \quad (\text{A17})$$

$$h = T_{br} \frac{\ln(P_C/1.01325)}{1 - T_{br}} \quad (\text{A18})$$

where P_{vr} , T_r , T_{br} are reduced vapor pressure, reduced temperature and reduced boiling temperature, respectively. At this point, the procedure by which β , γ , and m depends on the type of the considered compound. Compounds are divided into three categories: nonpolar, polar and hydrogen-bonded compounds. For nonpolar compounds (e.g., olefins and ethers), the following equations are used:

$$\beta = -4.26700 - \frac{221.79}{h^{2.5} \exp(0.0384h^{2.5})} + \frac{3.8126}{\exp(2272.44/h^3)} + \Delta^* \quad (\text{A19})$$

$$m = 0.78425 \exp(0.089315h) - \frac{8.5217}{\exp(0.74826h)} \quad (\text{A20})$$

where Δ^* equals zero, except for Hydrogen and Helium, and γ is calculated by Equation A15. For polar compounds other than water and alcohol, the following equations are used:

$$m = 0.466 T_C^{0.166} \quad (\text{A21})$$

$$\gamma = 0.08594 \exp(7.462 \times 10^{-4} T_C) \quad (\text{A22})$$

And for water and alcohols:

$$m = 0.0052 M^{0.29} T_C^{0.72} \quad (\text{A23})$$

$$\gamma = \frac{2.464}{M} \exp(9.8 \times 10^{-6} M T_C) \quad (\text{A24})$$

where M is the molar weight. For these two categories, β is calculated as:

$$\beta = \frac{\gamma}{b} - \frac{ah}{b} \quad (\text{A25})$$

- Estimation of vapor pressure as indicated in the Reid's Property Data Bank [88]:

For each tabulated compound, this method allows estimating the vapor pressure by means of three different equations:

$$\ln(P_v/P_C) = (1-x)^{-1} [(VPA)x + (VPC)x^{1.5} + (VPC)x^3 + (VPD)x^5] \quad (\text{A26})$$

$$x = 1 - T/T_C$$

$$\ln P_v = VPA - VPB/T + (VPC) \ln T + (VPD) P_v/T^2 \quad (\text{A27})$$

$$\ln P_v = VPA - VPB/(T + VPC) \quad (\text{A28})$$

where VPA , VPB , VPC , and VPD are tabulated coefficients (Table A16).

Table A16 Coefficients for the estimation of vapor pressure [88]

Compound	Eq.	VPA	VPB	VPC	VPD
isobutene	A26	-6.95542	1.35673	-2.4522	-1.4611
isobutane	A26	-6.95579	1.5009	-2.52717	-1.49776
<i>trans</i> -2-butene	A27	43.517	4174.56	-5.041	1995.0
<i>cis</i> -2-butene	A26	-6.88706	1.15941	-2.19304	-3.12758
methanol	A26	-8.54796	0.76982	-3.1085	1.54481
ethanol	A26	-8.51838	0.34163	-5.73683	8.32581
1-propanol	A26	-8.05594	0.0425183	-7.51296	6.89004
1-butanol	A26	-8.00756	0.53783	-9.3424	6.68692
methyl <i>tert</i> -butyl ether	A26	-7.82516	2.95493	-6.94079	12.17416
<i>tert</i> -butyl alcohol	A28	10.2346	2658.29	-95.50	

- Hankinson-Brobst-Thomson (HBT) method for the estimation of molar volume

Estimation of the molar volume, V , through the Hankinson-Brobst-Thomson (HBT) method can be accomplished by the following expressions [88,89]:

$$V = V_S \left(1 - c \ln \frac{\beta + P}{\beta + P_v} \right) \quad (\text{A30})$$

$$\beta/P_C = -1 + a(1-T_r)^{1/3} + b(1-T_r)^{2/3} + c(1-T_r) + d(1-T_r)^{4/3} \quad (\text{A31})$$

where:

$$\begin{aligned} a &= -9.070217 & b &= 62.45326 \\ c &= j + k\omega_{SRK} & d &= -135.1102 \\ e &= \exp(f + g\omega_{SRK} + h\omega_{SRK}^2) & f &= 4.79594 \\ g &= 0.250047 & h &= 1.14188 \\ j &= 0.0861488 & k &= 0.034483 \end{aligned}$$

in which V_S is the saturated liquid volume at the vapor pressure, P_v . The value of ω_{SRK} is the acentric factor that causes the Soave equation of state to give the best fit to pure component vapor pressures. It can be found as a tabulated value for several compounds [88]. When ω_{SRK} is unavailable, values of ω , calculated by Equation A13, can be used instead.

Values of V_S can be obtained through the following relations [173]:

$$V_S = V^* V^{(0)} \left[1 - \omega_{SRK} V^{(\delta)} \right] \quad (\text{A32})$$

$$V^{(0)} = 1 + a(1-T_r)^{1/3} + b(1-T_r)^{2/3} + c(1-T_r) + d(1-T_r)^{4/3} \quad (\text{A33})$$

$$V^{(\delta)} = \frac{e + fT_r + gT_r^2 + hT_r^3}{T_r - 1.00001} \quad (\text{A34})$$

where:

$$\begin{aligned} a &= -1.52816 & b &= 1.43907 & c &= -0.81446 \\ d &= 0.190454 & e &= -0.296123 & f &= 0.386914 \\ g &= -0.296123 & h &= -0.0480645 \end{aligned}$$

Equation A32 can be used in the range $0.25 < T_r < 0.95$, and Equation A33 in the range $0.25 < T_r < 1.0$. Values of V^* are tabulated parameters, which are close to the critical volume. Thus, when V^* is not available, V_C can be used instead. Values of P_v were preferentially estimated as indicated in the Reid's Property Data Bank [88] or, when unavailable, through estimation of P_{vr} by the method of Gómez-Thodos.

- Estimation of liquid mixtures molar volume

The following equations are the recommended mixing rules for the HBT method [88]:

$$T_{Cm} = \frac{\sum_i \sum_j x_i x_j V_{ij}^* T_{Cij}}{V_m^*} \quad (\text{A35})$$

$$V_m^* = \frac{1}{4} \left[\sum_i x_i V_i^* + 3 \left(\sum_i x_i V_i^{*2/3} \right) \left(\sum_i x_i V_i^{*1/3} \right) \right] \quad (\text{A36})$$

$$V_{ij}^* T_{Cij} = (V_i^* T_{Ci} V_j^* T_{Cj})^{1/2} \quad (\text{A37})$$

$$\omega_{SRKm} = \sum_i x_i \omega_{SRKi} \quad (\text{A38})$$

$$P_{Cm} = \frac{(0.291 - 0.080 \omega_{SRKm}) RT_{Cm}}{V_m^*} \quad (\text{A39})$$

where x_i and x_j are molar fractions of the compounds i and j , respectively. The subindex m in Equations A35 to A39 indicates that the corresponding property is referred to that of the mixture. Likewise, P_v in Equation A30, should be substituted by P_{vm} , which is calculated as follows [88]:

$$P_{vm} = P_{Cm} P_{rm} \quad (\text{A40})$$

$$\log_{10} P_{rm} = P_{rm}^{(0)} + \omega_{SRKm} P_{rm}^{(1)} \quad (\text{A41})$$

$$P_{rm}^{(0)} = 5.8031817 \log_{10} T_{rm} + 0.07608141 \alpha \quad (\text{A42})$$

$$P_{rm}^{(1)} = 4.86601 (\log_{10} T_{rm} + 0.03721754 \alpha) \quad (\text{A43})$$

$$\alpha = 35.0 - \frac{36.0}{T_{rm}} - 96.736 \log_{10} T_{rm} + T_{rm}^6 \quad (\text{A44})$$

$$T_{rm} = \frac{T}{T_{Cm}} \quad (\text{A45})$$

- Hildebrand solubility parameter for individual compounds

The Hildebrand solubility parameter for liquid-phase individual compounds, δ_j , at a given temperature, T , can be estimated by the following equation:

$$\delta_j = \sqrt{\frac{\Delta H_{vap,j} - RT}{V_j}} \quad (\text{A46})$$

where $\Delta H_{vap,j}$ is the enthalpy of vaporization of the compound j and V_j is its molar volume at a given temperature and pressure.

- Hildebrand solubility parameter for liquid mixtures

The Hildebrand solubility parameter for liquid-phase mixtures, δ_m , can be calculated as follows:

$$\delta_m = \sum_j \Phi_j \delta_j \quad (\text{A47})$$

where Φ_j is the volume fraction of the compound j . If additive volumes are considered, volume fractions can be calculated as:

$$\Phi_j = \frac{x_j \frac{M_j}{\rho_j}}{\sum_k x_k \frac{M_k}{\rho_k}} \quad (\text{A48})$$

- Hildebrand solubility parameter for solids

The Hildebrand solubility parameters at 298 K of some of the ion-exchange resins used in this work were estimated by means of a group-contribution method, by using the following equation [149]:

$$\delta_p = \sqrt{\frac{\sum_i x_i E_{coh,i}}{\sum_i x_i V_i}} \quad (\text{A49})$$

where x_i corresponds to the molar fraction of the structural group i , and $E_{coh,i}$ and V_i to the contributions to cohesion energy and to molar volume, respectively, of the structural group i . The different structural groups that were used, along with their corresponding $E_{coh,i}$ and V_i are listed in Table A17.

Table A17 Cohesion energy and molar volume contributions [149]

Structural group	E_{coh} [cal mol ⁻¹]	V [cm ³ mol ⁻¹]
>CH-	820	-1
-CH ₂ -	1180	16.1
-C ₆ H ₅ -	7630	71.4
-C ₆ H ₄ -	7630	52.4
-C ₆ H ₃ -	7630	33.4
-SO ₃ H	4500	27.6
-Cl	2760	24

In order to compute molar fractions of each structural group, divinylbenzene (DVB) contents for each resin were considered as: 7%wt. for low cross-linked resins, 12%wt. for medium cross-linked resins, and 20%wt. for high cross-linked resins. These weight

percentages are referred to the amount of DVB in the monomer mixture. This simplification was done because the actual amount of DVB in most commercial resins is usually unavailable. Then, molar fractions were calculated through mass fractions, which can be obtained by the following relations:

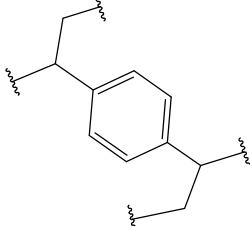
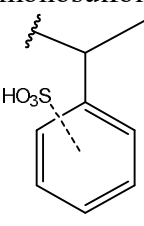
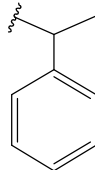
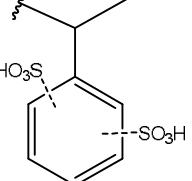
$$\%DVB = \frac{x_{DVB}}{x_{ST} + x_{DVB}} \quad (A50)$$

$$I = x_{SO_3H} + x_{ST} + x_{DVB} + x_{Cl} \quad (A51)$$

where $\%DVB$ is expressed as a fraction of unity and x_i are mass fractions. The subindexes DVB , ST , SO_3H , and Cl are referred to divinylbenzene, styrene, sulfonic groups, and chlorine, respectively. Values of x_{Cl} and x_{SO_3H} should be experimentally determined, e.g., by elemental analysis and titration against standard base.

At this point, when considering the different degrees of sulfonation that the used resins present, a distinction has to be made between non-sulfonated styrene rings (for partially sulfonated resins only), monosulfonated styrene rings, and bisulfonated styrene rings (for oversulfonated resins only). For the sake of clarity, Table A18 lists the number and type of structural groups within DVB and styrene other than sulfonic groups or chlorine atoms.

Table A18 Considered structural groups for the resins constituents

Constituent	Number	Structural group	Constituent	Number	Structural group
	2	>CH-	ST, monosulfonated 	1	>CH-
	2	-CH ₂ -		1	-CH ₂ -
	1	-C ₆ H ₄ -		1	-C ₆ H ₄ -
ST, non-sulfonated 	1	>CH-	ST, bisulfonated 	1	>CH-
	1	-CH ₂ -		1	-CH ₂ -
	1	-C ₆ H ₅ -		1	-C ₆ H ₃ -

- Estimation of molecular length

To estimate molecular lengths, distances and angles between atoms in molecules at their minimum energy conformation must be retrieved. For that purpose, ChemBio3D, which is included in the ChemBioOffice Suite software, was used. Among other features, this software allows obtaining such information. As example, Figure A1 is provided in

which a molecule of ethanol is depicted. Listed in Table A19 are the bond distances and angles for the ethanol molecule.

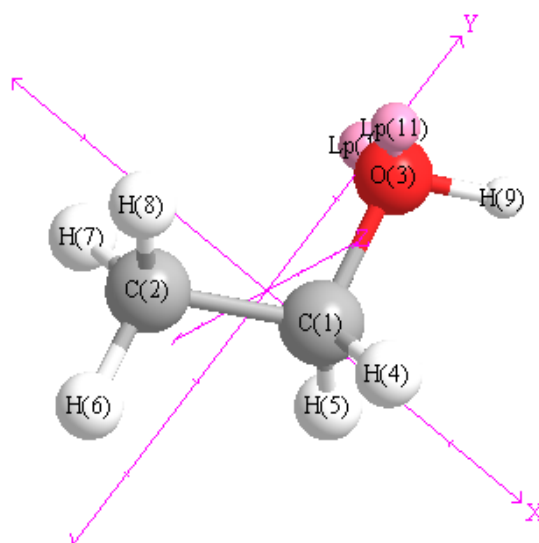


Figure A1 Molecule of ethanol

Table A19 Distances and angles between atoms in a molecule of ethanol

Atoms	Distance [Å]	Angle [rad]
O(3)-H(9)	0.961	
C(2)-H(8)	1.113	
C(2)-H(7)	1.113	
C(2)-H(6)	1.113	
C(1)-H(5)	1.111	
C(1)-H(4)	1.111	
C(1)-O(3)	1.408	
C(1)-C(2)	1.514	
H(9)-O(3)-C(1)		1.88
H(8)-C(2)-H(7)		1.91
H(8)-C(2)-H(6)		1.91
H(8)-C(2)-C(1)		1.92
H(7)-C(2)-H(6)		1.90
H(7)-C(2)-C(1)		1.92
H(6)-C(2)-C(1)		1.91
H(5)-C(1)-H(4)		1.92
H(5)-C(1)-O(3)		1.89
H(5)-C(1)-C(2)		1.93
H(4)-C(1)-O(3)		1.89
H(4)-C(1)-C(2)		1.93
O(3)-C(1)-C(2)		1.89

From this information, lengths in the three dimensions can be calculated by trigonometric relations. For instance, in the z direction, the distance between atoms H(5) and H(4) is:

$$d_{H(4)-H(5)} = \left[d_{C(1)-H(4)}^2 + d_{C(1)-H(5)}^2 - 2d_{C(1)-H(4)}d_{C(1)-H(5)} \cos(\alpha_{H(5)-C(1)-H(4)}) \right]^{1/2} \quad (\text{A51})$$

where d and α are the corresponding distances and angles listed in Table A19. Thus, following the example, 1.8, 3.3, and 4.1 Å would be the maximum molecular lengths in the z, x, and y directions, respectively, for the ethanol molecule.

- Modified UNIFAC-Dortmund method for the estimation of activities

The modified UNIFAC-Dortmund method is a group-contribution model which allows the estimation of liquid-phase activity coefficients, γ_i , in nonelectrolyte systems, as a function of temperature and composition. The activity coefficient is calculated as the summation of a combinatorial part (γ_i^C), which represents the contribution of the excess entropy due to the different shapes and sizes of the considered molecules, and a residual part (γ_i^R), which represents the contribution of the excess enthalpy caused by energetic interactions between molecules, as follows [85]:

$$\gamma_i = \ln \gamma_i^C + \ln \gamma_i^R \quad (\text{A52})$$

The combinatorial part, which depends not on temperature, can be determined by means of the following relations [85]:

$$\ln \gamma_i^C = 1 - V_i' + \ln V_i' - 5q_i \left[1 - \frac{V_i}{F_i} + \ln \left(\frac{V_i}{F_i} \right) \right] \quad (\text{A53})$$

$$V_i' = \frac{r_i^{3/4}}{\sum_j x_j r_j^{3/4}} \quad V_i = \frac{r_i}{\sum_j x_j r_j} \quad F_i = \frac{q_i}{\sum_j x_j q_j} \quad (\text{A54})$$

$$r_i = \sum_k \nu_k^{(i)} R_k \quad q_i = \sum_k \nu_k^{(i)} Q_k \quad (\text{A55})$$

where r_i and q_i are the relative van der Waals volume and surface area, respectively, of the molecule i , and $\nu_k^{(i)}$ is number of structural groups of the type k in the molecule i . Values of r_i and q_i can be obtained from R_k and Q_k , which are tabulated parameters (Table A20), and represent the van der Waals volume and surface area, respectively, of the structural group k .

The residual part, which is temperature-dependent, can be determined by means of the following relations [85]:

$$\ln \gamma_i^R = \sum_k \nu_k^{(i)} \left(\ln \Gamma_k - \ln \Gamma_k^{(i)} \right) \quad (\text{A56})$$

$$\ln \Gamma_k = Q_k \left[1 - \ln \left(\sum_m \Theta_m \Psi_{mk} \right) - \sum_m \frac{\Theta_m \Psi_{km}}{\sum_n \Theta_n \Psi_{nm}} \right] \quad (\text{A57})$$

$$\Theta_m = \frac{Q_m X_m}{\sum_n Q_n X_n} \quad X_m = \frac{\sum_j v_m^{(j)} x_j}{\sum_j \sum_n v_m^{(j)} x_j} \quad (\text{A58})$$

$$\Psi_{nm} = \exp \left(-\frac{a_{nm} + b_{nm} T + c_{nm} T^2}{T} \right) \quad (\text{A59})$$

where Γ_k and $\Gamma_k^{(i)}$ are the activity coefficients of the group k in the mixture and in the pure compound i , respectively; Θ_m and X_m are the area fraction and the mole fraction, respectively, of the group m ; Ψ_{nm} is the group interaction parameter; and a_{nm} , b_{nm} , and c_{nm} are tabulated coefficients (Table A21).

Table A20 R_k and Q_k parameters and group assignment for the modified UNIFAC-Dortmund method [85]

Main group	Subgroup	no	R_k	Q_k
1 "CH ₂ "	CH ₃	1	0.6325	1.0608
	CH ₂	2	0.6325	0.7081
	CH	3	0.6325	0.3554
	C	4	0.6325	0.0000
2 "C=C"	CH=CH	6	1.2832	1.2489
	CH ₂ =CH	7	1.2832	1.2489
	CH=C	8	1.2832	0.8962
5 "OH"	OH (p)	14	1.2302	0.8927
	OH (t)	82	0.6895	0.8345
7 "H ₂ O"	H ₂ O	16	1.7334	2.4561
13 "CH ₂ O"	CH ₂ O	25	1.1434	1.2495

Table A21 Modified UNIFAC-Dortmund group interaction parameters [85]

Main group		a_{nm} [K]	b_{nm}	c_{nm} [K ⁻¹]	a_{mn} [K]	b_{mn}	c_{mn} [K ⁻¹]
n	m						
1	2	189.66	-0.2723	0.0	-95.418	0.6171×10^{-1}	0.0
1	5	2777.0	-4.6740	0.1551×10^{-2}	1606.0	-4.7460	0.9181×10^{-3}
1	7	1391.3	-3.6156	0.1144×10^{-2}	-17.253	0.8389	0.9021×10^{-3}
1	13	233.10	-0.3155	0.0	-9.6540	-0.3242×10^{-1}	0.0
2	5	2649.0	-6.5080	0.4822×10^{-2}	1566.0	-5.8090	0.5197×10^{-2}
2	7	778.30	0.1482	0.0	-1301.0	4.0720	0.0
2	13	733.30	-2.5090	0.0	-844.30	2.9450	0.0
5	7	-801.90	3.8240	-0.7514×10^{-2}	1460.0	-8.6730	0.1641×10^{-1}
5	13	1102.0	-7.1760	0.9698×10^{-2}	1631.0	-7.3620	0.1176×10^{-1}
7	13	-197.50	0.1766	0.0	140.70	0.5679×10^{-1}	0.0

Appendix III Estimated properties

In this section, some of the properties estimated by the methods described in the previous section are listed (especially the estimated values which are not explicitly provided in previous chapters). Comparison between values obtained by different methods and/or literature data is provided, when available.

Table A22 Comparison of thermochemical data at 298 K

Compound	Literature		Joback	Modified Benson	
	$\Delta_f H_{j,LIQ}^\circ$ ^a	$S_{j,LIQ}^\circ$ ^a	$\Delta_f H_{j,LIQ}^\circ$	$\Delta_f H_{j,LIQ}^\circ$	$S_{j,LIQ}^\circ$
isobutene	-37.50	215.4 ^b	-43.28	-38.67	223.0
methanol	-239.2	126.8	-254.2	-239.1	127.2
ethanol	-277.6	160.7	-280.6	-274.9	159.8
1-propanol	-302.6	193.6	-306.2	-300.6	192.2
1-butanol	-327.3	225.8	-327.7	-326.4	224.5
methyl <i>tert</i> -butyl ether	-313.6	265.3	-317.8	-307.0	265.3
ethyl <i>tert</i> -butyl ether	-349.9	297.9 ^c	-340.3	-342.8	297.9
propyl <i>tert</i> -butyl ether	-372.2 ^b	333.5 ^b	-363.2	-368.6	330.3
butyl <i>tert</i> -butyl ether	-403.3 ^c	-	-389.6	-394.3	362.7

^a Unless specified, values have been taken from [92]. ^b [22]. ^c [93]

Table A23 Comparison of molar heat capacities, C_p [J (mol K)⁻¹]

T [K]	methanol			ethanol			
	Literature ^a	Růžička-Domalski	Missenard	Literature ^a	Literature ^b	Růžička-Domalski	Missenard
298.15	80.7	88.2	84.7	113.5	114.2	116.7	112.9
303.15	82.1	90.9	86.9	116.0	116.7	119.3	115.3
313.15	85.5	96.7	91.4	121.6	121.8	124.8	120.1
323.15	89.5	102.9	96.1	127.8	127.2	130.8	125.1
333.15	93.9	109.6	100.8	134.2	132.9	137.2	130.1
343.15	98.4	116.7	105.5	140.7	138.9	144.1	135.2
353.15	102.8	124.3	110.2	146.9	145.3	151.3	140.3
363.15	106.8	132.4	114.8	152.7	151.9	159.0	145.4
373.15	110.4	140.9	119.4	157.8	158.9	167.1	150.3
383.15	113.1	150.0	123.8	162.0	166.2	175.7	155.2

^a [23]. ^b [105]

Table A24 Comparison of molar heat capacities, C_p [$J (mol K)^{-1}$]

T [K]	1-propanol		1-butanol	
	Růžička-Domalski	Missenard	Růžička-Domalski	Missenard
298.15	146.4	141.2	176.2	169.4
303.15	149.3	143.7	179.3	172.1
313.15	155.4	148.8	185.9	177.5
323.15	161.9	154.1	192.9	183.2
333.15	168.8	159.5	200.4	188.9
343.15	176.2	165.0	208.4	194.8
353.15	184.1	170.5	216.8	200.6
363.15	192.3	175.9	225.6	206.5
373.15	201.0	181.3	235.0	212.3
383.15	210.2	186.6	244.7	218.0

Table A25 Comparison of molar heat capacities, C_p [$J (mol K)^{-1}$]

T [K]	methyl <i>tert</i> -butyl ether			ethyl <i>tert</i> -butyl ether			
	Literature ^a	Růžička-Domalski	Missenard	Literature ^a	Literature ^b	Růžička-Domalski	Missenard
298.15	184.4	187.5	204.6	218.7	220.3	215.9	232.9
303.15	186.2	189.2	206.2	221.0	222.3	217.5	234.5
313.15	189.6	192.6	209.3	225.5	226.3	220.7	238.0
323.15	193.2	196.1	212.7	230.1	230.4	224.1	241.7
333.15	196.9	199.8	216.3	234.8	234.6	227.4	245.6
343.15	200.6	203.5	220.0	239.5	238.9	230.9	249.8
353.15	204.5	207.4	224.0	244.5	243.3	234.4	254.2
363.15	208.5	211.4	228.2	249.5	247.9	238.0	258.8
373.15	212.6	215.5	232.7	254.6	252.5	241.7	263.7
383.15	216.8	219.8	237.5	259.9	257.2	245.5	268.9

^a [23]. ^b [105]**Table A26** Comparison of molar heat capacities, C_p [$J (mol K)^{-1}$]

T [K]	propyl <i>tert</i> -butyl ether		butyl <i>tert</i> -butyl ether	
	Růžička-Domalski	Missenard	Růžička-Domalski	Missenard
298.15	245.7	261.1	275.5	289.3
303.15	247.5	262.9	277.6	291.3
313.15	251.3	266.7	281.8	295.4
323.15	255.1	270.8	286.2	299.8
333.15	259.0	275.0	290.6	304.4
343.15	263.0	279.6	295.2	309.3
353.15	267.2	284.3	299.9	314.5
363.15	271.4	289.4	304.7	320.0
373.15	275.6	294.7	309.6	325.7
383.15	280.0	300.3	314.6	331.7

Table A27 Boiling temperature, critical temperature, critical pressure, V^* , and ω_{SRK}

Compound	T_b^a [K]	T_c^a [K]	P_c^d [bar]	V^{*f} [L mol ⁻¹]	ω_{SRK}^f
isobutene	266.25	417.9	40.0	0.2369	0.196
isobutane	261.43	408.14	36.5	0.2568	0.183
<i>trans</i> -2-butene	274.03	428.63	39.9	0.2367	0.215
<i>cis</i> -2-butene	276.87	435.58	42.0	0.2311	0.204
methanol	337.85	512.58	80.9	0.1198	0.554
ethanol	351.44	513.92	61.4	0.1752	0.638
1-propanol	370.35	536.78	51.7	0.2305	0.625
1-butanol	390.81	563.05	44.2	0.2841	0.593
methyl <i>tert</i> -butyl ether	328.35	497.1	33.7	0.3249	0.267
ethyl <i>tert</i> -butyl ether	346.1 ^b	516.67	31.1 ^c	0.3785 ^g	0.296 ⁱ
propyl <i>tert</i> -butyl ether	370.6 ^c	558.21	28.3	0.4285 ^h	0.307 ⁱ
butyl <i>tert</i> -butyl ether	397 ^d	576.09 ^e	25.4 ^e	0.4905 ^g	0.380 ^j
<i>tert</i> -butyl alcohol	355.57	506.21	39.7	0.2876	0.613
2,4,4-trimethyl-1-pentene	374.59	553	26.8	0.451	0.221
2,4,4-trimethyl-2-pentene	378.06	558	26.8	0.4493	0.236

^a Unless specified, values from [145]. ^b [174]. ^c [175]. ^d [176]. ^e Estimated by Joback method. ^f Unless specified, values from [88]. ^g V_c estimated by Joback method. ^h V_c from [145]. ⁱ ω from [145]. ^j ω from Equation A13, through estimation of P_{vr} by Gómez-Thodos method

Table A28 Enthalpy of vaporization, ΔH_{vap}

Compound	ΔH_{vap} [kJ mol ⁻¹]							
	Temperature [K]							
	313.15	323.15	333.15	343.15	353.15	363.15	373.15	383.15
isobutene	19.2	18.5	17.7	16.9	16.0	14.9	13.8	12.5
isobutane	18.0	17.3	16.5	15.6	14.6	13.5	12.2	10.7
<i>trans</i> -2-butene	20.6	19.9	19.2	18.5	17.6	16.8	15.8	14.7
<i>cis</i> -2-butene	21.2	20.5	19.8	19.1	18.2	17.4	16.4	15.3
methanol	36.9	36.2	35.5	34.7	34.0	33.1	32.3	31.4
ethanol	42.5	41.7	40.9	40.0	39.1	38.2	37.2	36.2
1-propanol	47.3	46.3	45.3	44.3	43.3	42.2	41.1	39.9
1-butanol	48.7	48.1	47.4	46.7	46.1	45.3	44.6	43.9
methyl <i>tert</i> -butyl ether	29.3	28.6	27.8	27.1	26.3	25.5	24.6	23.8
ethyl <i>tert</i> -butyl ether	31.3	30.7	30.1	29.5	28.8	28.1	27.4	26.7
propyl <i>tert</i> -butyl ether	33.6	33.1	32.5	32.0	31.4	30.8	30.2	29.6
butyl <i>tert</i> -butyl ether	39.0	38.4	37.9	37.3	36.7	36.0	35.4	34.7
<i>tert</i> -butyl alcohol	44.9	43.5	42.2	40.8	39.3	37.9	36.3	34.8
2,4,4-trimethyl-1-pentene	34.9	34.3	33.7	33.1	32.4	31.8	31.1	30.4
2,4,4-trimethyl-2-pentene	36.6	35.9	35.3	34.5	33.8	33.1	32.3	31.5

Table A29 Compounds molar volumes, V , by HBT method at 1.5 MPa

Compound	V [L mol ⁻¹]							
	Temperature [K]							
	313.15	323.15	333.15	343.15	353.15	363.15	373.15	383.15
isobutene	0.098	0.101	0.104	0.107	0.110	0.114	0.120	0.127
isobutane	0.109	0.112	0.115	0.119	0.123	0.129	0.137	0.149
<i>trans</i> -2-butene	0.096	0.098	0.101	0.104	0.107	0.110	0.114	0.119
<i>cis</i> -2-butene	0.093	0.095	0.097	0.100	0.103	0.106	0.109	0.114
methanol	0.041	0.041	0.042	0.043	0.044	0.044	0.045	0.046
ethanol	0.058	0.059	0.060	0.061	0.062	0.063	0.065	0.066
1-propanol	0.075	0.076	0.078	0.079	0.080	0.081	0.083	0.084
1-butanol	0.092	0.093	0.094	0.096	0.097	0.098	0.100	0.102
methyl <i>tert</i> -butyl ether	0.120	0.122	0.124	0.126	0.128	0.131	0.133	0.136
ethyl <i>tert</i> -butyl ether	0.136	0.138	0.140	0.143	0.145	0.147	0.150	0.153
propyl <i>tert</i> -butyl ether	0.149	0.151	0.153	0.155	0.157	0.159	0.162	0.164
butyl <i>tert</i> -butyl ether	0.166	0.168	0.170	0.172	0.174	0.176	0.179	0.181
<i>tert</i> -butyl alcohol	0.097	0.099	0.100	0.102	0.104	0.106	0.108	0.110
2,4,4-trimethyl-1-pentene	0.161	0.163	0.165	0.167	0.170	0.172	0.175	0.177
2,4,4-trimethyl-2-pentene	0.159	0.161	0.163	0.166	0.168	0.170	0.173	0.175

Table A30 Hildebrand solubility parameter for individual compounds, δ_j , at 1.5 MPa

Compound	δ_j [MPa ^{1/2}]							
	Temperature [K]							
	313.15	323.15	333.15	343.15	353.15	363.15	373.15	383.15
isobutene	13.00	12.52	12.01	11.46	10.87	10.21	9.46	8.57
isobutane	11.91	11.42	10.90	10.33	9.71	8.99	8.16	7.09
<i>trans</i> -2-butene	13.67	13.24	12.77	12.28	11.75	11.17	10.53	9.81
<i>cis</i> -2-butene	14.13	13.69	13.23	12.73	12.21	11.64	11.02	10.33
methanol	29.01	28.45	27.88	27.29	26.68	26.05	25.40	24.72
ethanol	26.18	25.67	25.16	24.63	24.09	23.53	22.95	22.34
1-propanol	24.35	23.88	23.41	22.93	22.44	21.93	21.41	20.87
1-butanol	22.40	22.08	21.76	21.43	21.09	20.74	20.38	20.01
methyl <i>tert</i> -butyl ether	14.90	14.56	14.22	13.87	13.50	13.12	12.72	12.30
ethyl <i>tert</i> -butyl ether	14.51	14.23	13.95	13.66	13.36	13.05	12.73	12.40
propyl <i>tert</i> -butyl ether	14.41	14.18	13.95	13.71	13.46	13.21	12.95	12.68
butyl <i>tert</i> -butyl ether	14.82	14.60	14.38	14.15	13.92	13.68	13.43	13.19
<i>tert</i> -butyl alcohol	24.22	23.75	23.28	22.79	22.28	21.76	21.22	20.66
2,4,4-trimethyl-1-pentene	14.09	13.87	13.64	13.40	13.16	12.91	12.66	12.39
2,4,4-trimethyl-2-pentene	14.44	14.21	13.98	13.74	13.50	13.25	13.00	12.73

List of tables and figures

Table 1.1 Properties of fuels blended with different amounts of ethanol.....	4
Table 1.2 Properties of some fuel ethers	6
Table 1.3 Popular characterization techniques for ion-exchange resins	15
Table 2.1 Source, purity, and analysis of used materials	29
Table 2.2 Physical and chemical properties of catalysts.....	30
Table 2.3 Morphological properties of resins both in dry and in water-swollen state. .	31
Table 3.1 Thermochemical data of involved chemical species (standard state, liquid at 1 atm and 298.15 K)	43
Table 3.2 Theoretically determined standard enthalpy, free energy and entropy changes, as well as the corresponding thermodynamic equilibrium constants, of alkyl <i>tert</i> -butyl ether syntheses in the liquid phase at 298.15 K	43
Table 3.3 Molar heat capacity coefficients of the equation $C_p^o [J mol^{-1} K^{-1}] = a + bT + cT^2 + dT^3$, where T is expressed in K	51
Table 3.4 Temperature dependence parameters of K , $\Delta_r H^o$, $\Delta_r S^o$, and $\Delta_r G^o$, for the considered reactions when $\Delta_r H^o = f(T)$. Uncertainties refer to a 95% confidence interval.....	54
Table 3.5 Standard molar enthalpy ($kJ mol^{-1}$), entropy ($J (mol K)^{-1}$) and free energy ($kJ mol^{-1}$) changes of alkyl <i>tert</i> -butyl ether syntheses in the liquid phase at 298.15 K. Uncertainties refer to a 95% confidence interval.....	54
Table 3.6 Readjusted thermochemical data of the ethers produced if $\Delta_r H^o = f(T)$ (standard state, liquid at 1 atm and 298.15 K)	55
Table 3.7 Estimated values of the liquid phase standard molar enthalpy change of reaction, $\Delta_r H^o$, for the studied reactions, when it is considered as temperature dependent.....	56
Table 4.1 Relevant properties of involved compounds.....	60
Table 5.1 Reaction rates for alkyl <i>tert</i> -butyl ethers. Standard uncertainty for replicated experiments is presented. $T = 333 K$, $R^o_{A/O} = 1.0$, $d_p = 0.25-0.40 mm$, $WHSV > 500 h^{-1}$	84
Table 5.2 Alcohols properties	84
Table 5.3 Estimated values of each resin Hildebrand solubility parameter at 298 K...	86
Table 5.4 Data analysis for coded regressors.....	89
Table 6.1 Molecular length, Ogston distribution coefficients, K_O , in different density domains of swollen polymer, molecular weight and random coil diameter, Φ_d , of considered reactants	99

Table 7.1 Isobutene selectivity towards products and byproducts at $t = 300$ min. Standard uncertainty for replicated experiments is presented	117
Table 7.2 Reactants initial concentration and conversion and selectivity at $t = 300$ min for individual and simultaneous processes. A-35, catalyst load = 0.16%wt., $d_p = 0.25$ - 0.40 mm, 750 rpm, $T = 333$ K	125
Table 8.1 Physical properties of A-35	131
Table 8.2 Possible forms of the adsorption term in kinetic expressions for PTBE and BTBE individual syntheses	137
Table 8.3 Preselected PTBE kinetic equations	142
Table 8.4 Equations #770, #68, #1,121, and #185 for PTBE kinetics	144
Table 8.5 Adsorption thermodynamic relations calculated from the selected PTBE kinetic equation. Standard uncertainties are indicated	146
Table 8.6 Preselected BTBE kinetic equations	147
Table 8.7 Free energy change of adsorption, $\Delta G_{a,j}^o$, calculated from equations #59, #176, and #293 for the BTBE synthesis. Standard uncertainties are indicated ..	151
Table 8.8 Equations #89, #86, #92, #88, #87, #91, and resulting averaged equation for the BTBE synthesis reaction kinetics	152
Table 8.9 Averaged equation from equations #66 and #68, estimated parameters values, and thermodynamic relations for the BTBE synthesis reaction.	153
Table 8.10 Fitted values for the apparent kinetic constant, minimal WSSE, and effectiveness factor (η) for each individual experiment affected by mass transfer limitations in the synthesis of BTBE	154
Table 8.11 Most relevant kinetic equations for the simultaneous syntheses of ETBE and BTBE	158
Table 8.12 Kinetic equations parameters, and thermodynamic relations for the simultaneous syntheses of ETBE and BTBE	160
Table 8.13 Fitted values for the apparent kinetic coefficients, minimal WSSE, and effectiveness factor (η) for each individual experiment affected by mass transfer limitations in the simultaneous syntheses of ETBE and BTBE	160
Table 8.14 Quoted adsorption enthalpies in the gas-phase, $\Delta H_a^o(g)$, for methanol, ethanol and 1-propanol on Amberlyst TM 15, enthalpy of vaporization, $\Delta H_a^o(vap)$, and calculated adsorption enthalpies in the liquid-phase, $\Delta H_a^o(l)$..	164
Table A1 Measured reaction medium composition (major compounds) in the MTBE synthesis reaction and calculated mass-action ratios, Γ_x , Γ_y and Γ_a , for each experimental run	177
Table A2 Measured reaction medium composition (major compounds) in the ETBE synthesis reaction and calculated mass-action ratios, Γ_x , Γ_y and Γ_a , for each experimental run	178
Table A3 Measured reaction medium composition (major compounds) in the ETBE synthesis reaction and calculated equilibrium constants, K_x , K_y and K , for each experimental run	179

Table A4 Measured reaction medium composition at equilibrium in the PTBE synthesis reaction and calculated equilibrium constants, K_x , K_y and K , for each experimental run.....	180
Table A5 Measured reaction medium composition at equilibrium in the BTBE synthesis reaction and calculated equilibrium constants, K_x , K_y and K , for each experimental run.....	181
Table A6 Experimental conditions and reactants conversion at the final reaction time for the study on the ETBE synthesis byproducts formation	182
Table A7 Experimental conditions and initial reaction rates for the synthesis of PTBE using 0.25-0.40 mm A-35 particles as catalyst	183
Table A8 Experimental conditions and initial reaction rates for the synthesis of BTBE using 0.25-0.40 mm A-35 particles as catalyst.....	183
Table A9 Experimental conditions and initial reaction rates for the simultaneous syntheses of ETBE and BTBE using A-35 as catalyst.....	184
Table A10 Possible forms of the adsorption term in kinetic expressions for the simultaneous syntheses of ETBE and BTBE	185
Table A11 Joback group contributions for different properties	186
Table A12 Modified Benson method group contributions for enthalpy and entropy changes of formation	187
Table A13 Missenard method group contributions for molar heat capacity.....	188
Table A14 Růžička-Domalski method group contributions for molar heat capacity	188
Table A15 Coefficients for the modified Benson equation.....	189
Table A16 Coefficients for the estimation of vapor pressure.....	191
Table A17 Cohesion energy and molar volume contributions	194
Table A18 Considered structural groups for the resins constituents.....	195
Table A19 Distances and angles between atoms in a molecule of ethanol	196
Table A20 R_k and Q_k parameters and group assignment for the modified UNIFAC-Dortmund method.....	198
Table A21 Modified UNIFAC-Dortmund group interaction parameters.....	198
Table A22 Comparison of thermochemical data at 298 K.....	199
Table A23 Comparison of molar heat capacities, C_p [J (mol K) ⁻¹]	199
Table A24 Comparison of molar heat capacities, C_p [J (mol K) ⁻¹]	200
Table A25 Comparison of molar heat capacities, C_p [J (mol K) ⁻¹]	200
Table A26 Comparison of molar heat capacities, C_p [J (mol K) ⁻¹]	200
Table A27 Boiling temperature, critical temperature, critical pressure, V^* , and ω_{SRK}	201
Table A28 Enthalpy of vaporization	201
Table A29 Compounds molar volumes by HBT method at 1.5 MPa.....	202
Table A30 Hildebrand solubility parameter for individual compounds at 1.5 MPa..	202

Figure 1.1 Projections on transport.....	3
Figure 1.2 Main fuel ethers syntheses reactions	6
Figure 1.3 European fuel ethers production capacities in 2011 (kt/y)	7
Figure 1.4 IFP process for MTBE.....	9
Figure 1.5 Snamprogetti process for MTBE	10
Figure 1.6 Philips etherification process	11
Figure 1.7 Schematic representation of sulfonated PS-DVB ion-exchange resins	14
Figure 1.8 Hydrated (left) and undissociated (right) sulfonic groups attached to the polymeric matrix of an ion-exchange resin.....	16
Figure 1.9 Schematic representation of the swollen-state morphology of macroreticular ion-exchange resins.....	18
Figure 1.10 Schematic representation of the elementary steps occurring during a catalytic reaction.....	19
Figure 2.1 ISEC morphological pattern of the gel-type phase.....	32
Figure 2.2 Schematic diagram of the fixed bed reactor setup	33
Figure 2.3 Schematic diagram of the batch reactor setup	34
Figure 3.1 Main reactions involved	42
Figure 3.2 Experimental mass-action ratio, Γ_a , variation with LHSV for the MTBE experiments.....	45
Figure 3.3 Comparison between values for MTBE equilibrium constant	45
Figure 3.4 Molar fraction evolution in time for the ETBE synthesis in a batch experiment at $T = 323$ K, and outlet stream steady-state molar fraction variation with LHSV for the ETBE synthesis in fixed-bed experiments at $T = 333$ K	46
Figure 3.5 Comparison between values for ETBE equilibrium constants.....	47
Figure 3.6 Evolution in time of PTBE molar fraction in batch experiments at different $R_{A/O}^o$ and temperatures.....	48
Figure 3.7 Comparison between values for PTBE equilibrium constant.....	48
Figure 3.8 Evolution in time of BTBE molar fraction in batch experiments at different $R_{A/O}^o$ and temperatures.....	49
Figure 3.9 Comparison between values for BTBE equilibrium constant.....	50
Figure 3.10 Van't Hoff plot when considering reaction enthalpy change constant within the temperature range ($\Delta_r H^o \neq f(T)$)	50
Figure 3.11 Variation of the molar heat capacity with temperature.....	52
Figure 3.12 Van't Hoff plot considering reaction enthalpy as function of temperature ($\Delta_r H^o = f(T)$)	53
Figure 4.1 Reaction network in the ETBE synthesis using C_4 as isobutene source	59
Figure 4.2 Example chromatogram after 300 min of experiment	62
Figure 4.3 Molar fraction evolution of major and minor chemical species	63

Figure 4.4 Selectivity of isobutene and ethanol towards products vs. total conversion .	64
Figure 4.5 Variation with temperature of the isobutene selectivity towards TMP-1 after 300 min of reaction.	65
Figure 4.6 TMP-1 and TMP-2 formation vs. time at different $R_{A/O}^{\circ}$	66
Figure 4.7 Variation with temperature of the ethanol selectivity towards DEE at $t_{\text{exp}} = 300$ min.	67
Figure 4.8 Ethanol conversion at $t_{\text{exp}} = 300$ min against temperature at different $R_{A/O}^{\circ}$.	67
Figure 4.9 DEE formation against $R_{A/O}^{\circ}$ at different temperatures at $t_{\text{exp}} = 300$ min ...	68
Figure 4.10 Variation with temperature of the isobutene selectivity towards TBA at $t_{\text{exp}} = 300$ min.	69
Figure 4.11 Evolution of TBA formation at different temperatures.	70
Figure 4.12 Variation with temperature of the ethanol selectivity towards ESBE at $t = 300$ min.	71
Figure 4.13 ESBE formation vs. time at different temperatures.	71
Figure 4.14 Total byproducts formation vs. time with two different catalysts.	72
Figure 4.15 Evolution of products distribution in terms of isobutene selectivity to TBA, ETBE, TMP-1, and TMP-2 with A-35 and CT-275.	73
Figure 5.1 Main reactions involved.	81
Figure 5.2 Isobutene conversion with different catalysts vs. $W_{\text{cat}}/F_{\text{IB}}$ at 333 K and $R_{A/O}^{\circ} = 1.0$ for the studied reaction systems.	82
Figure 5.3 Influence of external mass transport on the rate at 333 K and $R_{A/O}^{\circ} = 1.0$. ..	83
Figure 5.4 Influence of internal mass transport on the rate at 333 K and $R_{A/O}^{\circ} = 1.0$..	83
Figure 5.5 Isobutene reaction rate values for different catalysts versus number of alcohol carbon atoms, dipole moment, and Hildebrand solubility parameter.	85
Figure 5.6 Isobutene reaction rate values for each synthesis reaction versus differences between the Hildebrand solubility parameter of the polymer, δ_P , and that of the medium, δ_M	87
Figure 5.7 Reaction rate as a function of catalysts acid capacity.	88
Figure 5.8 Relative importance of regressors versus number of alcohol carbon atoms. ..	90
Figure 5.9 Reaction rate fit for the considered reactions.	90
Figure 5.10 Response surfaces for the syntheses of MTBE, ETBE, PTBE, and BTBE. ...	91
Figure 5.11 Reaction rate vs. $[H^+]/V_{\text{sp}}$	92
Figure 6.1 ISEC morphological pattern of the gel-phase.	100
Figure 6.2 Reaction rate fit for the sixteen catalysts in the MTBE reaction.	103
Figure 6.3 TOF distribution for each characteristic polymer chain density for the MTBE experiments.	103
Figure 6.4 Reaction rate fit for the sixteen catalysts in the ETBE reaction.	104
Figure 6.5 TOF distribution for each characteristic polymer chain density for the ETBE experiments.	105
Figure 6.6 Reaction rate fit for the four considered reactions.	106

Figure 6.7 k_R values versus alcohol molecular length	107
Figure 6.8 TOF distribution for each characteristic polymer chain density	107
Figure 7.1 Reaction scheme	113
Figure 7.2 Initial ETBE and BTBE reaction rate vs. initial ethanol molar fraction ..	114
Figure 7.3 Dependence of the initial ETBE and BTBE reaction rate on the acid sites density in the swollen gel phase volume.....	115
Figure 7.4 TOF^o displayed by each catalyst	116
Figure 7.5 Initial etherification rate vs. initial isobutene molar fraction	118
Figure 7.6 Evolution in time of the liquid-phase ethanol/1-butanol molar ratio at $T = 333$ K with A-35.....	119
Figure 7.7 Isobutene selectivity towards ETBE and BTBE as a function of isobutene conversion	120
Figure 7.8 Isobutene selectivity towards ETBE and BTBE as a function of isobutene conversion	120
Figure 7.9 Isobutene selectivity towards main products as a function of temperature for a given isobutene conversion level.....	121
Figure 7.10 Arrhenius plot of the initial etherification rates	122
Figure 7.11 Dependence of initial rates on temperature.....	123
Figure 7.12 Mole evolution in time of the main compounds for ETBE and BTBE individual syntheses	124
Figure 7.13 Mole evolution in time of the main compounds in the simultaneous syntheses.....	125
Figure 8.1 Studied reaction systems.....	129
Figure 8.2 Arrhenius plot of reaction rate data	133
Figure 8.3 Inverse of WSSE values for each equation fitted to PTBE kinetic data ..	141
Figure 8.4 Comparison between experimental and calculated PTBE reaction rates from equation #68, and residuals distribution	145
Figure 8.5 Inverse of WSSE values for each equation applied to BTBE kinetic data...	146
Figure 8.6 Comparison between experimental and calculated BTBE reaction rates from equation #59, and residuals distribution	149
Figure 8.7 Comparison between experimental and calculated BTBE reaction rates from equation #176, and residuals distribution	150
Figure 8.8 Comparison between experimental and calculated BTBE reaction rates from equation #293, and residuals distribution	150
Figure 8.9 Comparison between experimental and calculated BTBE reaction rates obtained with the equation averaged from equations #89, #86, #92, #88, #87, and #91, and residuals distribution	152
Figure 8.10 Comparison between experimental and calculated BTBE reaction rates obtained with the equation averaged from equations #66 and #68, and residuals distribution.....	154

Figure 8.11 Comparison between experimental and calculated BTBE reaction rates obtained with the equation averaged from equations #89, #86, #92, #88, #87 and #91, and residuals distribution. Experimental rates were free of mass transfer limitations or affected by mass transfer limitations 155

Figure 8.12 Comparison between experimental and calculated BTBE reaction rates obtained with the equation averaged from equations #66 and #68, and residuals distribution. Experimental rates were free of mass transfer limitations or affected by mass transfer limitations 155

Figure 8.13 Inverse of WSSE values for each fitted equation in the simultaneous syntheses of ETBE and BTBE..... 156

Figure 8.14 Comparison between experimental and calculated ETBE and BTBE reaction rates from equation #101,607 and residuals distribution 159

Figure 8.15 Comparison between experimental and calculated ETBE and BTBE reaction rates estimated by the averaged equation and residuals distribution... 159

Figure 8.16 Comparison between experimental and calculated ETBE and BTBE reaction rates from equation #101,607 affected by mass transfer limitations and residuals distribution..... 161

Figure 8.17 Arrhenius plot of the obtained apparent kinetic coefficients for the individual syntheses of PTBE and BTBE, for the simultaneous syntheses of ETBE and BTBE and for the ETBE individual synthesis from literature 162

Figure A1 Molecule of ethanol..... 196

Literature

- [1] United Nations, Department of Economic and Social Affairs, Population Division. World Population Prospects: The 2015 Revision, Key Findings and Advance Tables. Working Paper No. ESA/P/WP.241, 2015.
- [2] BP, BP Energy Outlook to 2035, London, 2016.
- [3] McKinsey Global Institute, McKinsey Sustainability & Resource Productivity Practice. R. Dobbs, J. Oppenheim, F. Thompson, S. Mareels, S. Nyquist, S. Sanghvi, Resource Revolution: Tracking Global Commodity Markets, 1st ed., 2013.
- [4] BP, BP Energy Outlook to 2035, London, 2015.
- [5] BP, BP Statistical Review of World Energy, 64th ed., London, 2015.
- [6] BP, BP Statistical Review of World Energy, 65th ed., London, 2016.
- [7] Renewable Fuels Association. Going Global: 2015 Ethanol Industry Outlook, 2015.
- [8] E. Gnansounou, A. Dauriat, J. Sci. Ind. Res. 64 (2005) 809–821.
- [9] The American Heritage[®] Dictionary of the English Language, 5th ed., Houghton Mifflin Harcourt Publishing Company, Boston, 2015.
- [10] W. Dabelstein, A. Reglitzky, A. Schütze, K. Reders. Automotive Fuels, in: Ullmann's Encyclopedia of Industrial Chemistry, Wiley-VCH Verlag GmbH & Co. KGaA, 2007.
- [11] R. Luque, L. Herrero-Davila, J.M. Campelo, J.H. Clark, J.M. Hidalgo, D. Luna, J.M. Marinas, A.A. Romero, Energy Environ. Sci. 1 (2008) 542–564.
- [12] G. Najafi, B. Ghobadian, T. Tavakoli, D.R. Buttsworth, T.F. Yusaf, M. Faizollahnejad, Appl. Energy 86 (2009) 630–639.
- [13] Stockholm University, ATRAX AB, Autoemission KEE Consultant AB, AVL MTC AB, R. Westerholm, K.E. Egeback, B. Rehnlund, M. Henke. Blending of Ethanol in Gasoline for Spark Ignition Engines, Stockholm, 2005.
- [14] US Department of Energy, National Renewable Energy Laboratory, R.L. McCormick, J. Yanowitz. Effect of Ethanol Blending on Gasoline RVP, 2012.
- [15] Renewable Fuels Association, R.E. Reynolds, T.G. Bridge, A. Kasperson, G. Herwick, B. Sauer, Changes in Gasoline IV Manual, 2009.
- [16] B.K. Bailey. Performance of ethanol as a transportation fuel, in: C.E. Wyman (Ed.), Handbook on Bioethanol: Production and Utilization, p. 37–60, CRC Press, 1996.
- [17] E. Christensen, J. Yanowitz, M. Ratcliff, R.L. McCormick, Energy & Fuels 25 (2011) 4723–4733.
- [18] R. Cascone, Chem. Eng. Prog. 104 (2008) S4–S9.
- [19] R. González, Performance of AmberlystTM 35 in the Synthesis of ETBE from Ethanol and C₄ Cuts, PhD Thesis, University of Barcelona, 2011.

- [20] CONCAWE, Gasoline ether oxygenate occurrence in Europe, and a review of their fate and transport characteristics in the environment. Report no. 4/12. Brussels, 2012.
- [21] R. Soto, C. Fité, E. Ramírez, R. Bringué, M. Iborra, *Green Process. Synth.* 3 (2014) 321–333.
- [22] J.A. Linnekoski, A.O.I. Krause, A. Holmen, M. Kjetså, K. Moljord, *Appl. Catal. A Gen.* 174 (1998) 1–11.
- [23] J.F. Izquierdo, F. Cunill, M. Vila, M. Iborra, J. Tejero, *Ind. Eng. Chem. Res.* 33 (1994) 2830–2835.
- [24] C. Oost, U. Hoffmann, *Chem. Eng. Sci.* 51 (1996) 329–340.
- [25] W.R. Mirabella, in: 6th Annu. Glob. Refin. Summit 2012, Barcelona, 2012.
- [26] J. Van Gerpen, *Fuel Process. Technol.*, 86 (2005) 1097–1107.
- [27] M. Pera-Titus, M. Bausach, J. Tejero, M. Iborra, C. Fité, F. Cunill, J.F. Izquierdo, *Appl. Catal. A Gen.* 323 (2007) 38–50.
- [28] G. Egloff, P.M. Van Arsdell, *J. Inst. Pet.* 27 (1941) 121–142.
- [29] B.H. Gwynn, J.H. Hirsch, US Patent 2 743 302 A, 1956.
- [30] D. Gubisch, K. Armbrust, A. Kaizik, B. Scholz, R. Nehring, US Patent 6 015 928 A, 2000.
- [31] T. Tsuchida, S. Sakuma, T. Takeguchi, W. Ueda, *Ind. Eng. Chem. Res.* 45 (2006) 8634–8642.
- [32] P.H. Pfromm, V. Amanor-Boadu, R. Nelson, P. Vadlani, R. Madl, *Biomass and Bioenergy* 34 (2010) 515–524.
- [33] K. Srirangan, L. Akawi, X. Liu, A. Westbrook, E.J. Blondeel, M.G. Aucoin, M. Moo-Young, C.P. Chou, *Biotechnol Biofuels* 6 (2013) 139–152.
- [34] R. Jain, Y. Yan, *Microb Cell Fact* 10 (2011) 97–106.
- [35] O. V. Berezina, N. V. Zakharova, C. V. Yarotsky, V. V. Zverlov, *Appl. Biochem. Microbiol.* 48 (2012) 625–638.
- [36] K.F. Yee, A.R. Mohamed, S.H. Tan, *Renew. Sustain. Energy Rev.* 22 (2013) 604–620.
- [37] B. Torck, A. Convers, L. Asselineau, M. Hellin, US Patent 4 310 710, 1982.
- [38] A.T. Quitain, S. Katoh, M. Goto. Synthesis of Biomass-Derived Gasoline Fuel Oxygenates by Microwave Irradiation, in: Z. Fang (Ed.), *Liquid, Gaseous and Solid Biofuels - Conversion Techniques*, p. 357–374, InTech, 2013.
- [39] F. Ancillotti, G. Oriani, E. Pescarollo, US Patent 4 071 567, 1978.
- [40] C.W. Zahn, US Patent 5 245 087, 1993.
- [41] J.F. Knifton, J.R. Sanderson, P.E. Dai, US Patent 5 162 592, 1992.
- [42] J.F. Knifton, P.S.E. Dai, US Patent 5 449 839, 1995.
- [43] K.L. Rock, M. Korpelshoek, *PTQ Catalysis* (2008) 45–51.
- [44] A. Akelah, D.C. Sherrington, *Chem. Rev.* 81 (1981) 557–587.

- [45] B. Corain, M. Zecca, K. Jeřábek, *J. Mol. Catal. A Chem.* 177 (2001) 3–20.
- [46] R.L. Albright, *React. Polym. Ion Exch. Sorbents* 4 (1986) 155–174.
- [47] O. Okay, *Prog. Polym. Sci.* 25 (2000) 711–779.
- [48] D.C. Sherrington, *Chem. Commun.* (1998) 2275–2286.
- [49] O. Deutschmann, H. Knözinger, K. Kochloefl, T. Turek. *Heterogeneous Catalysis and Solid Catalysts*, in: *Ullmann's Encycl. Ind. Chem.*, Wiley-VCH Verlag GmbH & Co. KGaA, Weinheim, Germany, Germany, 2009.
- [50] A. Chakrabarti, M.M. Sharma, *React. Polym.* 20 (1993) 1–45.
- [51] L. Hanková, L. Holub, K. Jeřábek, *React. Funct. Polym.* 66 (2006) 592–598.
- [52] F.M. Coutinho, R.R. Souza, A.S. Gomes, *Eur. Polym. J.* 40 (2004) 1525–1532.
- [53] J. Guilera, L. Hanková, K. Jeřábek, E. Ramírez, J. Tejero, *React. Funct. Polym.* 78 (2014) 14–22.
- [54] S. Schlick, E. Bortel, K. Dyrek, *Acta Polym.* 47 (1996) 1–15.
- [55] K. Jeřábek, L. Holub, in: *13th Int. IUPAC Conf. Polym. Org. Chem.*, Montreal, 2009.
- [56] R. Bringué, E. Ramírez, M. Iborra, J. Tejero, F. Cunill, *J. Catal.* 304 (2013) 7–21.
- [57] T. Doğu, N. Boz, E. Aydın, N. Oktar, K. Murtezaoglu, G. Doğu, *Ind. Eng. Chem. Res.* 40 (2001) 5044–5051.
- [58] B.C. Gates, W. Rodriguez, *J. Catal.* 31 (1973) 27–31.
- [59] F. Ancillotti, M. Massi Mauri, E. Pescarollo, *J. Catal.* 46 (1977) 49–57.
- [60] F. Ancillotti, M. Massi Mauri, E. Pescarollo, L. Romagnoni, *J. Mol. Catal.* 4 (1978) 37–48.
- [61] T. Uematsu, *Bull. Chem. Soc. Jpn.* 45 (1972) 3329–3333.
- [62] R. Thornton, B.C. Gates, *J. Catal.* 34 (1974) 275–287.
- [63] S.K. Ihm, M.J. Chung, K.Y. Park, *Ind. Eng. Chem. Res.* 27 (1988) 41–45.
- [64] J.H. Ahn, S.K. Ihm, K.S. Park, *J. Catal.* 113 (1988) 434–443.
- [65] K. Jeřábek, *Anal. Chem.* 57 (1985) 1598–1602.
- [66] K. Jeřábek, *Anal. Chem.* 57 (1985) 1595–1597.
- [67] K. Jeřábek, *Collect. Czechoslov. Chem. Commun.* 46 (1981) 1577–1587.
- [68] L. Holub, K. Jeřábek, *J. Mol. Catal. A Chem.* 231 (2005) 21–26.
- [69] K. Jeřábek, L. Hanková, Z. Prokop, E.G. Lundquist, *Appl. Catal. A Gen.* 232 (2002) 181–188.
- [70] K. Jeřábek, L. Hanková, L. Holub, *J. Mol. Catal. A Chem.* 333 (2010) 109–113.
- [71] K. Jeřábek, in: *ACS Symp. Ser.*, American Chemical Society, 1996, pp. 211–224.
- [72] G. Ertl, H. Knözinger, F. Schülth, J. Weitkamp (Eds.), *Handbook of Heterogeneous Catalysis*, 2nd ed., Wiley-VCH Verlag GmbH & Co. KGaA, Weinheim, Germany, 2008.

- [73] J.M. Smith, *Chemical Engineering Kinetics*, 2nd ed., McGraw-Hill, New York, 1970.
- [74] J.F. Izquierdo, F. Cunill, J. Tejero, M. Iborra, C. Fité, *Cinética de Las Reacciones Químicas*, 1st ed., Universitat de Barcelona, Barcelona, 2004.
- [75] M. Granollers, *Liquid-Phase Oligomerization of Isoamylenes over Solid Acid Catalysts*, PhD Thesis, University of Barcelona, 2012.
- [76] J. Guilera, E. Ramírez, C. Fité, M. Iborra, J. Tejero, *Appl. Catal. A Gen.* 467 (2013) 301–309.
- [77] L. Nemeč, V. Blum, P. Rinke, M. Scheffler, *Phys. Rev. Lett.* 111 (2013) 065502.
- [78] G. Zhao, J. Li, X. Wang, *Chem. Eng. J.* 173 (2011) 185–190.
- [79] M. Martínez, A.H. Ahmed, A.P. Loh, R.E. Oswald, *Biochemistry* 53 (2014) 3790–3795.
- [80] A.B. Wöhri, P. Hillertz, P.-O. Eriksson, J. Meuller, N. Dekker, A. Snijder, *Mol. Membr. Biol.* 30 (2013) 169–83.
- [81] M.I. Sohel, M.W. Jack, *Bioresour. Technol.* 102 (2011) 2617–22.
- [82] P.M. Mortensen, J.D. Grunwaldt, P.A. Jensen, K.G. Knudsen, A.D. Jensen, *Appl. Catal. A Gen.* 407 (2011) 1–19.
- [83] M.R. Nanda, Z. Yuan, W. Qin, H.S. Ghaziaskar, M.-A. Poirier, C.C. Xu, *Fuel* 117 (2014) 470–477.
- [84] M. Iborra, C. Fité, J. Tejero, F. Cunill, J.F. Izquierdo, *React. Polym.* 22 (1993) 65–76.
- [85] J. Gmehling, J. Li, M. Schiller, *Ind. Eng. Chem. Res.* 32 (1993) 178–193.
- [86] M. Vila, F. Cunill, J.F. Izquierdo, J. González, A. Hernández, *Appl. Catal. A Gen.* 117 (1994) L99–L108.
- [87] J. Tejero, A. Calderón, F. Cunill, J.F. Izquierdo, M. Iborra, *React. Funct. Polym.* 33 (1997) 201–209.
- [88] R.C. Reid, J.M. Prausnitz, B.E. Poling, *The Properties of Gases and Liquids*, 4th ed., McGraw-Hill, New York, 1987.
- [89] B.E. Poling, J.M. Prausnitz, O. John Paul, R.C. Reid, *The Properties of Gases and Liquids*, 5th ed., McGraw-Hill, New York, 2001.
- [90] E.S. Domalski, E.D. Hearing, *J. Phys. Chem. Ref. Data* 17 (1988) 1637.
- [91] E.S. Domalski, E.D. Hearing, *J. Phys. Chem. Ref. Data* 22 (1993) 805–1159.
- [92] D.R. Lide, *CRC Handbook of Chemistry and Physics*, 85th ed., CRC Press, Boca Raton, FL, 2004.
- [93] K.G. Sharonov, Y.B. Mishentseva, A.M. Rozhnov, E.A. Miroshnichenko, L.I. Korchatova, *J. Chem. Thermodyn.* 23 (1991) 636–642.
- [94] F. Colombo, L. Cori, L. Dalloro, P. Delogu, *Ind. Eng. Chem. Fundam.* 22 (1983) 219–223.
- [95] A. Rehfinger, U. Hoffmann, *Chem. Eng. Sci.* 45 (1990) 1605–1617.
- [96] J.F. Izquierdo, F. Cunill, M. Vila, J. Tejero, M. Iborra, *J. Chem. Eng. Data* 37 (1992) 339–343.

- [97] T. Zhang, R. Datta, *Ind. Eng. Chem. Res.* 34 (1995) 730–740.
- [98] A. Wyczęsany. Thermodynamics of Ether Production, in: H. Hamid, M.A. Ali (Eds.), *Handbook of MTBE and Other Gasoline Oxygenates*, Marcel Dekker Inc., New York, 2004.
- [99] L. Solà, M.A. Pericàs, F. Cunill, M. Iborra, *Ind. Eng. Chem. Res.* 33 (1994) 2578–2583.
- [100] O. Françoisse, F.C. Thyron, *Chem. Eng. Process. Process Intensif.* 30 (1991) 141–149.
- [101] M. Vila, F. Cunill, J.F. Izquierdo, J. Tejero, M. Iborra, *Chem. Eng. Commun.* 124 (1993) 223–232.
- [102] K.L. Jensen, R. Datta, *Ind. Eng. Chem. Res.* 34 (1995) 392–399.
- [103] K.G. Sharonov, A.M. Rozhnov, A.V. Korol'kov, S.Y. Karaseva, E.A. Miroshnichenko, L.I. Korchatova, *J. Chem. Thermodyn.* 27 (1995) 751–753.
- [104] C. Gómez, F. Cunill, M. Iborra, F. Izquierdo, J. Tejero, *Ind. Eng. Chem. Res.* 36 (1997) 4756–4762.
- [105] R. Soto, C. Fité, E. Ramírez, R. Bringué, F. Cunill, *Chem. Eng. Res. Des.* 92 (2014) 644–656.
- [106] V. Macho, M. Kavala, M. Polievka, M. Okresa, W. Piecka, *Ropa Uhlie* 24 (1982) 397.
- [107] P.M. Słomkiewicz, *Appl. Catal. A Gen.* 313 (2006) 74–85.
- [108] K.G. Sharonov, Y.B. Mishentseva, A.M. Rozhnov, E.A. Miroshnichenko, L.I. Korchatova, *J. Chem. Thermodyn.* 23 (1991) 141–145.
- [109] E.S. Domalski, E.D. Hearing. Condensed Phase Heat Capacity Data, in: P.J. Linstrom, W.G. Mallard (Eds.), *NIST Chemistry WebBook*, NIST Standard Reference Database Number 69, National Institute of Standards and Technology, Gaithersburg MD.
- [110] M.M. Sharma, *React. Funct. Polym.* 26 (1995) 3–23.
- [111] M.A. Harmer, Q. Sun, *Appl. Catal. A Gen.* 221 (2001) 45–62.
- [112] F. Aiouache, S. Goto. Ethanol-Based Oxygenates from Biomass, in: H. Hamid, M.A. Ali (Eds.), *Handbook of MTBE and Other Gasoline Oxygenates*, Marcel Dekker Inc., New York, 2004.
- [113] K.F. Wong, C.A. Eckert, *J. Chem. Eng. Data* 14 (1969) 432–436.
- [114] R.H. Perry, D.W. Green, J.O. Maloney, *Perry's Chemical Engineers' Handbook*, McGraw-Hill, New York, 2008.
- [115] API Bulletin 2500, American Petroleum Institute, January, 1955.
- [116] API Bulletin 2513, American Petroleum Institute, February 1959.
- [117] API Bulletin 2516, American Petroleum Institute, February 1962.
- [118] API Bulletin 2518, American Petroleum Institute, February 1962.
- [119] F. Ancillotti, V. Fattore, *Fuel Process. Technol.* 57 (1998) 163–194.

- [120] R. Meusinger, R. Moros, *Fuel* 80 (2001) 613–621.
- [121] M.L. Honkela, A. Root, M. Lindblad, A.O.I. Krause, *Appl. Catal. A Gen.* 295 (2005) 216–223.
- [122] J. Gmehling, J. Lohmann, A. Jakob, J. Li, R. Joh, *Ind. Eng. Chem. Res.* 37 (1998) 4876–4882.
- [123] V.J. Cruz, J.F. Izquierdo, F. Cunill, J. Tejero, M. Iborra, C. Fité, R. Bringué, *React. Funct. Polym.* 67 (2007) 210–224.
- [124] E. Giménez, Estudio comparativo de la reacción de obtención del ETBE en fase líquida sobre tres resinas polisulfonadas como catalizadores, BSc Thesis, University of Barcelona, 2001.
- [125] M. Umar, A.R. Saleemi, S. Qaiser, *Catal. Commun.* 9 (2008) 721–727.
- [126] M. Umar, A.R. Saleemi, B. Saha, *Nucl.* 46 (2009) 101–107.
- [127] M. Di Girolamo, M. Lami, M. Marchionna, E. Pescarollo, L. Tagliabue, F. Ancillotti, *Ind. Eng. Chem. Res.* 36 (1997) 4452–4458.
- [128] R.A. Meyers, *Handbook of Petroleum Refining Processes*, 3rd ed., McGraw-Hill, New York, 2004.
- [129] M.L. Honkela, A.O.I. Krause, *Catal. Letters* 87 (2003) 113–119.
- [130] J.F. Izquierdo, M. Vila, J. Tejero, F. Cunill, M. Iborra, *Appl. Catal. A Gen.* 106 (1993) 155–165.
- [131] J. Tejero, F. Cunill, J.F. Izquierdo, M. Iborra, C. Fité, D. Parra, *Appl. Catal. A Gen.* 134 (1996) 21–36.
- [132] R.S. Karinen, M.S. Lylykangas, A.O.I. Krause, *Ind. Eng. Chem. Res.* 40 (2001) 1011–1015.
- [133] W.S. Gallaway, M.J. Murray, *J. Am. Chem. Soc.* 70 (1948) 2584–2586.
- [134] H.J. Panneman, A.A.C.M. Beenackers, *Ind. Eng. Chem. Res.* 34 (1995) 3817–3825.
- [135] H.J. Panneman, A.A.C.M. Beenackers, *Ind. Eng. Chem. Res.* 34 (1995) 4318–4325.
- [136] C. Fité, J. Tejero, M. Iborra, F. Cunill, J. F. Izquierdo, D. Parra, C. Fité, *Appl. Catal. A Gen.* 169 (1998) 165–177.
- [137] F. Cunill, M. Vila, J.F. Izquierdo, M. Iborra, J. Tejero, *Ind. Eng. Chem. Res.* 32 (1993) 564–569.
- [138] C. Fité, M. Iborra, J. Tejero, J.F. Izquierdo, F. Cunill, *Ind. Eng. Chem. Res.* 33 (1994) 581–591.
- [139] A. Moronta, J. Luengo, Y. Ramírez, J. Quiñónez, E. González, J. Sánchez, *Appl. Clay Sci.* 29 (2005) 117–123.
- [140] O.S. Pavlov, S. A. Karsakov, S.Y. Pavlov, *Russ. J. Appl. Chem.* 82 (2009) 1117–1122.
- [141] M. Cadenas, R. Bringué, C. Fité, E. Ramírez, F. Cunill, *Top. Catal.* 54 (2011) 998–1008.
- [142] R.S. Karinen, J.A. Linnekoski, A.O.I. Krause, *Catal. Letters* 76 (2001) 81–87.

- [143] L.K. Rihko, J.A. Linnekoski, A.O.I. Krause, *J. Chem. Eng. Data* 39 (1994) 700–704.
- [144] L. Solà, M.A. Pericàs, F. Cunill, J.F. Izquierdo, *Ind. Eng. Chem. Res.* 36 (1997) 2012–2018.
- [145] C.L. Yaws, P.K. Narasimhan. *Critical Properties and Acentric Factor - Organic Compounds*, in: C.L. Yaws (Ed.), *Thermophysical Properties of Chemicals and Hydrocarbons*, p. 1–95, William Andrew, Norwich NY, 2009.
- [146] R. Stewart, *The Proton: Applications to Organic Chemistry*, Academic Press Inc., London, 1985.
- [147] C. Buttersack, *React. Polym.* 10 (1989) 143–164.
- [148] R.S. Karinen, A.O.I. Krause, *Appl. Catal. A Gen.* 188 (1999) 247–256.
- [149] T. Matsuura, *Synthetic Membranes and Membrane Separation Processes*, CRC Press Inc., Boca Raton FL, 1993.
- [150] C. Fité, J. Tejero, M. Iborra, F. Cunill, J.F. Izquierdo, *AIChE J.* 44 (1998) 2273–2279.
- [151] U. Grömping, *J. Stat. Softw.* 17 (2006) 1–27.
- [152] A.T. Bell, *Science* 299 (2003) 1688–1691.
- [153] L.K. Rihko-Struckmann, P. V Latostenmaa, A.O.I. Krause, *J. Mol. Catal. A Chem.* 177 (2001) 41–47.
- [154] T. Crispin, I. Halász, *J. Chromatogr. A* 239 (1982) 351–362.
- [155] S.Y. Chee, S.N. Gan, *J. Appl. Polym. Sci.* 111 (2008) 1185–1189.
- [156] D.E. López, J.G. Goodwin, D.A. Bruce, E. Lotero, *Appl. Catal. A Gen.* 295 (2005) 97–105.
- [157] K. Jeřábek, *Kem. U Ind.* 62 (2013) 171–176.
- [158] P.M. Słomkiewicz, *J. Chromatogr. A* 1034 (2004) 169–174.
- [159] Ó. Santín, *Estudio del control de las etapas físicas en las síntesis de MTBE y ETBE*, MSc Thesis, University of Barcelona, 2005.
- [160] W.J. Casey, D.J. Pietrzyk, *Anal. Chem.* 45 (1973) 1404–1409.
- [161] A. Gicquel, B. Torck, *J. Catal.* 83 (1983) 9–18.
- [162] D. Parra, J. Tejero, F. Cunill, M. Iborra, J.F. Izquierdo, *Chem. Eng. Sci.* 49 (1994) 4563–4578.
- [163] K. Sundmacher, R.S. Zhang, U. Hoffmann, *Chem. Eng. Technol.* (1995) 269–277.
- [164] C.L. Yaws, K.Y. Li. *Solubility Parameter and Liquid Volume - Organic Compounds*, in: C.L. Yaws (Ed.), *Thermophysical Properties of Chemicals and Hydrocarbons*, p. 597–643, William Andrew, Norwich NY, 2009.
- [165] H. Akaike. *Information theory and an extension of the maximum likelihood principle*, in: E. Parzen, K. Tanabe, G. Kitagawa (Eds.), *Selected Papers of Hirotugu Akaike*, p. 199–213, Springer, New York, 1998.
- [166] K.P. Burnham, D.R. Anderson, *Model Selection and Multimodel Inference: A Practical Information - Theoretic Approach*, 2nd ed., Springer Science & Business Media, 2002.

- [167] M.R.E. Symonds, A. Moussalli, *Behav. Ecol. Sociobiol.* 65 (2011) 13–21.
- [168] N. Oktar, K. Mürtezaoğlu, G. Doğu, T. Doğu, *Can. J. Chem. Eng.* 77 (1999) 406–412.
- [169] P. Słomkiewicz, *Adsorpt. Sci. Technol.* 24 (2006) 239–256.
- [170] W.E. Acree Jr., J.S. Chickos, Phase Transition Enthalpy Measurements of Organic and Organometallic Compounds, in: P.J. Linstrom, W.G. Mallard (Eds.), NIST Chemistry WebBook, NIST Standard Reference Database Number 69, National Institute of Standards and Technology, Gaithersburg MD.
- [171] J.F. Ogilvie, *Comput. Chem.* 8 (1984) 205–207.
- [172] C.L. Yaws, M.A. Satyro. Enthalpy of Vaporization - Organic Compounds, in: C.L. Yaws (Ed.), *Thermophysical Properties of Chemicals and Hydrocarbons*, p. 309–400, William Andrew, Norwich NY, 2009.
- [173] G.H. Thomson, K.R. Brobst, R.W. Hankinson, *AIChE J.* 28 (1982) 671–676.
- [174] M.S.H. Fandary, A.S. Aljimaz, J.A. Al-Kandary, M.A. Fahim, *J. Chem. Eng. Data* 44 (1999) 1129–1131.
- [175] J.F. Norris, G.W. Rigby, *J. Am. Chem. Soc.* 54 (1932) 2088–2100.
- [176] T.W. Campbell, W. Burney, T.L. Jacobs, *J. Am. Chem. Soc.* 72 (1950) 2735–2736.

1. Introducció

Les resines de bescanvi iònic funcionalitzades són materials de base polimèrica que es poden utilitzar com a catalitzadors en una gran varietat de reaccions químiques per formar productes desitjats, de manera altament selectiva i a velocitats comercialment rendibles. Entre aquests catalitzadors, les resines sulfòniques han assolit una importància cabdal a l'hora de dur a terme alguns processos industrials molt importants com, per exemple, el procés d'eterificació d'isoolefines per obtenir èters ramificats.

La producció d'èters ramificats, que s'utilitzen com a additius oxigenats antidetonants en la formulació de les gasolines comercials, es va convertir en un dels processos industrials més importants, sobretot a Europa, quan es van retirar les gasolines amb plom, als anys noranta del segle XX. Dels èters comercials que s'empren actualment, en destaquen, pel volum de producció mundial, el metil *terc*-butil èter (MTBE) i l'etil *terc*-butil èter (ETBE). Aquests èters s'obtenen per mitjà d'un procés de reacció catalítica entre 2-metilpropè (isobutè) i metanol i etanol, respectivament, utilitzant resines de bescanvi iònic sulfonades i d'estructura macroreticulada com a catalitzadors.

D'altra banda, actualment es considera convenient utilitzar matèries primeres renovables per a la producció de combustibles, atès que això permet reduir l'impacte ambiental del sector del transport en un context en el qual la flota mundial de vehicles augmenta considerablement. En aquest sentit, la tendència general ha estat fer ús d'etanol d'origen renovable, però els últims anys aquesta opció ha suscitat controvèrsia, atès que la producció d'etanol per mitjà de processos de fermentació de biomassa competeix directament amb la producció d'aliments.

De manera alternativa, hi ha un interès creixent en l'ús d'altres alcohols que també es poden obtenir per mitjà de processos fermentatius però que no competeixen amb la producció alimentària. Així, per exemple, l'ús d'1-propanol i, especialment, d'1-butanol suscita interès tant en el món de la recerca com en el comercial. L'eterificació d'isobutè amb 1-propanol i 1-butanol produeix, respectivament, propil *terc*-butil èter (PTBE) i butil *terc*-butil èter (BTBE). Aquests èters presenten un seguit de propietats que poden comportar beneficis potencials com a additius per a combustibles (per exemple, una disminució de les emissions per evaporació, augment del contingut energètic, immiscibilitat en aigua i higroscopicitat baixa). Per tant, aquesta és una de les alternatives que podrien comportar una millora efectiva de la formulació de les gasolines comercials a curt termini.

Tot i que la producció industrial d'MTBE i d'ETBE està molt estesa, l'ús de resines de bescanvi iònic com a catalitzadors comporta certs fenòmens fisicoquímics rellevants que avui dia continuen sense haver-se entès completament. En conseqüència, calen estudis que intentin aportar nous coneixements pel que fa al comportament catalític d'aquests materials. Per això, en aquesta tesi, s'estudien diversos aspectes relacionats amb el funcionament catalític de resines de bescanvi iònic, sulfòniques i macroreticulades, en les reaccions de síntesi en fase líquida d'MTBE, ETBE, PTBE i BTBE (figura 1).

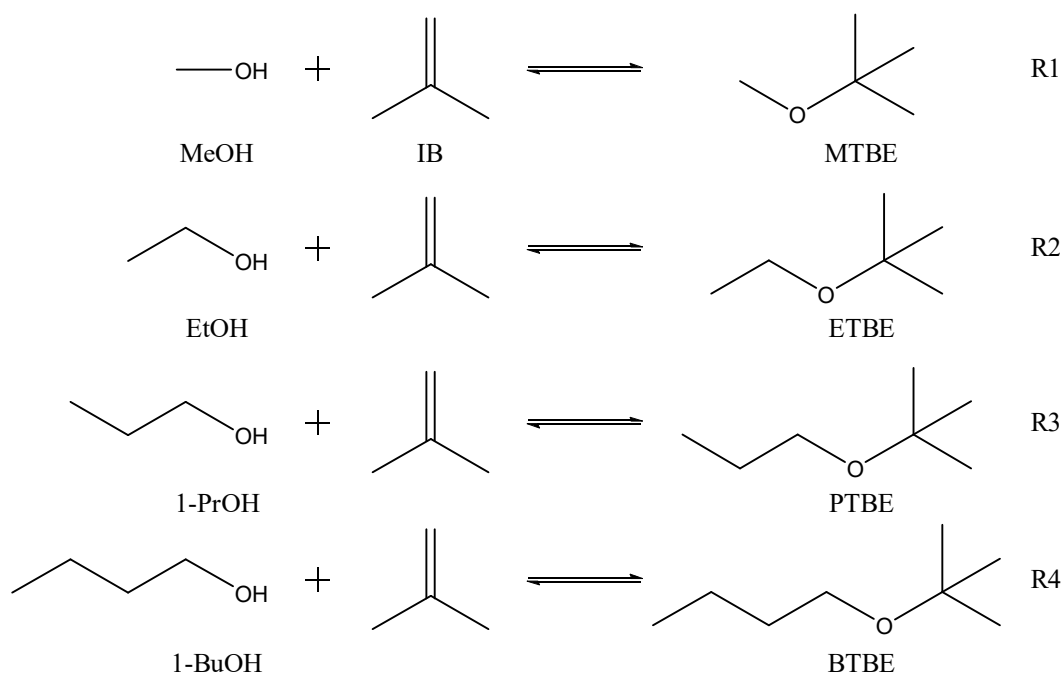


Figura 1 Reaccions estudiades

Les reaccions que apareixen a la figura 1 són, de fet, una sèrie de reaccions anàlogues en les quals poden aparèixer canvis de les propietats del medi de reacció, a causa, principalment, de la mida d'alguns dels compostos que hi participen. D'aquesta manera, es pot avaluar la influència de les característiques de diferents resines i dels medis de reacció sobre el desenvolupament de les reaccions de síntesi estudiades.

Així doncs, amb l'objectiu general d'aprofundir en el coneixement del comportament catalític d'aquests materials, s'han establert els objectius específics següents:

1. Estudi de l'equilibri termodinàmic de les reaccions de síntesi d'MTBE, ETBE, PTBE i BTBE en fase líquida.
2. Anàlisi de la distribució de productes per a aquest tipus de síntesi i determinació de les condicions d'operació que afavoreixen la formació de subproductes en les reaccions estudiades.
3. Ampliació del coneixement del comportament catalític de les resines de bescanvi iònic per mitjà de l'establiment de relacions entre les seves característiques i el nivell d'activitat catalítica que presenten.
4. Estudi de viabilitat d'un procés mitjançant el qual s'obtinguin èters diferents de manera simultània.
5. Anàlisi cinètica de les síntesis proposades emprant els catalitzadors potencialment més adients.

2. Experimental

2.1 Materials

Per a la realització d'aquest treball, s'han utilitzat els reactants següents: metanol (amb un contingut màxim del 0,005% màssic d'aigua), etanol (0,02% màssic d'aigua màxim), 1-propanol (0,005% màssic d'aigua màxim), 1-butanol (0,005% màssic d'aigua màxim) i isobutè pur (>99,9% GC) o, alternativament, una mescla sintètica d'hidrocarburs C₄ com a font d'isobutè. La composició d'aquesta mescla pretén emular la d'una fracció C₄ industrial d'una unitat d'FCC: 25% isobutè, 40% isobutà i 35% *trans*-2-butè. D'altra banda, en els procediments analítics s'han emprat diversos compostos, els quals es poden generar com a productes o subproductes de reacció: 2-metil-2-propanol (TBA, >99,7% GC), dietilèter (DEE, >99,5% GC), 2-metoxi-2-metilpropà (MTBE, >99,9% GC), 2-etoxi-2-metilpropà (ETBE, >95,0% GC), 2-etoxibutà (ESBE, >99,7% GC), 2-4-4-trimetil-1-pentè (TMP-1, >98% GC) i 2-4-4-trimetil-2-pentè (TMP-2, >98% GC). També s'han utilitzat els compostos 2-metil-2-propoxipropà (PTBE, >99% GC) i 1-*terc*-butoxibutà (BTBE, >98% GC), els quals es van sintetitzar al laboratori i es van purificar per mitjà d'una extracció i una rectificació en una columna Vigreux.

Tots els catalitzadors que s'han emprat en aquesta tesi són resines àcides de bescanvi iònic, d'estirè i divinilbenzè, sulfonades i macroreticulades. Majoritàriament, es tracta de resines comercials; concretament, són les resines següents: Amberlyst™ 15 (A-15, Rohm & Haas SAS), A-16, A-35, A-36, A-39, A-40, A-46, A-48, A-70; Purolite® CT175 (CT-175, Purolite Ltd.), CT-252, CT-275, i Lewatit® K 2620 (K2620, Lanxess AG). També s'han emprat quatre resines que s'havien sintetitzat en un estudi previ [53], les resines 306, 406, 606 i 806. Les característiques dels catalitzadors utilitzats es mostren a les taules 1 i 2.

Taula 1 Propietats físiques i químiques dels catalitzadors

Catalitzador	%DVB ^a	Capacitat àcida ^b [meq H ⁺ g _{cat} ⁻¹]	Tipus de sulfonació ^c	$-\Delta H_{Ads}^{NH_3}$ ^d [kJ mol ⁻¹]	d _{p,m} ^f [μm]	T _{màx} ^h [K]
A-15	Alt	4,81	C	110 ± 3 ^e	740	393
A-16	Mitjà	4,80	C	108 ± 3 ^e	600-800 ^g	403
A-35	Alt	5,32	O	113 ± 3	623	423
A-36	Mitjà	5,40	O	117 ± 2 ^e	630	423
A-39	Baix	4,81	C	111 ± 3 ^e	-	403
A-40	Alt	5,01	O	111 ± 3 ^e	580-800 ^g	413
A-46	Alt	0,87	S	108 ± 3 ^e	-	393
A-48	Alt	5,62	O	113 ± 3 ^e	-	413
A-70 ⁱ	Baix	2,65	C	117 ± 2 ^e	570	463
CT-175	Alt	4,98	C	114 ± 1 ^e	940	403
CT-252	Mitjà	5,40	O	115 ± 3 ^e	780	403
CT-275	Alt	5,20	O	113 ± 3	746	403
K2620	Alt	5,07	O	109 ± 3	620	413
306	Alt	0,81	S	-	-	-
406	Alt	0,99	S	-	-	-
606	Alt	1,89	P	-	-	-
806	Alt	3,10	P	-	-	-

^a Classificació considerada de grau de reticulació: baix (<9%), mitjà (9-14%), alt (>14%). ^b Valoració sobre base estandarditzada. ^c Sulfonació convencional (C), sobresulfonació (O) i sulfonació parcial (P). ^d Entalpia d'adsorció d'amoníac. ^e [75], ^f Diàmetre de partícula mitjà per difracció amb làser en aire. ^g Diàmetre de partícula segons dades del fabricant. ^h Temperatura d'operació màxima segons el fabricant. ⁱ Resina clorada.

Taula 2 Propietats morfològiques dels catalitzadors en estat sec i inflats en aigua

Catalitzador	ρ^a [g cm ⁻³]	Estat sec: adsorció-desorció de N ₂ a 77 K ^b				Inflat en aigua: mètode ISEC			
		S_{BET}^c [m ² g ⁻¹]	S_g [m ² g ⁻¹]	V_{g}^d [cm ³ g ⁻¹]	$d_{\text{m,porus}}^e$ [nm]	Macro/mesoporus			Fase gel
						$S_{\text{àrea}}$ [m ² g ⁻¹]	V_{porus} [cm ³ g ⁻¹]	d_{porus}^e [nm]	V_{sp} [cm ³ g ⁻¹]
A-15	1,416	42,0	41,3	0,328	31,8	192	0,616	12,8	0,765
A-16	1,401	1,69	1,75	0,013	29,7	46,2	0,188	16,3	1,129
A-35	1,542	29,0	35,6	0,210	23,7	199	0,720	14,5	0,613
A-36	1,567	21,0	21,2	0,143	27,0	68,0	0,259	15,2	1,025
A-39	1,417	0,09	0,065	0,0003	17,6	56,1	0,155	11,1	1,624
A-40	1,431	0,22	0,32	0,0006	7,5	11,0	0,125	45,5	0,442
A-46	1,137	57,4	54,8	0,263	19,2	186	0,470	10,1	0,523
A-48	1,538	33,8	32,1	0,249	31,0	186	0,568	12,2	0,620
A-70	1,514	0,018				66,1	0,220	13,3	1,257
CT-175	1,498	28,0	26,6	0,30	45,1	90,7	0,615	27,1	0,908
CT-252	1,493	22,4	19,9	0,221	44,4	132	0,491	14,9	0,981
CT-275	1,506	20,3	30,2	0,377	50,1	209	0,772	14,7	0,806
K2620	1,428	28,7	30,6	0,188	27,3	163,8	0,498	12,16	0,942
306	1,112	38,1	40,6	0,267	26,4	156	0,408	10,5	1,247
406	1,129	35,8	39,6	0,272	27,5	136	0,643	18,9	0,934
606	1,177	30,4	33,5	0,233	27,8	122	0,652	21,3	0,951
806	1,263	26,5	29,0	0,198	28,0	62,2	0,455	29,3	1,250

^a Densitat d'esquelet mesurada per desplaçament d'He (Accupic 1330). ^b Mostres assecades al buit (0,001 MPa, 383 K), ^c Mètode BET (Brunauer-Emmett-Teller). ^d Volum de N₂ adsorbit a pressió relativa (P/P₀) = 0,99.

^e $d_{\text{m,porus}} = 4V_{\text{g}}/S_{\text{g}}$ o $d_{\text{porus}} = 4V_{\text{porus}}/S_{\text{àrea}}$, respectivament.

La selecció de resines inclou polímers amb un grau de reticulació baix (A-39 i A-70), mitjà (A-16, A-36 i CT-252) i alt (A-15, A-35, A-40, A-46, A-48, CT-175, CT-275, K2620, 306, 406, 606 i 806). Pel que fa al tipus de sulfonació, hi ha resines que presenten sulfonació convencional (A-15, A-16, A-39, A-70 i CT-175), la qual cosa implica que hi ha aproximadament un grup sulfònic per anell d'estirè; sobresulfonació (A-35, A-36, A-40, A-48, CT-252, CT-275 i K2620), més d'un grup sulfònic per anell; o sulfonació parcial (A-46, 306, 406, 606 i 806), és a dir, amb menys d'un grup sulfònic per anell d'estirè. De les resines parcialment sulfonades, se'n distingeix el subgrup format per l'A-46, la 306 i la 406, atès que es considera que estan sulfonades principalment en la superfície de les microesferes [53]. Quant a la resina A-70, cal destacar que part dels àtoms d'hidrogen de la seva estructura s'han substituït per àtoms de clor, cosa que li confereix una estabilitat tèrmica i una força àcida superiors [76].

Pel que fa a la morfologia de la fase gel dels catalitzadors, descrita mitjançant la tècnica ISEC [65,66], la distribució de fraccions de volum de densitat de cadena característica es mostra a la figura 2.

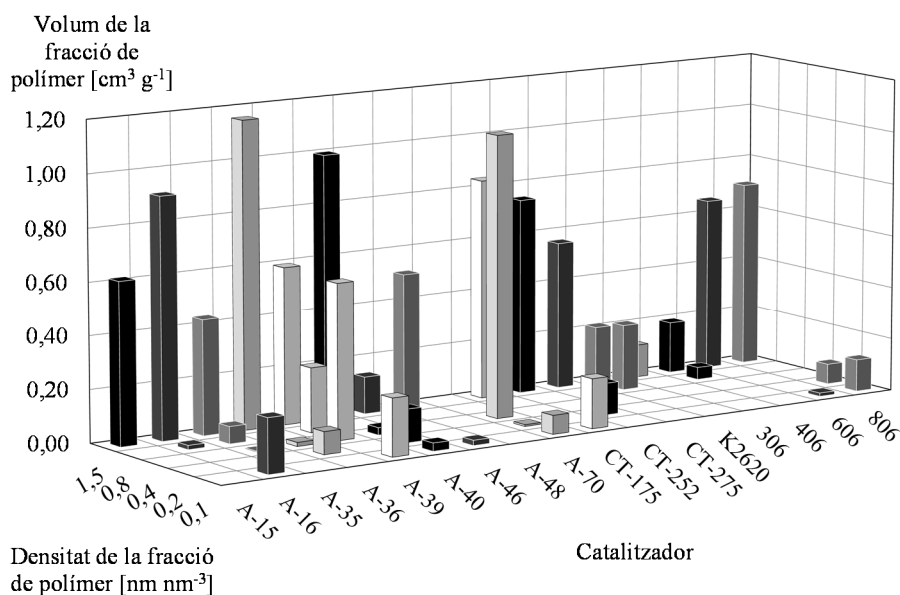


Figura 2 Distribució de volums de la fase gel dels catalitzadors

2.2 Dispositius experimentals

Per a la realització dels experiments s'han utilitzat dos dispositius experimentals diferents: un reactor de llit fix i un reactor discontinu de tanc agitat.

El dispositiu amb reactor de llit fix (figura 3) està format per un o més microreactors (longitud: 150 mm, diàmetre intern: 7 mm) submergits en un bany termostàtic que permet mantenir el reactor a la temperatura desitjada.

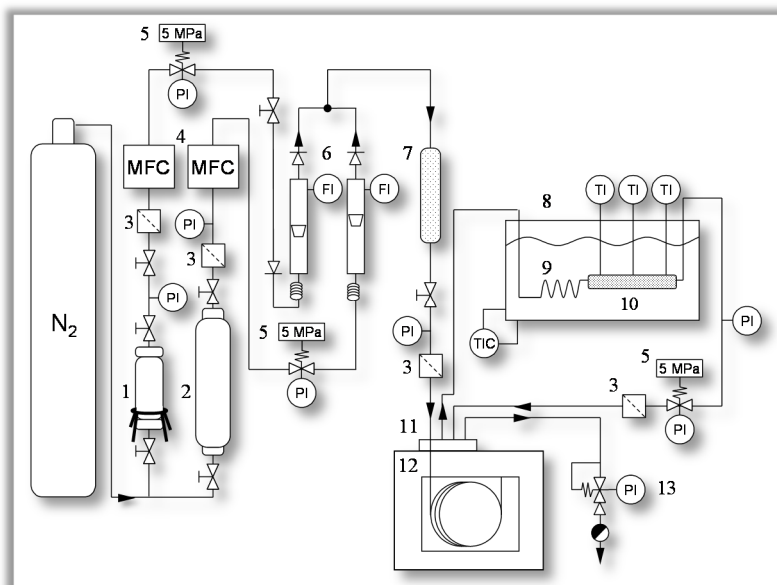


Figura 3 Diagrama del dispositiu de reactor de llit fix: 1. Contenidor olefínic, 2. Dipòsit alcohòlic, 3. Filtre de $2\mu\text{m}$, 4. Controlador de cabal màssic, 5. Vàlvula de seguretat, 6. Vàlvula sense retorn, 7. Mesclador, 8. Bany termostàtic, 9. Serpentí calefactor, 10. Reactor, 11. Vàlvules de mostreig, 12. Cromatògraf de gasos, 13. Regulador de contrapressió

En els casos en què s'han volgut dur a terme experiments amb un llit catalític isoterm, el catalitzador s'ha diluït amb partícules de carbur de silici (el qual és inert) del mateix rang de mida de partícula que el catalitzador. La relació màssica inert/catalitzador sempre s'ha mantingut per sota del límit, prèviament establert, a partir del qual hi pot haver alteracions de flux (per sota de 300). A més, segons el tipus d'experiment, el règim d'operació d'aquest dispositiu pot ser diferencial o integral. Per tal d'operar en règim diferencial, cal no superar un cert límit de conversió al reactor. Aquest límit generalment se situa al voltant del 10% en el tipus de reaccions que es tracten en aquesta tesi. Aquest fet ha limitat la quantitat de catalitzador que es pot introduir al reactor a cada temperatura. Pel que fa a l'operació en règim integral, no cal limitar la conversió ni, en conseqüència, la massa de catalitzador del reactor.

Al llarg de cada experiment, s'ha analitzat la composició tant del corrent d'entrada com del de sortida del reactor. Per fer-ho, s'han pres mostres periòdicament per mitjà de dues vàlvules pneumàtiques que injecten 2 μL de líquid pressuritzat a un cromatògraf de gasos 7890A equipat amb una columna capil·lar i un detector de flama d'ionització.

El dispositiu amb reactor discontinu de tanc agitat (figura 4) està format per un reactor encamisat d'acer inoxidable de 200 cm^3 equipat amb un inductor de catalitzador. La temperatura al reactor es controla amb un bany termostàtic. En els experiments realitzats en aquest dispositiu, s'ha analitzat l'evolució de la composició del medi de reacció amb un cromatògraf de gasos 6890 acoblat a un detector selectiu de masses HP5973N.

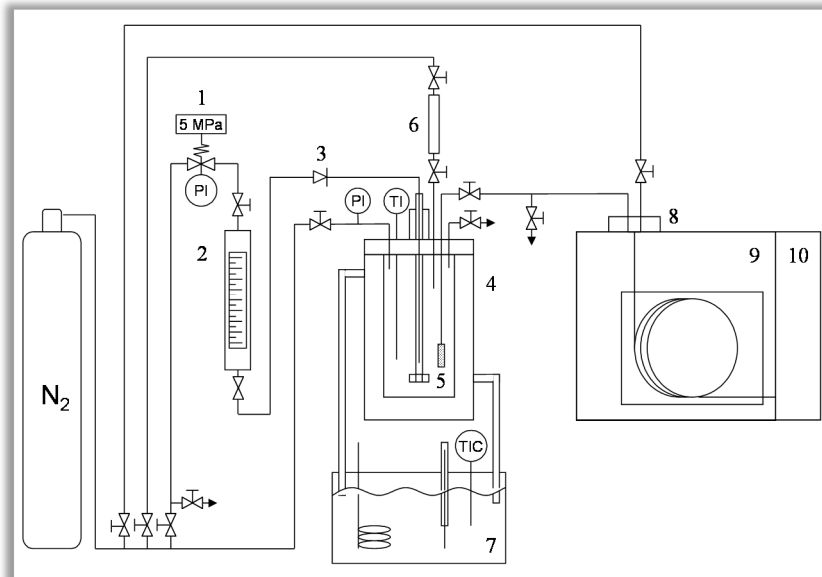


Figura 4 Diagrama del dispositiu amb reactor discontinu: 1. Vàlvula de seguretat, 2. Bureta de pressió, 3. Vàlvula sense retorn, 4. Reactor, 5. Filtre de 2 μm , 6. Inductor de catalitzador, 7. Bany termostàtic, 8. Vàlvula de mostreig, 9. Cromatògraf de gasos, 10. Detector selectiu de masses

3. Resultats

3.1 Equilibri químic

A l'hora de considerar si la implantació d'un procés pot tenir possibilitats d'èxit industrialment, en primer lloc, cal realitzar estudis que permetin determinar-ne les propietats termodinàmiques corresponents mitjançant un treball experimental contrastat. En el cas dels processos que s'estudien en aquesta tesi, hi ha un bon nombre de referències bibliogràfiques relatives a les síntesis d'MTBE i d'ETBE, però en canvi n'hi ha poques que facin referència a la síntesi d'èters més pesats d'estructura similar. A més, especialment pel que fa a l'ETBE, hi ha certes discrepàncies entre els diferents estudis disponibles.

Així doncs, en aquesta tesi s'ha estudiat l'equilibri químic de les reaccions de síntesi d'MTBE, ETBE, PTBE i BTBE per addició de l'alcohol corresponent (metanol, etanol, 1-propanol o 1-butanol, respectivament) a l'isobutè (figura 1), en fase líquida, en un rang de temperatures de 313 a 383 K i utilitzant resines de bescanvi iònic com a catalitzador. D'aquesta manera, els resultats obtinguts en aquesta tesi pel que fa als sistemes més estudiats (MTBE i ETBE) es poden comparar amb el que hi ha publicat a la literatura, cosa que permet avaluar la solidesa dels procediments seguits per a l'obtenció de resultats en el conjunt de les quatre reaccions analitzades, incloent-hi les menys estudiades (PTBE i BTBE).

La majoria dels experiments s'han realitzat en un reactor discontinu de tanc agitat utilitzant la resina de bescanvi iònic A-35 com a catalitzador, però a més també s'ha fet servir el dispositiu amb reactor de llit fix, operant en règim integral, i fins a tres resines més, per tal de demostrar que ni el tipus d'operació ni el catalitzador afecten els valors de les propietats termodinàmiques d'una reacció química.

Pel que fa als principals resultats obtinguts, a la figura 5 es mostra la dependència amb la temperatura dels valors de les constants d'equilibri químic, que s'han calculat a partir de les relacions d'activitats dels compostos corresponents (equació 1).

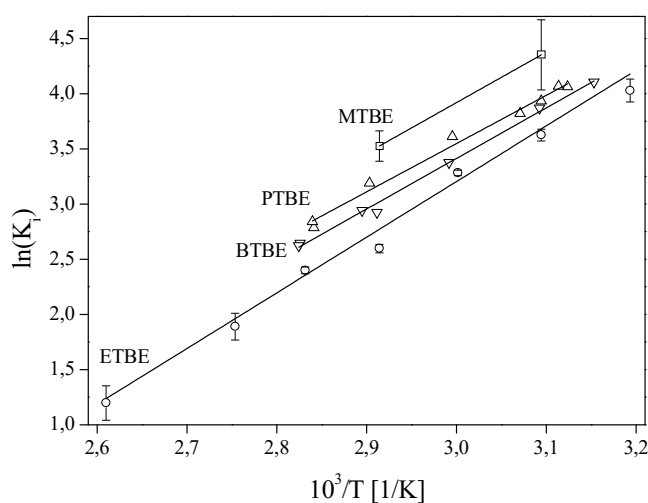


Figura 5 Dependència dels valors de les constants d'equilibri amb la temperatura. Les barres d'error corresponen a un nivell de confiança del 95%. Les rectes indiquen els valors predits per les equacions 2-5

$$K_i \equiv \prod_{j=1}^S (a_j)_{e_i}^{v_j} = \left(\prod_{j=1}^S (\gamma_j)_{e_i}^{v_j} \right) \left(\prod_{j=1}^S (x_j)_{e_i}^{v_j} \right) \equiv K_{\gamma_i} \cdot K_{x_i} \quad (1)$$

Els valors dels increments d'entalpia i entropia de reacció es poden estimar a partir dels pendents i les ordenades, respectivament, de les expressions que s'ajusten millor als resultats obtinguts:

$$\ln K_{MTBE} = \frac{(4.540 \pm 1.190)}{T} - (9,7 \pm 3,5) \quad (2)$$

$$\ln K_{ETBE} = \frac{(4.860 \pm 210)}{T} - (11,46 \pm 0,60) \quad (3)$$

$$\ln K_{PTBE} = \frac{(4.360 \pm 430)}{T} - (9,52 \pm 1,29) \quad (4)$$

$$\ln K_{BTBE} = \frac{(4.570 \pm 340)}{T} - (10,30 \pm 0,99) \quad (5)$$

Si es considera que l'increment d'entalpia de reacció no és constant en l'interval de temperatures que s'estudia, l'increment d'entalpia s'expressa per mitjà de l'equació de Kirchoff, a partir de la capacitat calorífica molar, en fase líquida, dels compostos corresponents:

$$\frac{d\Delta_r H^\circ}{dT} = \sum_{j=1}^S v_j C_{P_j}^\circ \quad (6)$$

$$C_{P_j}^\circ [J \text{ mol}^{-1} K^{-1}] = a + bT + cT^2 + dT^3 \quad (7)$$

A partir d'aquí, es poden obtenir els valors dels increments d'entalpia, entropia i energia lliure de Gibbs de la reacció, tenint en compte les relacions següents:

$$\ln K = I_H - \frac{I_K}{RT} + \frac{a}{R} \ln T + \frac{b}{2R} T + \frac{c}{6R} T^2 + \frac{d}{12R} T^3 \quad (8)$$

$$\text{en què: } a = \sum_{j=1}^S v_j a_j; b = \sum_{j=1}^S v_j b_j; c = \sum_{j=1}^S v_j c_j; d = \sum_{j=1}^S v_j d_j$$

$$\Delta_r H^\circ = I_K + aT + \frac{b}{2} T^2 + \frac{c}{3} T^3 + \frac{d}{4} T^4 \quad (9)$$

$$\Delta S^\circ = RI_H + a + a \ln T + bT + \frac{c}{2} T^2 + \frac{d}{3} T^3 \quad (10)$$

$$\Delta G^\circ = I_K - RI_H T - aT \ln T - \frac{b}{2} T^2 - \frac{c}{6} T^3 - \frac{d}{12} T^4 \quad (11)$$

Finalment, a la taula 3 es mostren els valors obtinguts de les diferents propietats termodinàmiques de les quatre reaccions que s'han estudiat.

Taula 3 Valors dels increments d'entalpia [kJ mol^{-1}], entropia [J (mol K)^{-1}] i energia lliure de Gibbs [kJ mol^{-1}] molars estàndard per a les reaccions de síntesi d'alquil *terc*-butil èters en fase líquida a 298,15 K. Els errors associats corresponen a un nivell de confiança del 95%

Reacció	Propietat	$\Delta_r H^\circ \neq f(T)$	$\Delta_r H^\circ = f(T)$	Teòric	Estudis previs			
MTBE	$\Delta_r H^\circ$	-38 ± 10	-37 ± 10	-36,9	-37,7 ^a	$-39,1 \pm 0,8^b$	$-38,0 \pm 0,8^b$	-36,1 ^c
	$\Delta_r S^\circ$	-80 ± 30	-80 ± 30	-76,9		$-85,3 \pm 0,5^b$	$-81,7 \pm 0,5^b$	-75,4 ^c
	$\Delta_r G^\circ$	-13 ± 13	-14 ± 13	-14,0	-14,0 ^a	$-13,7 \pm 0,8^b$	$-13,6 \pm 0,8^b$	-13,7 ^c
ETBE	$\Delta_r H^\circ$	$-40,4 \pm 1,7$	$-38,5 \pm 1,7$	-34,8	$-44,3 \pm 2^d$	-41,1 ^e	$-35,45 \pm 1,94^f$	$-36,3 \pm 7,2^g$
	$\Delta_r S^\circ$	-95 ± 5	-89 ± 5	-78,2		-94,9 ^e	$-82,37 \pm 5,99^f$	$-81,3 \pm 21,4^g$
	$\Delta_r G^\circ$	-12 ± 2	-12 ± 2	-11,5		-12,8 ^e		$-12,1 \pm 4,5^g$
PTBE	$\Delta_r H^\circ$	-36 ± 4	-34 ± 3	-32,1	$-26,4^h$			
	$\Delta_r S^\circ$	-79 ± 11	-71 ± 10	-75,5	$-53,0^h$			
	$\Delta_r G^\circ$	-13 ± 5	-12 ± 4	-9,6				
BTBE	$\Delta_r H^\circ$	-38 ± 3	-35 ± 3	-38,5	$-34,8 \pm 2,7^i$			
	$\Delta_r S^\circ$	-86 ± 8	-76 ± 9	-78,6	$-75,8 \pm 7,7^i$			
	$\Delta_r G^\circ$	-12 ± 4	-12 ± 4	-15,1				

^a [95]. ^b [96]. ^c [98]. ^d [100]. ^e [102]. ^f [103]. ^g [105]. ^h [22]. ⁱ [108].

3.2 Formació de subproductes

Tot i que l'ús d'èters ramificats com a additius de la gasolina està molt estès a la Unió Europea, especialment l'ETBE, no hi ha gaires treballs que se centrin en la formació de subproductes. Tanmateix, és ben sabut que en el procés industrial d'obtenció d'ETBE se'n formen, de subproductes, els quals són indesitjables, atès que empitjoren la qualitat de la gasolina. Per tant, per poder optimitzar el procés d'obtenció d'ETBE, cal ampliar el coneixement relatiu a les condicions que afavoreixen la formació de subproductes.

Així doncs, l'objecte d'estudi d'aquest apartat són les principals reaccions secundàries que tenen lloc simultàniament amb la síntesi d'ETBE (figura 6). Els experiments s'han dut a terme en el reactor discontinu de tanc agitat, en el rang de temperatures de 323 a 383 K i utilitzant resines de bescanvi iònic com a catalitzadors; principalment s'ha emprat l'A-35, però també la CT-275.

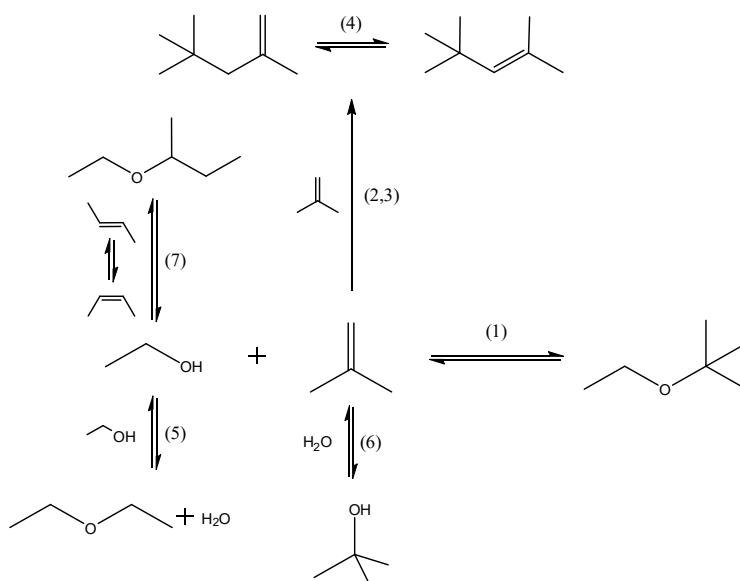


Figura 6 Xarxa de reaccions en la síntesi d'ETBE utilitzant fracció C₄ com a font d'isobutè:

1. Eterificació d'isobutè amb etanol, 2,3. Oligomerització d'isobutè per formar els dímers TMP-1 i TMP-2, 4. Reacció d'isomerització entre TMP-1 i TMP-2, 5. Deshidratació d'etanol per formar DEE i aigua, 6. Hidratació d'isobutè per formar TBA, 7. Eterificació de 2-butè amb etanol per formar ESBE

A la figura 7 es mostra l'evolució de la fracció molar de les diferents espècies químiques involucrades en aquest sistema de reaccions per a un experiment dut a terme a una temperatura de 383 K, amb una raó molar inicial alcohol/olefina ($R^{\circ}_{A/O}$) de 0,5 i utilitzant 10 g d'A-35 com a catalitzador. En aquestes condicions, l'aparició de reaccions secundàries està fortament afavorida.

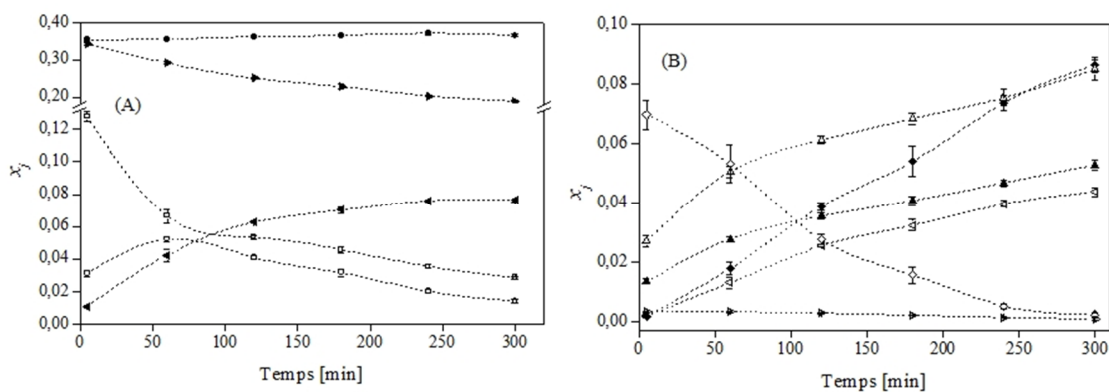


Figura 7 Evolució de la fracció molar dels compostos majoritaris (A) i minoritaris (B).

$T = 383$ K, $R^{\circ}_{A/O} = 0,5$, A-35, càrrega de catalitzador = 10% màssic, $d_p = 0,25-0,40$ mm, 500 rpm. Les barres d'error indiquen l'error estàndard per als experiments replicats.

x_{IB} (□), x_{EtOH} (○), $x_{isobutà}$ (●), $x_{trans-2-butè}$ (▶), $x_{cis-2-butè}$ (◀), x_{ETBE} (◇), x_{TBA} (▷), x_{DEE} (◁), x_{ESBE} (◆), x_{TMP-1} (△), x_{TMP-2} (▲)

De les reaccions secundàries estudiades, la de formació de dímers és la més important. La selectivitat d'isobutè per formar TMP-1 i TMP-2 pot arribar a valors de més del 60% i del 30%, respectivament, a 383 K i amb una raó molar inicial etanol/isobutè de 0,5. Pel

que fa a la reacció d'isomerització entre TMP-1 i TMP-2, cal destacar que aquest cas constitueix una excepció respecte de la norma general quant a l'estabilitat d'alquens isòmers, atès que el TMP-1 és més estable que el TMP-2. La formació de DEE és pràcticament inexistent a temperatures de fins a 343 K, però a 363 i 383 K augmenta molt, especialment si hi ha un excés d'etanol en la mescla inicial de reactants. En aquest cas, la selectivitat d'etanol pel DEE arriba al 50% a 383 K. La formació de TBA es dona en quantitats molt petites. A 383 K i en excés d'etanol, la selectivitat d'isobutè pel TBA al final de l'experiment ($t = 300$ min) assoleix un valor màxim del 7%. Cal esmentar, però, que la síntesi de TBA és una reacció molt ràpida en comparació amb la resta de reaccions secundàries. Això comporta que, en qualsevol de les condicions assajades, la formació de TBA arribi a equilibri químic al llarg dels experiments i que, posteriorment, l'equilibri es desplaci a l'esquerra arran del caràcter irreversible d'altres reaccions secundàries. Finalment, pel que fa a la formació d'ESBE, cal esmentar que pràcticament és inexistent a 323 i a 343 K. En canvi, a 383 K i en excés d'isobutè, la selectivitat d'etanol per l'ESBE pot arribar a valors del 50%.

A partir dels resultats obtinguts, s'ha pogut concloure que totes les reaccions secundàries es veuen afavorides per temperatures elevades. Pel que fa a la concentració inicial de reactants, un excés d'isobutè promou la formació de dímers d'isobutè i d'ESBE, mentre que un excés d'etanol afavoreix les formacions de DEE i de TBA.

Adicionalment, s'han seleccionat tres experiments en què la formació de subproductes ha estat elevada i s'han repetit amb un altre catalitzador, la resina CT-275, per comprovar si hi ha diferències respecte del comportament catalític observat amb la resina A-35. Les condicions experimentals per a aquests experiments han estat les següents: a temperatures altes (363 i 383 K), s'han fet dos experiments amb una raó molar inicial alcohol/olefina de 0,5, és a dir, en excés d'olefina; a la temperatura més elevada (383 K), s'ha realitzat un experiment amb una raó etanol/isobutè d'1,0, és a dir, amb la relació estequiomètrica.

En l'experiment a 363 K i excés d'isobutè, s'ha observat que la formació de subproductes és més elevada en el cas de l'A-35 que en el de la CT-275. Aquest fet s'explica per la major capacitat àcida de l'A-35, cosa que la fa més activa en general, i per la superfície específica, la qual també és superior a la de la CT-275 ($29 \text{ m}^2 \text{ g}^{-1}$ versus 20,3, respectivament), cosa que pot permetre que els reactants accedeixin més fàcilment als centres actius. En aquest cas, resulta adient explicar el comportament catalític de les resines per mitjà de les propietats morfològiques en estat sec i no pas en estat d'inflament, atès que, en excés d'isobutè (i de la resta de components de la mescla C_4), és probable que l'estructura de la resina es trobi pràcticament col·lapsada.

Quan la temperatura augmenta fins a 383 K, amb la mateixa concentració inicial de reactants, la resina CT-275 produeix una quantitat de subproductes superior. En analitzar els subproductes formats, es pot comprovar que l'augment en la formació de dímers d'isobutè és molt més pronunciat en els experiments amb la CT-275 que en els experiments amb l'A-35. En aquest cas, l'explicació més coherent està relacionada amb

les diferències quant al diàmetre dels porus de les dues resines (la CT-275 presenta uns porus molt amples, de 50,1 nm, i l'A-35, en canvi, de només 23,7 nm). En aquest sentit, és probable que els dímers formats puguin arribar a bloquejar, si més no de manera parcial, els porus de l'A-35 i a impedir que la reacció continuï progressant. En canvi, en el cas de la CT-275, aquest efecte no és prou determinant, a causa del fet que els porus d'aquesta resina són més grans.

Finalment, pel que fa la formació de subproductes en els experiments a 383 K i relació estequiomètrica, pràcticament no hi ha diferències entre els dos catalitzadors, ni en termes de producció ni en termes de selectivitat. Això indica que en aquestes condicions la morfologia dels catalitzadors no té un paper determinant en els processos catalítics. En canvi, les condicions d'operació, especialment la temperatura i la càrrega de catalitzador, determinen el progrés de les diferents reaccions que es produeixen, en funció de la cinètica de cadascuna. Per tant, la reacció de síntesi d'ETBE, que és relativament ràpida, pot arribar a equilibri, però després, a causa de la demanda de reactants generada per les reaccions secundàries, es desplaça a l'esquerra.

3.3 Influència de les propietats de les resines sobre la seva activitat catalítica

Com s'ha vist, la síntesi d'alquil *terc*-butil èters se sol dur a terme utilitzant resines àcides de bescanvi iònic com a catalitzadors. Concretament, s'empren resines sulfonades d'estructura macroreticulada. Ara bé, tot i que aquest tipus de síntesi està molt estesa, especialment a Europa, manquen treballs que analitzin si hi ha correlacions entre l'activitat catalítica de les resines i les seves propietats. En conseqüència, en aquesta tesi s'ha realitzat un estudi centrat a avaluar la influència de les característiques pròpies d'aquests catalitzadors en les reaccions de síntesi d'MTBE, ETBE, PTBE i BTBE (figura 1).

A més, com s'ha esmentat prèviament, les reaccions estudiades en aquesta tesi constitueixen una sèrie de reaccions anàlogues en les quals pot aparèixer una variació de les propietats del medi a causa de la mida dels compostos que hi estan involucrats. Aquesta possible variació també pot influir en el desenvolupament dels processos catalítics mitjançant els quals es duen a terme aquestes reaccions.

Pel que fa al procediment experimental, cal esmentar que els experiments duts a terme en aquest estudi s'han realitzat en el reactor de llit fix, operant en règim diferencial, a una temperatura de 333 K i utilitzant setze resines de bescanvi iònic diferents. La raó molar d'alimentació alcohol/isobutè s'ha fixat en 1,0 i s'ha utilitzat la mescla C₄ com a font d'isobutè. Pel que fa als resultats obtinguts, s'expressen en termes de velocitat de reacció intrínseca, és a dir que les etapes de transferència de matèria, externa i interna, no afecten significativament els valors de velocitat de reacció obtinguts. Això s'ha pogut determinar gràcies a la realització d'experiments previs, l'objectiu dels quals ha estat, precisament, determinar les condicions d'operació que garanteixen que aquests efectes siguin negligibles.

En primer lloc, s'ha procedit a avaluar la reactivitat dels diferents alcohols amb l'isobutè o, en altres paraules, s'ha analitzat quin efecte poden tenir les diferents propietats del medi sobre la reactivitat d'aquests sistemes. Atès que l'única diferència entre els quatre sistemes de reacció és la mida de l'alcohol lineal primari, aquesta anàlisi s'ha centrat en les propietats dels alcohols. En termes de la velocitat de reacció observada en funció de l'alcohol utilitzat, els resultats mostren que, per a un grup de catalitzadors, l'ordre de reactivitat és 1-butanol > 1-propanol > etanol > metanol. Concretament, els catalitzadors que segueixen aquest ordre són les resines A-15, A-35, A-36, A-40, A-48, CT-175, CT-252 i CT-275. Per contra, per a un segon grup de catalitzadors, el metanol és més reactiu que l'etanol, concretament per a les resines A-16, A-39, A-46, A-70, 306, 406, 606 i 806.

Tal com es mostra a la figura 8, la velocitat de consum d'isobutè augmenta en augmentar la mida de l'alcohol. Així, els valors de velocitat de reacció registrats per a la síntesi de BTBE són els més elevats, seguits pels de PTBE, la magnitud dels quals correspon, aproximadament, a la meitat dels de BTBE, i els valors més baixos corresponen a les síntesis d'MTBE i ETBE, les quals presenten valors de velocitat de reacció molt similars. Aquests resultats coincideixen amb els d'estudis anteriors disponibles a la bibliografia [59,60].

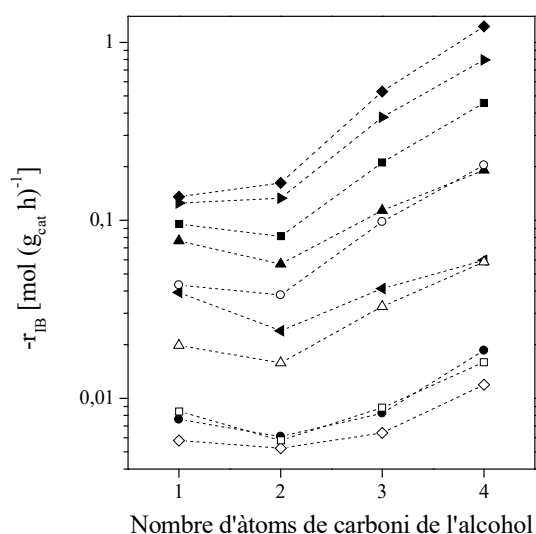


Figura 8 Valors de velocitat de reacció per a diferents catalitzadors respecte del nombre d'àtoms de carboni de l'alcohol. $T = 333 \text{ K}$, $R_{A/O}^{\circ} = 1,0$, $d_p = 0,25\text{-}0,40 \text{ mm}$, $\text{WHSV} > 500 \text{ h}^{-1}$. A-16 (■), A-35(◆), A-39 (▲), A-46 (●), A-70 (◄), CT-275 (►), 306 (◇), 406 (□), 606 (△), 806 (○)

A la figura 8 s'observa que, en termes de velocitat de reacció, la posició relativa de cada catalitzador respecte de la resta roman pràcticament inalterable independentment de la reacció considerada. Aquest fet podria suggerir que hi ha una relació entre la morfologia del catalitzador i l'activitat que presenta. Per tal de verificar o refutar aquesta hipòtesi, s'ha utilitzat la metodologia de superfícies de resposta, amb la finalitat de trobar la propietat o el conjunt de propietats dels catalitzadors que pugui explicar la variabilitat de velocitats de reacció observada per a cadascuna de les quatre reaccions que s'han estudiat.

D'aquesta anàlisi, n'han sorgit uns models empírics, mostrats a les equacions 12-15, que, amb el menor nombre de paràmetres possible, són capaços de descriure fidelment les velocitats de reacció observades (el valor R^2 ajustat mínim és de 0,977). Tots quatre models, i els paràmetres que inclouen, són estadísticament significatius amb un 95% de nivell de confiança.

$$\text{MTBE: } \sqrt{-r_{IB}} = +0,0592 + 0,0585 [H^+] - 0,0272 V_{sp} \quad (12)$$

$$\text{ETBE: } \sqrt{-r_{IB}} = +0,0124 + 0,0825 [H^+] - 0,0023 V_{sp} - 0,0206 [H^+] V_{sp} \quad (13)$$

$$\text{PTBE: } \sqrt{-r_{IB}} = -0,0681 + 0,1796 [H^+] + 0,0520 V_{sp} - 0,0709 [H^+] V_{sp} \quad (14)$$

$$\text{BTBE: } \sqrt{-r_{IB}} = -0,0981 + 0,2877 [H^+] + 0,0531 V_{sp} - 0,1217 [H^+] V_{sp} \quad (15)$$

Aquests models, que es representen a la figura 9, permeten constatar que dues propietats de les resines de bescanvi iònic, concretament la capacitat àcida ($[H^+]$) i el volum de polímer expansible de la fase gel del catalitzador (V_{sp}), determinen l'activitat catalítica de les resines.

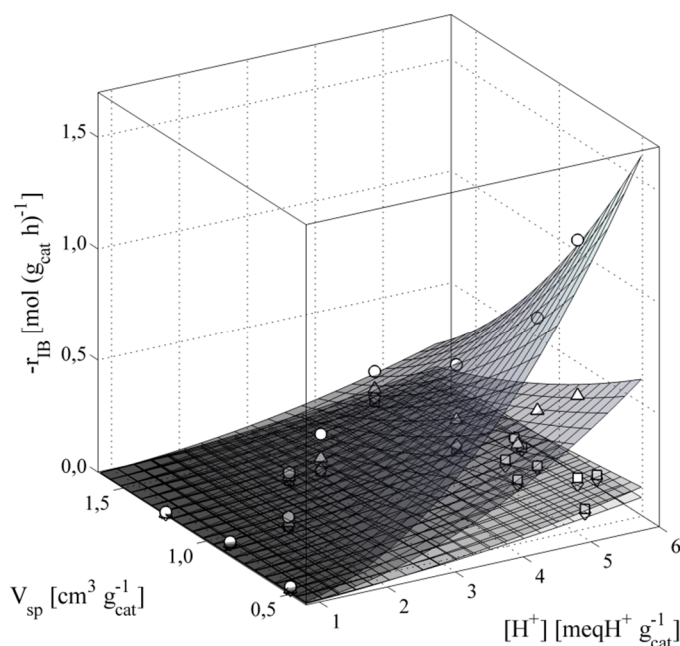


Figura 9 Superfícies de resposta corresponents a les síntesis d'MTBE (\diamond), ETBE (\square), PTBE (Δ) i BTBE (\circ)

Com s'observa a la figura 9, les velocitats de reacció augmenten a mesura que el catalitzador té més capacitat àcida i menys V_{sp} , independentment de la reacció considerada. Això s'explica pel fet que aquesta combinació de factors, o propietats, afavoreix que hi hagi concentracions locals de grups sulfònics elevades, cosa que pot permetre que els reactants es coordinin simultàniament amb més d'un centre actiu a la vegada.

Si es compara l'activitat catalítica de les resines en les diferents reaccions, es pot observar que la principal diferència entre les superfícies de resposta correspon al pendent del pla tangent amb V_{sp} per a valors elevats de capacitat àcida. Aquest fet

implica que l'efecte de la conformació espacial sobre la velocitat de reacció és més acusat per als alcohols més grans, les cadenes d'hidrocarburs dels quals podrien interactuar amb la matriu polimèrica dels catalitzadors.

Així doncs, aquesta anàlisi permet correlacionar l'activitat catalítica dels catalitzadors amb la concentració de grups sulfònics en la fase gel de les resines. Per aquest motiu, s'ha volgut aprofundir en l'efecte que té la morfologia de la fase gel sobre l'activitat catalítica seguint l'aproximació de Jeřábek et al. [69]. Per tant, s'ha desenvolupat un model empíric que té en compte la capacitat àcida i la distribució de fraccions de polímer en la fase gel, determinada mitjançant la tècnica ISEC [65,66].

Aquest model empíric permet computar la velocitat de reacció global com una suma de contribucions de cadascuna de les fraccions de polímer de la fase gel, tal com es mostra a l'equació 16,

$$r_n = \sum_{i=0.1}^{1.5} r_i = \sum_{i=0.1}^{1.5} \left[TOF_i \cdot [H^+]_n \cdot \left(\frac{V_{SP,i}}{\sum_{j=0.1}^{1.5} V_{SP,j}} \right) \right] \quad (16)$$

en què TOF_i és un paràmetre ajustable que correspon a l'activitat específica de la fracció de polímer i [$\text{mol (meqH}^+ \text{ h)}^{-1}$].

Aquest model s'ha ajustat als resultats obtinguts per a les síntesis d'MTBE i d'ETBE, per separat i diferenciant els dos grups de catalitzadors que mostren un comportament diferent quant a l'ordre de reactivitat dels alcohols (així, les resines A-15, A-35, A-36, A-40, A-48, CT-175, CT-252 i CT-275 s'han designat com a grup A i les resines A-16, A-39, A-46, A-70, 306, 406, 606 i 806 com a grup B). S'ha comprovat que el model prediu satisfactòriament les velocitats de reacció observades per a totes dues síntesis i, a més, especialment en el cas de les resines del grup A, permet diferenciar una de les fraccions de polímer de la resta, la que presenta una densitat de cadena característica de $0,4 \text{ nm nm}^{-3}$, pel fet que presenta una activitat específica superior a les altres. Aquest fet implica que l'eficàcia global dels grups sulfònics situats en aquesta regió de polímer és superior a la dels grups sulfònics situats a qualsevol altra regió, cosa que està relacionada amb l'accessibilitat dels reactants a aquests centres actius. Així, per a regions més denses, l'accés dels reactants als centres actius pot estar parcialment restringit, cosa que en fa disminuir l'eficàcia global, i, en regions menys denses, la concentració de centres actius pot ser massa baixa per permetre que els reactants es coordinin amb més d'un centre actiu simultàniament, cosa que també fa disminuir la contribució d'aquests centres actius a la velocitat de reacció.

Consegüentment, s'ha plantejat una generalització del model empíric per a les quatre reaccions estudiades. Per fer-ho, ha calgut introduir una modificació a l'expressió de l'equació 16: s'ha substituït el paràmetre TOF_i per TOF_i^R , el qual es defineix en funció

de la reacció de formació d'MTBE i dels coeficients de distribució d'Ogston dels diferents alcohols a través de cada fracció de polímer:

$$TOF_i^R = k_R \cdot TOF_i^{MTBE} \cdot \frac{K_{O,i}^{MetOH}}{K_{O,i}^{ROH}} \quad (17)$$

- en què:
- TOF_i^R : activitat específica de la fracció de polímer i per a la reacció R [mol (meqH⁺ h)⁻¹]
 - k_R : constant de proporcionalitat per a la reacció R
 - TOF_i^{MTBE} : activitat específica de la fracció de polímer i per a la reacció de formació d'MTBE [mol (meqH⁺ h)⁻¹]
 - $K_{O,i}^{MetOH}$: coeficient de distribució d'Ogston del metanol a través de la fracció de polímer i
 - $K_{O,i}^{ROH}$: coeficient de distribució d'Ogston de l'alcohol lineal primari corresponent a través de la fracció de polímer i

Mitjançant l'ajust simultani de les equacions 16 i 17 a totes les dades experimentals, però mantenint la separació entre els grups A i B, s'han obtingut els valors dels paràmetres TOF_i^R i k_R que minimitzen la suma quadràtica de les diferències entre els valors experimentals i calculats de les velocitats de reacció per a les quatre reaccions estudiades. A la figura 10 es mostren els valors de TOF_i^R per a cadascun dels grups de catalitzadors segons la densitat de cadena característica de les fraccions de polímer presents a la fase gel dels catalitzadors.

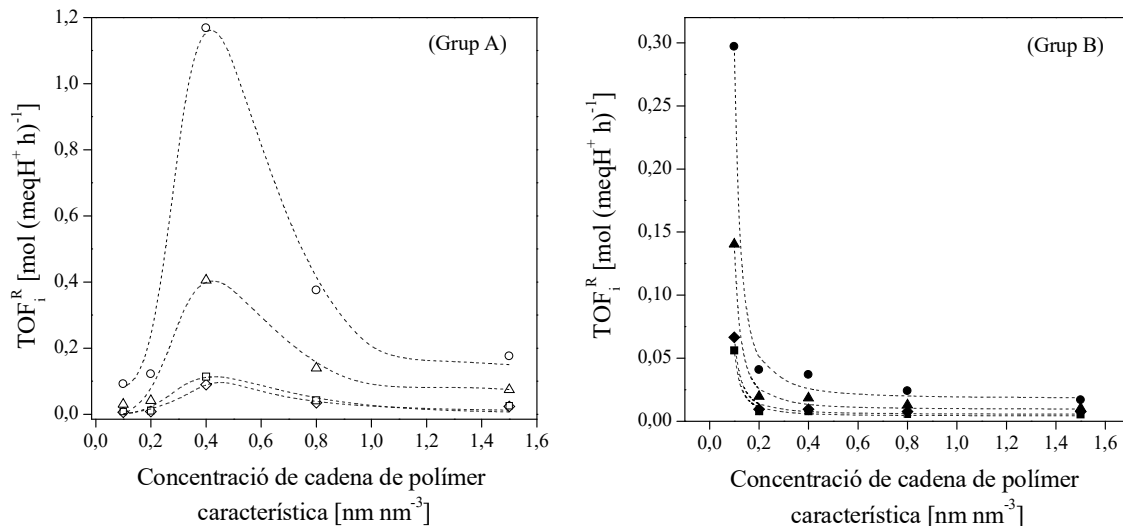


Figura 10 Distribució de TOF de cada densitat característica de fracció de polímer.

$T = 333 \text{ K}$, $R_{AO}^0 = 1,0$, $d_p = 0,25\text{-}0,40 \text{ mm}$, $WHSV > 500 \text{ h}^{-1}$.

Grup A (símbols blancs): MTBE (\diamond), ETBE (\square), PTBE (Δ) i BTBE (\circ).

Grup B (símbols negres): MTBE (\blacklozenge), ETBE (\blacksquare), PTBE (\blacktriangle) i BTBE (\bullet).

De la figura 10, se'n desprèn que els catalitzadors del grup A, que són els més interessants pel que fa a la producció industrial d'alquil *terc*-butil èters, atès que són els més actius, presenten una fracció de polímer (la de $0,4 \text{ nm nm}^{-3}$) en què l'eficàcia dels grups sulfònics és superior a la de la resta pels motius que s'han indicat prèviament. Aquesta fracció de polímer presenta avantatges independentment de la reacció considerada. Com es pot observar, els valors de TOF_i^R dels catalitzadors del grup A augmenten a mesura que augmenta la mida dels alcohols implicats en la reacció *R*, tal com ho fa la reactivitat dels alcohols en la figura 9.

Pel que fa als catalitzadors del grup B, sembla que la fracció de polímer més afavorida és la menys densa, mentre que per a la resta de fraccions de polímer s'arriba a eficàcies pràcticament nul·les. En aquest cas, sembla més coherent suposar que la baixa densitat de cadena d'aquesta regió pot facilitar l'accés dels reactants a fraccions de polímer veïnes, en les quals la concentració de grups sulfònics és més elevada, que no pas interpretar els resultats en funció de les possibilitats de coordinació entre reactants i centres actius.

Finalment, des del punt de vista dels fabricants de resines de bescanvi iònic, els resultats que es mostren en aquest apartat permeten identificar el conjunt de característiques que afavoreixen l'activitat catalítica d'aquests materials en el tipus de reaccions que s'estudien. En aquest sentit, les resines més adients per actuar com a catalitzadors en la síntesi d'alquil *terc*-butil èters són les que tenen una capacitat àcida elevada, una estructura més aviat rígida, és a dir, poca capacitat d'inflament, i una fase gel en què predominen les fraccions de polímer amb una densitat de cadena mitjana, de $0,4 \text{ nm nm}^{-3}$. En general doncs, les resines que mostren unes característiques més similars a les que s'han descrit són resines sobresulfonades i amb un grau de reticulació elevat.

3.4 Síntesi simultània d'ETBE i BTBE amb resines de bescanvi iònic

D'altra banda, s'ha realitzat un estudi amb l'objectiu d'avaluar la viabilitat d'un procés de síntesi d'ETBE i de BTBE alhora, utilitzant resines de bescanvi iònic. Els avantatges principals que pot implicar un procés d'aquestes característiques són que permetria que els fabricants disposessin de flexibilitat operativa per adaptar-se a les demandes del mercat i disponibilitat de matèries primeres i que, a més, poguessin utilitzar productes de fermentació que ja contenen tots dos alcohols, etanol i 1-butanol, com és el cas de la fermentació ABE (en què s'obté acetona, 1-butanol i etanol), per exemple. D'aquesta manera, doncs, es poden estalviar etapes de separació. Addicionalment, hi ha estudis previs que indiquen que les velocitats de reacció globals poden ser sensiblement superiors a les del procés de síntesi d'ETBE, cosa que també pot comportar uns estalvis operatius significatius [39,59]. Les reaccions estudiades en aquest apartat es mostren a la figura 11.

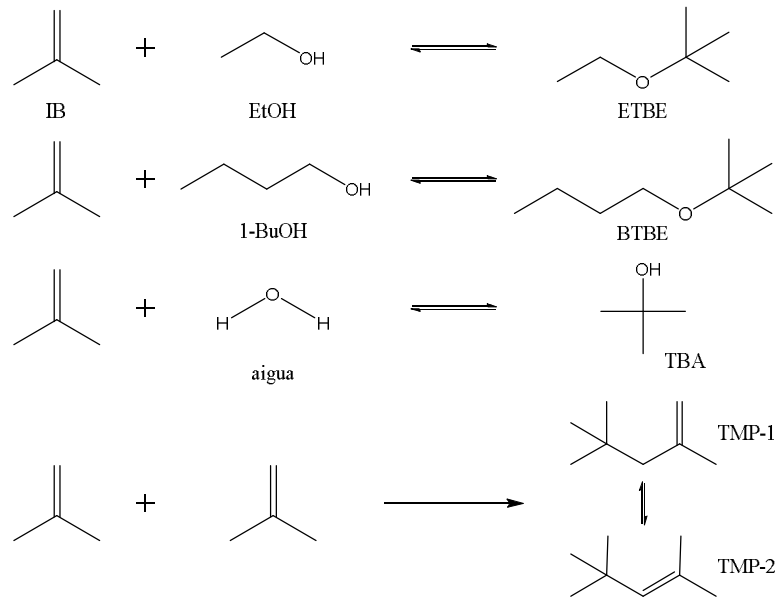


Figura 11 Esquema de reaccions

Així, per a aquest estudi, s'han realitzat experiments en el reactor discontinu de tanc agitat, en un rang de temperatures de 315 a 353 K, utilitzant sis resines de bescanvi iònic comercials diferents (A-16, A-35, A-39, A-46, A-70 i CT-275) com a catalitzadors, amb diferents concentracions de reactants.

Els resultats principals indiquen que l'A-35 és el catalitzador més idoni per a aquest procés, tant en termes de velocitat de reacció com de baixa formació de subproductes (figura 12). També es pot observar que hi ha una relació de proporcionalitat entre la velocitat de reacció de totes dues síntesis i la concentració de centres actius en la fase gel del catalitzador. A més, en aquest estudi s'ha comprovat que l'etanol s'adsorbeix preferentment, per davant de l'1-butanol, en totes les resines utilitzades, cosa que fa que la velocitat de producció d'ETBE sigui, generalment, superior a la de BTBE.

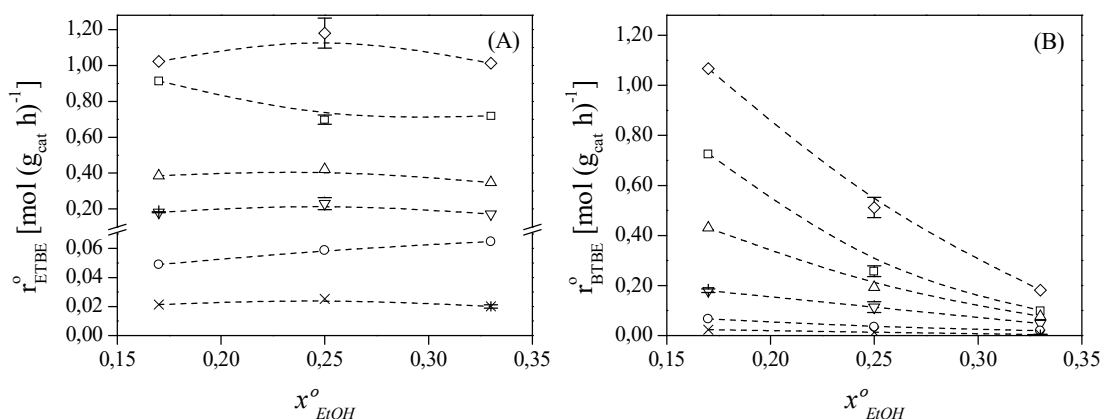


Figura 12 Velocitat de reacció inicial d'ETBE (A) i de BTBE (B) respecte de la fracció molar d'etanol en la mescla inicial de reactants. Les barres d'error indiquen l'error estàndard dels experiments replicats. T = 333 K, $R_{A/O}^{\circ} = 1,0$, $d_p = 0,25-0,40$ mm, 750 rpm.

A-35 (◇), CT-275 (□), A-16 (△), A-39 (▽), A-70 (○) i A-46 (×)

D'altra banda, també s'ha comprovat que la velocitat de reacció de totes dues síntesis augmenta en augmentar la concentració d'isobutè en la mescla inicial de reactants, tal com ja descriuen estudis previs [59,136,138]. Pel que fa a l'efecte de la temperatura sobre el desenvolupament de les reaccions estudiades, cal destacar el fet que la síntesi de BTBE es veu més afectada per limitacions de transferència de matèria que la d'ETBE, cosa que es pot explicar per la mida de les molècules que hi estan implicades. A més, les limitacions en la difusió d'1-butanol, o del producte resultant, el BTBE, també afecten el transport de la resta d'espècies.

En relació amb la comparació entre els sistemes individuals (les síntesis d'ETBE i de BTBE per separat) i el sistema simultani, s'ha pogut comprovar que la formació de subproductes és sensiblement inferior en el cas del procés simultani. A més, la velocitat de consum global d'isobutè és molt superior en el sistema simultani que en la síntesi d'ETBE.

3.5 Anàlisis cinètiques

Al llarg d'aquesta tesi s'ha estudiat la formació de diversos alquil *terc*-butil èters. D'aquests èters, n'hi ha dos, el PTBE i el BTBE, dels quals es poden trobar molt poques referències bibliogràfiques. Paral·lelament, a l'apartat anterior, s'ha proposat un sistema de reacció en el qual es poden obtenir ETBE i BTBE simultàniament. Per tant, per a aquests tres sistemes, s'ha trobat adient estudiar-ne les cinètiques de formació. Per fer-ho, s'han realitzat experiments tant en el reactor de tanc agitat com en el de llit fix, en un rang de temperatures de 317 a 354 K i utilitzant o bé isobutè pur o bé la mescla sintètica d'hidrocarburs C₄ com a fonts d'isobutè. L'estudi cinètic s'ha dut a terme amb la resina A-35 com a catalitzador.

Mitjançant el formalisme Langmuir-Hinshelwood-Hougen-Watson (LHHW), i considerant la introducció d'un terme d'interacció entre la resina i el medi reactiu [136,150], s'han desenvolupat tots els models cinètics que poden descriure les reaccions, sota l'assumció que qualsevol de les etapes de reacció del procés catalític poden ser l'etapa limitant de velocitat. Seguidament, les expressions resultants s'han ajustat sistemàticament a les dades cinètiques que es podien considerar lliures d'efectes significatius de les etapes de transferència de matèria, externa i interna. Els valors òptims dels paràmetres de les equacions cinètiques s'han calculat per minimització de la suma quadràtica ponderada de les diferències entre els valors observats i calculats (WSSE), per mitjà de l'algoritme de Levenberg-Marquardt:

$$WSSE = \sum \left(\frac{r_{exp} - r_{calc}}{w} \right)^2 \quad (18)$$

El factor de ponderació, w , és la velocitat mitjana de reacció de cadascuna de les síntesis, en els casos de les cinètiques de PTBE i BTBE, i la velocitat màxima de reacció de cadascuna de les reaccions, en els casos de les cinètiques de producció simultània d'ETBE i BTBE.

D'aquesta manera, s'ha seleccionat un conjunt de models que són capaços de descriure les dades experimentals de manera acurada. D'aquests models, se n'han rebutjat aquells que presenten algun paràmetre amb una incertesa estàndard associada del 100% o més de la magnitud del propi paràmetre. A més, també s'han rebutjat aquells models que presenten alguna incongruència termodinàmica. Així, per a cadascuna de les reaccions, s'ha pogut obtenir un conjunt de models capaços de descriure acuradament els valors observats de velocitat de reacció, que contenen paràmetres estadísticament significatius i que compleixen les restriccions termodinàmiques.

A l'hora de seleccionar el millor model, o conjunt de models, per a cadascuna de les reaccions, s'ha adoptat el criteri d'informació d'Akaike (AIC) [166,167], cosa que ha permès seleccionar els models que es mostren a continuació.

Sistemes de reacció de síntesi individual de PTBE de BTBE:

$$r_{PTBE} = \frac{k'_{PTBE} \left(a_{IB} a_{1-PrOH} - \frac{a_{PTBE}}{K_{EqPTBE}} \right)}{a_{1-PrOH} + k_{PTBE} a_{PTBE}} \exp \left[\frac{\bar{V}_M \phi_P^2}{RT} (\delta_M - \delta_P)^2 \right] \quad (19)$$

$$k'_{PTBE} \left[\frac{\text{mol}}{\text{g}_{cat} \text{h}} \right] = \exp \left[(0,366 \pm 0,014) - (9,04 \pm 0,08) \cdot 10^3 \left(\frac{1}{T} - \frac{1}{327,7} \right) \right]$$

$$k_{PTBE} = \exp \left[-(1,37 \pm 0,07) - (9,1 \pm 0,4) \cdot 10^3 \left(\frac{1}{T} - \frac{1}{327,7} \right) \right]$$

$$\delta_P \left[\text{MPa}^{1/2} \right] = (20,5 \pm 0,3)$$

$$r_{BTBE} = \frac{k'_{BTBE} \left(a_{IB} a_{1-BuOH} - \frac{a_{BTBE}}{K_{EqBTBE}} \right)}{a_{1-BuOH} + k_{BTBE} a_{BTBE}} \exp \left[\frac{\bar{V}_M \phi_P^2}{RT} (\delta_M - \delta_P)^2 \right] \quad (20)$$

$$k'_{BTBE} \left[\frac{\text{mol}}{\text{g}_{cat} \text{h}} \right] = \exp \left[(1,151 \pm 0,010) - (9,22 \pm 0,14) \cdot 10^3 \left(\frac{1}{T} - \frac{1}{328,6} \right) \right]$$

$$k_{BTBE} = \exp \left[-(1,1 \pm 0,6) \right]$$

$$\delta_P \left[\text{MPa}^{1/2} \right] = 17,0 \pm 0,3$$

Sistema de reacció de síntesi simultània d'ETBE i de BTBE:

$$r_{ETBE} = \frac{k'_{ETBE} \left(a_{IB} a_{EtOH} - \frac{a_{ETBE}}{K_{EqETBE}} \right)}{a_{EtOH} + k_{1-BuOH} a_{1-BuOH} + k_{ETBE} a_{ETBE}} \exp \left[\frac{\bar{V}_M \phi_P^2}{RT} (\delta_M - \delta_P)^2 \right] \quad (21)$$

$$r_{BTBE} = \frac{k'_{BTBE} \left(a_{IB} a_{1-BuOH} - \frac{a_{BTBE}}{K_{EqBTBE}} \right)}{a_{EtOH} + k_{1-BuOH} a_{1-BuOH} + k_{ETBE} a_{ETBE}} \exp \left[\frac{\bar{V}_M \phi_P^2}{RT} (\delta_M - \delta_P)^2 \right] \quad (22)$$

$$k'_{BTBE} \left[\frac{\text{mol}}{\text{g}_{\text{cat}} \text{h}} \right] = \exp \left[-(0,32 \pm 0,04) - (10,2 \pm 0,3) \cdot 10^3 \left(\frac{1}{T} - \frac{1}{333,6} \right) \right]$$

$$k_{BTBE} \left[\frac{\text{mol}}{\text{g}_{\text{cat}} \text{h}} \right] = \exp \left[-(0,79 \pm 0,02) - (8,62 \pm 0,19) \cdot 10^3 \left(\frac{1}{T} - \frac{1}{333,6} \right) \right]$$

$$k_{BTBE} = \exp \left[-(2,36 \pm 0,11) - (10,9 \pm 0,8) \cdot 10^3 \left(\frac{1}{T} - \frac{1}{333,6} \right) \right]$$

$$k_{ETBE} = \exp[0,21 \pm 0,07]$$

$$\delta_p \left[\text{MPa}^{1/2} \right] = 25,99 \pm 0,10$$

L'ajust de les expressions 19-22 a les dades experimentals per a cadascun dels sistemes estudiats es mostra a les figures 13-15. En aquestes figures s'inclouen totes les dades experimentals, independentment del dispositiu experimental que s'ha utilitzat o si les velocitats de reacció presenten limitacions a causa de l'etapa de transferència de matèria interna.

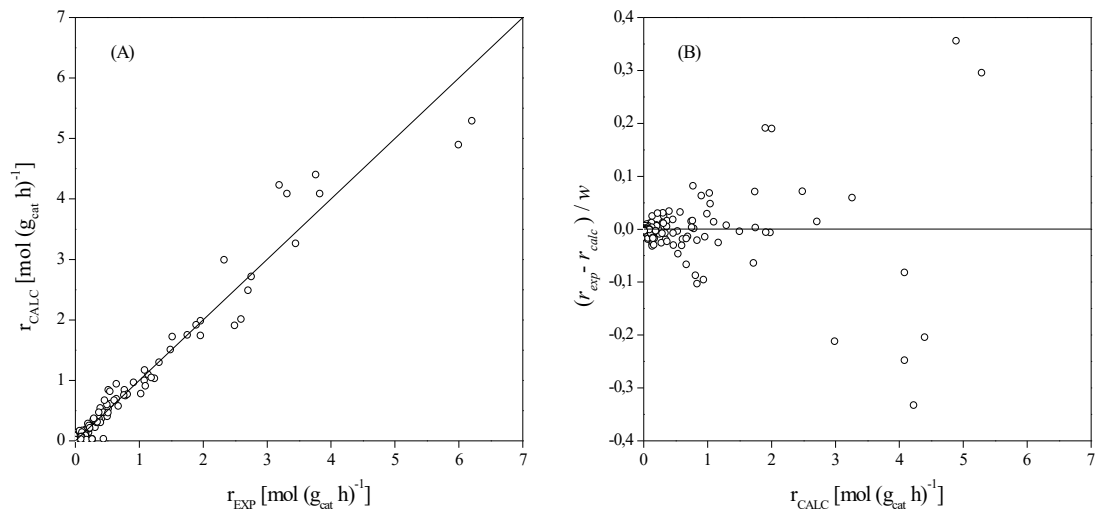


Figura 13 Velocitats de reacció de síntesi de PTBE calculades mitjançant l'equació 19 vs. velocitats experimentals (A) i distribució dels residuals (B)

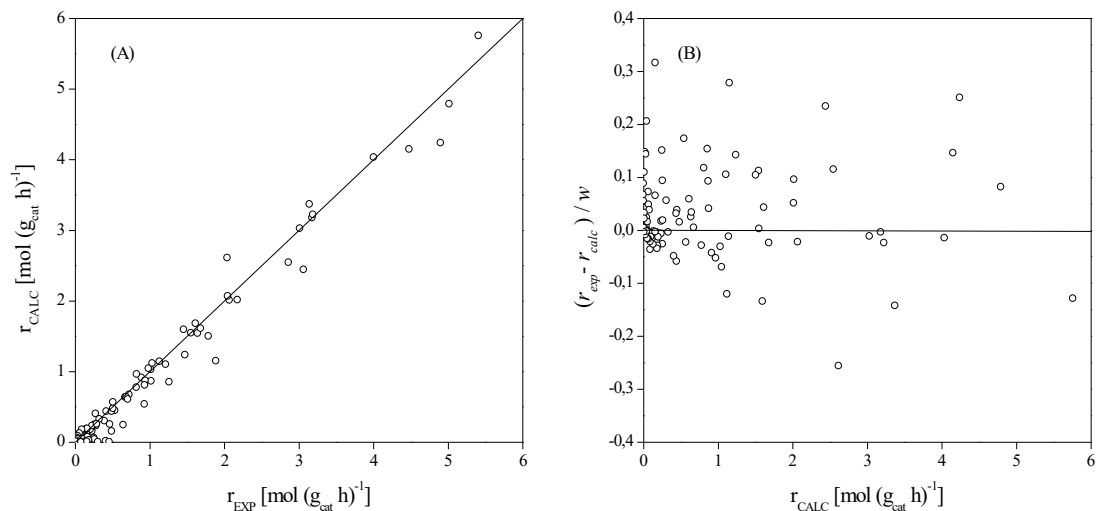


Figura 14 Velocitats de reacció de síntesi de BTBE calculades mitjançant l'equació 20 vs. velocitats experimentals (A) i distribució dels residuals (B)

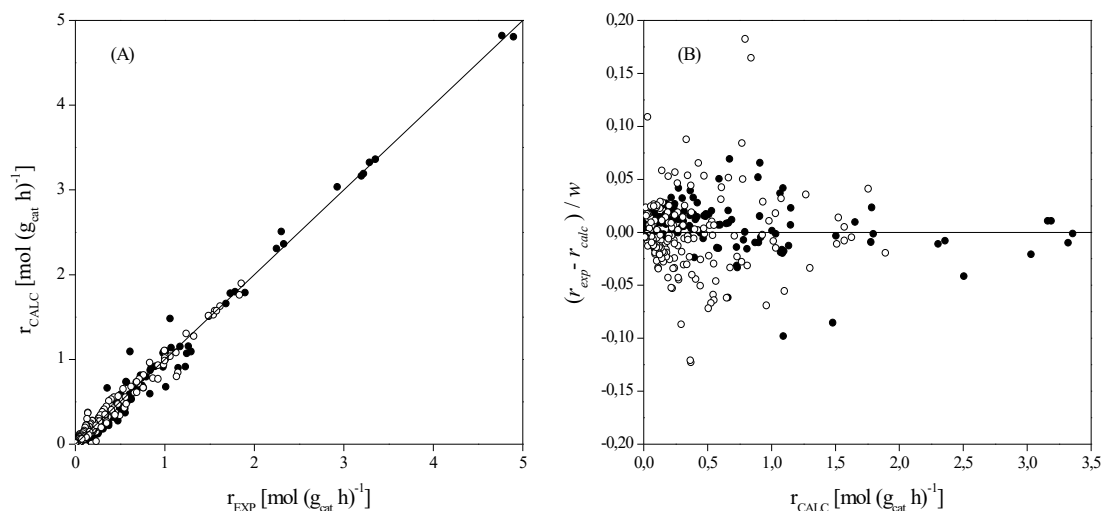


Figura 15 Velocitats de reacció de síntesi d'ETBE i de BTBE calculades mitjançant les equacions 21 i 22, respectivament, vs. velocitats experimentals (A) i distribució dels residuals (B). ETBE (●), BTBE (○).

Així, els models que descriuen millor les cinètiques de les reaccions de síntesi que s'han estudiat indiquen que el mecanisme de reacció més probable és del tipus Eley-Rideal i que l'etapa limitant de velocitat del procés global de reacció és la de reacció en superfície. Les reaccions es poden descriure de la manera següent: una molècula d'alcohol s'adsorbeix en un centre actiu del catalitzador, reacciona amb una molècula d'isobutè del medi i produeix una molècula, adsorbida, de l'èter corresponent, que finalment es desorbeix. En tots els casos, el nombre de centres actius vacant és menyspreable, la qual cosa és consistent amb reaccions en fase líquida.

Pel que fa a l'energia d'activació de les reaccions estudiades, els valors obtinguts són $(75,1 \pm 0,7)$, $(76,6 \pm 1,1)$ i (84 ± 3) kJ mol⁻¹ per a les síntesis de PTBE, BTBE i ETBE, respectivament. Aquests valors són molt similars als de les síntesis d'MTBE i d'ETBE que s'havien obtingut en estudis anteriors [19,95,100,136,138,161,162].

4. Conclusions

En l'estudi que s'ha dut a terme en relació amb l'equilibri químic de les síntesis d'MTBE, ETBE, PTBE i BTBE s'han determinat les propietats termodinàmiques de les quatre reaccions i s'han estimat els increments d'entalpia i entropia de formació dels èters corresponents. Tal com s'esperava, ni el mode d'operació del reactor ni el catalitzador utilitzat afecten el valor de les propietats termodinàmiques de les síntesis estudiades. També s'ha constatat que les quatre reaccions són reversibles i exotèrmiques, motiu pel qual la conversió dels reactants disminueix en augmentar la temperatura d'operació. A partir dels valors de les constants d'equilibri, es pot afirmar que les limitacions termodinàmiques a què estan sotmeses aquestes reaccions no són significativament diferents.

Pel que fa a la formació de subproductes en la síntesi d'ETBE, s'ha constatat que totes les reaccions secundàries associades a aquesta síntesi es veuen afavorides per un increment de la temperatura d'operació. El tipus de subproductes formats, principalment està relacionat amb la composició inicial de reactants. Així, un excés d'olefina afavoreix tant la formació de dímers d'isobutè, la qual és la reacció secundària més important en termes quantitativs, com la formació d'ESBE, que només s'ha produït en quantitats significatives a les temperatures més elevades (363 i 383 K). En canvi, l'excés d'alcohol a la mescla de reactants inicial afavoreix les formacions de DEE i de TBA, el qual és el subproducte que s'ha format en una extensió inferior. En relació amb la comparació del comportament catalític de les resines A-35 i CT-275, s'ha pogut determinar que la CT-275 produeix una quantitat superior de subproductes a la temperatura més elevada (383 K), tot i que també produeix més quantitat d'ETBE.

A l'hora de relacionar les propietats dels catalitzadors amb el grau d'activitat catalítica en les reaccions de síntesi d'MTBE, ETBE, PTBE i BTBE, s'ha determinat que les característiques que tenen una correlació estadísticament significativa amb la velocitat de reacció observada són la capacitat àcida i el volum expansible de la fase gel de les resines. En aquest sentit, les resines amb una capacitat àcida superior (és a dir, amb un nombre de centres actius més elevat) i un volum expansible inferior (és a dir, que presenten una estructura més rígida) són les més actives. L'efecte de l'estructura esdevé més determinant a mesura que incrementa la mida de les molècules implicades en aquestes síntesis. A més, la velocitat de reacció augmenta en augmentar la mida de les molècules implicades. Addicionalment, s'ha presentat un model empíric que correlaciona l'estructura de la fase gel dels catalitzadors (és a dir, la distribució de volums de les fraccions de polímer de densitat de cadena diferents) amb la velocitat de reacció observada en les quatre síntesis.

L'estudi de la producció simultània d'ETBE i BTBE utilitzant resines de bescanvi iònic com a catalitzador ha permès determinar que, de tots els catalitzadors estudiats, la resina A-35 és el catalitzador més adient per dur a terme aquest procés. D'altra banda, s'ha trobat una relació de proporcionalitat entre les velocitats de reacció observades per a totes dues síntesis i la concentració de grups sulfònics en la fase gel dels catalitzadors. Així mateix, s'ha determinat que l'etanol s'adsorbeix preferentment en totes les resines assajades. A més, s'ha comprovat que el procés de síntesi simultània de tots dos èters té avantatges significatius respecte de la producció de cada èter en processos individuals, tant pel que fa a una formació de subproductes inferior com pel que fa a un consum global d'isobutè superior.

Finalment, s'ha dut a terme una anàlisi cinètica de les reaccions estudiades. Segons els resultats obtinguts, el mecanisme de reacció més probable és del tipus Eley-Rideal i l'etapa controlant de la velocitat global del procés de síntesi és la de reacció en superfície. Les reaccions que s'han estudiat es poden descriure de la manera següent: una molècula d'alcohol s'adsorbeix en un centre actiu del catalitzador, reacciona amb una molècula d'isobutè del medi i produeix una molècula, adsorbida, de l'èter corresponent, que finalment es desorbeix.

Agraïments

En primer lloc, vull agrair la direcció i les aportacions del Carles Fité i el Roger Bringué. Al llarg d'aquest temps, he tingut l'oportunitat d'aprendre'n molt, de tots dos, i, sens dubte, aquesta tesi no hauria estat possible sense el seu guiatge. També vull fer extensiu el meu agraïment a la resta de membres del grup de Catàlisi i Cinètica Aplicada, que m'han donat l'oportunitat de treballar amb ells.

En mirar enrere, m'adono de la quantitat de companys amb qui he tingut l'ocasió de compartir moments (i més d'un problema) al laboratori. En aquest sentit, vull fer esment del meu primer mentor, el Rafa, així com de la Marta, el Carlos, la Madelin i la María Ángeles. D'altra banda, no puc deixar d'agrair la col·laboració de la Vanessa Arellano, la Laura Cazacu, la Júlia Athayde i la Silvia Cañavera, amb qui vaig treballar en algunes de les fases experimentals que han acabat formant part d'aquest treball. Resulta curiós adonar-se de la quantitat de feina que poden fer juntes persones tan diferents. Més enllà dels companys de laboratori, també vull fer esment dels companys i amics que he anat fent a la universitat i al departament, incloent-hi els professors i el personal administratiu.

Faig una menció especial (perquè sí, perquè vull) als altres dos membres de GUISOBA, el Jordi i el Rodrigo, amb qui tantes vegades hem arreglat (i espatllat) el món en una mena de tertúlies, sovint poc organitzades i injustificades, que tant podien tractar temes fonamentals per al desenvolupament de la ciència (com, per exemple, el gruix de neu previst a la cara nord dels Pirineus aquell cap de setmana o els detalls més punyents de la batalla de Trafalgar) com altres temes més aviat intrascendents (com ara què devia ser allò de la fase gel).

Crec que també és just i necessari agrair la paciència que han tingut amb mi la resta d'amics (els extrauniversitaris, vull dir) i la meva família (especialment la meva mare) perquè, inexplicablement, encara toleren la meva poca presència en actes socials i perquè, d'alguna manera, també han contribuït a enriquir aquesta llarga etapa formativa que espero que no s'acabi mai.

Aina, a tu et deixo pel final. Et deixo pel final perquè aquesta és una part complicada. També et deixo pel final, no ens enganyem, per incorporar un cert efecte de teatralitat i dramatisme. Però també és cert que et deixo pel final perquè crec que tota història (i aquesta és l'última pàgina d'aquesta història) ha de tenir un gran final. I els millors finals solen ser oberts. Solen fer pensar que, més enllà del que s'ha llegit, hi ha tot allò que encara no s'ha escrit. I en tenim moltes, de coses per escriure. De manera que a tu, Aina, més enllà d'agrair-te el suport que m'has ofert fins ara, el que vull és convidar-te a seguir omplint pàgines i pàgines plegats.

